Multi-physics modeling of the intake line of an internal combustion engine

Mohamad Yassine

THESE DE DOCTORAT DE

L'ÉCOLE CENTRALE DE NANTES
COMUE UNIVERSITE BRETAGNE LOIRE

ECOLE DOCTORALE N° 602
Sciences pour l'Ingénieur
Spécialité : « ***Energétique, Thermique, Combustion***»

Par

« Mohamad YASSINE »

« Multi-physics modeling of the intake line of an internal combustion engine »

Thèse présentée et soutenue à « Nantes », le « 28 janvier 2019 »
Unité de recherche : *Laboratoire de recherche en Hydrodynamique, Énergétique et Environnement Atmosphérique*

Rapporteurs avant soutenance :

Antoine Dazin Professeur des Universités, ENSAM Lille
Yannick Bailly Professeur des Universités, Université de Franche-Comté

Composition du Jury :

Président :	Antoine Dazin	Professeur des Universités, ENSAM Lille
Examinateurs :	Yannick Bailly	Professeur des Universités, Université de Franche-Comté
	Christelle Périlhon	Maître de Conférences HDR, CNAM Paris
Dir. de thèse :	David Chalet	Professeur des Universités, Ecole Centrale de Nantes
Co-enc. de thèse	Haitham Mezher	Ingénieur de Recherche, Ecole Centrale de Nantes

Invité
Jérôme Migaud Ingénieur Mann+Hummel

Acknowledgment

The work in this PhD Thesis is done in a joined International Teaching and Research Chair entitled "Innovative Intake and Thermo-management Systems" between Ecole Centrale de Nantes and MANN+HUMMEL.

Firstly, I would like to express my sincere gratitude to my advisor Mr. David CHALET, Full Professor in the LHEEA laboratory of Ecole Centrale de Nantes, for the continuous support of my PhD study and related research, for his patience, motivation, and immense knowledge. His guidance helped me in all the time of research and writing of this thesis. I could not have imagined having a better advisor and mentor for my PhD study.

I would also like to thank to Mr. Jerome MIGAUD, Director Innovation Transportation in MANN+HUMMEL Group, for his scientific contribution and his technical expertise. I cannot forget to thank Mr. Haitham MEZHER, Doctor and Application/Business Development Engineer in Gamma Technologies, for the technical support it has given me. I have learned a lot from the fruitful discussions we had during my research study.

Besides my advisors, I would like to thank the rest of my thesis committee: Prof. Antoine DAZIN, Prof. Bailly YANNICK, and Dr. Christelle PERILHON , for their insightful comments and encouragement, but also for the hard question which incented me to widen my research from various perspective.

I would also like to take this opportunity to thank Mr. Quentin MONTAIGNE and Mr. Antoine BOUEDEC for their contribution to ensure the good functioning of the experimental test benches during my research study.

And finally, last but not the least; I would like to thank my family and my friends for providing me with unfailing support and continuous encouragement throughout my years of study and through the process of researching and writing this thesis. This accomplishment would not have been possible without them. Thank you.

Table of Contents

Nomenclature

Latin symbols	
a	*Local sound speed (m/s)*
a_i	*Weighting coefficient (m/s)*
a_0	*Sound speed (m/s)*
$A(W)$	*Vector of thermodynamics variables in gas dynamic conservative equation (-)*
A	*Surface (m^2)*
$\hat{A}$	*Transfer matrix pole (w.u)*
$\hat{A}$	*Pole of state space representation (w.u)*
B_I	*Amplitude of incident wave (mbar)*
B_{II}	*Amplitude of retrograde wave (mbar)*
$\hat{B}$	*Transfer matrix pole (w.u)*
$\hat{B}$	*Pole of state space representation (w.u)*
C	*Torque (N.m)*
C	*Capacitance (F)*
C_p	*Specific heat of air at constant pressure (J/kg/K)*
C_v	*Specific heat of air at constant volume (J/kg/K)*
C_d	*Discharge coefficient (w.u)*
$\hat{C}$	*Transfer matrix pole (w.u)*
$\hat{D}$	*Pole of state space representation (w.u)*
D	*Diameter (m)*
$\hat{D}$	*Transfer matrix pole (w.u)*
$\hat{D}$	*Pole of state space representation (w.u)*
E	*Internal energy (J)*
E_0	*Total internal energy(J)*
e	*Internal energy per unit area (J/m)*
f	*Frequency (Hz)*
$f_{friction}$	*Friction coefficient (w.u)*
FFT (.)	*Fast Fourier transform of (.)*

G	*Friction forces vector ($m.s^{-2}$)*
H	*Enthalpy (J/kg)*
H_0	*Total enthalpy (J/kg)*
h_0	*Total Enthalpy per unit area (J/kg/m)*
I	*Input of neural network system (-)*
J	*Jacobian Matrix (w.u)*
k_0	*Real wave number (1/m)*
K	*Coefficient of resistance (w.u)*
Lap (.)	*Laplace transform of (.)*
L	*Length (m)*
L	*Inductance (H)*
M	*Mach Number (w.u)*
N	*Engine Rotational Speed (rpm)*
O	*Output of neural network system (-)*
P	*Pressure in frequency domain (Pa)*
p	*Pressure (mbar)*
p_a	*Relative pressure (mbar)*
p_0	*Mean pressure (mbar)*
q_m	*Air mass flow rate (kg/h)*
$q_{m\,exc}$	*Air mass flow excitation (kg/h)*
Q_m	*Air mass flow rate in Laplace domain (-)*
Q	*Quality factor (w.u)*
$\dot{Q}$	*Heat flux exchanged with walls (w/m^2)*
q	*Heat exchange (w/m^2)*
R	*Resistance (Ω)*
R	*Reflection coefficient (w.u)*
R_E	*Reflection coefficient in moving medium (w.u)*
r	*Ideal gas constant mass (J/kg/K)*

r_h	*Hyperbolic radius (m)*
r(x)	*Reflection coefficient at a certain position (w.u)*
s	*Laplace Variable (w.u)*
S	*Source Vector (w.u)*
TF	*Transfer Function (mbar/kg/h)*
t	*Time (s)*
T	*Temperature (K)*
T_{ref}	*Reference temperature (19 ° C)*
u	*Fluid velocity (m/s)*
U	*Fluid velocity in Laplace domain (-)*
V	*Vector of thermodynamics variables in gas dynamic non-conservative equation (-)*
W	*Vector of thermodynamics variables in gas dynamic conservative equation (-)*
$\dot{W}$	*Heat exchange through the system (w/m^2)*
X_{steady}	*Static losses coefficient (mbar/(Kg.h))*
$X_{inertia}$	*Global inertial parameter (1/m)*
X_i	*Inertial parameter of mode i (1/m)*
$\bar{X}$	*Mean value of a quantity (-)*
x	*Position (m)*
z	*Acoustic impedance model (mbar/kg/h)*
z_c	*Characteristic impedance (1/(m.s))*
z_{cc}	*Complex characteristic impedance (1/(m.s))*
z_{c0}	*Specific impedance of the medium (1/(m.s))*

Greek symbols	
Δt	*Time step (s)*
Δx	*Length Interval (m)*
Δf	*Bandwidth (Hz)*
Δp	*Pressure losses (mbar)*

ΔL	*Length correction (m)*
Δqm	*Air mass flow rate difference (kg/h)*
α	*Attenuation Coefficient (1/m)*
β	*Complex wave number (1/m)*
γ	*Specific Heat ratio (w.u)*
δ	*Uncertainty (w.u)*
ε	*Damping Factor (w.u)*
ξ	*Mass energy loss coefficient (1/m)*
η	*Volumetric Efficiency (w.u)*
λ	*Wavelength (m)*
$\dot{\lambda}$	*Friction coefficient of Darcy (-)*
σ	*Standard deviation (w.u)*
ρ	*Density (kg/m^3)*
ϑ	*Damping coefficient of exponential filter (-)*
χ	*Parametric coefficient of artificial viscosity (w.u)*
ω	*Pulsation (rad/s)*

Index	
0	*Initial*
act	*Actual*
atm	*Atmospheric*
cyl	*Cylinder*
est	*Estimated*
exp	*experimental*
i	*Mode*
imp	*Imposed*
isen	*Isentropic*
max	*Maximum*

measured	*Measured value*
Native	*Modeling of the intake system using 1D non-linear approach*
p	*piston*
ref	*Reference*
rel	*Relative*
th	*Theoretical*
Useful	*Final useful position of the shut off component*

Acronyms	
0D	*Zero – Dimensional*
1D	*One - Dimensional*
3D	*Three – Dimensional*
BDC	*Bottom Dead Center*
CA	*Crank Angle*
CAC	*Charge Air Cooler*
CFD	*Computational Fluid Dynamics*
CFL	*Courant-Friedrichs-Lewy*
CO	*Carbon Monoxide*
CO_2	*Carbon Dioxide*
CPU	*Central Processing Unit*
CUC	*Clean Up Component*
DEN	*Denominator*
DFB	*Dynamic Flow Bench*
diff	*Difference*
Disp	*Displacement*
DNS	*Direct Numerical Resolution*
DOC	*Diesel Oxidation Catalyst*
DoE	*Design of Experiment*

DPF	*Diesel Particulate Filter*
EGR	*Exhaust Gas Recirculation*
FFT	*Fast Fourier Transform*
FRM	*Fast Running Models*
GT/TF	*GT-Power/ Transfer Function model*
HC	*Hydrocarbon*
ICE	*Internal Combustion Engine*
IVC	*Intake Valve Closing*
IVO	*Intake Valve Opening*
MOC	*Method of characteristics*
NEDC	*New European Driving Cycle*
NH_3	*Ammonia*
NO_x	*Nitric Oxide and Nitrogen Dioxide*
NUM	*Numerator*
OEM	*Original Equipment Manufacturers*
OS	*Operating System*
PM	*Particulate Matter*
RAM	*Random Access Memory*
RANS	*Reynolds Averaged Navier-Stokes*
RDE	*Real Driving Emissions*
Re	*Reynolds number*
RT	*Real Time*
RSS	*Root Sum Square*
SCR	*Selective Catalytic Reduction*
TDC	*Top Dead Center*
TF	*Transfer Function*
TPA	*Three Pressure Analysis*
TMFC	*Two microphones Four calibrations*

TMTC	*Two microphones Three calibrations*
TVD	*Total Variation Diminishing*
VDFB	*Virtual Dynamic Flow Bench*
VVT	*Variable Valve Timing*
WLTC	*Worldwide harmonized Light vehicle Test Cycle*
WLTP	*Worldwide harmonized Light vehicle Test Protocol*

Other Symbols	
+	*Direct*
-	*Retrograde*
$\partial / \partial x$	*Partial derivative according to x axis*
$\partial / \partial t$	*Partial derivative according to time*
d / dx	*Total derivative according to x axis*
d / dt	*Total derivative according to x axis*
D / Dt	*Mathematic operator*
$\lvert TF \rvert$	*Modulus of transfer function*
$\lvert u \rvert$	*Absolute value of velocity*
$\overrightarrow{grad}\, p$	*Pressure forces*
$\overrightarrow{\overline{\overline{grad}}} V$	*Convective acceleration*
$\overrightarrow{div}\, \overline{\overline{\tau}}$	*Molecular viscosity forces*
$\vec{V}$	*Velocity Vector*
$\vec{f}$	*Forces vector*
$\otimes$	*Convolution product*

Introduction

The automotive industry evolution is quite important. The technical development and new innovations continue to evolve internal combustion engines. Nowadays, Diesel and Gasoline engines dominate the market in Europe, while other technologies, such as hybrid cars, electric cars and more technologies occupy less than 1% of the market. However, internal combustion engine is likely to remain dominant in road vehicles in the short and medium term perspective. Herefore, engine manufacturers are concerned by the reduction of pollutant emissions, such as: NO_x, CO, HC, and PM that deteriorate air quality and contribute to global warming (caused by CO_2 emissions). The technical development and new innovations continue to evolve internal combustion engines to meet emission regulations that are increasingly severe (Figure 1). In Europe, pollutant emissions are measured on different test drive cycles (NEDC, WLTC, Artemis, etc…). The cycles differ mainly in their ability to represent statistically real world conditions. New European Driving Cycle (NEDC) is a reference cycle for homologating vehicles until Euro 6c. This later will be replaced by a Worldwide harmonized Light vehicle Test Cycle (WLTC), which covers a wider band of acceleration, speed combinations and is more dynamic (Figure 2). A new emission regulation test, known as "Real Driving Emissions" (RDE), has been introduced alongside the WLTP laboratory test to ensure that cars meet emissions limits in a much wider range of driving conditions.

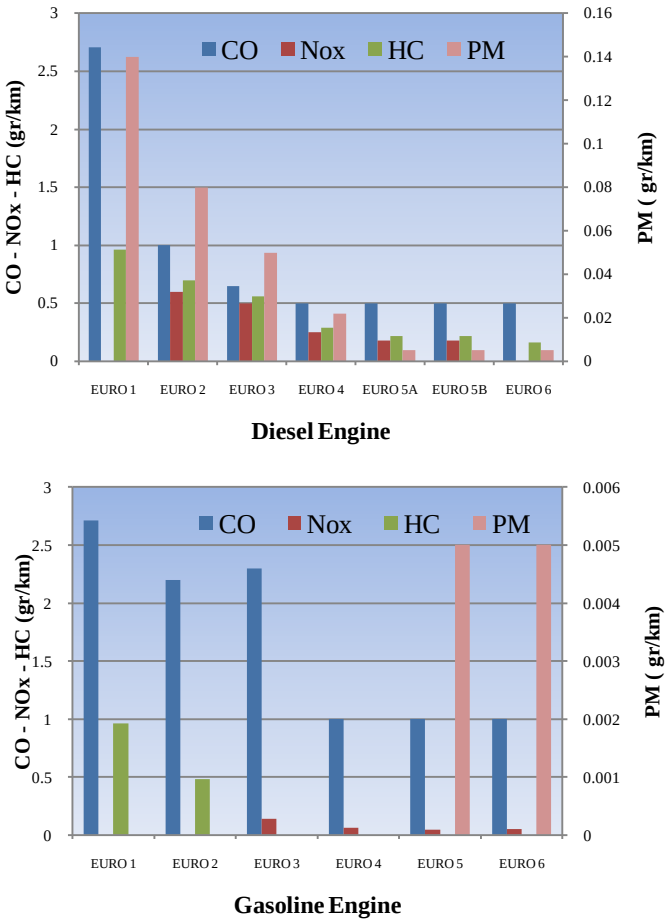

Figure 1 - European Emissions Standards Generations for Diesel and Gasoline Engines[1]

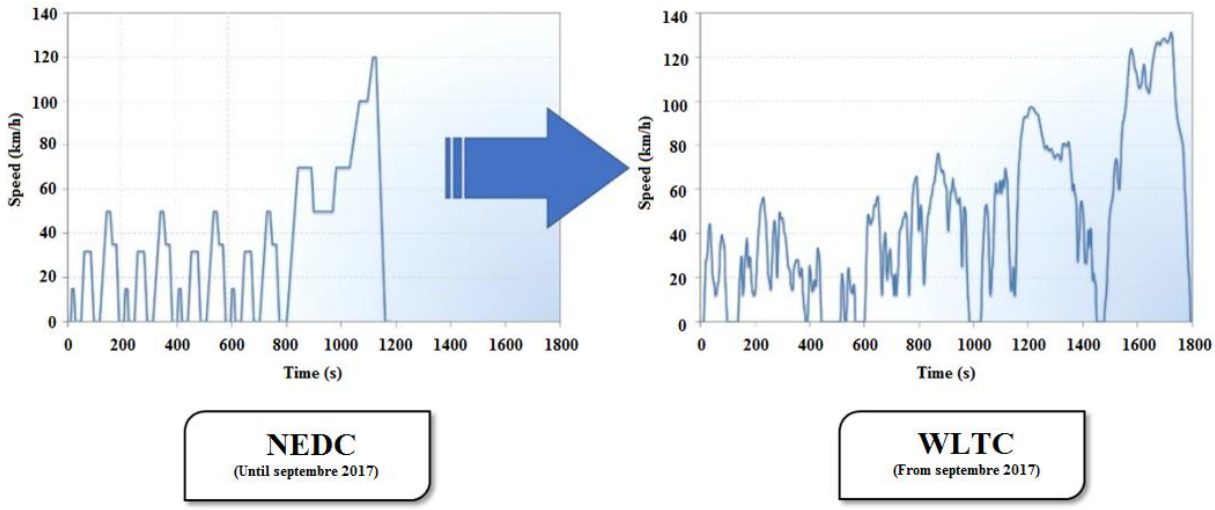

Figure 2 – NEDC to WLTC promotion[2]

Automotive industries are in constant evolution and the competition among carmakers to introduce the most innovative solutions is growing day by day in order to improve engine's performance. For example, in order to reduce the emissions, new technologies were added to the exhaust system of the engine, called exhaust after-treatment systems, to reduce the level of emissions generated by fuel combustion (DOC, SCR, and DPF). Recently a new system is added to the previous systems to avoid NH_3 leakage called "CUC". Consequently, with all of these technologies, the internal combustion engine becomes more sophisticated and hard to manage. Therefore, experimental tests on an engine test bench are primordial to study engine's behavior under different conditions. This phase is called "Engine Calibration". The aim of this stage is to find a compromise between power, consumption, pollutant emissions, and noise. However, this procedure is time and cost consuming. Since time is a major factor in engine design and production, here comes the importance of engine simulation codes and models. Through these models, virtual engine calibration models can be done. Since few years, simulation is being used widely in automotive industries. Instead of building costly prototypes and expending fuel for doing tests on a real engine, simulation became a good solution before taking new decisions. For example, concerning the study of the air flow behavior in air intake manifolds, which is considered compressible and unsteady, the models are based on thermo-dynamical equations. These equations can be 3D, 2D, 1D or 0D. Commercial software usually use one-dimensional or zero-dimensional representations, since three-dimensional models are time consuming and could only be used to study the behavior of isolated engine components. The 3D models are difficult to use for complete engine simulations. As well as for the two-dimensional models, they are only useful to simulate components with particular shape and always require a significant simulation time. The one-dimensional models allow simulations of a complete engine while maintaining acceptable accuracy. However, because of the many components that are added to the engine simulation model, the simulation time of one-dimensional models becomes higher than the real time. For this reason, zero-dimensional models were recently used. These latter allow to calculate the thermodynamic variables only at well-defined points of the studied component, and thus do not pass through a discretization of it. This allows to significantly reducing the computation time, while maintaining sufficient accuracy at the desired points. However, the

flow in the intake system of the internal combustion engine for example is three-dimensional and not easy to model. The reason behind this is the presence of different physical phenomena such as wave action, geometry variations, pressure losses, vibrations, heat transfer. The technologies added to the intake system such as EGR, turbo-charger, CAC, Air filter, etc…made the modeling of the flow through it more complex. Then, with zero-dimensional models, the results of simulation will not be precise.

The capacity of these virtual models to represent some of the physical phenomena versus their simulation time remains a challenge (Figure 3).

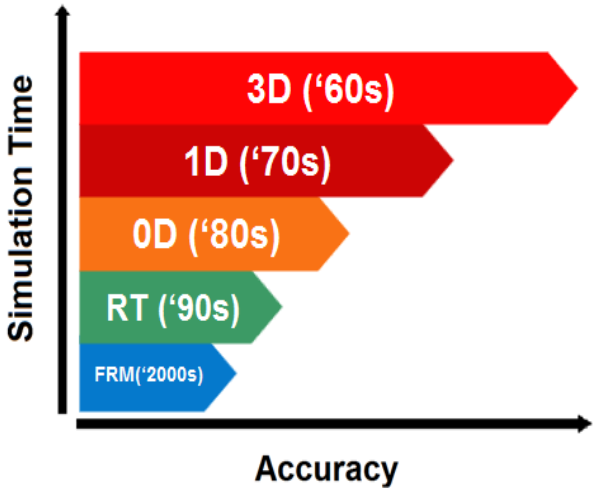

Figure 3 – Accuracy VS Simulation Time of the Engine Models

Engine emissions and performances are mainly influenced by the gas dynamics in intake and exhaust systems. For example, engine volumetric efficiency is mainly dependent on the instantaneous pressure across the intake and exhaust valves. In order to improve engine breathing, the intake system should be perfectly designed. Reducing the pressure drop of different intake system parts of the engine (manifold and runner's design, junctions, etc...) and ensuring proper acoustic tuning help improving the volumetric efficiency of the engine.

Concerning the study of gas dynamics and the propagation of pressure waves in the intake system of an internal combustion engine, a precise modeling is needed in order to obtain good results. Unfortunately, the computational time for these simulations is considered as high compared to the real time. Here comes the main objective of this PhD thesis. The work presented in this manuscript provides a complete study of the gas dynamics in the intake system of the internal combustion model, and helps to elaborate a new model of the flow behavior especially at the intake valve of the cylinder. This model will be implemented in commercial software in order to reduce the simulation time of the complete engine model. The final results will be compared to one-dimensional native model and experimental results. The ability of the model to represent the physical phenomena will be discussed according to the precision criterion of the volumetric efficiency and the instantaneous pressure upstream of the intake valve.

After a short introduction, the present manuscript is structured as follows:

- ***Chapter I:*** *The engine simulation models history are presented in this chapter. A brief description about each model and their advantages/demerits helps to understand the main objective of this work. Model based equations helps usually understanding the physics behind the equations.*

- ***Chapter II:*** *The experimental and numerical tools used in this PhD are described. Each facility and software served to accomplish and validate the model.*

- ***Chapter III:*** *This is the main section of the work, where the main model is presented. The model history and its optimization procedure are presented. Only the theory behind the methodology is presented in this chapter, the model validation and the experimental results will be shown in chapter V.*

- ***Chapter IV:*** *Based on acoustic equations, new model identification is presented. The new methodology permits to replace a test bench, presented in chapter II. The aim of the study in this chapter is to shorten the main model identification procedure.*

- ***Chapter V:*** *The main model validation is presented in this chapter. Experimental test benches are used to validate the model. This step helps to show the capacity of the model to reproduce the reality by taking into account the main physical phenomena, which occur in the intake system of an internal combustion engine.*

I. Bibliography

Internal combustion engine performance is directly conditioned by the mass of air introduced in the cylinder. This air mass determines the maximum amount of fuel that can be injected and therefore the total energy available. This latter is transformed into mechanical energy on a shaft, frictions and heat losses. The optimization of this quantity of air requires the study of the flow that takes place in the intake system. This optimization is done by determining the lengths and sections of the ducts, volumes of the different elements, as well as the characteristics of the distribution (diameter and number of valves, maximum lift, etc...). In this section, the literature survey study of the air flow behavior in the intake system of an internal combustion engine is presented. Different representations helped to model the unsteady behavior of the air. The advantages and the demerits of each model will be discussed and then main challenge will be identified.

I.1. Numerical Simulation

Recently, modeling and simulation in research and development field for internal combustion engine has been largely developed. Simulation became a good solution before taking new decisions. Nowadays, a multitude of simulation codes dedicated to engine simulation are available on the market (such as GT-Power, AMESim, Wave, etc…). In Table I-1, a summary of the advantages and the demerits of numerical simulation in internal combustion field allow understanding the importance of this latter as well as its limitations.

Numerical Simulation	
Advantage	*Demerits*
- Cost Saving : instead of doing tests on a real engine and expending fuel, simulation can rather be a good solution to save money - Time saving: once the model is ready to use, it allows replacing experimental tests used for engine optimization. - Understanding the physical meaning of a certain phenomenon through physical models - Once the model in the simulation software is ready to use, it is then possible to evaluate engine performance under different configurations and operating conditions, by making the quickly the necessary modifications - Virtual sensors allow to obtain values of different thermodynamic variables, with high sampling rate, in parts of engine where it is difficult to implement sensors in reality	- Commercial software are usually expensive compared to the open source codes. The access to the source and its modification is very limited for obvious reasons of commercial property. The setting of this type of codes requires a detailed knowledge of the engine geometry. - Open source code can be an alternative solution but it is not friendly use. - The time dedicated for the calibration phase is still considered as high. - Numerical instabilities can affect the final results - Some numerical models (such as neural models /fast running models) depend on engine tests. It is a primary step for model learning

Table I-1 - Advantages and demerits of numerical simulation

The ideal model is the one which helps to get more advantages than the demerits presented in Table I-1. This is exactly the main objective of the work presented in this PhD thesis.

I.2. Models History

The simulation codes are classified according to their complexity, precision and computational time. However, precision criterion versus simulation time remains a challenge in engine optimization, design and production. Recently, carmakers are more dependent on simulation since engine's behavior was perfectly studied using many physical approaches [3][4][5]. Concerning the study of flow behavior in air intake system, which is considered compressible and unsteady, many studies provided a scope of intake system optimization to maximize engine air filling[6][7]. Many models have been used in intake system modeling, where pressure waves phenomena is taken into consideration. These latter are generated by intake valves periodic motion and piston's displacement during admission phase. Nowadays, the challenge is to find a model which gives high accuracy level with minimum simulation time.

Figure I-1 presents the global approaches used in internal combustion engine simulation. It is clear that the tendency nowadays is to apply physics in industries. In other words, the recent models are friendly use and help to achieve certain objectives as fast as possible Once the physical properties of certain phenomena are identified (work began since 1950), then the next step is to find the easiest and the fastest way to reach the goal.

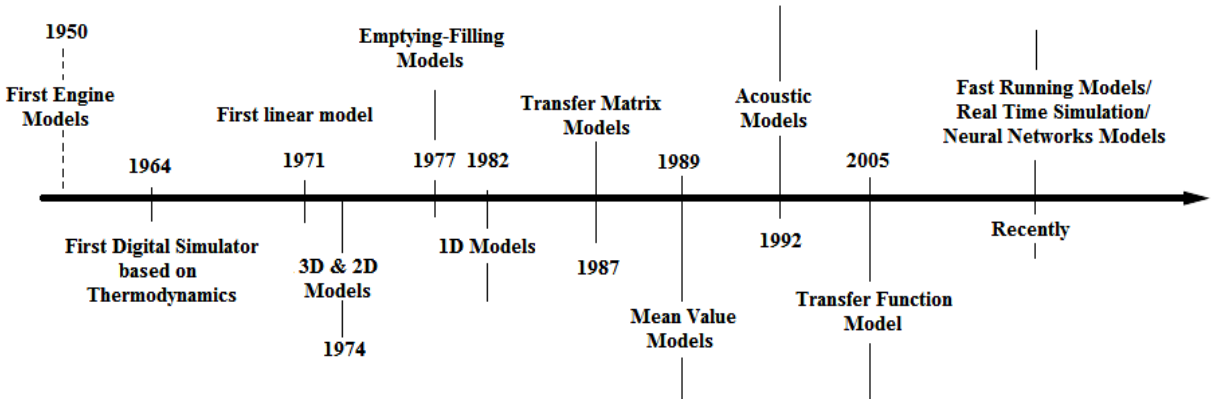

Figure I-1 – Approaches History

Figure I-2 illustrated the global models used for automotive application in function of accuracy and computational time. Logically, when high accuracy level is demanded, the computational time of the model will increase. The position of the model suggested in this PhD work is indicated by a green solider. The objective of this work is to apply physics for engine optimization purposes. This can be done by the use of a model, which takes into consideration the main physical phenomena that exist in the intake system of an internal combustion (IC) engine.

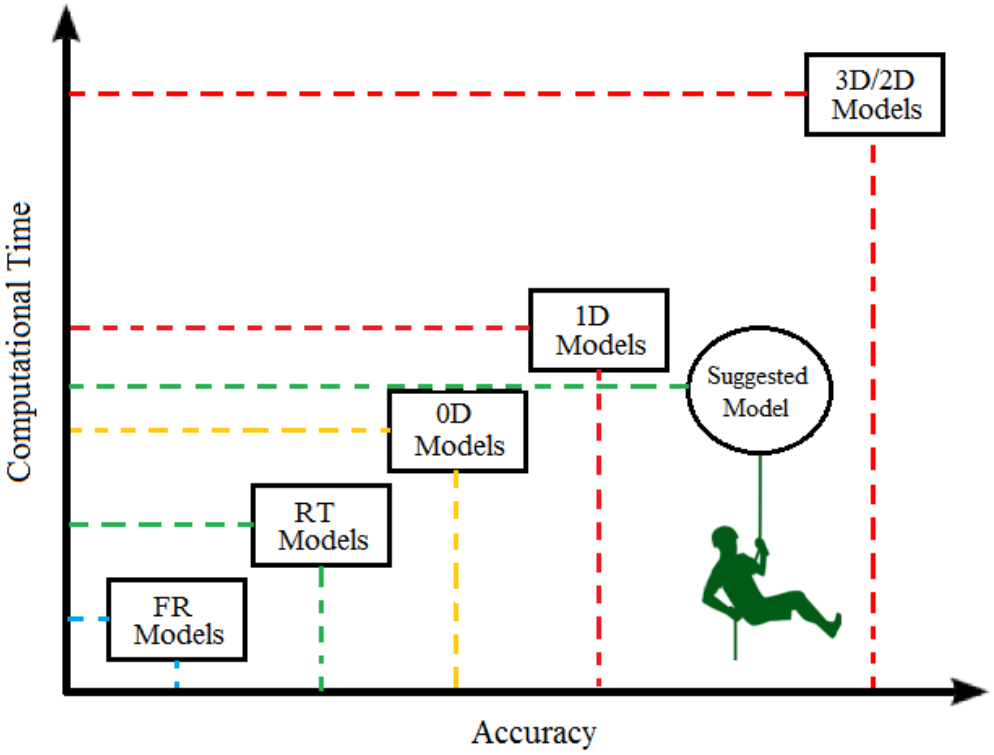

Figure I-2 - Models = f (Accuracy, Computational Time)

The literature study presented in this chapter allows a better understanding of the main objective of the present work. A brief description of each approach is presented, as well as their advantages and limits.

I.2.1 Three Dimensional Approach

Using the three-dimensional equations of Newtonian fluids, also called "Navier-Stokes" equations (based on mass, momentum and energy conservation laws) the physical phenomena that take place in the intake system of an internal combustion engine is studied and analyzed. The incompressible form of these equations can be written as follows:

$$\rho\left(\frac{\partial\vec{V}}{\partial t}+\overline{\overline{grad}}\vec{V}\cdot\vec{V}\right)=\vec{f}-\overrightarrow{grad}\,p+\overrightarrow{div}\,\overline{\overline{\tau}} \qquad \text{(I-1)}$$

It allows taking into consideration the tree-dimensional effects of the turbulent flow. A discretization of the studied element (Mesh) is needed (Figure I-4). Coupled with defining the initial and boundary conditions, the element is subjected to some iterative numerical resolutions in order to identify the thermodynamic parameters. A direct numerical resolution (DNS) of Navier-Stokes equations is possible, with fine meshes and very small time step. The results showed a good accuracy level [8]. Several models are used and they are based on Reynolds decomposition applied to the Navier-Stokes equations (RANS). In order to complete the system of equations, turbulence models are used (k-ε models, Mixing Length models, Spalart-Almaras models, etc…)[9][10][11][12].

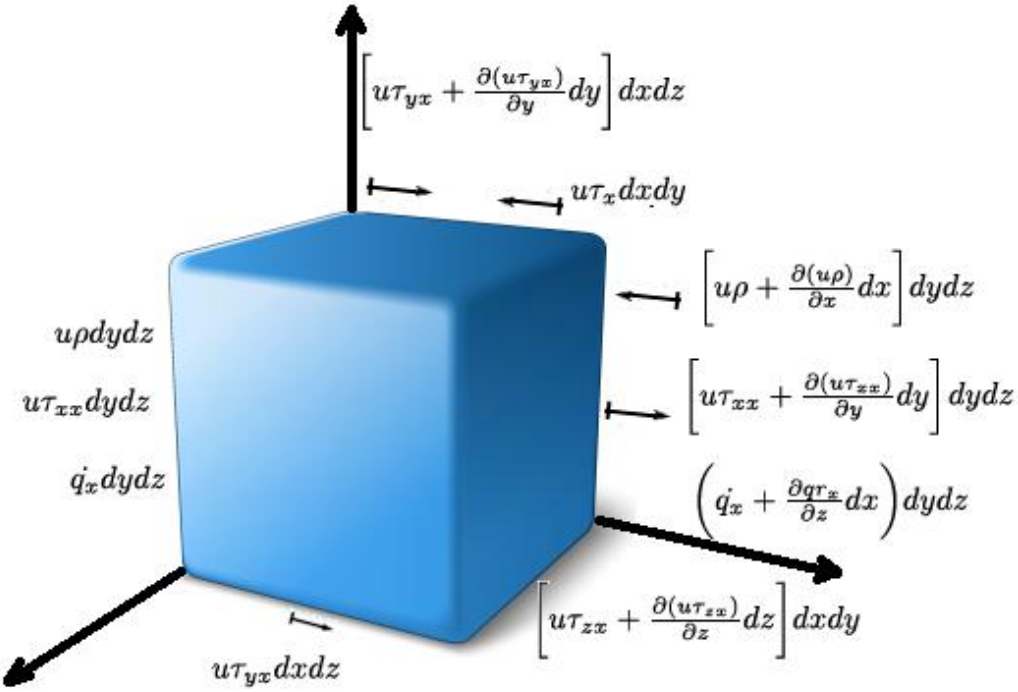

Figure I-3 - Forces applied on each cell

These models are the basis of existing three-dimensional software. For example, Mahe [13] used 'Fluent' software in order to model his experimental test bench. This latter allowed him measuring certain thermodynamic variables at different positions. This cannot be easy to do experimentally.

The three-dimensional models are used for complex geometries modeling where other approaches do not help to get good results. However, these models need the use of a super computer and it is time consuming.

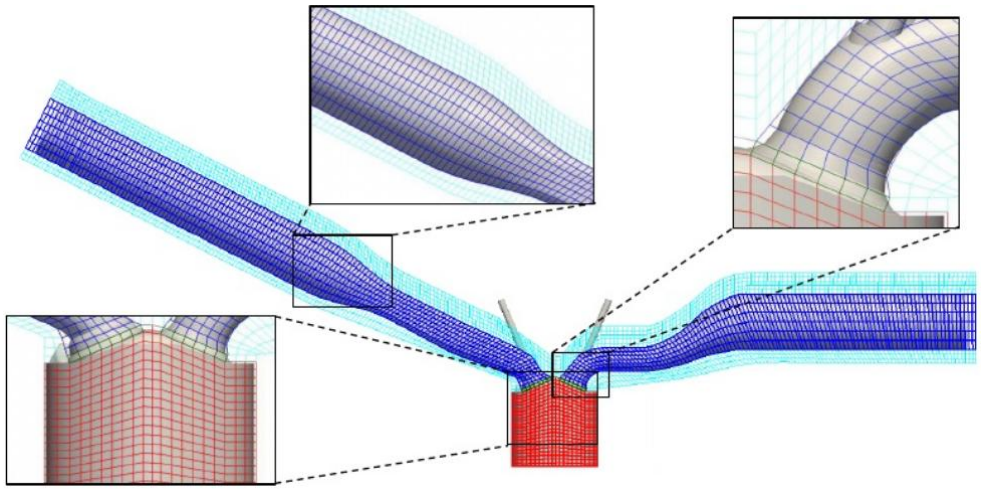

Figure I-4 - Mesh discretization of intake system, cylinder and exhaust system [8]

I.2.2 Two Dimensional approach

Similar to the three dimensional approach, but this time the Navier-Stokes equations are only differentiated with respect to x and y. There is no dependence of anything on z.

Many authors used this approach for modelling purposes in automotive filed [14][15][16]. The accuracy of these models is considered high and it is also dedicated to complex geometries. Same as three dimensional approaches, such models are time consuming and relatively difficult to use for complete system simulation in automotive field.

I.2.3 One Dimensional approach

The one-dimensional approach consists in neglecting the internal shear stresses that meshes perform on each other. When the length-diameter ratio of the tube is high, the flow through it can be considered one-dimensional. In this case, the pressure and the velocity of the fluid at a certain position on the tube are constants. These models are the basis of many automotive commercial software since their computational time is acceptable compared to three-dimensional models. In the case of a complex geometry, one-dimensional models do not guaranty good results (such as intake manifold). Then, some discharge coefficients are added to improve the flow modeling (model tuning).

I.2.3.1. Equations of Gas dynamics

The first equation corresponds to the conservation of mass (continuity equation):

$$\frac{\partial(\rho A)}{\partial t}+\frac{\partial(\rho u A)}{\partial x}=0 \tag{I-2}$$

The geometry section is represented by *F*. The second equation corresponds to the conservation of momentum:

$$\frac{\partial(\rho u A)}{\partial t}+\frac{\partial(\rho u^2+p)A}{\partial x}-p\frac{\partial A}{\partial x}+\frac{1}{2}\rho u^2 f_{friction}\pi D=0 \tag{I-3}$$

It expresses the fundamental equation of dynamics. The term $\frac{1}{2}\rho u^2 f_{friction}\pi D$ corresponds to the force that takes into account the friction effect between the flow and the fixed walls. This force is due to the viscosity effects of the fluid. It is proportional to the friction coefficient, which is a number without dimension, and to the hydraulic diameter or equivalent diameter D.

Bannister *et al.*[17] introduced the term G in the equation (I-3), which is equal to:

$$G=\frac{1}{2}u|u|f_{friction}\frac{4}{D} \tag{I-4}$$

The term $u|u|$ is used to ensure that the friction always oppose the direction of the fluid movement. Finally, equation (I-3) can be written as follow:

$$\frac{\partial(\rho u)}{\partial t}+\frac{\partial(\rho u^2+p)}{\partial x}+p\frac{u^2}{A}\frac{\partial f_{friction}}{\partial x}+\rho G=0 \tag{I-5}$$

To be noted that the use of friction term in equation (I-5) is the only way to include the effects of fluid viscosity. The gases are sufficiently diluted to neglect the internal stresses[6]. The coefficient of friction f is a measure of shear stress (or shear force per unit area) that turbulent flow exerts on the wall of a pipe. It is a dimensionless parameter. Many authors worked on the modeling of this coefficient [15] to [22].

When the fluid is incompressible and has as negligible coefficient of expansion, the continuity and the momentum equations are sufficient to identify the two unknown functions p and u. However, when the density depends on pressure and temperature, two other equations linking the four unknown functions (p, u, ρ and T) must be added.

The third equation is the energy equation. It expresses the way in which heat exchange takes place. This is a typical formulation of the first law of thermodynamics.

$$\dot{Q} - \dot{W} = \frac{\partial E_0}{\partial t} + \frac{\partial H_0}{\partial x} dx \tag{I-6}$$

Where E_0 and H_0 are respectively the internal energies and total enthalpy:

$$E_0 = e_0 \rho A dx = (e + \frac{1}{2} u^2) \rho A dx \tag{I-7}$$

$$H_0 = h_0 \rho A u = (e_0 + \frac{p}{\rho}) \tag{I-8}$$

The term $\dot{Q}$ in equation (I-6) represents the heat flux exchanged with the walls:

$$\dot{Q} = q \rho A dx \tag{I-9}$$

The second term $\dot{W}$ in equation (I-6) represents the heat exchange through the system, it is equal to zero. Using equations (I-7), (I-8) and (I-9), equation (I-6) can be then written as follow:

$$q \rho A dx = \frac{\partial (e_0 \rho A dx)}{\partial t} + \frac{\partial (h_0 \rho A u)}{\partial x} dx \tag{I-10}$$

The system of equations is therefore identified from the equations (I-2), (I-5) and (I-10). These latter are hyperbolic equations with partial derivative. A common characteristic to the solutions of these equations is that some information is transmitted by the "waves" that propagate at the speed of sound with respect to the fluid, while others informations move at the velocity of the fluid itself.

An additional equation is needed in order to obtain a system of four equations with four unknowns. The gas state equation expresses the existing relation between the pressure, density and temperature. The gas is considered as ideal:

$$p = \rho r T \tag{I-11}$$

$$e = C_v T = \frac{r}{\gamma - 1} T = \frac{p}{\rho (\gamma - 1)} \tag{I-12}$$

$$h = C_p T = \frac{\gamma r}{\gamma - 1} T = \frac{\gamma p}{\rho(\gamma - 1)} = \frac{a^2}{(\gamma - 1)} \tag{I-13}$$

Winterbone *et al.*[6][26] wrote the system of equations identified previously in two different ways: conservative form and non-conservative form. The conservative form consists in writing Euler equations as follow:

$$\frac{\partial W}{\partial t} + \frac{\partial A(W)}{\partial x} = S \tag{I-14}$$

Where *W*, *A* (W) and *S* are respectively:

$$W = \begin{bmatrix} \rho \\ \rho u \\ \frac{p}{\gamma - 1} + \frac{1}{2}\rho u^2 \end{bmatrix} \tag{I-15}$$

$$A(W) = \begin{bmatrix} \rho u \\ p + \rho u^2 \\ u\left(\frac{p\gamma}{\gamma - 1} + \frac{1}{2}\rho u^2\right) \end{bmatrix} \tag{I-16}$$

$$S = \begin{bmatrix} \frac{-\rho}{A} u \frac{dA}{dx} \\ \frac{-\rho}{A} u^2 \frac{dA}{dx} - \rho G \\ -\left(\rho \frac{u^2}{2} + \frac{p\gamma}{\gamma - 1}\right) \frac{u}{A} \frac{dA}{dx} + pqe \end{bmatrix} \tag{I-17}$$

The non-conservative form consists on eliminating the terms that contain products, thus:

$$\frac{\partial V}{\partial t} + \mathrm{A} \frac{\partial V}{\partial x} = S \tag{I-18}$$

Where,

$$V = \begin{bmatrix} \rho \\ u \\ p \end{bmatrix} \tag{I-19}$$

$$\mathrm{A} = \begin{pmatrix} u & \rho & 0 \\ 0 & u & \dfrac{1}{\rho} \\ 0 & a^2\rho & u \end{pmatrix} \tag{I-20}$$

$$S = \begin{bmatrix} \dfrac{-\rho}{F} u \dfrac{dA}{dx} \\ -G \\ \dfrac{-a^2 \rho u}{A} \dfrac{dA}{dx} + (1-\gamma)\rho(qe + uG) \end{bmatrix} \tag{I-21}$$

It has been indicated that these two systems of equations are mathematically similar [6], but the numerical resolution of the non-conservative form leads to a numerical scheme where the total mass of the system is not conserved. The conservative form corresponds to 1D equations of Euler[6]. The non-conservative form is used in Method of characteristics (MOC). Both quasi one-dimensional forms result from a simplification of multi-dimensional equations of Eulerian integral formulation. In order to evaluate the consequences of these simplifications, Winterbone *et al.*[6] classified the terms in their decreasing order of magnitude according to some simulations of the flow in the intake manifold an engine: effect of section variation, effect of frictions with the walls and finally the heat transfer. Bulaty *et al.*[27] replaced the variables by their average values which represent the nominal operation of the engine. They discovered that the terms of energy dissipation by conduction in the fluid are negligible compared to the terms of energy dissipation by friction and by heat exchange.

I.2.3.2. Acoustic Approach

Acoustic approach was used for modeling the pressure wave propagation in the intake system of the internal combustion engine [28][29][30]. Non-linearity of the equations presented in the previous section is a major problem in fluid dynamics field. This implies that there is no general solution of these equations. Acoustics is considered a first order approximation in which the effects of non-linearity are neglected.

A. Acoustic wave propagation:

The following assumptions are then made:

- Heat exchange ↔ q=0
- Frictions ↔ $f_{friction}$=0
- Section variation↔ $\frac{dA}{dx} = 0$
- u_0=0, p_0=0 and ρ_0=0

Then, the fundamental equations of gas dynamics can be simplified:

$$\frac{\partial \rho}{\partial t} + u\frac{\partial \rho}{\partial x} + \rho\frac{\partial u}{\partial x} = 0 \tag{I-22}$$

$$\frac{\partial u}{\partial t} + u\frac{\partial u}{\partial x} + \frac{1}{\rho}\frac{\partial u}{\partial x} = 0 \tag{I-23}$$

$$\frac{\partial \rho}{\partial t} = \frac{1}{a^2}\frac{\partial p}{\partial t} \tag{I-24}$$

The theory consists on considering that the fluid is subjected to a disturbance of small amplitude, then:

$$u = \partial u \tag{I-25}$$

$$p = \partial p \tag{I-26}$$

$$\rho = \partial \rho \tag{I-27}$$

The notation given by Borel[31] was adopted in the writing of the previous relations. This notation is a bit different than the one used by Winterbone and Pearson [6][32], which is rather based on the work of Davies [33].

By simply replacing the previous variables in equations (I-22), (I-23) and (I-24), the three equations called "classical wave equations" or the equations of propagation of the acoustic wave are then obtained:

$$\frac{\partial^2(\partial p)}{\partial t^2} = a_0^2\frac{\partial^2(\partial p)}{\partial x^2} \tag{I-28}$$

$$\frac{\partial^2(\partial u)}{\partial t^2} = a_0^2\frac{\partial^2(\partial u)}{\partial x^2} \tag{I-29}$$

$$\frac{\partial^2(\partial \rho)}{\partial t^2} = a_0^2\frac{\partial^2(\partial \rho)}{\partial x^2} \tag{I-30}$$

The analytical solutions of the previous equations can be written as follow:

$$\delta p(x,t) = B_I f_I(a_0 t - x) + B_{II} f_{II}(a_0 t + x) \tag{I-31}$$

$$\delta u(x,t) = \frac{1}{\rho_0 a_0}[B_I f_I(a_0 t - x) - B_{II} f_{II}(a_0 t + x)] \quad \text{(I-32)}$$

$$\delta \rho(x,t) = \frac{1}{a_0^2}[B_I f_I(a_0 t - x) + B_{II} f_{II}(a_0 t + x)] \quad \text{(I-33)}$$

The solution of the propagation equation of the acoustic wave is the sum of two functions. The effect produced is the superposition of two phenomena:

- Direct acoustic wave : $\delta p^+ = B_I f_I(a_0 t - x)$
- Retrograde acoustic wave: $\delta p^- = B_{II} f_{II}(a_0 t + x)$

Then, equation (I-31) can be written as follow:

$$\delta p = \delta p^+ + \delta p^- \quad \text{(I-34)}$$

The physical significance of the decomposition of pressure fluctuations is that the direct and retrograde pressure waves propagate without any interaction. But in reality this is not the case, this remains evident when solving the non-linear equations of flow. In any case, it is always interesting from a physical point of view to consider the flow as the result of the superposition of two components, but this resultant flow cannot be calculated directly by the addition or subtraction of these two components pressure components. However, it is still possible to obtain the values of these components as explained by Payri *et al.* [34]. In fact, acoustic theory is able to describe the flow in the pipes, mainly in the complex systems but the interaction between the pipes and the acoustic source is poorly represented: the acoustic source is not considered as a variant as with time.

In general, any periodic function is a sum of sinusoidal or harmonic signals whose frequencies are the integer multiples of the fundamental frequency [31][35]:

$$\delta p = B_I \cos(\omega t - k_0 x) + B_{II} \cos(\omega t + k_0 x) \quad \text{(I-35)}$$

Equation (I-35) can be expressed using complex number[36]:

$$\delta p(x,t) = (B_I e^{-jk_0 x} + B_{II} e^{jk_0 x}) e^{j\omega t} \quad \text{(I-36)}$$

Where $\omega = 2\pi f$ and $k_0 = \frac{\omega}{a_0}$ are respectively the pulsation and the wave number.

Borel [31] presented a complete study about acoustic wave behavior when it is faced to an obstacle.

However, in reality the propagation of the pressure waves in the pipes of an internal combustion engine involves losses: the thermal processes due to the viscosity of the fluid next to the walls, the turbulence of the flow itself, heat dissipation and heat conduction. Then the level of entropy can no longer be considered constant and the transformations are no longer

isentropic. In this case, the effect of the mean Mach number M cannot be neglected because the pressure and the air mass flow rate variables will be influenced by this number.
Munjal [35] wrote the wave equation for a viscous moving medium, introducing a visco-thermal attenuation coefficient and a loss coefficient per unit length:

$$\left[\frac{D^2}{Dt^2} - a_0^2 \frac{\partial^2}{\partial x^2} + 2(\xi u + a_0 \alpha)\frac{D}{Dt}\right] p = 0 \tag{I-37}$$

Where $\frac{D}{Dt} = \frac{\partial}{\partial t} + u\frac{\partial}{\partial x}$

The term $2(\xi u + a_0\alpha)$ corresponds to the visco-thermal effect and the average flow.

The term α is the visco-thermal attenuation coefficient given by the following equation [33]:

$$\alpha = \left(\frac{1}{r_h a_0}\right)\sqrt{\left(\frac{\omega}{2\rho_0}\right)}\left[1 + \left(\sqrt{\gamma} - \frac{1}{\sqrt{\gamma}}\right)\sqrt{\left(\frac{1}{P_r}\right)}\right] \tag{I-38}$$

The complex wave number is defined in equation (I-39)[35]:

$$\beta^{\pm} = \mp\left(\frac{\alpha + \xi M + jk_0}{1 \pm M}\right) \tag{I-39}$$

The complex characteristic impedance in viscous moving medium is presented by the following equation[35]:

$$z_{cc} = z_{c0}\left(1 - \frac{\alpha + \xi M}{k_0} + j\,\frac{\alpha + \xi M}{k_0}\right) \tag{I-40}$$

Where z_{c0} is the specific impedance for a simple tube, and it is expressed in the following equation [35]:

$$z_{c0} = \frac{a_0}{A} = \frac{\sqrt{\gamma r T}}{A} \tag{I-41}$$

Hence, the analytical solution of the equation (I-37)

$$p(x,t) = p^+ + p^- = [B_I \exp(-\beta^+ x) + B_{II} \exp(\beta^- x)]\exp(j\,\omega t) \tag{I-42}$$

$$qm(x,t) = \frac{1}{z_{cc}}[B_I \exp(-\beta^+ x) - B_{II} \exp(\beta^- x)]\exp(j\,\omega t) \tag{I-43}$$

For cylinder filling optimization, it is useful to increase the pressure upstream of the intake valve. However, high pressure value condition corresponds to the higher impedance value at the same place. So by maximizing the impedance upstream of the valve, the pressure response will be high and therefore the cylinder filling can be improved. Wave propagation remains important even at high engine speed [37] and for turbocharged engines [38][39]. Using acoustic theory, the compressor modeling is done [40][41][42]. Acoustic model can be

coupled with other approaches, such as CFD, MOC, 1D and 0D [28][43][44][45][46][47][48][49].

B. Acoustic impedance model

The characteristic acoustic impedance "z" of the medium in which the wave propagates, characterizes the behavior of the geometry of the medium when it faces a disturbance. In fact, the pressure variation imposed by the passage of a wave introduces a speed variation whose value depends on a specific characteristic. The pressure-velocity ratio is given by equation (I-44) [31][33][36][50]:

$$z(x) = \frac{\delta p}{\delta u} = \rho_0 a_0 \frac{f_I(a_0 t - x) + f_{II}(a_0 t + x)}{f_I(a_0 t - x) - f_{II}(a_0 t + x)} \tag{I-44}$$

Munjal used the air mass flow rate instead of velocity vector [35]:

$$z(x) = \frac{p(x)}{q_m(x)} = z_{c0} \frac{B_I \exp(-\beta^+ x) + B_{II} \exp(\beta^- x)}{B_I \exp(-\beta^+ x) - B_{II} \exp(\beta^- x)} \tag{I-45}$$

In the case of a tube of length L, the characteristic impedance at x=L can be written in function of the characteristic impedance at x=0 and the specific impedance of the medium[51].

$$z(L) = z_{c0} \frac{z(0) + j z_{c0} \tan(k_0 L)}{z_{c0} + j z(0) \tan(k_0 L)} \tag{I-46}$$

In internal combustion engine application, the first two cases exist:

- Open ended tube: this case corresponds to the admission phase (Figure I-5). The volume of the cylinder is considered big enough to consider that the tube at the intake valve is an open ended tube:

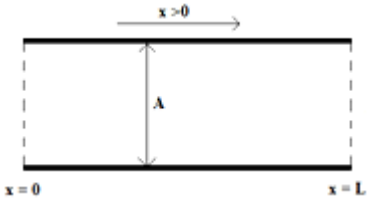

Figure I-5 - Open ended tube

The impedance at the extremities is equal to zero, since the pressure variation at these positions is negligible. Then from equation (I-46):

$$z(0) = z(L) = 0 \Rightarrow \tan(k_0 L) = 0 \Rightarrow k_0 L = n\pi$$
$$\Rightarrow L = \frac{n\pi}{k_0} = \frac{n\pi}{\frac{2\pi}{\lambda}} \Rightarrow L = n\frac{\lambda}{2}$$
$$\rightarrow f_{1/2} = \frac{a_0}{2L} n \qquad \text{(I-47)}$$

Where, n=1, 2, 3…N.
This frequency corresponds to the half wave resonance of the tube.

- Open-close ended tube: this case corresponds to the phase after closing the intake valve (Figure I-6). The volume of the cylinder is considered big enough to consider that the tube at the intake valve is an open-close ended tube:

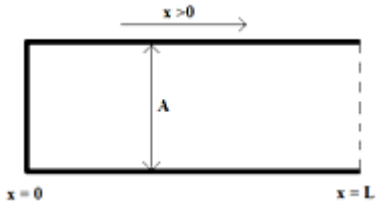

Figure I-6 - Open-close ended tube

In this case, the boundary conditions are:

- For x=L, the pressure variation is negligible $\Rightarrow z(L) = 0$
- For x=0, air mass flow rate variation is negligible since this end is close $\Rightarrow z(0) \rightarrow \infty$

Then from equation (I-46):

$$z(L) = 0 \Rightarrow \frac{1}{j\tan(k_0 L)} \rightarrow 0 \Rightarrow \tan(k_0 L) \rightarrow \infty \Rightarrow k_0 L = (2n-1)\frac{\pi}{2}$$
$$\Rightarrow L = \frac{(2n-1)\frac{\pi}{2}}{k_0} = \frac{(2n-1)\frac{\pi}{2}}{\frac{2\pi}{\lambda}}$$
$$\Rightarrow L = (2n-1)\frac{\lambda}{4}$$
$$\rightarrow f_{1/4} = \frac{a_0}{4L}(2n-1) \qquad \text{(I-48)}$$

Where, n=1, 2, 3…N.

This frequency corresponds to the quarter wave resonance of the tube.

Desmet [51] identified the acoustic impedance in the cases of complex geometries (section variation of the geometry is included). Harrison *et al.* [26][27][37] used the acoustic impedance to understand the nature of the acoustic waves generated during the closure of the intake valve and to characterize the intake flow of a single-cylinder engine. The model suggested in this PhD work is based on this acoustic approach, specifically on impedance model.

C. Two Pressure sensor method

This method is used since 1970. According to Desmet [51], the simplest and most effective way to obtain the impedance in a reference plane is to measure the pressure and the volume velocity in the same reference plane. The method consists in using two pressure sensors or two microphones located in a straight tube under the excitation of a speaker (Figure I-7):

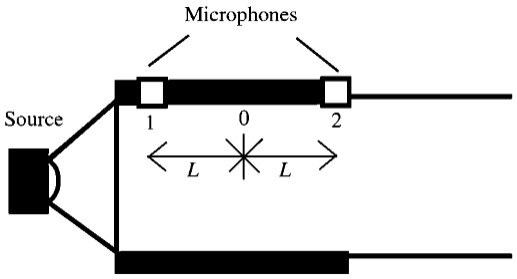

Figure I-7 - Two sensors configuration[51]

In Figure I-7, the pressure values at position1 and 2 are related to the pressure and velocity at position 0. The following equation is written as follow:

$$\begin{pmatrix} p_0 \\ u_0 \end{pmatrix} = \begin{pmatrix} \dfrac{1}{\cos \beta L} & 0 \\ 0 & \dfrac{1}{jz_c \sin \beta L} \end{pmatrix} \begin{pmatrix} \dfrac{p_1 + p_2}{2} \\ \dfrac{p_1 - p_2}{2} \end{pmatrix} \tag{I-49}$$

Thus, if the distance 2L is too small or close to the half wave length, the method will not be valid. In addition, this method does not take into consideration the source impedance. Thus, precise measurements are not guaranteed. This method can be improved by using a known source, which is the principle of TMTC [51] and TMFC [52] method.

Using equation (I-42), the pressure at position 1 and 2 can be written as follow:

$$p(x_1,t) = [B_I \exp(-\beta^+ x_1) + B_{II} \exp(\beta^- x_1)] \exp(j\omega t) \tag{I-50}$$

$$p(x_2,t) = [B_I \exp(-\beta^+ x_2) + B_{II} \exp(\beta^- x_2)] \exp(j\omega t) \tag{I-51}$$

Thus, the amplitude of the pressure responses can be identified using equations (I-50) and (I-51). Harrison *et al.*[28] used this method to characterize the pressure waves in the intake line of a single-cylinder engine in order to calculate the acoustic impedance. Unfortunately, this method does not take into consideration the difference between an open and a closed valve in automotive application.

This method is also used in the determination of the reflection coefficient by identifying the direct and retrograde components of the wave.

D. Reflection coefficient model

This methodology consists in representing each acoustic element by the incident and the retrograde characteristic of the wave. The geometry of the intake line of an engine has complexities, because of the presence of geometric discontinuities (sudden section variation) and thermodynamic discontinuities (CAC). In fact, in front of a discontinuity, part of the incident wave is reflected. Thus, it will be useful to characterize the behavior of the pressure waves as a function of the pressure reflection coefficient [33]:

$$r(x) = \frac{p^{-}_{(x)}}{p^{+}_{(x)}} = \frac{p^{-}_{(0)}.\exp(+jk_0x)}{p^{+}_{(0)}.\exp(-jk_0x)} = |r(x)|.\exp(+2jk_0x) \tag{I-52}$$

The characteristic impedance can be written using the reflection coefficient:

$$z(x) = \frac{p(x)}{q_m(x)} = \frac{p^{+}_{(x)} + p^{-}_{(x)}}{\frac{1}{z_{co}}\left(p^{+}_{(x)} - p^{-}_{(x)}\right)} = z_{co}\frac{1+r(x)}{1-r(x)} \tag{I-53}$$

This formulation was used in the flow modeling of the intake system of a single cylinder engine [26][27][50][53].

In the case of a tube open to the atmosphere at its end or to a chamber having a large volume, the reflection coefficient is written in the following form:

$$r = -R.\exp[-2jk_0(L + \Delta L)] \tag{I-54}$$

Where ΔL is a virtual length extension (Figure I-8). This quantity is added to the physical real length of the tube, since the reflection does not occur exactly at the open end.

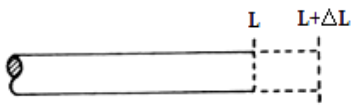

Figure I-8 - Tube extension representation

This phenomenon is due to flow unsteadiness and viscosity losses. The value of ΔL was identified by many authors[50][54][55][58].

Peters *et al.* [59] took into consideration the Mach number in reflection coefficient determination for a better representation of the wave propagation:

$$R_E = R^2 \left(\frac{1-M}{1+M} \right)^2 \tag{I-55}$$

Mezher *et al.* [60][61] have used this characterization to identify a transfer matrix for complex geometries of intake line of the engine (the charge air cooler "CAC").

E. Transfer Matrix Methodology

For a supercharged engine, modeling of the intake part requires a precise simulation methodology, because of the complexity of the elements existing on this line. In addition, to account for the effects of pressure waves in this modeling, through the elements that make up the intake line, is required.

The transfer matrix of a system, also called transmission matrix or 4-pole representation, is a linear system that connects the input and output variables[44]. By using the pressure and air mass flow rate variables, the transfer function an aero-acoustic element can be written as follow[35]:

$$\begin{pmatrix} P_2 \\ Q_{m_2} \end{pmatrix} = \begin{bmatrix} \widehat{A} & \widehat{B} \\ \widehat{C} & \widehat{D} \end{bmatrix} \begin{pmatrix} P_1 \\ Q_{m_1} \end{pmatrix} \tag{I-56}$$

Munjal [35] identified a transfer matrix for the case of acoustic excitation in inviscid moving medium, of a simple tube. To *et al.* [60][61] developed a methodology to find the transfer matrix of an unknown system, using two pressure sensors upstream of the system and two downstream sensors. Tao *et al.*[64] presented all the techniques that are established for the purpose of calculating the poles of the transfer matrix. Mezher's work [65] is based on this transfer matrix methodology. The new model is implemented in a non-linear simulation software code as a modeling improvement method (especially for CAC application), in which mean flow and high pressure fluctuation were taken into account (acoustical extended method).

Finally, as a conclusion, acoustic approach is essential in the study of vibratory phenomena, but from a simulation point of view, the number of equations used remains important and requires a high calculation time.

I.2.3.3. Method of Characteristics (MOC)

It is the first method used for flow simulation in internal combustion engine[66]. Borel [31] presented a detailed description of this methodology. Benson [67] improved the MOC method by taking into account the section variations, frictions and heat exchanges. The method consists in transforming the partial differential gas dynamics equations into a total derivative

system. The MOC method and its variants are first order accurate in space and time and they are based on a non-conservative form of the gas dynamics equations.

Pressure, velocity and temperature evolution laws can be precisely identified, as a function of time, using this methodology. In addition, it can be applied in the regions where the fluid behavior identification is the interest of engine manufactures.

On the other hand, the use of the MOC as a graphical method has some problems, such as the ability to compute the characteristics either at constant time or constant position only. Linear interpolation between calculated points decreases first order accuracy.

Since non-conservative form of gas dynamics and the hypothesis of isentropic flow are adopted, the methodology is limited to shock waves. Many authors updated this methodology in order to take into account this phenomenon [68][69][70]. Their main problem is that they require many iterative resolutions which increase the computational time.

The characteristic method remained the only method adopted for the simulation of gas flows in the internal combustion engine until the appearance of the finite difference method.

I.2.3.4. Finite difference schemes

Shock waves can exist in the internal combustion engine, especially at the exhaust system. The gradients of the variables tend to infinity when shock waves appear in the main equations. Thus, the differential representation of the fundamental equations could not represent correctly the flow when the shock waves exist. LeVeque [71] has shown that numerical resolution schemes that are not based on a conservative formulation of the fundamental equations of gas dynamics, cannot converge to a physically correct solution when discontinuities are present. Then, conservative form is the best choice, where mass, momentum and energy are conserved whatever the nature of the flow is.

The integration of equation (I-14) leads to the following equations:

$$\left(W_i^{n+1} - W_i^{n}\right)\Delta x + \left(A_{i+1/2}^{n} - A_{i-1/2}^{n}\right)\Delta t = 0 \tag{I-57}$$

$$W_i^{n+1} = W_i^{n} - \frac{\Delta t}{\Delta x}\left(A_{i+1/2}^{n} - A_{i-1/2}^{n}\right) \tag{I-58}$$

Where W represents the average of dependant variables:

$$W_i = \frac{1}{\Delta x}\int_{x_i-1/2}^{x_i+1/2} W dx \tag{I-59}$$

And F the average flow across the cell boundaries over a time interval:

$$A_{i\pm1/2} = \frac{1}{\Delta t}\int_{t^n}^{t^{n+1}} F dt \tag{I-60}$$

However, system discretization will introduce some errors. These errors are related to the choice of Δx . The value of this latter depends on the smallest element of the system to be modeled. Thus, the time and the space step in the numerical resolution of the system have to be choosing in a way that error is not amplified. These variables are linked using Courant-Friedrichs-Lewy stability criterion to ensure the stability of the solution [72]:

$$\frac{\Delta t}{\Delta x} \leq CFL.Min\left(\frac{1}{a+|u|}\right) \tag{I-61}$$

The choice of CFL coefficient depends of the numerical scheme used. It is equal to one in the case of linear equations.

The Numerical schemes can be listed as follow:

A. Lax-Friedrichs scheme [73]

$$W_i^{n+1} = \frac{1}{2}\left[W_{i+1}^n + W_{i-1}^n\right] - \frac{\Delta t}{2\Delta x}\left[A_{i+1}^n - A_{i-1}^n\right] \tag{I-62}$$

This method is the first step of Lax-Wendroff Richtmyer method

B. Leapfrog scheme [26]

It the simplest method and allows to obtain a second order accuracy in space and time. It is the second step of Lax-Wendroff Richtmyer method:

$$W_i^{n+1} = W_i^{n-1} - \frac{\Delta t}{\Delta x}\left[A_{i+1}^n - A_{i-1}^n\right] \tag{I-63}$$

C. Lax-Wendroff scheme

$$W_i^{n+1} = W_i^n - \frac{\Delta t}{2\Delta x}\left[A_{i+1}^n - A_i^n\right] + \frac{(\Delta t)^2}{2(\Delta x)^2}\left[J_{i+1/2}^n\left(A_{i+1}^n - A_i^n\right) - J_{i-1/2}^n\left(A_i^n - A_{i-1}^n\right)\right] \tag{I-64}$$

Where $J = \frac{\partial F}{\partial W}$ is the Jacobian Matrix. And according Richtmyer and Morton [74], the form of this matrix, which has a conservative properties and reduces the computational time, is given by equation (I-65):

$$J_{i\pm1/2} = J\left[\frac{1}{2}\left(W_i + W_{i\pm1}\right)\right] \tag{I-65}$$

D. Lax-Wendroff Richtmyer Method[75]

It does not require the calculation of the Jacobian Matrix. This method consists of two steps and they are already presented in equations (I-62) and (I-63).

The values of $A_{i\pm1}^{n+1}$ in equation (I-63) depend on the values of $W_{i\pm1}^{n+1}$ equation (I-62).

E. MacCormack scheme [76]

In the case of linear equations, this method is similar to Lax-Wendroff one. This scheme does not only models flow in the forward direction, but also allows retrograde flow to be considered:

$$W_i^* = W_i^{n+1} - \frac{\Delta t}{\Delta x}\left(A_i^{n+1} - A_{i-1}^{n+1}\right) \tag{I-66}$$

$$W_i^{n+2} = \frac{1}{2}\left[W_i^{n+1} + W_i^* - \frac{\Delta t}{\Delta x}\left(A_{i+1}^* - A_i^*\right)\right] \tag{I-67}$$

F. W_α^β Classification [77]

There are two steps in this method (equations (I-68), which is called 'predictor', and (I-69), which is called 'corrector'):

$$W^* = W_{i+\beta}^{n+\alpha} = (1-\beta)W_i^n + \beta W_{i+1}^n - \alpha\frac{\Delta t}{\Delta x}\left[A_{i+1}^n - A_i^n\right] \tag{I-68}$$

$$W_i^{n+1} = W_i^n - \frac{\Delta t}{2\alpha.\Delta x}\begin{bmatrix}(\alpha-\beta)A_{i+1}^n + (2\beta-1)A_i^n \\ +(1-\alpha-\beta)A_{i-1}^n + A_{i+\beta}^{n+\alpha} - A_{i+\beta-1}^{n+\alpha}\end{bmatrix} \tag{I-69}$$

It is stable when CFL is lower than one [18].

G. Artificial Viscosity

The artificial viscosity is added to the numerical schemes in order to dampen the oscillations in shock profiles and to avoid numerical instabilities [78].

The general form of the related equation is given by the following equation:

$$W_i^{n+1} = W_i^* + \alpha\frac{\Delta t}{\Delta x}\Delta\left[\left|\Delta W_{i+1}^*\right|\Delta W_{i+1}^*\right] \tag{I-70}$$

Where $\Delta W_{i+1}^* = W_{i+1}^* - W_i^*$.

Lapidus [79] suggested the following form for the artificial viscosity:

$$\tilde{W}_{i+\beta}^{n+\alpha} = (1-\beta)W_i^n + \beta W_{i+1}^n - \alpha\left[\sigma.\left(A_{i+1}^n - A_i^n\right)\right] \tag{I-71}$$

$$W_{i+1}^{n} = W_{i}^{n} - \frac{\sigma}{2\alpha}\begin{bmatrix} (\alpha-\beta).A_{i+1}^{n} \\ +(2\beta-1).A_{i}^{n} \\ +(1-\alpha-\beta).A_{i-1}^{n} \\ +\tilde{A}_{i+\beta}^{n+\alpha} - \tilde{A}_{i+\beta-1}^{n+\alpha} \end{bmatrix} + \frac{\sigma}{2}\begin{bmatrix} \chi\left|u_{i+1}^{n} - u_{i}^{n}\right|.\left(W_{i+1}^{n} - W_{i}^{n}\right) \\ -\chi\left|u_{i}^{n} - u_{i-1}^{n}\right|.\left(W_{i}^{n} - W_{i-1}^{n}\right) \end{bmatrix} \quad \text{(I-72)}$$

Where χ is the parametric coefficient of artificial viscosity.
Then, the CFL coefficient can be written as follow:

$$CFL = \left[1 + \frac{\chi^{2}}{4}\right]^{1/2} - \frac{\chi}{2} \quad \text{(I-73)}$$

This criterion is more restrictive than the Courant-Friedrichs-Lewy condition [18].

Many other schemes were also used to solve the conservative form of gas dynamic equations [80][81][82][83].

As a conclusion, in general most one- dimensional simulation software are based on these schemes. In terms of precision, they guaranteed a good accuracy level. This latter varies according the assumptions made on the used scheme. However, in terms of computational time, the models based on finite difference schemes are also time consuming compared to the real time. And the non physical instabilities (in other words, numerical instabilities) faced during the iterations can affect the results.

I.2.4 Zero Dimensional Approach

In this approach, there is no spatial dependence; the different thermodynamic variables (pressure, temperature, density, etc...) vary only as a function of time. The development of the various zero-dimensional methods, cited below, aims to reduce the simulation time with a degree of precision considered sufficient for certain phenomena that the researcher wants to solve.

I.2.4.1. Emptying-Filling Method

The equations of mass and energy conservation are used to determine the thermodynamic variables at each time step. According to this method, the different parts of the inlet system of an internal combustion, in which the gases flow, are considered as independent open thermodynamic systems. These systems are filling up with gases contained in the upstream systems and then emptying in the downstream ones. The simulation time of the models based on this method is too fast compared to one-dimensional approaches[84]. However, this method neglects certain geometric details that can have preponderant effects. In other words, it is unable to distinguish two different geometries having the same overall volume. For this reason, model validity depends on the geometry studied for the intake system components[85]. The pressure wave propagation in the intake line and their effect cylinder filling of the engine cannot be taken into account using this method, because only the average pressure can be determined in the sections studied[86]. The main problem with this approach

is that the inertia of the fluid related to the length of the pipes and the engine rotational speed is not taken into account. The method is improved in inertial capacitive method.

I.2.4.2. Inertial Capacitive method

In this method, the contribution of the inertia of gas flow in the intake line will be taken into account, which increases the degree of precision of the model compared to the emptying method[86]. The computational time of the models based on this method is relatively fast compared to other approaches.

Despite taking into account the flow inertia, the inertial capacitive method is neglecting the compressible properties of the air. The flow nature is always considered stationary. Thus the use of this approach allows leads to low accurate results and wrong ones for particular cases, according to the geometry of the adopted line. In addition, the methodology does not take into consideration the effects of pressure waves in the intake line and their presence.

I.2.4.3. Mean value Model

It is a simple modeling method that calculates the average values of thermodynamic variables over several cycles, neglecting the effects of inertia as well as the pressure losses around the valve. For example, in order to estimate the average mass flow aspirated by the engine, the formula is given as follows:

$$q_m = \frac{\rho.Disp.N}{120} \tag{I-74}$$

The advantage of this method is that the equations used in the simulation code are simple algebraic equations with few differential equations. Chevalier *et al.*[87] used this method for singularities modeling (throttle valve, junctions, manifold, etc...). Model accuracy can be improved by taking into consideration the pressure losses of the system. However, complex geometries remain an obstacle for use of this approach. In addition, Mean Value model cannot calculate the instantaneous pressure and air mass flow rate variations in the intake line of an engine [88]. It is then impossible to determine either the effects of pressure waves on the flow, nor the backflow into the intake system and their consequences on engine filling. This method can be applied in the case of an engine running at low speed, since the effect of acoustic waves is neglected by the flow inertia on the cylinder filling.

As a conclusion, zero-dimensional models are perfect in term of computational time point of view. But when high accuracy level is demanded, the models based on these approaches do not guarantee good results.

I.2.5 Neural Network Black-Box Model

Also called Non-Linear black-box model, it is founded in the 50's. Recently automotive engineers are using this method in engine simulation field. Based on empirical parameters, the neural network model can reproduce, by learning, unknown complex phenomena. These models are valid for the whole engine's operating range and its short simulation time makes

real-time applications possible. The output and the input of the model are related by a hidden layer, in which system learning is implemented (Figure I-9). The internal parameters of the model are identified by minimizing a quadratic criterion during the learning process.

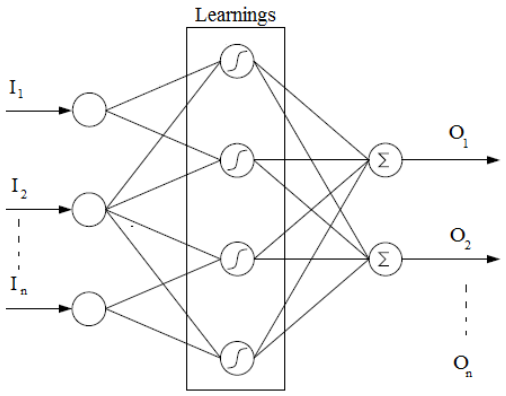

Figure I-9 - Neural Networks representation

It is a fast running model used often for pollutant emissions and cylinder pressure. Many authors in automotive filed used this model, especially when the physics in their studied system is complex and in certain cases it is unknown[89][90][91][92].

However, this method can be applied for a certain and specific objective. For example, if the simulation of a complete engine is demanded, then these models require a huge test campaign (which is not easy to do: cost and time consuming).

I.3. Modeling of different parts of an IC Engine

For a better understanding of the physical behavior of flow in the main parts of the engine and in order to well specify the parameters of these parts in the simulation software, a brief study on the modeling of different parts of the intake system of an internal combustion engine is presented.

Based on quasi-stationary hypotheses, the intake system of the engine can be modeled using a series of tubes connected to each other with a specific boundary conditions [6], [93].

I.3.1 Solid wall:

This is the case of a closed tube. An important property of such condition is that it does not transmit the flow, thus the velocity is equal to zero at this position. A wave is then reflected at this wall to a wave having the same amplitude. The reflection coefficient is usually assumed to be equal to 1.

$$R = \frac{p^-}{p^+} \tag{I-75}$$

For a better precision, the reflection coefficient must be measured and then introduced into calculations.

I.3.2 Section change:

This is the case of a sudden narrowing or enlargement of a section. One part of the wave is then reflected, while another part is transmitted through the section.

- Sudden Enlargement:

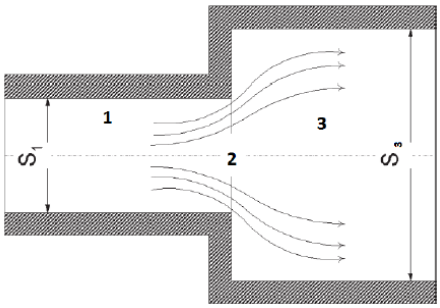

Figure I-10- Sudden Enlargement[94]

This configuration is presented in (Figure I-10) and the equations used for modelling the flow in this case are:

$$\rho_1 u_1 A_1 = \rho_3 u_3 A_3 \tag{I-76}$$

$$a_1^2 + \frac{\gamma - 1}{2} u_1^2 = a_2^2 + \frac{\gamma - 1}{2} u_2^2 = a_3^2 + \frac{\gamma - 1}{2} u_3^2 \tag{I-77}$$

$$A_3 \left(p_1 - p_3 \right) = \rho_3 u_3^2 A_3 - \rho_1 u_1^2 A_1 \tag{I-78}$$

$$A_2 = C_d A_3 \tag{I-79}$$

The coefficient C_d is used to take into account the disturbances of the flow considering that the flow passes through an intermediate state (state 2). This latter separates both zones where the flow can be considered as one-dimensional.

Many authors worked on identifying the coefficient C_d [7][95]. Considering an unsteady behavior of the flow in this section, the model proposed by Chalet *et al.*[94] have been validated on a shock tube and then compared to a CFD Fluent model.

It is important to note that the changes in the sections in internal combustion are rarely abrupt. However, they show a progressive change in section as shown in Figure I-11.

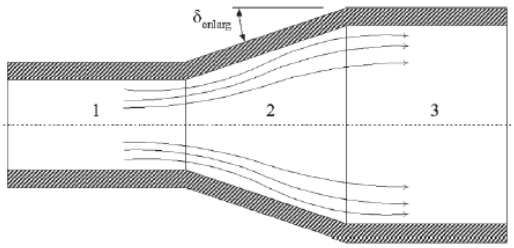

Figure I-11- Progressive Enlargement [94]

Chalet *et al.*[94] identified the friction parameter in gas dynamics equations in function of the angle at the top of the divergent δ_{enlarg} :

$$f_{enlarg} = \min\left(0.0155\delta_{enlarg} - 0.124\right) \tag{I-80}$$

They considered that this kind of singularity behaves like a sudden enlargement for angles of divergence greater than 40 degrees.

- Sudden narrowing:

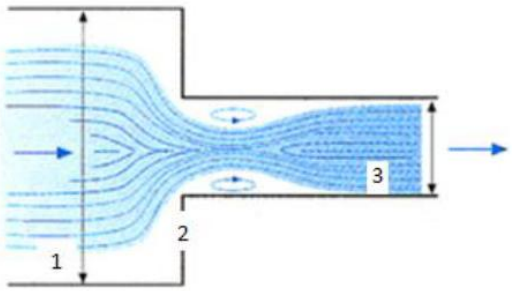

Figure I-12 - Sudden narrowing [94]

Figure I-12 shows a sudden narrowing of the section around the flow. This kind of singularity is characterized by the same system of equations (I-76) to (I-79):

$$\frac{p_1}{\rho_1^{\gamma}} = \frac{p_2}{\rho_2^{\gamma}} \tag{I-81}$$

Also a discharge coefficient C_d allows taking into account the appearance of disturbances in the flow and recirculation zones. This can be done by integrating the section 2 in the computation, and then the conservation equations of mass, momentum and energy are applied to the section 2 with the following equation:

$$A_2 = C_d A_1 \tag{I-82}$$

Chalet *et al.*[94] presented also the complete study for identifying the discharge coefficient for this case.

I.3.3 Bends

A large number of bends exist in the intake system of an internal combustion engine. Consequently, the modeling of this element is important. In one-dimensional models, this specific geometry is generally considered as three elements: two straight tubes separated by the curvature of the bend itself (Figure I-13).

Using CFD codes, Chalet *et al.*[94] found that the flow velocity is above the average in the area next to the inner wall of the bend. This velocity increasing is followed by pressure losses in this zone. These observations imply that the flow is no longer one-dimensional. It should be noted that the one-dimensional character is maintained before and after the discontinuity. One-dimensional approach can still be used at the bend but a suitable modification is needed [94][96].

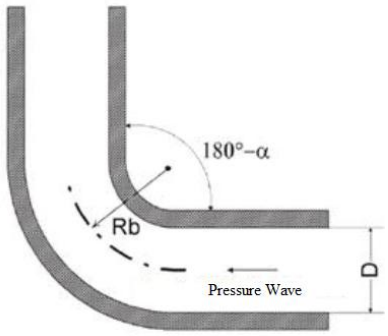

Figure I-13 - Bend representation [96]

I.3.4 Open end pipe

The equations used in this type of boundary condition are usually given by the method of characteristic (using mass, momentum and energy conservation laws). In addition, the equation which describes an isentropic flow is also used.

Incoming Flow case:

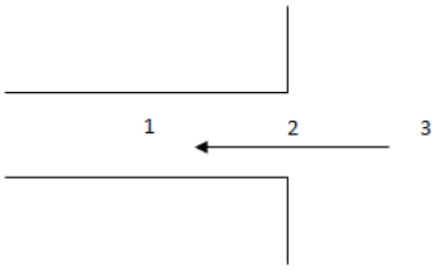

Figure I-14 - Incoming flow [97]

Figure I-14 presents the configuration and the system of equations can be presented as follow:

$$C_d \rho_2 u_2 A_2 = \rho_1 u_1 A_1 \tag{I-83}$$

$$a_1^2 + \frac{\gamma - 1}{2} u_1^2 = a_2^2 + \frac{\gamma - 1}{2} u_2^2 = a_3^2 \tag{I-84}$$

$$A_1 \left(p_1 - p_2 \right) = \rho_2 u_2^2 A_2 - \rho_1 u_1^2 A_1 \tag{I-85}$$

$$\frac{p_3}{\rho_3^\gamma} = \frac{p_2}{\rho_2^\gamma} \tag{I-86}$$

The discharge coefficient is a relation between the experimental air mass flow and the isentropic one.

$$C_d = \frac{q_{m_{exp}}}{q_{m_{isen}}} \tag{I-87}$$

Kirkpatrick [97] considered that the discharge coefficient is constant (equal to 0.65). Blair *et al.*[98] indicate that if the purpose was to make a simple comparison to highlight the improvement of a certain process of the flow, this method is completely adequate. However, if the aim is to incorporate C_d the value in an engine simulation model, then a precise definition of the discharge coefficient is needed. An ideal and actual discharge coefficient terms was introduced[98][99]. The first term compared the experimental mass flow rate to the mass flow calculated in a non-isentropic way. The second term represents better the reality since it is calculated with an iterative method based on the value of $q_{m_{exp}}$. The multidimensional effects are taken into account using the formulation of discharge coefficient presented by Blair *et al.* [98]. The one dimensional assumption remains correct in the pipe downstream of the open end, but only at a sufficient distance from the singularity. The model of discharge coefficient presented by Chalet *et al.* [100] is much more global and precise than the one presented by Blair *et al.* [98]. It takes into account the Mach number and the characteristics of the geometry.

Outgoing Flow case:

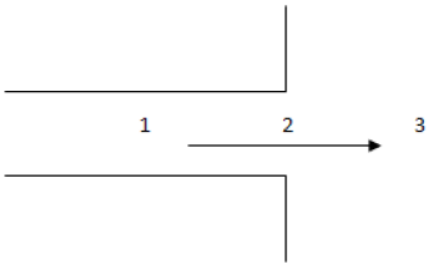

Figure I-15 - Outgoing flow[97]

At this discontinuity, the wave is reflected at the open end and transformed to expansion wave. A part of the wave is transmitted to the boundary 3. The system of equations, presented in Figure I-15, can be written as follow:

$$\rho_2 u_2 A_2 = C_d \rho_1 u_1 A_1 \tag{I-88}$$

$$a_1^2 + \frac{\gamma - 1}{2} u_1^2 = a_2^2 + \frac{\gamma - 1}{2} u_2^2 \quad \text{(I-89)}$$

$$p_2 = p_3 \quad \text{(I-90)}$$

$$\frac{p_1}{\rho_1^\gamma} = \frac{p_2}{\rho_2^\gamma} \quad \text{(I-91)}$$

The discharge coefficient at this singularity was also identified by Blair *et al.* [98].

I.3.5 Junction

Pressure wave propagation across a junction (Figure I-16) is an intrinsically multi-dimensional phenomenon [6]. Modeling such a flow with one-dimensional approaches is not simple because the complete geometry of the junction will not be presented (for example the case of an intake manifold of a four-cylinder engine).Two models are conventionally used for modeling the flow in a junction [5]: the first one is the constant pressure theory which assumes that the static pressure in all branches is the same. Although this method is proven to be easy to apply, simulation results compared to experimental one do not show good accuracy level. This method can be used when the velocity of the speed is low, but this is not always the case for real operating conditions of an engine. The second method is the momentum conservation law, which takes into account the direction of the flow in the different branches. Usually, pressure losses coefficients experimentally determined are used in this case. However, this method is a time consuming compared to the first one.

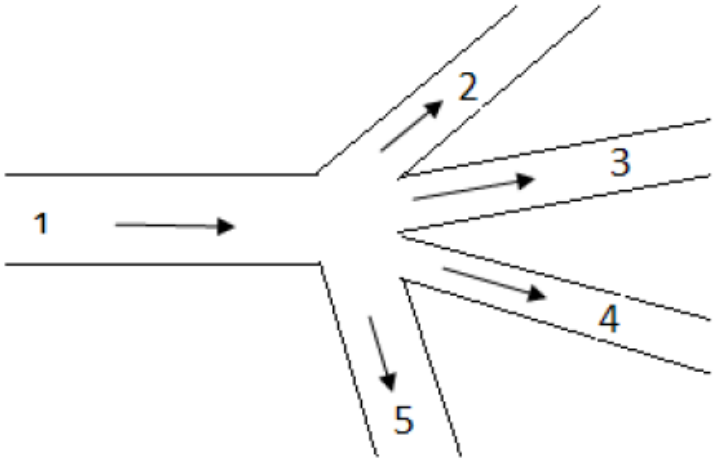

Figure I-16 - One-dimensional representation of a junction[32]

Dimitriadis *et al.* [5] proposed a calculation method that employs appropriate turbulence models. This method is based on CFD calculation to evaluate the pressure losses in a junction. However, this kind of techniques is still based on a stationary flow condition.

Based on the modelling of the junction with pressure losses, which is most used and having a good accuracy level for engine simulation application, many authors worked on modelling the flow behavior in a junction [6][96][101][102].

I.3.6 Valves

The connection between the intake or the exhaust runners and the cylinder is done through the valves. They play an important role in the design of internal combustion engine. The valves are essentially characterized by their opening periods, opening timing, frequency and the flow section available for flow. One-dimensional approach is usually used for flow modelling through the valve[32]. The flow is characterized using empirical data. The effective cross section and the discharge coefficient identifications are needed to characterize the pressure losses.

Figure I-17 corresponds to an intake valve where zone 1 represents the intake runner. Zone t and zone 2 represent respectively the throat and the in-cylinder boundary conditions.

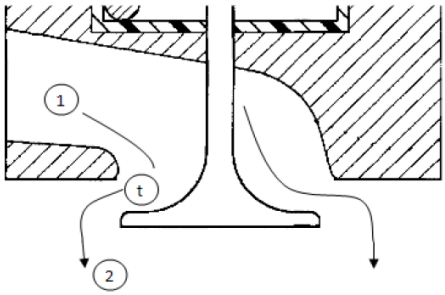

Figure I-17 - Flow representation through an intake valve[32]

The theoretical equations applicable to this kind of discontinuity, which is specific to an internal combustion engine, are given by:

$$\rho_t u_t A_t = C_d \rho_1 u_1 A_1 \tag{I-92}$$

$$a_2^2 = a_1^2 + \frac{\gamma - 1}{2} u_1^2 = a_t^2 + \frac{\gamma - 1}{2} u_t^2 \tag{I-93}$$

$$\frac{\rho_t}{\rho_2} = \left(\frac{p_t}{p_2} \right)^{\frac{1}{\gamma}} \tag{I-94}$$

The discharge coefficient C_d is measured experimentally in stationary state and then applied in the simulation in a quasi-stationary manner in order to improve the flow modeling through the valve as much as possible. Many authors also worked on identifying the discharge coefficient[6][19][103][104][27][106].

I.3.7 Throttle valve

The throttle valve in gasoline engine allows getting the correct air/fuel ratio in the cylinder to achieve the best combustion conditions. The mixture ratio is then controlled by the throttle valve since the quantity of fuel entering the cylinder is quantitatively related to the air flow in gasoline engine. The throttle valve behaves as a thermodynamic device, where the flow

through it is considered as adiabatic and subjected to pressure losses. Depending on the angle of opening of the throttle valve, the pressure losses can high or low.

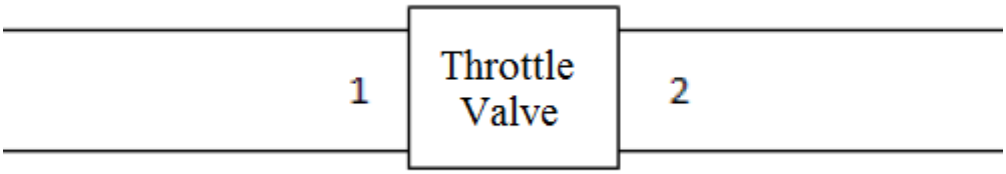

Figure I-18 - Throttle valve

The equations used in this kind of discontinuity (Figure I-18) are presented as follow:

$$\rho_2 u_2 A_2 = \rho_1 u_1 A_1 \tag{I-95}$$

$$a_1^2 + \frac{\gamma - 1}{2} u_1^2 = a_2^2 + \frac{\gamma - 1}{2} u_2^2 \tag{I-96}$$

$$\Delta p = p_1 - p_2 = f_c \left(\frac{\rho_1 u_1^2}{2} \right) \tag{I-97}$$

$$f_c = \frac{2K}{\gamma} \tag{I-98}$$

K is called coefficient of resistance. It is an empirical coefficient based on the work of Benson *et al.*[107]. K and f_c depend on Reynolds and Mach numbers. K is a function of the solidity and Reynolds number. The solidity is the ratio between obscured surface and the total area exposed to the gas [6]. Figure I-19 shows the values of K as a function of Reynolds number and Solidity. Figure I-20 shows the values of K in function of the square of mach number downstream the throttle valve.

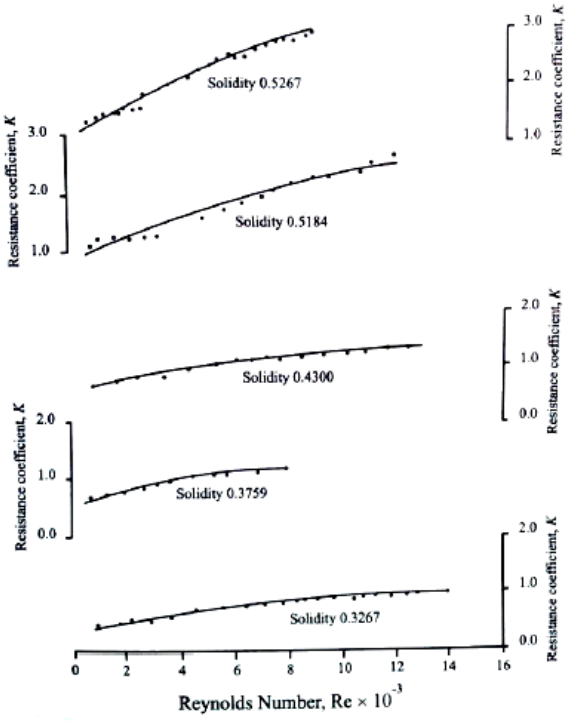

Figure I-19 - K=f (Re, Solidity)[32]

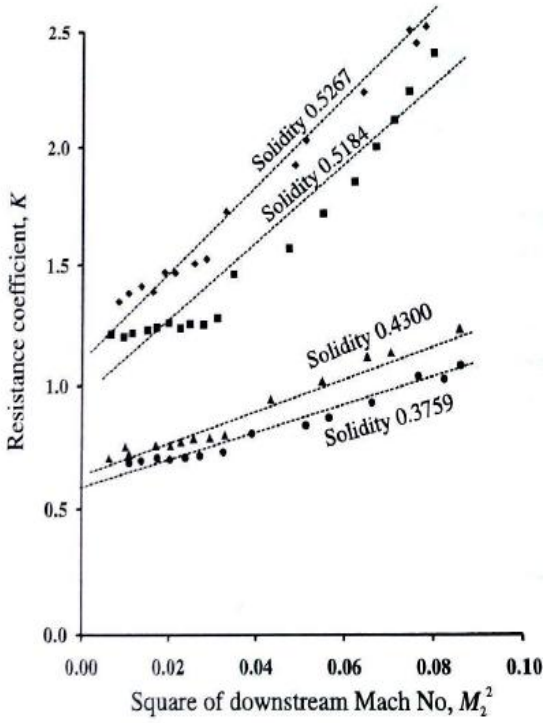

Figure I-20- K= f (Square of Mach number)[32]

Blair *et al.*[106] modelled the pressure losses across the throttle valve using their coefficient. They proved that the pressure drop characteristics largely depend on the relationship between the throttle and the pipe surfaces. It was then necessary to use throttle mapping model for discharge coefficients in order to use it in a precise simulation of the engine.

Harrison *et al.*[28] elaborated a model for the throttle valve based on acoustic approach. They considered that when the throttle valve is at full open position, the system behaves as a simple pipe. And when it is closing, their model takes the form of a sudden narrowing of the pipe and then a sudden enlargement. This discontinuity is supposed to reproduce the effect of pressure drop created by the angle of the throttle valve closing.

I.3.8 Other types of intake system parts

The flow behavior through other types of parts in the intake system of an internal combustion engine (such as CAC, Compressor, EGR, etc…) was also studied by many authors. Since only naturally aspirated engines will be used to validate the model introduced in this PhD work, the literature survey study about these parts will not be presented in this chapter.

The air flow behavior in the intake system of an internal combustion engine was studied in the literature survey chapter. The concept behind the wave action was clarified due to different models, especially the acoustic theory. However, each approach presents some advantages and some demerits. The challenge of the present research study is then identified, which is the compromise between accuracy and simulation time. Later on, a new methodology will be discussed, in which the model is based on transfer function concept.

II. Experimental and Numerical Tools

The literature survey study allows understanding the importance of the wave action in the intake system of the internal combustion engine. This phenomenon needs special means of investigations. In this section, experimental test benches and software, used in this PhD thesis, are described. A dynamic flow bench helps to find the natural frequencies of the intake system of internal combustion engine. The use of this bench is described as well as its architecture. The identified values from the dynamic flow bench allow creating a virtual system, which will be used in the simulation software. Finally, the experimental results, given by different engine test benches, help to validate the models presented in this work.

II.1. Dynamic Flow Bench

In the aim of studying pressure wave's propagation in different geometries of intake system of an internal combustion engine, a dedicated test bench called: "Dynamic Flow Bench" (DFB) is used. The advantage of this latter is to obtain pressure fluctuations which are similar to those observed in the intake system (mainly after closing the intake valve). A steady flow is established using an air pump, which helps to create suction and to determine the pressure losses in the geometry. The flow is then suddenly interrupted (within 0.5 ms) using a system equipped with a valve, actuated by a pneumatic piston. A resonance system of quarter-wave is then established (open-ended configuration) and the instantaneous pressure upstream the valve is measured. This pressure variation is correlated with the air mass flow rate in order to identify a "transfer function". This latter models the resonant frequencies and represents the dynamic behavior of the tested geometry. Later on, the identification procedure of the transfer functions is based using this test bench.

II.1.1 Bench Architecture

The objective of the dynamic flow bench is to generate pressure waves in a tested geometry. The bench works as follow (Figure II-3): an air pump "SuperFlow SF-1020" (number 1) is used to create suction in the tested part (the same direction of flow as in a real engine is respected). Thanks to the second option provided by this air pump (blow air mode instead of suction air mode), which is mandatory in order to ensure the sealing of the tested geometry mounted on the test bench, by adding a liquid that detects leakage. A control unit is implemented in the pump to control the air flow rate. A shutoff system interrupts roughly the flow (number 2). The tested geometry is placed on the upper side of the shutoff system (number 3). A by-pass system is actuated at the same time with the closing valve to maintain the flow in the pump (number 4). This experimental installation is controlled using a control unit (number 5). The instantaneous pressure at the end of the tested geometry (upstream the valve) is measured using a sensor and an acquisition system with a sampling frequency of 20 KHz (number 6 and 7). A LabVIEW program is made to control the acquisition process (Figure II-1 and Figure II-2).

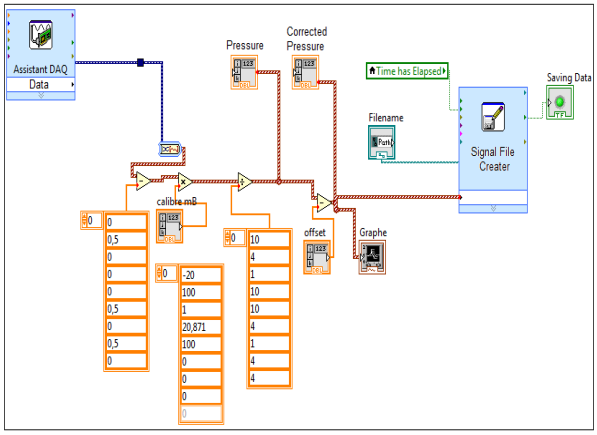

Figure II-1 – LabVIEW Software

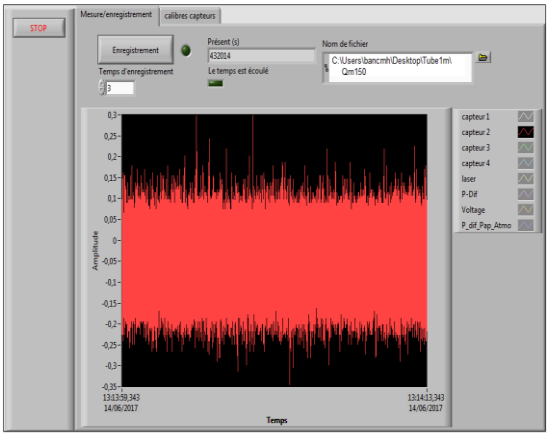

Figure II-2 – Acquisition Tool

The data are registered in Matlab files (.mat) on a computer using DIAdem software tool, which is designed by National Instruments Company to help engineers and scientists quickly locate, inspect, analyze and report on measurements (number 8). The atmospheric pressure and temperature in the cell are measured during the tests. However, the temperature of the aspirated air can increase after many tests. This phenomenon should not be neglected for the comparison between different results.

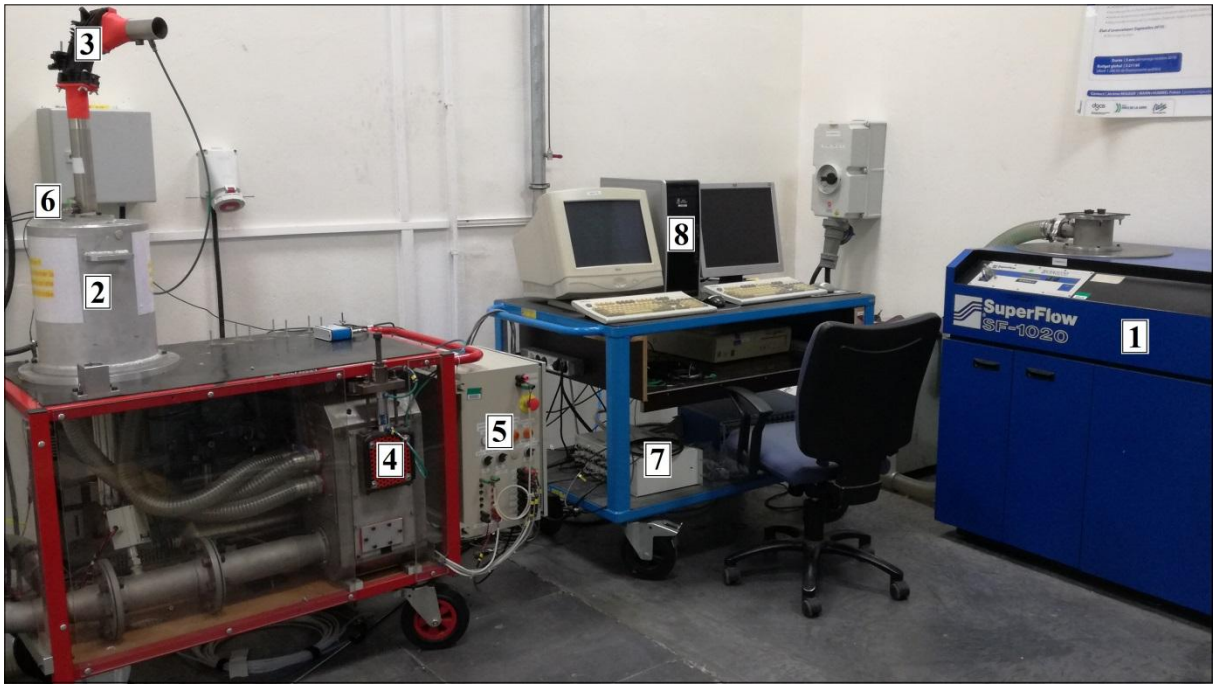

Figure II-3 – Dynamic Flow Bench

The physical operation of the experimental setup is presented in Figure II-4. The air mass flow rate vector is created using Matlab and described by equations (II-1) to (II-3).

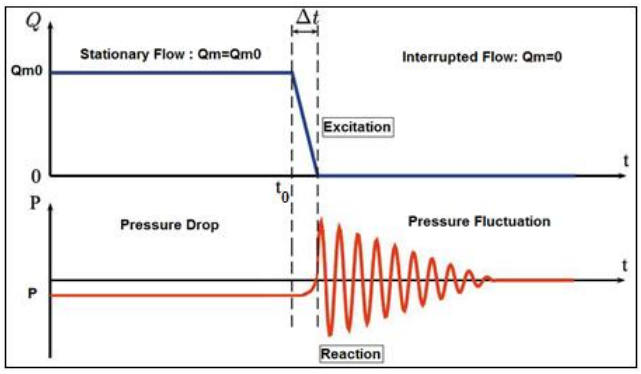

Figure II-4 - Physical Operation of DFB

$$qm = qm_0 \qquad t \le t_0 \tag{II-1}$$

$$qm = qm_0 \left[1 + \frac{1}{\Delta t}\left(t_0 - t\right) \right] \tag{II-2}$$

$$t_0 < t < t_0 + \Delta t$$

$$qm = 0 \quad t \ge t_0 + \Delta t \tag{II-3}$$

The air flow shutoff solution has been chosen for the dynamic flow bench because it is hard to create periodic air flow shutdown. The bench mechanics is easier with a fast shutdown system than a periodic rotating one.

The advantage of the air flow shutoff is the perfect segregation between the tested part and the facility after the shutdown. In fact, after closing the valve, the dynamic flow bench allows

identification of the natural frequencies of the tested geometry (the fundamental frequency and its harmonics). The natural frequency of a system is the frequency at which the system tends to vibrate when it is not disturbed by an outside force. For example, a tube of 1086 mm long and 32 mm diameter is characterized using the dynamic flow bench. The natural frequencies of the tested part referring to Figure II-5 are: 75, 225, 376, 529, 680, and 832 Hz. The dynamic flow bench represents both phenomena: quarter-wave and half-wave resonance systems. The frequencies of the peaks in Figure II-5 correspond to the resonance system of quarter-wave (fundamental frequency and its harmonics). The frequencies of the "inter-peaks" represent the resonance system of half-wave. The energy of these latter is considered as negligible.

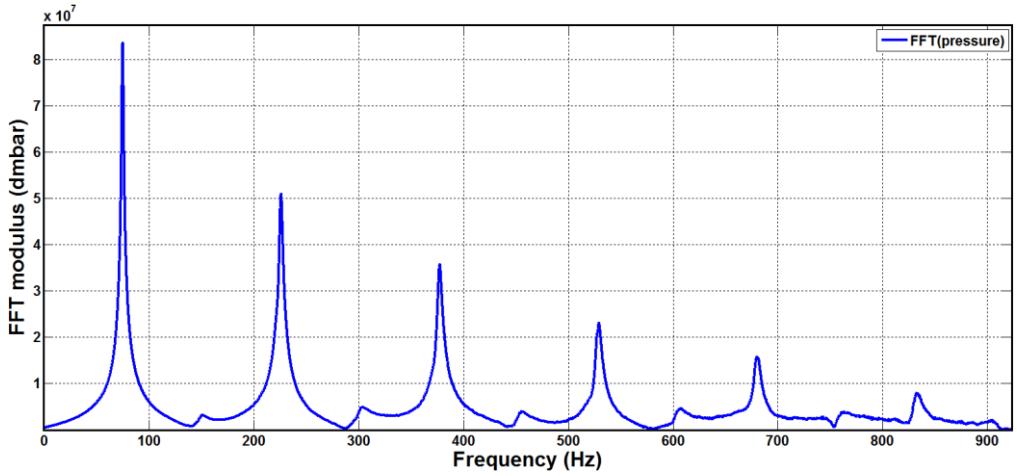

Figure II-5 – Fast Fourier Transform of the derivative of the instantaneous pressure upstream of the shutoff valve

The inconvenient of air flow shutoff system is the non-periodic character of the excitation, which means that the signal processing will be more difficult and the quality of the response in the frequency domain will be low compared to a periodic character one.

II.1.2 Bench Sensitivity Control

The engine sensitivity is about nearly 500 Hz. It means that the excitation on the dynamic flow bench has to be controlled to cover perfectly the range between 0 and 500 Hz.
Many parameters can affect the excitation response (in term of frequency range):

Shutoff component:

The bench provides four shutoff components with different slots: x = 3, 6, 9 and 12 mm (Figure II-6). In a packaging point of view and to be able to test high runner area of tested parts, a diameter of 40 mm has been chosen for the 4 components. The pressure losses increase when a shutoff component of low stroke value is chosen. For example, the component of 6 mm stroke value allows a 250 kg/h maximum value of suction rate. However, an aspirated air flow rate can reach 500 kg/h using the shutoff component of 12 mm.

Piston back pressure:

Valve closing is controlled by a piston, which is pneumatically actuated using compressed air in a cylinder. The pressure in the cylinder is regulated using a discharge control valve.
The piston speed is related to the cylinder pressure using equation(II-4)[108]:

$$\text{Piston speed}\left(\text{m/s}\right) = 3.3\text{x Back pressure}\left(\text{bar}\right) + 2.3 \qquad \text{(II-4)}$$

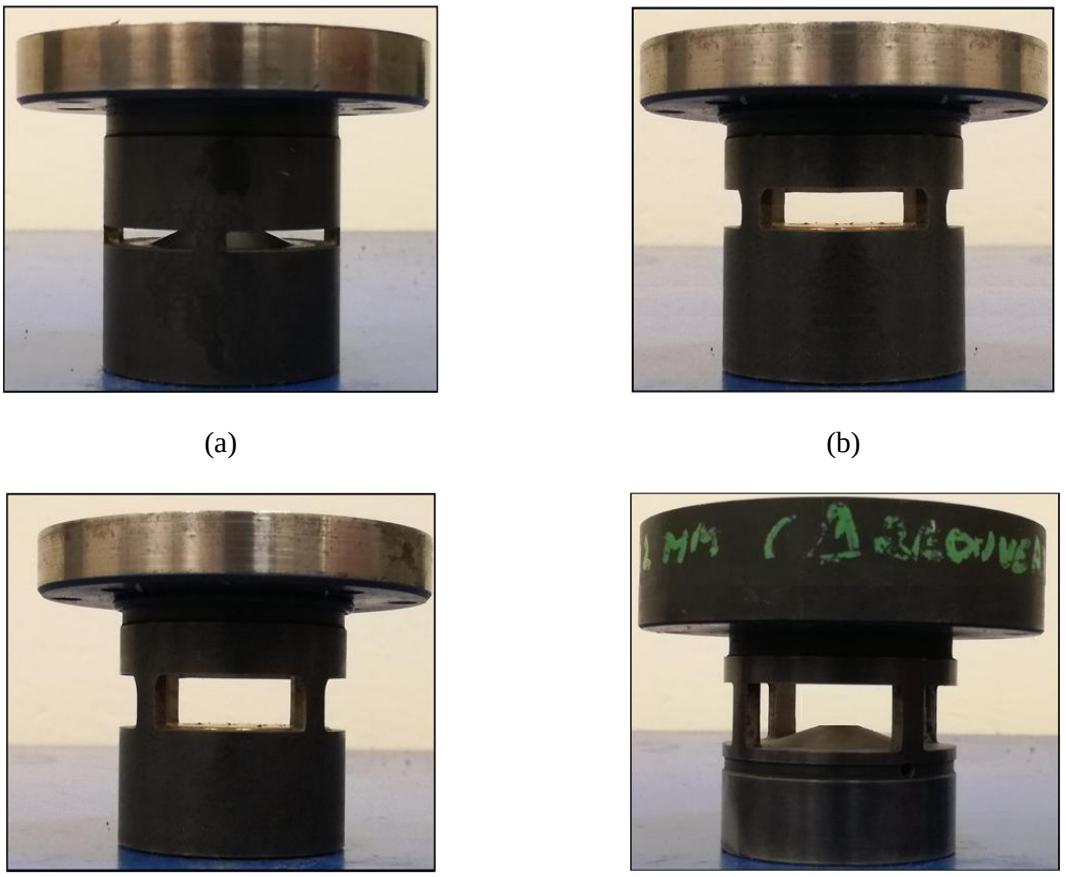

(a) (b)

(c) (d)

Figure II-6 – Shutoff components: (a) 3mm slot, (b) 6 mm slot, (c) 9 mm slot and (d) 12 mm slot

Valve displacement:

It is related to the useful stroke. The valve displacement can be detected using a Laser. The initial position of the valve is p_i = 0 (Figure II-7). At time t (shoot time), the shutoff is activated. The valve continues moving till the edge of the shutoff component. The position of the valve (at $p_{useful} = p_i$ + stroke), is the final useful position (Figure II-8).

Figure II-7 – Initial valve position

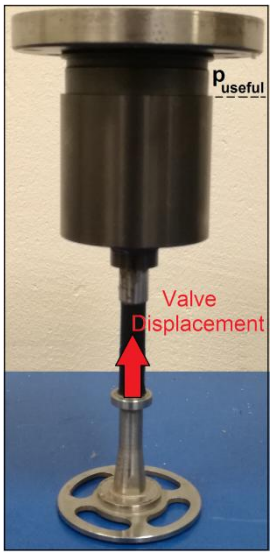

Figure II-8 – Useful valve position

Closing time:

Using Laser data, the closing time can be determined (Figure II-9). The shutoff component of 6 mm stroke is used in this example (useful stroke position in red line).

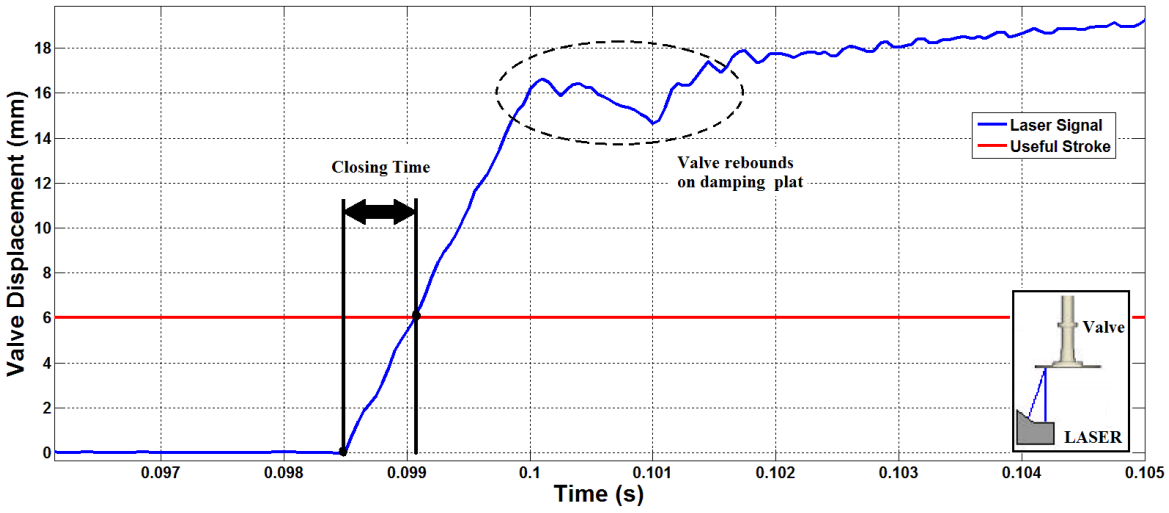

Figure II-9 - Laser data curve in function of time

Using laser sensor, four characteristics can be checked:

1. The closing time factor
2. The linearity of the valve closing
3. Bouncing oscillation level in order to avoid consecutive aspirations.
4. The valve shutoff speed factor:

$$\text{Val ve shutoff speed}(\text{m}/\text{s}) = \frac{\text{Valve displacement}}{\text{Closing time}} \qquad \text{(II-5)}$$

If the first three characteristics are outside the admissible range and not respected, tests are considered not valid.

The closing time effect of the valve on the relative pressure response is studied. The piston back pressure and the choice of the shutoff component affect the shutoff time (Figure II-10). To ensure security and shutdown valve durability, the back pressure limitation is about 2 bars. The high back pressure can destroy the shutoff valve. The shutoff component of 12 mm slot was eliminated in this study because consecutive aspirations can occur.

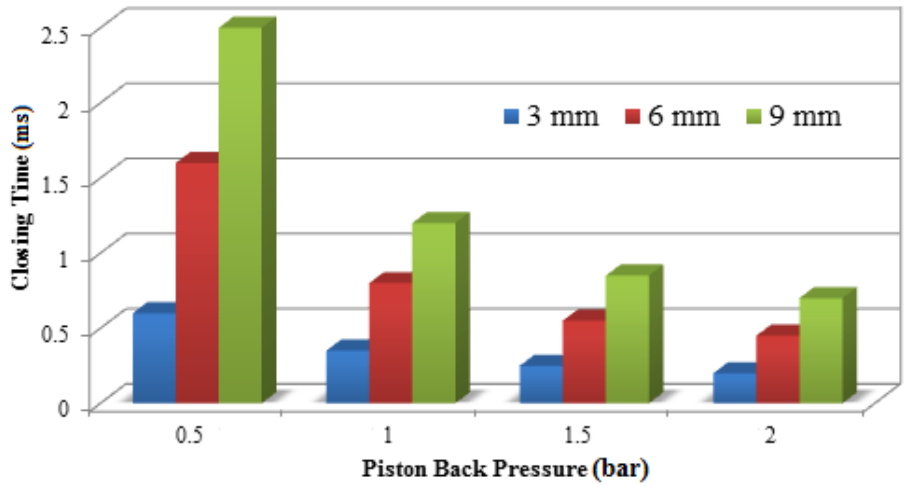

Figure II-10 – Closing time factor in function of piston back pressure and useful stroke

Different tests are done using 3 shutoff components (x=3, 6 and 9 mm) and four piston back pressures (0.5, 1, 1.5 and 2 bars). The closing time value of the valve should be around 0.5 ms to cover perfectly the range between 0-800 Hz of the signal [108]. The shutoff component of 3 mm at 0.5 bars can be used to get a closing time value of 0.5 ms. Unfortunately this small slot does not allow the pump to aspirate high air flow (maximum value of air mass flow rate is about 80 kg/h). The shutoff component of 9 mm allows suction of 400 kg/h maximum value. At 2 bars, the closing time value in this case is close to 0.5 ms. But after many tests, the shutoff valve is destroyed. Therefore, the shutoff component chosen is that of 6 mm stroke at 1.5 bars (allowing a 250 kg/h maximum value of suction rate).

II.1.3 Bench Calibration and Repeatability

Before any test campaign, this phase is mandatory. The mechanical parts and sensors of the bench have to be controlled periodically to ensure the constant quality of all measurements. It's a complicated task and the better way to proceed is to use an absolute reference to check the equipment reliability. The absolute reference chosen is a tube of 1086 mm long and 32 mm diameter and has been brought with 100 tests done with different excitation conditions (Figure II-11).

Figure II-11 – Dynamic Flow Bench test using the absolute reference

The bench repeatability is tested before the tests campaign. The piston back pressure was checked before the shoots (1.5 bars). This value can increase with time to reach 1.6 and 1.7 bars. A discharge valve was used in this case to regulate again the piston back pressure to 1.5 bars. Figure II-12 shows good repeatability of the test bench after 5 tests on the same geometry and at the same air mass flow value (150 kg/h).

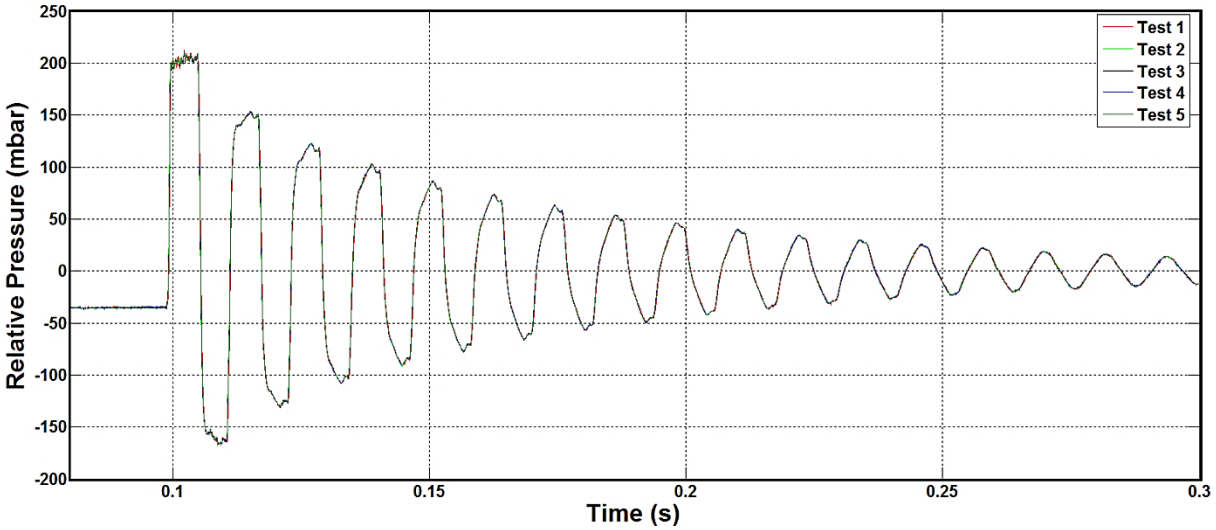

Figure II-12 – Study of repeatability using the absolute reference at 150 kg/h

To resume, the experimental setup runs with an excellent accuracy, reliability and repeatability (about 3% in an 800 Hz band pass), which allows us to have access to the dynamic behavior of intake geometries with measurements.

II.2. GT-Suite Software

In this work, the simulation software used to investigate the pressure waves in the intake system of the internal combustion engine is GT-Power (a part of GT-Suite software). It is a platform for multi-physics system simulation developed by Gamma Technologies, used by all major engine manufacturers and vehicle OEMs. GT-Power is a one-dimensional non-linear simulation tool which allows studying the engine behavior. It contains libraries for simulation and analysis of the air path, combustion, acoustics, cooling systems, fuel injection systems, lubrication systems, etc… An engine model in GT-Power can represent one or many of these systems and the interactions between them as well. GT-Power user can access to the thermodynamic variables using virtual sensors (Pressure, temperature, density, air mass flow rate, etc…). The principle of the one-dimensional computation, on which GT-Power is based, consists on discretizing a continuous geometry to sub-volumes in order to increase the accuracy of the calculation (Figure II-13).

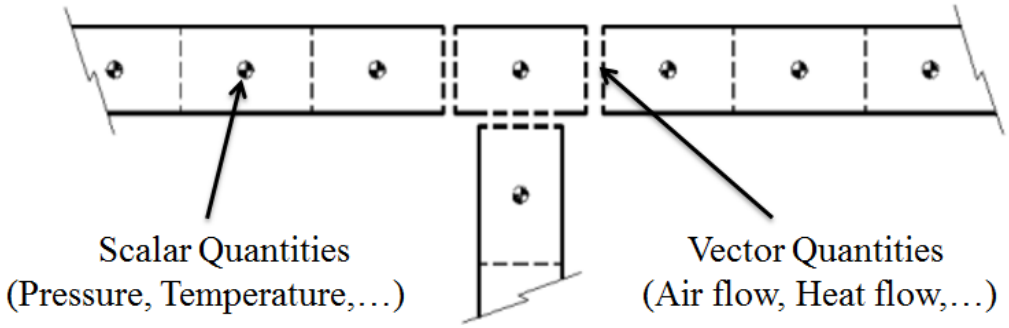

Figure II-13 – Decomposition of geometry on GT-Power [109]

The stability of GT-Power is regulated by a CFL condition CFL_{max}. The solver, which is based on both standard nonlinear Navier-Stokes and linear wave equations, constantly calculates the time step required to respect the following condition [109]:

$$CFL_{max} = \frac{\Delta t}{\Delta x}(|u| + a) \leq 0.8 \qquad \text{(II-6)}$$

GT-Power was chosen for different reasons:

- To simulate the flow in the intake system of different types of engines, for a better understanding of some related phenomena.
- High detailed modelling of the pulsating flow in the intake system of the internal combustion engine, which allows investigating the pressure wave propagation.
- Easy exploitation of simulation results and comparison with experimental data via integrated post-processing tools GT-Post

- It allows coupling the model in the sketch with other software as Simulink, OpenFOAM, Converge, Fluent, etc…(Figure II-14)
- It allows coupling of mathematical functions with the one-dimensional modeling of the geometries, allowing therefore Multi-Physics modeling.

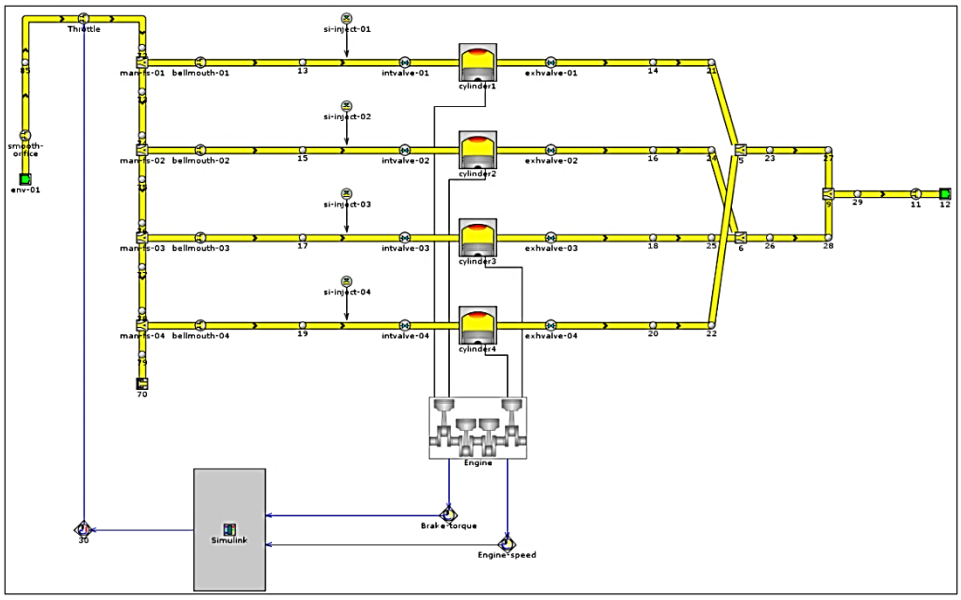

Figure II-14 – GT-Power / Simulink coupled model

Unfortunately, although operating according to 1D representation, GT-Power calculation time is not negligible. Furthermore, calibration phase of the model in the simulation software, based on experimental results, is not easy and takes a lot of time.

Vehicle Simulation, Real Time and Fast Running Models can be also performed using GT-Suite special libraries. These models are based on mean value models, experimental results and engine mapping. However, physical phenomena, such as pressure wave propagation, cannot be investigated (Figure II-15).

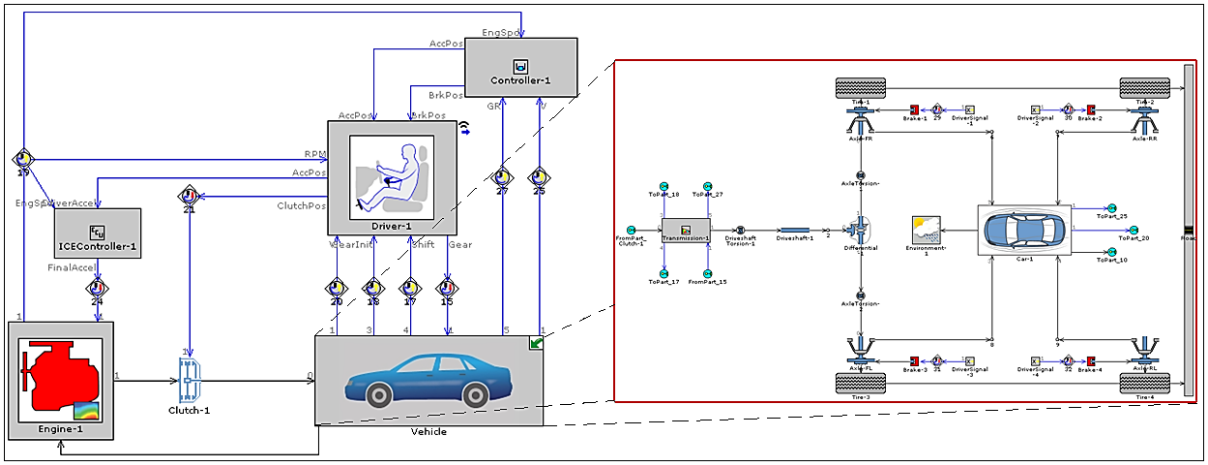

Figure II-15 – Real time simulation model of a vehicle using GT-Suite

It is quite easy to build a GT-Power model, from a geometrical point of view, since the simulation software is a graphical programming including a library of different engine components (cylinder, tubes, etc…). However, some parameters related to combustion for example, are difficult to be defined in GT-Power. Then a TPA (Three Pressure Analysis) model is commonly used to determine quantities that are difficult or impossible to measure directly such as: residuals, valve flows profiles, combustion apparent burn rate. These parameters should be defined in order to build a complete engine model. TPA consists in focusing on a cylinder, cutting-off the rest of the system and then replacing it by instantaneous measured port pressures (intake pressure, cylinder pressure, exhaust pressure) located near the cylinder.

Design of Experiments (DoE) can be also performed using GT-Power to calibrate engine model. Many test cases may be run simultaneously to screen the field of study. Based on a set of independent parameters, user can identify particular parameters define certain factors for model optimization.

The intake system of an internal combustion engine can be calibrated in GT-Power using the "Dynamic Flow Bench". First of all, the test bench is modelled in GT-Power software. The "Virtual Dynamic Flow Bench" concept is presented in (Figure II-16).

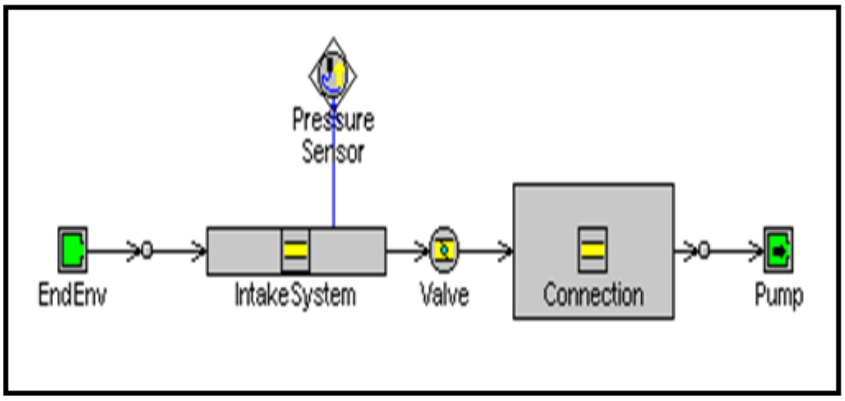

Figure II-16 – Virtual Dynamic Flow Bench model

The 'Pump' template helps to regulate the air mass flow excitation profile. The closing time is set to 0.5 ms, which is controlled using the 'Valve' template (according to equations (II-1) to (II-3)). 'EndEnv' template allows defining the atmospheric conditions during the test campaign. The tested part should be placed between 'EndEnv' and 'Valve' templates. In suction mode (before closing the valve), the pressure losses can be measured using the virtual sensor. The latter must be located at the same position on the geometry as the real sensor. The pressure losses depend on the geometry of the tested part and the air flow. When these parameters are well modelled in GT-Power, good agreement is then obtained between experimental results and GT-Power virtual model in terms of pressure losses. After closing the shutoff valve, a friction multiplier tuning is needed to model the pressure fluctuation (using DoE). Figure II-17 and Figure II-18 present a comparison between experimental (from test bench) and simulated (Virtual test bench) data in time and frequency domains. The intake system in this example is a simple tube of 985mm length and 30 mm. The sensor is located 40 mm away from the valve seat. The air flow rate aspirated by the pump is fixed to 160 kg/h.

During the experimental campaign, the atmospheric pressure and temperature in the cell is registered and integrated in the virtual model via 'EndEnv' template. The model shows good ability to reproduce the reality (up to 700 Hz). The intake system calibration is performed at specific operating points. In other words, for each aspirated air mass flow rate, the parameters tuning is necessary to reproduce perfectly the wave propagation in the intake system.

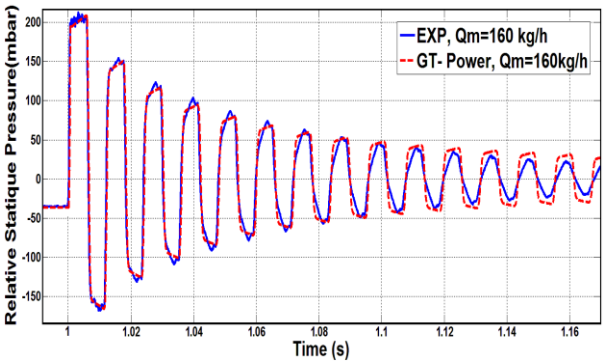

Figure II-17 – Relative pressure in function of time

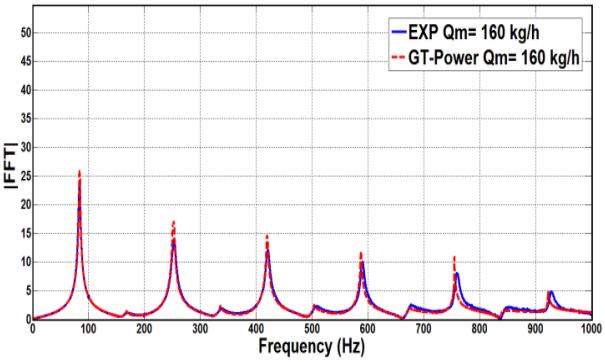

Figure II-18 – FFT modulus of relative pressure in frequency domain

Figure II-19 – DFB tests on EB2 intake system

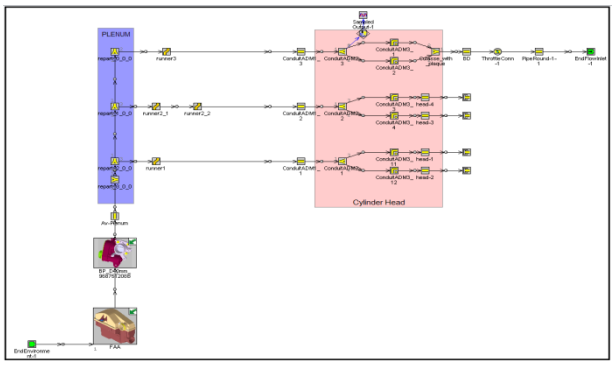

Figure II-20 – VDFB tests on EB2 intake system

Figure II-19 and Figure II-20 show the calibration process of the intake system of the three cylinder engine (EB2) using dynamic flow bench and GT-Power (this engine is detailed in section II.6).

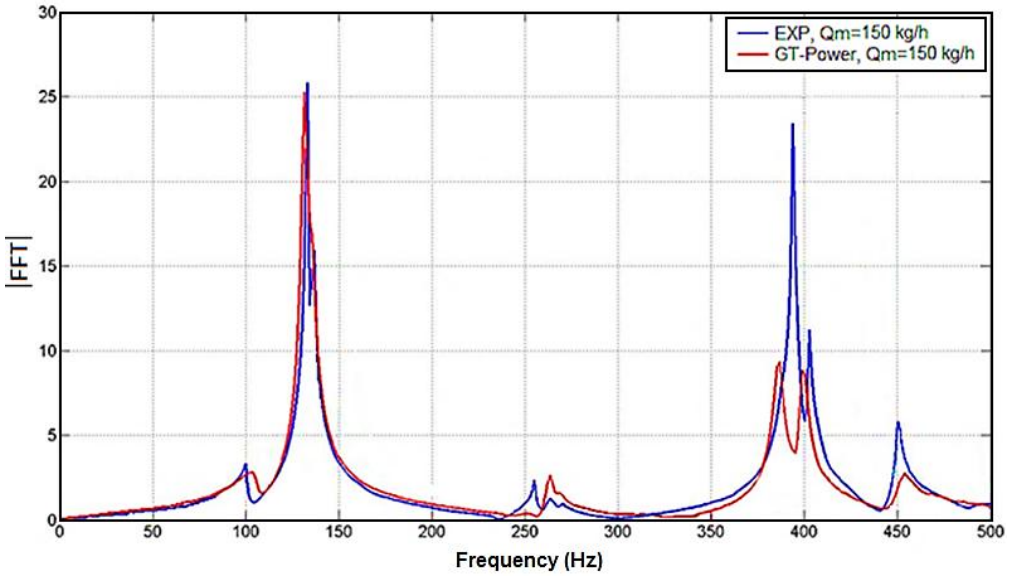

Figure II-21 – FFT modulus of relative pressure at third runner in frequency domain

At 150 kg/h, the intake system of the three cylinder engine is calibrated according to experimental data from the Dynamic Flow Bench (Figure II-21). The virtual model is calibrated by adding more pressure losses and changing the coefficient of friction in some parts in the intake line. The instantaneous relative pressure is registered using a sensor placed at the end of the third runner of the intake geometry (near the shutoff valve). The first and the second runners are tightly closed at their ends during the tests. The model shows good ability to reproduce the reality in term of frequency. In term of amplitude of the peaks, the virtual model shows the ability of well modeling the intake system up to 350 Hz. From that value, the virtual signal is more damped compared to experimental data.

II.3. MATLAB/Simulink

The name MATLAB stands for **MAT**rix **LAB**oratory and it is developed by MathWorks. MATLAB is a high level language for technical computing used as a tool for high-productivity research, development and analysis. Faster than traditional computing language: C, C++ and FORTRAN, MATLAB system consists of five main parts:

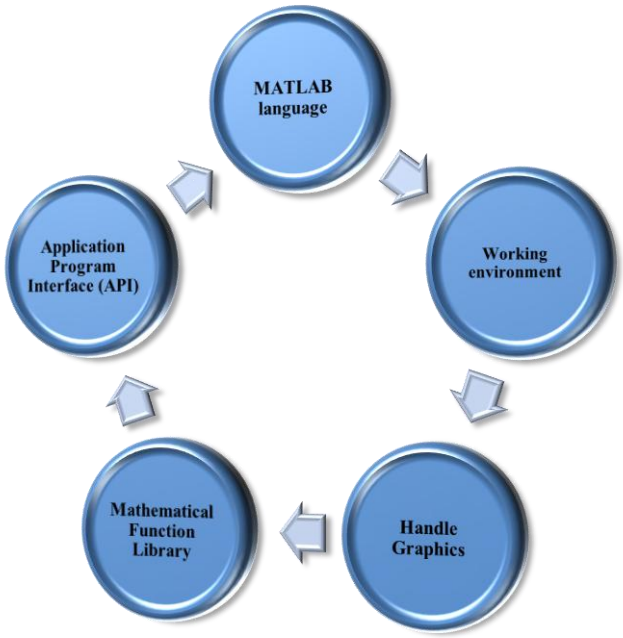

Figure II-22 – Main parts of MATLAB system

1. **MATLAB language:** This is a high-level matrix/array language with control flow statements, functions, data structures, input-output, and data-oriented programming features.
2. **MATLAB working environment:** This is a set of tools and facilities that user works with as MATLAB programmer. It includes facilities for managing variables in workspace user model and importing-exporting data.
3. **Handle graphics:** This is the MATLAB graphics system which includes high-level commands for two-dimensional and three-dimensional data visualization, image processing, animation and presentation graphics.
4. **MATLAB mathematical function library:** This is a big collection of computational algorithms ranging from elementary functions (sum, sine, cosine, etc…) to more sophisticated functions (matrix inverse, matrix eigen values, Fast Fourier Transforms, etc…)
5. **Matlab Application Program Interface (API):** In this library, user can write C and FORTRAN programs that interact with MATLAB. It includes facilities for calling routines from MATLAB, calling MATLAB as a computational engine, and for reading and writing MAT-files.

MATLAB includes a family of application-specific solutions called "Toolboxes". These latter extend MATLAB environment to solve particular classes of problems and allow user to learn and apply specialized technology. One of the toolboxes used in this work is: "System Identification Toolbox". This advanced toolbox provides MATLAB functions for constructing mathematical models of dynamic systems from measured input-output data. The recent versions of this toolbox allow the identification of Transfer Function linear model. In this PhD work, the intended Transfer Function is a linear relation between the instantaneous pressure (input of system) and the air mass flow rate (output of the system). From MATLAB

workspace, the input and the output of the system were imported. Then, by simply indicating a transfer function desired model identification and specifying the numerator and denominator model order, the new identified model will be generated with an error percentage. The detailed transfer function identification procedure will be presented later on.

Simulink, also developed by MathWorks, is a graphical programming environment for modeling, simulating and analyzing multi-domain dynamic systems. This graphical block diagramming tool offers a tight integration with the rest of MATLAB environment and can either drive MATLAB or be scripted from it. Simulink is widely used in automatic control and digital signal processing for multi-domain simulation and Model-Based Design (Figure II-23).

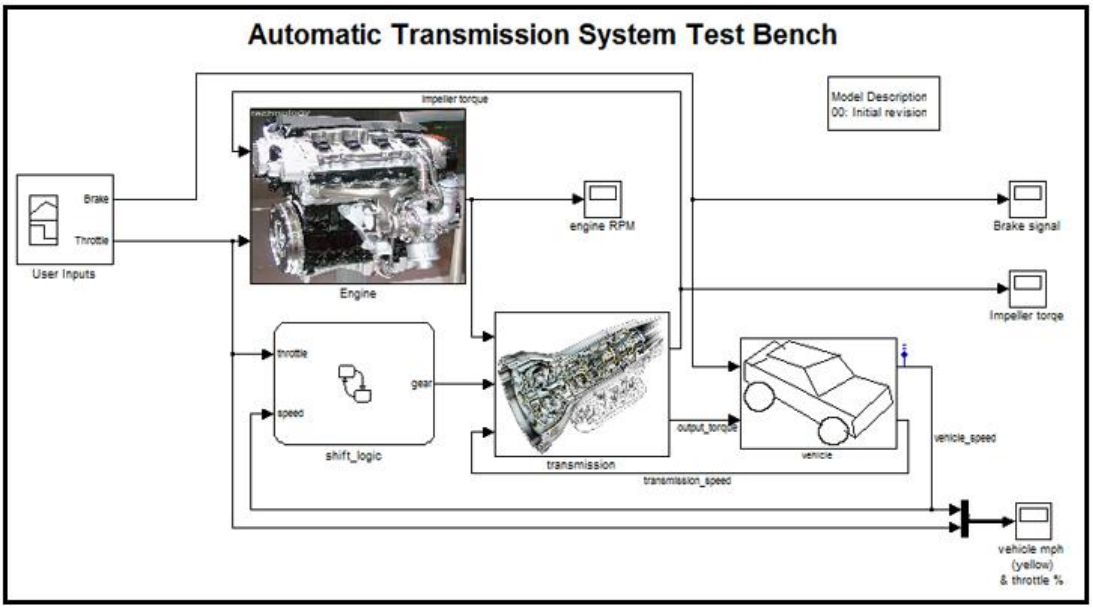

Figure II-23 – Vehicle Simulink simulation model [109]

II.4. Computer Hardware Characteristics

The speed of the simulations can be hardly correlated to the floating point math operations of the system. In general, several factors affect the performance of the simulation software: CPU (Central Processing Unit), Processors/Cores, RAM and OS (Operating System).

Table II-1 presents the hardware characteristics of the computer used for simulations during the PhD work (PC-LHEEA 114) and of the recommended ones by Gamma Technologies.

Computer system	PC-LHEEA 114	Recommended
CPU	3.4 GHz	3.4 GHz
Processors/Cores	8/Quad-Core	8/Quad-Core
RAM	8 GB	8GB
OS	64 bit (Windows)	32/64 bit (Windows)

Table II-1 – Hardware Characteristics of the Computer

Note that a GT-Power solver license is required for each core processing a simulation. A multi-core computer running with a single solver license is limited to solve one model at a time (parallel processing mode).

II.5. Hot-Film Air-Flow Sensor Calibration

To measure the average air mass flow rate aspirated by the internal combustion engine, a hot-film air-flow sensor is used (Figure II-24). It is a mini CTA probe supplied by Dantec Dynamics. The sensor is made of a wire whose resistance is measured at a determined temperature. The resistance parameter changes as a function of the temperature of the wire. The latter depends on the velocity of the fluid. The wire temperature variation induces a variation of its electrical resistance and subsequently of the voltage at its terminals. Then, the flow velocity can be determined. Knowing the density and the flow area, the air mass flow rate can be deduced. This device allows measuring low air flow (Calibrated range: 0.005 - 500 m/s, precision:$\pm$ 3% $\dot{m}$). The calibration phase of this sensor is compulsory before any measuring campaign. Therefore, a tube with fixed geometry and known dimensions, placed downstream a sonic nozzle, is used (Figure II-25). The new polynomial function is then identified (Figure II-26). The hot-film sensor is used only in the case of a single cylinder engine, were air mass flow rate value is not high for different engine rotational speed (the $Qm_{usefull}$ in Figure II-26 represents the range of use of the flow meter) . For other engines presented in this work, another air flow sensor is used and it will be described later on.

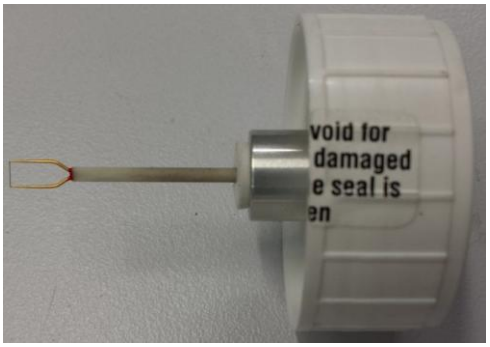

Figure II-24 – Mini CTA hot-film probe, Dantec Dynamics

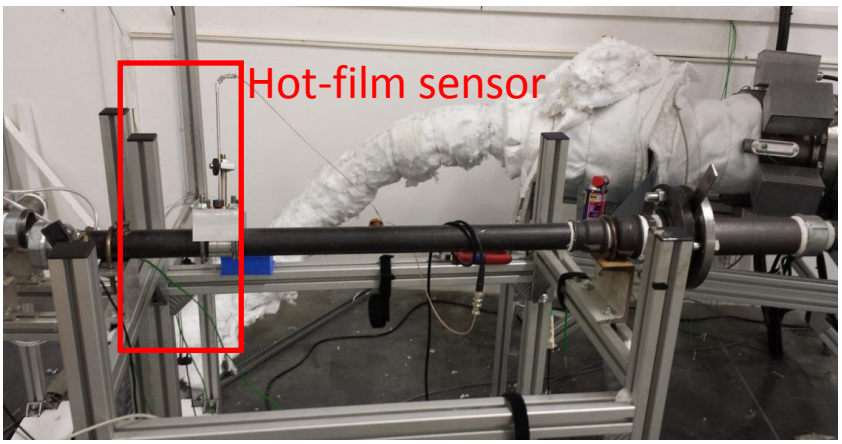

Figure II-25 – Calibration Process

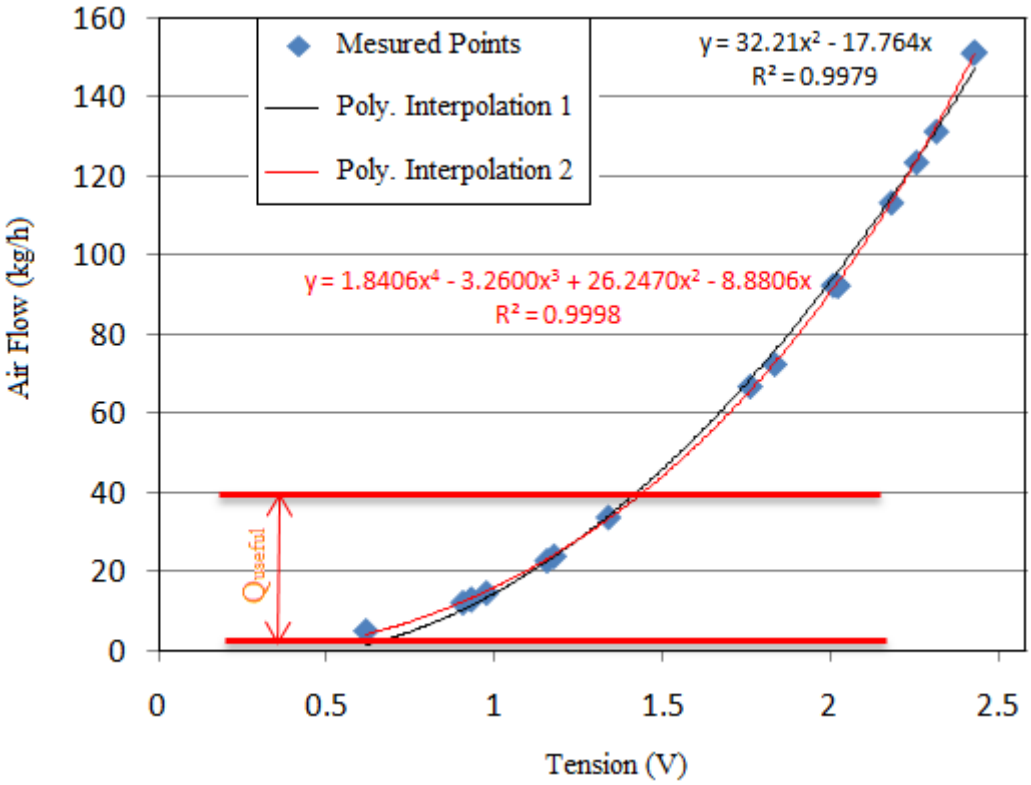

Figure II-26 - Flow Meter Calibration

II.6. Engine Descriptions:

In this section, the engines used for model validation are described. Different types of engines are presented: single cylinder, three cylinder and four cylinder engines.

II.6.1 Single Cylinder Engine

The first phase of model validation is the use of a single cylinder engine driven by electric motor. The engine is installed in LHEEA/TSM laboratory (Table II-2). In this PhD work, combustion in this engine is not taken into consideration for different reasons:

1. Better engine speed control: the crankshaft rotation speed depends on the electric motor speed.
2. The effect of fuel injection and combustion on the pressure upstream of the intake valve is negligible [3]
3. The control system of the driven engine is not sophisticated (no fuel injection, no spark ignition timing, etc…).

The intake geometry of the single cylinder engine is a simple tube of 985 mm long with an inner diameter of 30 mm (Figure II-27). Using KISTLER sensor (Calibrated Range: 0…5bar abs/±5 mbar error/0…80°C) with a 4624A piezo-resistive Amplifier, mounted 80 mm away from the valve seat, the instantaneous pressure upstream of the intake valve was measured. The cylinder pressure was also measured using 6117BFD17 sensor, which is mounted at the end of the spark plug (Calibrated Range: 0…200bar abs/±1.2 bar error/). Furthermore, the average air mass flow rate was measured at the exhaust system using a hot wire (Calibrated

Range: 0…50 kg/hr / ±0.5 kg/hr error). A volume of 200 L was mounted between the exhaust tube and the air flow sensor to have a stabilized flow while taking measurements (Figure II-28). Finally, the instantaneous pressure in function of crank angle (CA) was registered for different engine speed. Similarly, the volumetric efficiency for different engine speed was calculated using the air flow measurements provided by the sensor and the theoretical air mass flow rate as follows:

$$\eta = \frac{qm_{act}}{qm_{th}} \tag{II-7}$$

$$qm_{th} = \rho \times Disp \times \frac{N}{120} \tag{II-8}$$

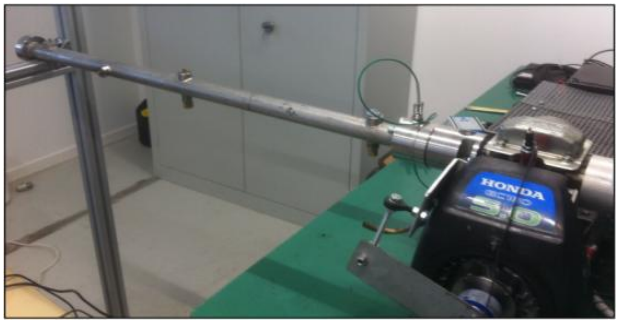

Figure II-27 – Single Cylinder Engine

Figure II-28 – 200 L volume

Engine characteristics	Manufacturer data
Model	Honda GC 160
Bore	64 mm
Stroke	50 mm
Compression Ratio	8.5:1
Total Displacement	160cm^3
Minimum RPM	1260 rpm
Maximum RPM	3000 rpm

Table II-2 – Engine Specifications

The engine was built in GT- Power software (Figure II-29). The characteristics of each part of the engine are well specified in each related template. First, the boundary conditions are specified using appropriate template (EndEnvironment Template). The atmospheric pressure and temperature are then specified. The intake and exhaust geometry and the cylinder head characteristics (length, diameter, surface roughness, heat exchange with walls, material, etc…) are specified using tube template. Both intake and exhaust valves are specified using valve template (The valves opening and closing time, maximum lift, diameter, etc…). The valve is closed at 253 °CA (Figure II-30). In cylinder template, engine specifications were implemented on corresponding parameter in the template. Engine operation point can be defined by user using the crank template. Engine operation running time can be specified by user as well. For example, user can define one second of real engine operation time. The simulation can be stopped automatically when model converges. The convergence criterion can be defined by user also. The criterion can be the in-cylinder air mass flow for example. A

value of this later is recommended by GT-Power, which is equal to 0.02kg/h. It means that the model convergence depends on this value. After many iterations (when $\Delta q_m \leq 0.02$) the simulation stops automatically.

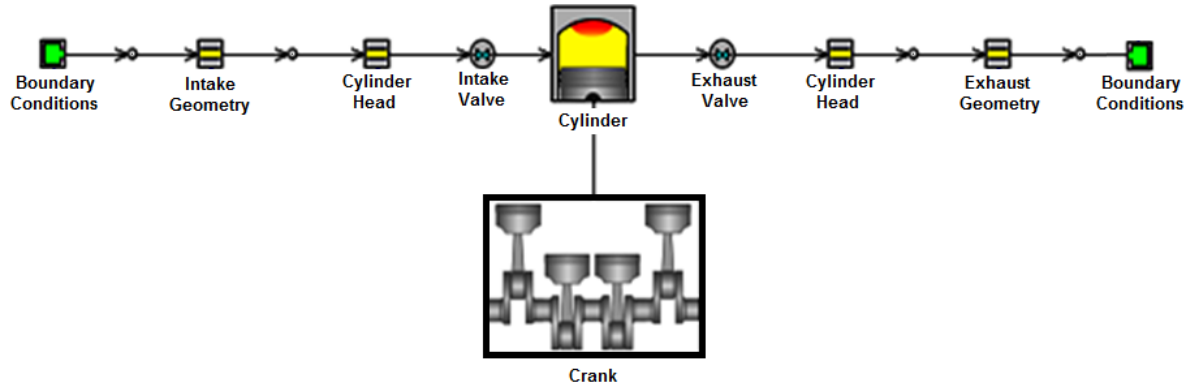

Figure II-29 - GT-Power Single Cylinder Engine Model

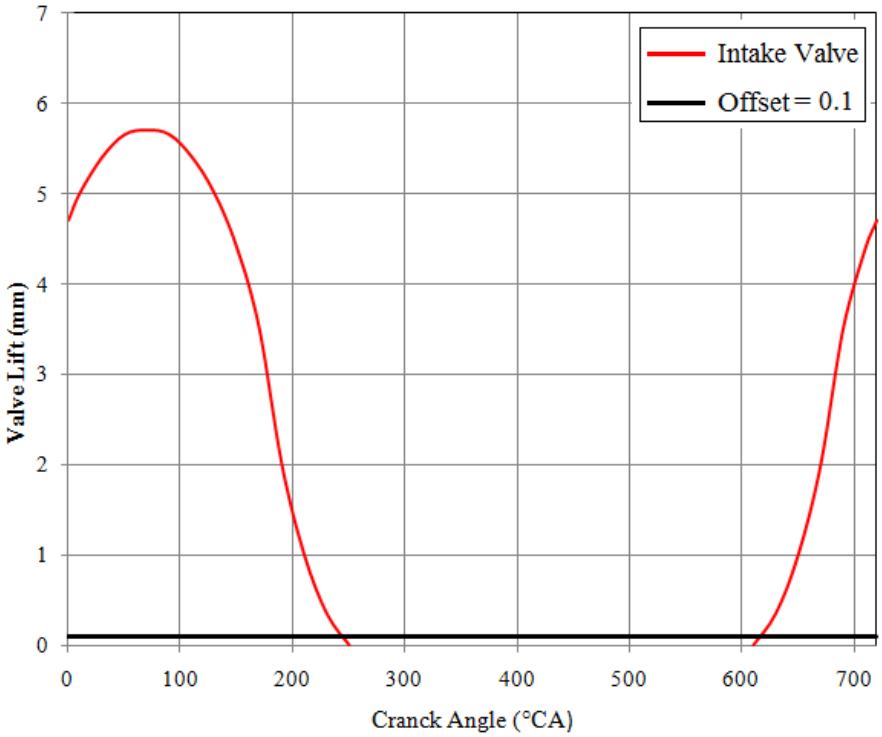

Figure II-30 -Intake Valve profile

The tuning of the virtual engine is based on the experimental results. This step is very important before implementing the identified transfer function model in the simulation software. Additional friction coefficients and length correction are applied on the intake and exhaust geometry of the engine. The virtual sensors are added to the engine and they are located at the same place as the real sensor in reality. In this case, and after certain iterations, the GT-Power Native model will be tuned and ready to use. The tuning is done for each engine operation point.

II.6.2 Three Cylinder Engines

EB2 is a 3 cylinder gasoline naturally aspirated PureTech (VTi) engine. Part of EB family, the engine specifications are presented in Table II-3.

Figure II-31 - Three Cylinder Engine

Engine characteristics	Manufacturer data
Model	EB2 PSA
Bore x Stroke	75 mm x 90.5mm
Compression Ratio	11:1
Total Displacement	1199 cm^3
Max Power	82ch @ 5750 rpm
Max Torque	118 N.m @ 2750 rpm
Valves per cylinder	4
Type of Injection	Indirect multi-port
Emission level	€5/6
VVT System	Yes

Table II-3 – Engine Specifications

The GT-Power engine model at full load was calibrated according to several tests on the engine. In addition, the intake system was separately calibrated using the real and the virtual dynamic flow bench (Figure II-21). The final virtual model is presented in Figure II-32, where only the intake system and the cylinders are shown. Three Kistler Sensors were added to the engine (Figure II-34). The sensors were implemented at the end of each runner (Figure II-36). Each sensor measures the relative pressure before the intake valves of each cylinder. The purpose behind these measured values is to have different experimental data, at different engine operating points, in order to validate the simulation results given by the transfer function model. The model is considered as accurate when measured and simulated relative pressures are close enough ($\Delta diff \rightarrow 0$). The experimental volumetric efficiency can be also calculated using the air mass flow meter, located at the intake system of the three cylinder engine (before the air filter) (Figure II-35)

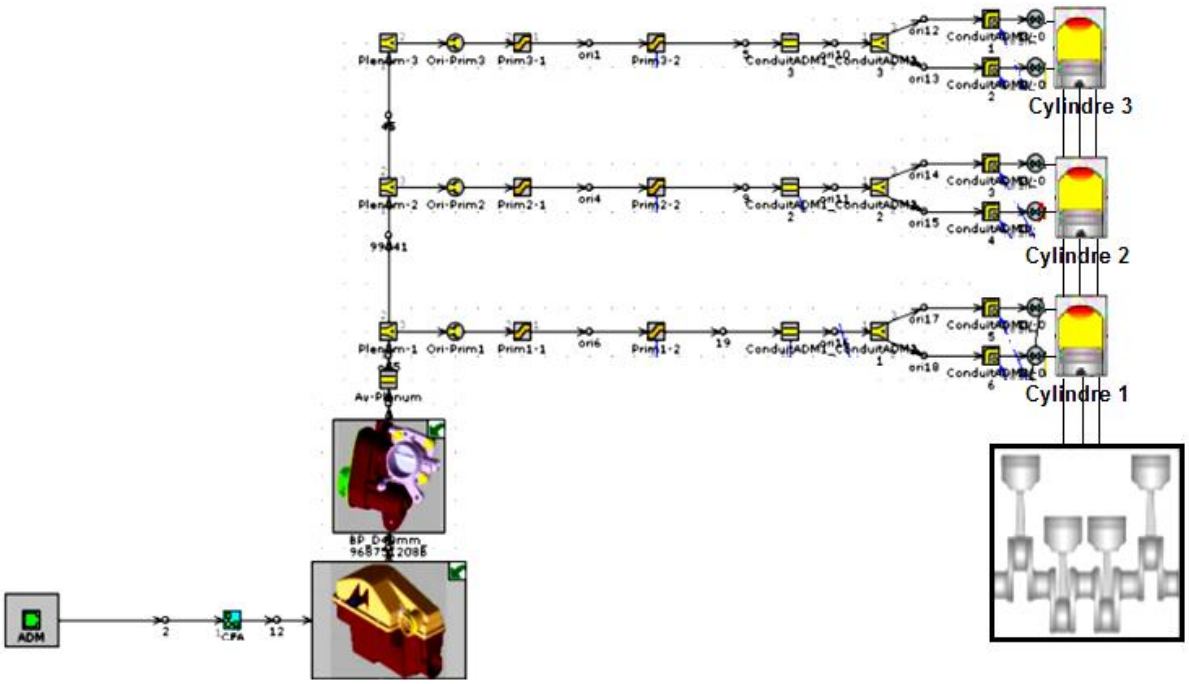

Figure II-32- Three Cylinder Engine Model

The main components in Figure II-32 are:

- Boundary conditions: This allows taking into consideration the atmospheric pressure and temperature. Air humidity and different other characteristics are also specified using the EndEnvironment template.

- Air filter: it is modeled using a set of tubes and junctions. Usually, this component is modeled/replaced by pressure losses coefficients.

- Throttle valve: in this template, valve dimensions can be specified. The opening valve position can be also modified by simply changing the corresponding parameter in this template.

- Cylinder: In this application, combustion is taken into consideration. The combustion laws are also specified in this template as well as the cylinder geometric specifications.

- Manifold: the volume of the manifold is specified using specific templates (junctions), where the position of the runners and the distances between them are also implemented to the model. Runners are modeled using tubes.

- Cylinder head: since two intake valves per cylinder exist, the cylinder head specification is not easy. A junction is used in order to specify the angle of the exit ports (linked to the intake valves).

- Intake valves: valve geometry parameters where specified used the proper template. The valve opening and closing time are specified as well (Figure II-33)

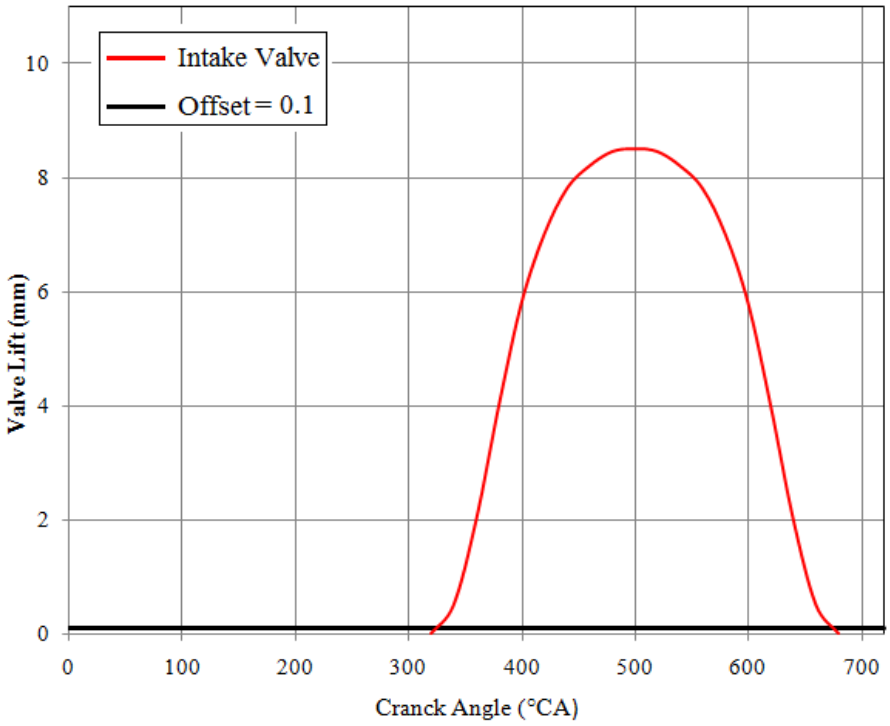

Figure II-33 - Intake Valve profile of cylinder number 1

Figure II-34Kistler Sensor and Amplifier

Figure II-35Air mass flow meter

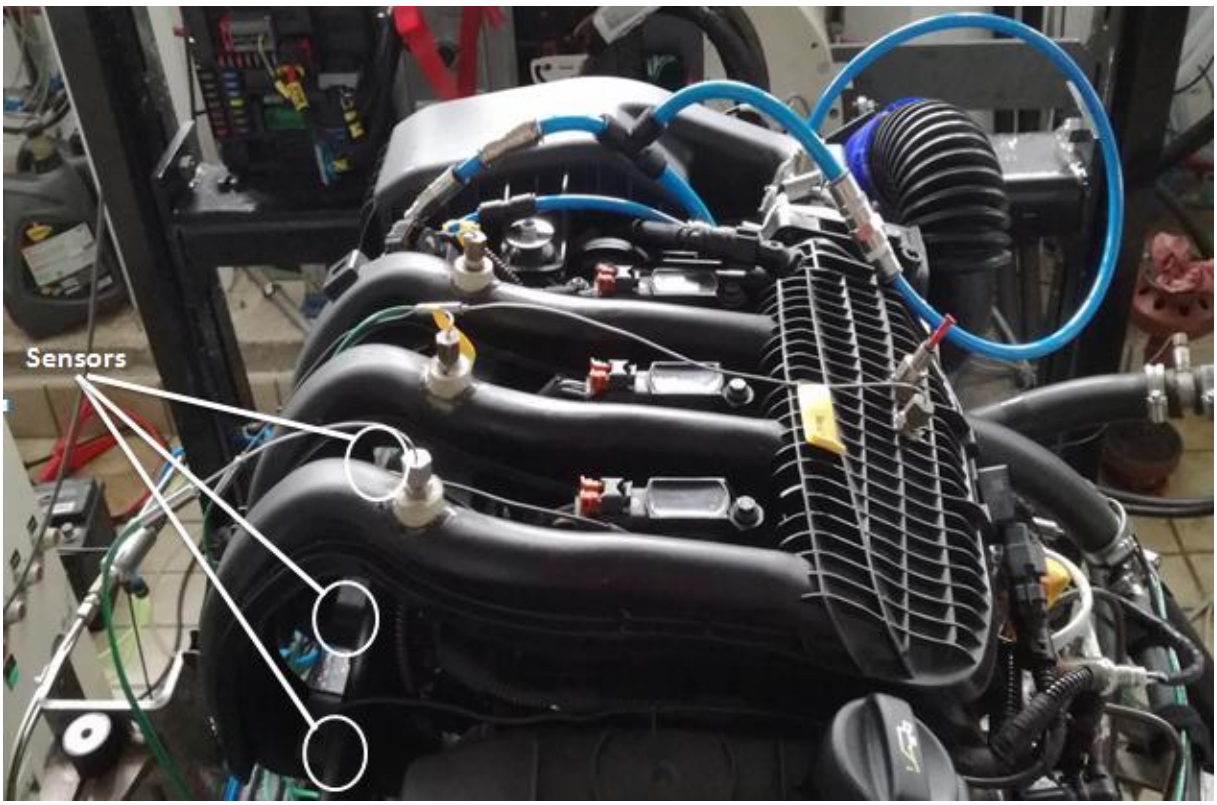

Figure II-36 Intake Manifold of the three cylinder engine

II.7. Uncertainty Calculation:

The physical models presented in this work will be compared to experimental results in order to validate the methodologies. However, uncertainty calculations are unavoidable before any model validation. Each measurement is subject to some uncertainties. The main sources of measurement uncertainties are: measuring instrument, the measured item, the environment, the operator, etc… Once the uncertainty in a measurement is evaluated, the result can be properly judged. It is important not to confuse the terms 'error' and 'uncertainty'. Since the 'error' is the difference between the true and the measured values of the measured object, the 'uncertainty' is a quantification of the doubt about the measurement result.

In this PhD work, five main sources of measurement uncertainty can exist:

1. Acquisition: amplifier, noise, reading, analogical-numerical conversion
2. Sensors: low precision sensor, measuring range, non-linearity in the measurement range.
3. Calibration: zero offset which is due to sensor components aging.
4. Installation: the air flow sensor, for example, should be placed before air filter were flow pulsations are not significant.
5. Environment, temperature, elevation, humidity, etc…

There are two approaches for uncertainty estimation [110]:

1. Type A: evaluation of uncertainty by statistical methods. Estimating by repeating the same measurements several times. The average of the measurements is then calculated (II-1) as well as the standard deviation (II-2). Finally the uncertainty is calculated using equation (II-3).

$$\overline{X} = \sum_{i=1}^{n} \frac{X_i}{n} \tag{II-1}$$

$$\sigma = \sqrt{\frac{\sum_{j=1}^{n} (X_j - \overline{X})^2}{n-1}} \tag{II-2}$$

$$\text{Uncertainty}_{type\ A} = \frac{\sigma}{\sqrt{n}} \tag{II-3}$$

2. Type B: evaluation of uncertainty by non-statistical methods. In other words, uncertainty is calculated from past experience of the measurements, calibration certificates, manufacturer's specifications, published information, etc... These informations give the lower and the upper limits of the uncertainty. The distribution between these limits is considered as uniform (rectangular distribution (Figure II-37)). In this case, the uncertainty is calculated using equation (II-4).

$$\text{Uncertainty}_{type\ B} = \frac{Full\ width}{\sqrt{3}} \tag{II-4}$$

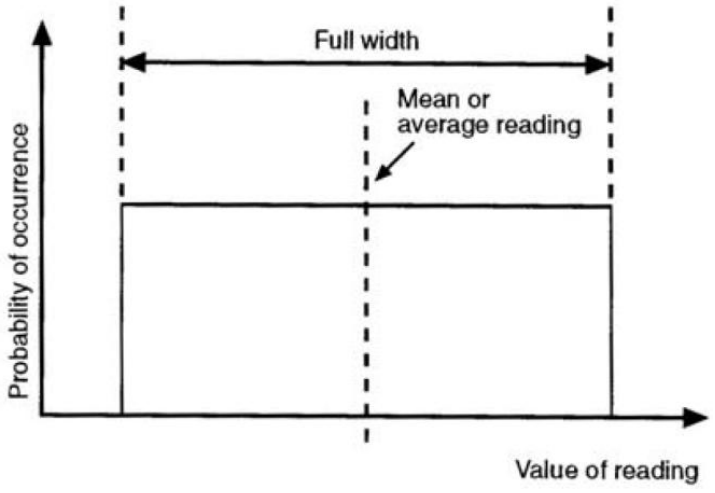

Figure II-37 – Sketch of a rectangular distribution[110]

If $X=f(Y_j)$, with $j=1,2,3,\ldots, n$, the root-sum-square (RSS) method is used to find the uncertainty on X (II-5) [111].

$$\delta X = \sqrt{\sum_{j=1}^{n}\left(\frac{\partial X}{\partial Y_j}\delta Y_j\right)^2} \tag{II-5}$$

In this work, the thermodynamic variables measured using sensors are:

- The pressure
- The air mass flow rate

Thus, the uncertainty calculation of these variables is based on the following equations:

- Pressure variable:

The static pressure measured upstream the intake valve is given by equation (II-6):

$$p = p_{relative-measured} + p_{atm-measured} \tag{II-6}$$

$$\delta_p = \sqrt{\left(\frac{\partial p}{\partial p_{relative-measured}}\delta_{p\ relative-measured}\right)^2 + \left(\frac{\partial p}{\partial p_{atm-measured}}\delta_{p\ atm-measured}\right)^2} \tag{II-7}$$

$$\delta_p = \sqrt{\left(\delta_{p\ relative-measured}\right)^2 + \left(\delta_{p\ atm-measured}\right)^2} \tag{II-8}$$

Where δ_p is the uncertainty of measured pressure.

- Air mass flow rate:

The corrected value of the air mass flow is a function of the total pressure and temperature:

$$qm_{corrected} = qm.\frac{\sqrt{\frac{T^*}{T_{ref}}}}{\frac{p^*}{p_{ref}}} \tag{II-9}$$

$$\delta_{qm_{corrected}} = \sqrt{\left(\frac{\partial qm_{corrected}}{\partial qm}\delta_{qm}\right)^2 + \left(\frac{\partial qm_{corrected}}{\partial T_1^*}\delta_{T_1^*}\right)^2 + \left(\frac{\partial qm_{corrected}}{\partial p_1^*}\delta_{p_1^*}\right)^2} \tag{II-10}$$

$$\delta_{qm_{corrected}} = \sqrt{\left(\sqrt{\frac{T_1^*}{T_{ref}}}.\frac{p_{ref}}{p_1^*}\delta_{qm}\right)^2 + \left(\frac{qm.p_{ref}}{2p_1^*\sqrt{T_{ref}\,T_1^*}}\delta_{T_1^*}\right)^2 + \left(\frac{qm.p_{ref}.\sqrt{T_1^*}}{\left(p_1^*\right)^2.\sqrt{T_{ref}}}\delta_{p_1^*}\right)^2} \tag{II-11}$$

Where $\delta_{qm_{corrected}}$ is the uncertainty of air mass flow rate.

For each sensor, the uncertainty is then calculated in Table II-4:

Sensor	Type	Range	Precision	Uncertainty
Pressure	KISTLER 4624A piezo-resistive sensor	[0-5] bar	±5 mbar	5/√3
	Cylinder pressure sensor 6117BFD17	[0-200] bar	±1.2 bar	1.2/√3
	Atmospheric pressure sensor	[0.8-1.1] bar	±3 mbar	3/√3
Air Mass flow	Mini CTA- hot wire	[0-50] kg/h	±0.5 kg/h	0.5/√3
Temperature	THGN810	[-30- 60]°C	±0.1°C	0.1/√3

Table II-4 - Characteristics of each sensor used in experimental tests

All the numerical and experimental facilities presented in this chapter helped to achieve the main objective of this PhD work. The dynamic flow bench and Matlab are used for the identification of transfer functions. GT-Power software is used for the complete engine simulation, where the identified transfer functions will be implemented. And finally the experimental test benches allowed validating the simulation results (and then proving the high accuracy level of the model) are presented.

III. Transfer Function Model

From a physical point of view, when the frequency of the excitation source is equal to the natural frequency of an element, the system tends to vibrate with the highest amplitude values. This phenomenon is called "Resonance". In internal combustion engine, the excitation source is the intake valve. The frequency of opening-closing of this latter is related to the engine rotational speed. For a particular engine operating point, the frequency of the valve is equal to the natural frequency of the intake system. Thus a resonance of the system will occur. A wave will propagate in the system with a high amplitude .This phenomenon leads to a high pressure value at the intake valve position. By taking advantage of this high energy before the intake valve opening (IVO), engine filling can be improved. The transfer function is a source impedance measurement method when the tested geometry is considered to be the acoustic load. The natural frequencies of an element can be identified using dynamic flow bench. The transfer function contains informations related to the flow behavior, such as inertia, damping coefficient, frequencies and harmonics. In this chapter, the transfer function identification methodology and model improvement will be presented. Later on, the model validation will prove the ability of this function to model the unsteady and compressible behavior of the flow. The challenge is still the accuracy of the model versus simulation time. After making the coupling with the one-dimensional non-linear code, the results will be discussed according the accuracy and the computational time of the new model compared to the one-dimensional native approach.

III.1. Introduction

The firing order of the engine, piston motion and the valve timing are leading to a transient pressure excitation [112]. The intake valve is the main source of unsteadiness of the flow in the intake system of an internal combustion engine. The valve helps the engine to breath when it is open (flow source) and creates pressure waves while and after closing (excitation source). In the first case, the intake system is open at both ends. Then the pressure waves created is considered as negligible compared to the case were the intake system is open at one end (after closing the valve) [31]. The resulting pressure propagation in the intake system has a significant effect on the volumetric efficiency. Acoustic supercharging occurs at a specific engine rotational speed, when the pressure upstream the intake valve is high at the intake valve closing time. This natural overcharge phenomenon is called "Ram effect". The volumetric efficiency can be improved at low and medium engine rotational speed with the help of pressure wave propagation [26][113]. As shown in the literature study about this topic, many authors tried to elaborate models which help to simulate perfectly the flow behavior in the intake system. The computational time of these models is considered as too high compared to the real time engine operation. Other authors neglected some important phenomena, such as the wave action, in order to reduce the computational time of their models. The final results did not show good accuracy level. It is well known that the one-dimensional approaches take into account the unsteady behavior of the air flow in the intake system of internal combustion engine. In fact, the precision of these models increases by increasing the nodes number (by decreasing the length interval). Unfortunately, the computational time of one-dimensional models increases when high precision of the model is needed. For this reason, the idea behind the Transfer Function model was born.

The objective is to replace the geometries in the simulation code, which are modeled using one-dimensional schemes, by a function which allows conserving the accuracy level with less computational time. Taking for example the intake system of the internal combustion engine, this geometry was built in the simulation software using templates (tubes, junctions, air filter, etc…). The modeling of these templates is based on one-dimensional schemes. The informations which is offered with these templates are:

- The pressure value between the input and the output of the whole intake system and the calculated pressure losses values (roughness of the internal surface, damping parameter, etc...)
- The physical parameter of each part of the intake system (length, diameter, etc…). These main parameters affect the pressure upstream the intake valve. They specify the natural frequencies of the geometry as well.
- Calculate the heat transfer of each part's wall

The resultant calculated useful value from all of the informations listed before is the pressure upstream the intake valve, which controls the volumetric efficiency of the engine. If the new model can reproduce the same response with less computational time, this will not affect the global results of the main model (consumption, emissions etc…). But it will help to get results faster and this is exactly the aim of the study presented in this manuscript.

The Transfer Function is then a zero dimensional linear model which correlates input information to an output response. In this work, the Transfer function is the ratio between relative pressure (output of the system) and air mass flow rate (excitation source). It is a source impedance measurement method when the tested geometry is considered to be the acoustic load. The transfer function is equal to the impedance at the part's outlet (in the position close to the intake valve). The transfer function includes complete information about resonance frequencies, inertia and damping of the intake line at a specific point. In addition, this mathematical function allows prediction of the pressure wave behavior created by any unsteady flow excitation.

For the case of multi-cylinder engine, the intake system is always in a configuration where it is open at both ends (since at least one valve is open per engine cycle). Then, even the half wave resonance frequencies should be taken into consideration in the final model.

The complete methodology will be presented in this chapter: identification process, calibration, implementation in the simulation software and finally the validation procedure.

III.2. Model History:

III.2.1 General description of the model

The idea has been presented by Fontana *et al*. [108][114] as a new methodology for evaluating the thermodynamic properties of the air in the intake system of an internal combustion engine. The method consists in stimulating an intake system using air flow as an excitation profile, and then registers the pressure response of this geometry. Compared to the models presented in the literature of this topic, Fontana's idea presented two innovative concepts:

- The use of a dynamic flow bench to generate pressure waves which are similar to those observed on a real engine after closing the intake valve. As presented in Chapter II, the air mass flow level has to be representative of the engine and has to be exactly known in time and frequency domain. A particular attention is paid on the very quick valve closing time of the testing equipment, in a way to measure the dynamic behavior in the largest possible bandwidth.
- The relative pressure variation is measured using a sensor located on the tested geometry and near the shutoff component of the dynamic flow bench. The pressure response has to be induced only by tested part with no influences of the measurement facility itself.

The transfer function is then a linear relation between relative pressure and air mass flow rate. The data offered by the dynamic flow bench after doing tests, allow finding the measured transfer function:

$$TF_{measured} = \frac{FFT\,(p_{relative})}{FFT\,(qm_{imp})} \tag{III-1}$$

Fontana *et al.* [114] built a mathematical model (in s-domain) of the air intake system based on the electrical analogy, which uses the well-known results of the RLC circuits.

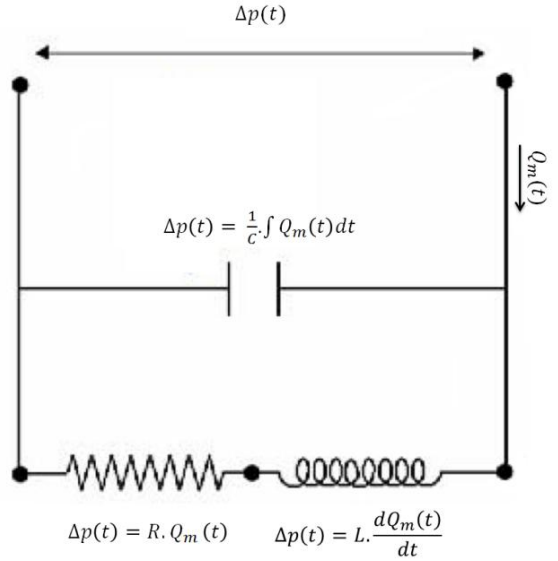

Figure III-1 – Parallel RLC electric circuit

The simplified model is a second order model illustrated by Figure III-1 and defined by:

- Air mass oscillation = Induction L
- Delimited volume = Capacitance C
- Energy dissipation = Resistance R
- Air mass flow = Electrical current
- Relative pressure = Differential voltage

The differential equation of this second order electrical model (III-2) describes the unsteady response of air (relative pressure) in function of the resonance pulsation of the system ω_0, the damping factor which represents the dissipation energy through the part ε, the inertia parameter $X_{inertia}$ (source of the ram effect) and the steady parameter X_{steady} which is calculated using the pressure drop in steady flow conditions on the dynamic flow bench.

$$\frac{1}{\omega_0}\frac{d^2 p_{rel}}{dt^2}+\frac{2\varepsilon}{\omega_0}\frac{dp_{rel}}{dt}+p_{rel}=X_{steady}qm_{imp}+X_{inertia}\frac{dqm_{imp}}{dt} \tag{III-2}$$

The transfer function is then identified using Laplace representation applied in equation (III-2). Using the modal decomposition theory [50], the complete model is then a superposition of second order systems:

$$TF(s)=\left(X_{steady}+sX_{inertia}\right)\sum_{i}^{n}\frac{a_i}{\left(\frac{s}{\omega_{0i}}\right)^2+2\varepsilon_i\left(\frac{s}{\omega_{0i}}\right)+1} \tag{III-3}$$

Where n is the number of natural frequencies of the tested part (including fundamental frequency and its harmonics) and a_i represents the energy proportion of each resonance modes, also called weight coefficient:

$$\sum_{i}^{n} a_i = 1 \tag{III-4}$$

Thus, the function is a complex vector with n lines and one column. The number of samples in the vector can be specified by user (using a window function). In order to quantifies the transfer function with the resonance frequencies and corresponding damping factors, the transfer function should be written in s-domain. For this reason, an identification process is performed using a mathematical multivariable optimization tool that searches for the best combination of parameters [115]. This identification procedure is internally developed by Mann+Hummel.

Fontana *et al.* [114] used this methodology to study the leakage of "Active Intake Manifold" (Figure III-2). Active manifold is usually characterized by a mechanical switching system, which varies the runner length depending on the rotational engine speed. However, a resonance effect at low rotational engine speed, which allows improving the cylinder filling at this engine operation point, can occur using a configuration with long runners. A configuration with short runners is used to get the resonance effect at high rotational engine speed.

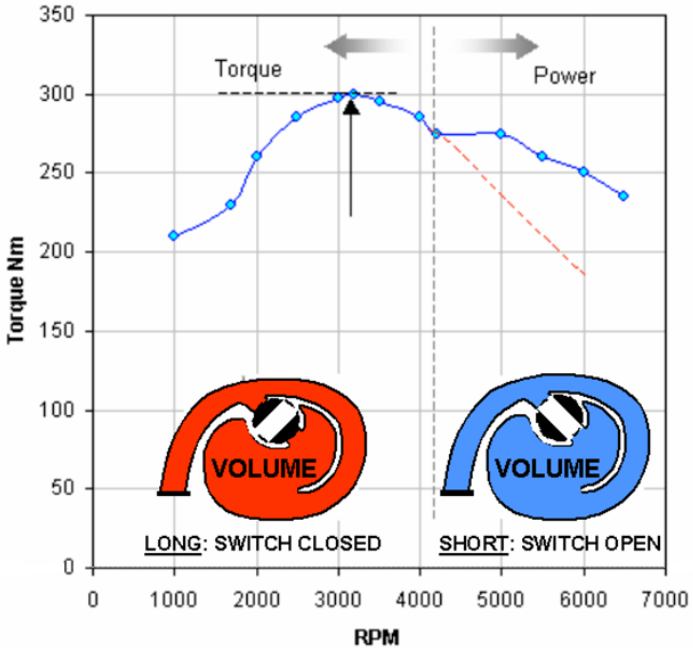

Figure III-2 – Active Intake Manifold [114]

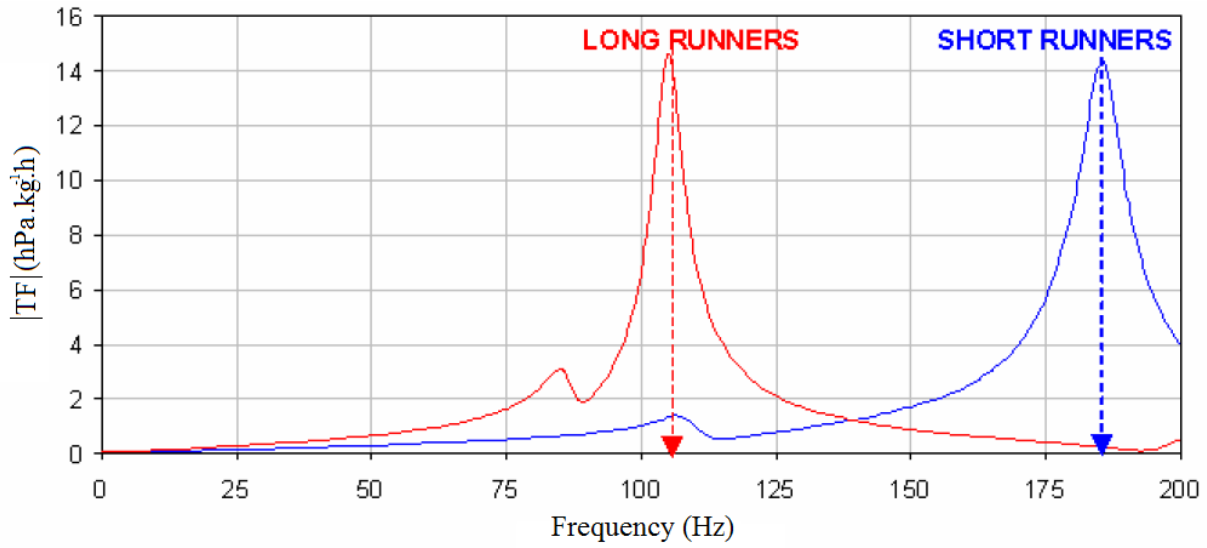

Figure III-3 – Modulus of TF of two configuration (with long runner and short runner) [114]

Using identified transfer functions for each configuration (Figure III-3), the switch point at a specific rotational engine speed can be determined to increase the maximum power of the engine while keeping a good drivability. The leakage effect on the pressure upstream the intake valve can be determined as well using these transfer functions (Figure III-4).

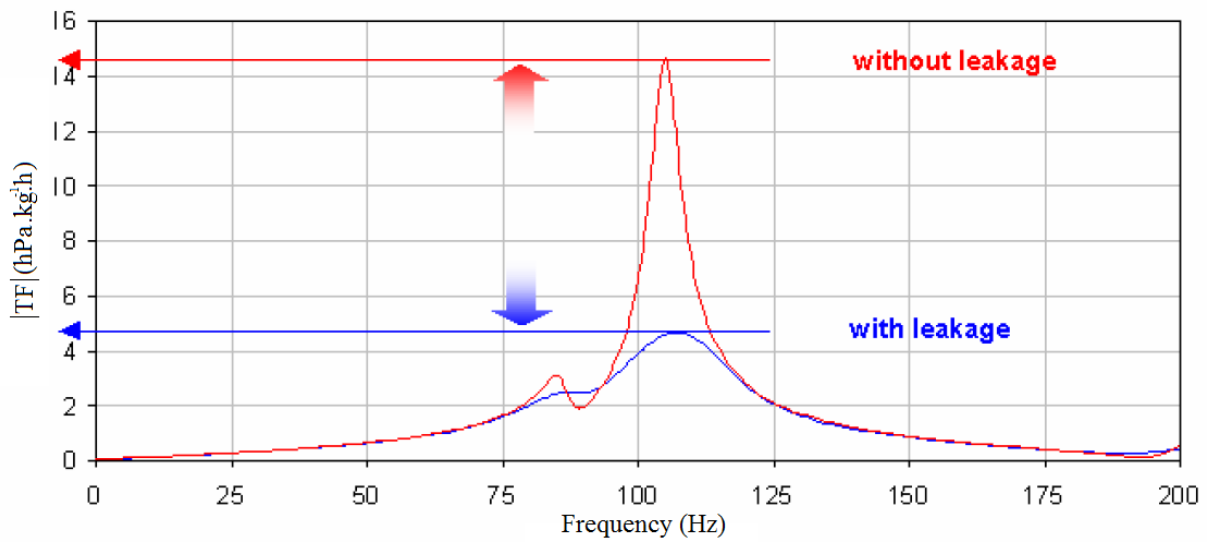

Figure III-4 – Leakage effect on the amplitude of the transfer function [114]

Chalet *et al.*[116][117][118][49] and Mahe *et al.*[13][119] used mechanical analogy to build a mathematical model of the air intake system that takes into account non-steady effects of flow. The simplified model is also a second order model illustrated and defined by:

- Air mass oscillation = Mass M
- Viscous effects = Damper C
- Compressible characteristic of air = Spring K
- Flow velocity = Derivative of the mass displacement

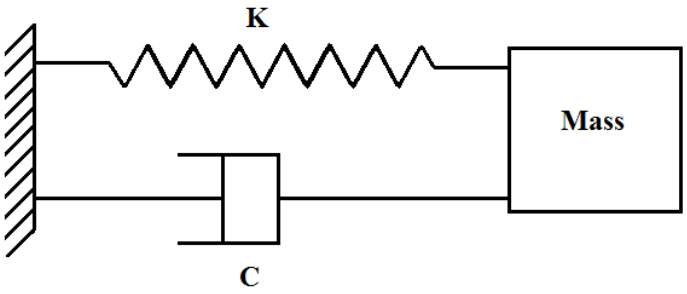

Figure III-5 – A mass spring damper system

Based on this analogy, the differential equation of the system is identified:

$$\frac{d^2p}{dt^2} + 2\varepsilon\omega_0 \frac{dp}{dt} + \omega_0^2 p = X_{inertia} \frac{du}{dt} \tag{III-5}$$

This latter does not take into account static pressure. In other words, the differential equation (III-5) describes the system only after closing the shutoff component, where static and relative pressures were dissociated. The air mass flow rate was replaced by velocity parameter as well in Equation (III-5). The Transfer Function is then defined by solving the differential equation in frequency domain:

$$TF(s) = \frac{P(s)}{U(s)} = \sum_i^n \frac{a_i X_{inertia} s}{s^2 + 2\varepsilon_i \omega_{0i} s + \omega_{0i}^2} \tag{III-6}$$

The parameter of transfer function model are identified using a shock tube (for more details please refer to [119][120]) and an automated identification process based on least squares method. The main purpose of the work of Mahe[13] is to qualify the impact of the intake system on the internal combustion engine filling. Therefore, the intake geometry is replaced by its transfer function in the engine simulation software (GT-Power) (Figure III-7). This coupling is made using Simulink (Figure III-8). This latter receives the air flow signal from GT-Power model, and then provides it the pressure response calculated from the transfer function. The model was validated on a single cylinder engine. The model validation was conducted using precision criterion on volumetric efficiency (III-7) and on instantaneous pressure upstream of the intake valve (III-8).

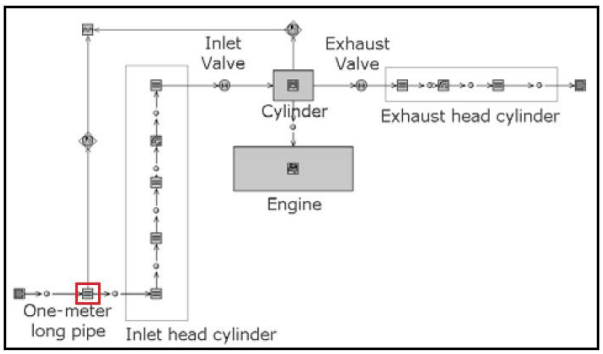

Figure III-6 – GT-Power Native Model

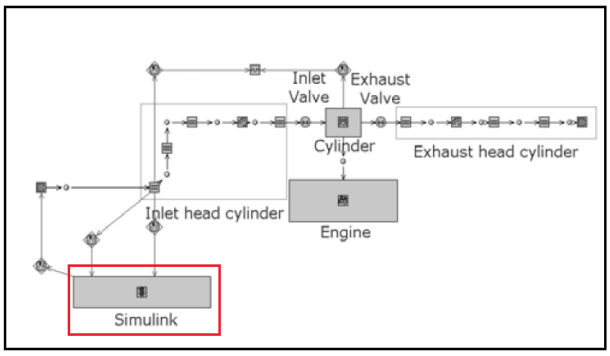

Figure III-7 – GT-Power/Simulink Coupled Model

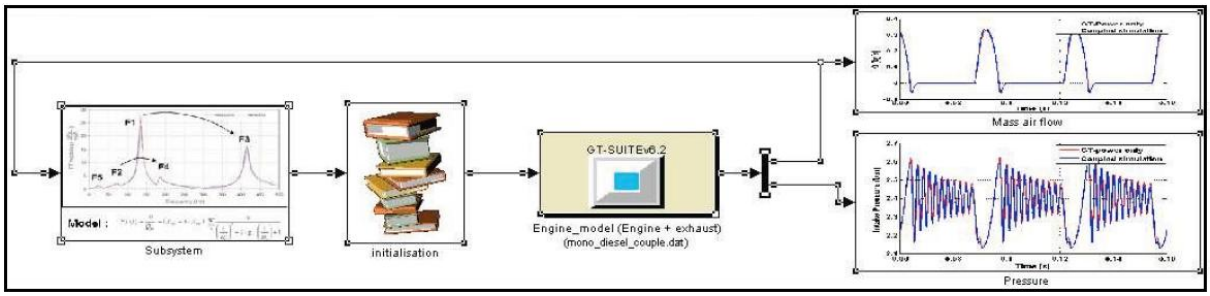

Figure III-8 – Simulink routine

$$qm_{th} = \rho Disp \frac{N}{120} \tag{III-7}$$

$$\eta = \frac{q_{mexp}}{qm_{th}} \tag{III-8}$$

The same analogy is used by Mezher *et al.*[121]. However, the velocity is replaced by air mass flow rate parameter in equation (III-5).

$$TF(s) = \frac{P(s)}{Qm(s)} = \sum_{i}^{n} \frac{a_i X_{inertia} s}{\left(\frac{s}{\omega_{0i}}\right)^2 + 2\frac{\varepsilon_i}{\omega_{0i}} s + 1} \tag{III-9}$$

The difference between equations (III-3) and (III-9) is that the transfer function is modeling only relative pressure after closing the shutoff valve on the dynamic flow bench. The static pressure or pressure losses will be added to the transfer function in the simulation using the same methodology of Chalet *et al.*[116]. Based on Bode Diagram, the transfer function parameters $\varepsilon_i, \omega_{0i}, X_{inertia}$ are identified. Once the tests on the dynamic flow bench are done, the modulus of the transfer function (based on equation (III-1)) is plotted in function of frequency. For the case of a simple geometry, a tube of length L and diameter D for example, the pressure waves generated by the dynamic flow bench before closing the shutoff valve are insignificant compared to the pressure losses values. This phenomenon is not modeled in the transfer function. Once the shutoff component of the DFB is activated, the system is then

open at one end and close at the other end. Referring to Figure II-18, the modulus of the measured transfer function presents peaks with low amplitude. This is due to nonlinear effects where the open end is acting as close end because of high wave velocity. Mezher *et al.*[121]considered that these peaks do not affect the transfer function response. Then only peaks with high amplitude, which correspond to quart wave resonance profile, are considered in the transfer function model. These fundamental frequencies (also called resonance frequencies) of the tested geometry can be easily specified. They correspond to the frequencies of the peaks presented in the modulus of the transfer function. In order to identify the parameters of the transfer function, a quality factor is used for each resonance mode i. This latter represents the damping rate of an oscillator. Based on Tooley's work [122], the quality factor can be determined using equation (III-10), where Δf_i represents the bandwidth of each resonance mode where the signal loses 3 dB of maximum amplitude of the peaks. These intermediate calculations allow user to find the damping factor of each resonance mode (III-12). Using equation (III-13)), the inertia parameter can be deduced.

$$Q_i = \frac{f_i}{\Delta f_i} \tag{III-10}$$

$$\Delta f_i = f_{2i} - f_{1i} \tag{III-11}$$

$$\varepsilon_i = \frac{1}{2Q_i} \tag{III-12}$$

$$\left|TF_i\right| = \frac{a_i X_{inertia} \pi f_i}{\varepsilon_i} \tag{III-13}$$

If the model can reproduce the Bode diagram of the measured curve (same amplitude and bandwidth of the peaks), then the identified parameters of the transfer function are perfectly modeling the physical phenomena of the pressure wave's propagation. In this way, the complete transfer function model can be perfectly representative of the system. Mezher *et al.*[121]tested this methodology on different tubes, and the results showed good correlation between identified model and the measured transfer function.

Using a shock tube, the parameters of the transfer function are linked to the geometry characteristics (Length and diameter) in order to be able to identify them without experimental tests on the dynamic flow bench equations (III-14) to (III-17) [121].

$$f_i = \frac{c_0}{4\left(L + \Delta L\right)}(2i - 1) \tag{III-14}$$

$$X_{inertia} = 0.7207\frac{L}{A} \tag{III-15}$$

$$\varepsilon(\%) = 0.6178\left(\frac{L}{A}\right)^{0.1741} \times f^{0.5} \tag{III-16}$$

$$L_i = \frac{L}{i} \tag{III-17}$$

Note that these equations are valid only for a simple geometry. The resonance frequencies are determined at ambient temperature. These frequencies can also be numerically identified at different temperature values according to the following equation:

$$f(T) = f(T_{amb}) \cdot \sqrt{\frac{T_{amb}}{T}} \tag{III-18}$$

Where $f(T)$ is the new resonance frequency at a desired temperature and $f(T_{amb})$ is the resonance frequency measured at the ambient temperature.

Finally, and in order to take advantage of the identified transfer function in simulation process, the function is then integrated in the simulation software (GT-Power) in the same way as in the work of Mahe [13]. The same single cylinder engine is used to validate the results and to show the ability of the new identification process in replacing the numerical identification of the transfer function. The identification process presented by Mezher[121] allows a better understanding of the different parameters of the transfer function and their interactions.

Mezher [65] integrated the position coordinate in the transfer function model:

$$TF(s) = \frac{P(s)}{Qm(s)} = \sum_{i}^{n} \frac{a_i X_{inertia} \cos(k_{oi} x) s}{\left(\frac{s}{\omega_{0i}}\right)^2 + 2\frac{\varepsilon_{x,i}}{\omega_{0i}} s + 1} \tag{III-19}$$

The transfer function can be identified, therefore, at different positions on the intake system. Mezher's transfer matrix methodology [60], [61], [123]–[125] is based on the equation (III-19).

III.2.2 Pressure losses calculation:

The pressure losses in the intake system of an internal combustion engine depend on the air flow passing through it. Two types of pressure losses are responsible for pressure drops along geometry: major losses and minor losses (resulted from changes in geometry)[126]. Major losses are caused by air viscosity (friction of molecules between them and along duct walls). The famous equation of major losses in a circular duct is:

$$\Delta p_{m,i} = \lambda . \frac{L_i}{D_i} . \frac{\rho}{2} u^2 \tag{III-20}$$

The friction coefficient of Darcy λ depends on flow pattern (laminar and turbulent flow). Using Reynolds number, this coefficient can be determined (Moody diagram).

Minor losses are resulted from changes in geometry (disruption of flow). Bernoulli's equation is often used to calculate the pressures losses in function of the geometrical characteristics of

the air intake system components and the average speed of the piston. The total pressures upstream and downstream of each component can be related using equation:

$$\Delta p_i = \xi_i . \frac{\rho}{2} u^2 \tag{III-21}$$

ξ_i is the mass energy loss coefficient which depends on the geometrical characteristics of the components and can be found easily in the literature or may be determined experimentally. Since the flow is considered as quasi-stationary during suction phase, then the fluid velocity can be related to the piston velocity using equation:

$$A_p \overline{u_p} = A u \tag{III-22}$$

Thus, the pressure losses of the whole intake geometry can be deduced:

$$\Delta p = \sum_i \Delta p_i = \rho \overline{u_p} . \sum_i \xi_i . \left(\frac{A_p}{A_i} \right)^2 \tag{III-23}$$

An analogy between pressure losses to be calculated and the reference losses at iso-Reynolds can be made.

According to Fontana *et al.* [114], the steady coefficient in Equation (III-3) is represented on the transfer function by its value at null frequency. Then it is the ratio between the pressure losses at the intake valve and the initial masse flow rate established on the dynamic flow bench before closing the shutoff component:

$$X_{steady} = TF(s=0) = \frac{P(t \le t_0)}{Qm(t \le t_0)} \tag{III-24}$$

In order to build a complete multi-physical model which could replace perfectly the intake geometry of the internal combustion engine, the pressure losses should be added to the transfer function in the routine. Mahe[13] and Mezher[65] dissociated the static pressure from the relative pressure in the transfer function model. Mahe [13] calculated the major and the minor losses of the geometry taking into account Reynolds number, while Mezher[65] used experimental results from dynamic flow bench to find the general loss coefficient as a relation between pressure drop and the square of the air mass flow rate aspirated by the SuperFlow at:

$$loss_{coefficient} = \frac{\Delta p}{(qm_{steady})^2} \tag{III-25}$$

III.2.3 Conclusion

In general, the aim of the previous works was to replace one dimensional representation by a zero dimensional approach. Different transfer function methodologies were discussed in the previous section (Figure III-9).

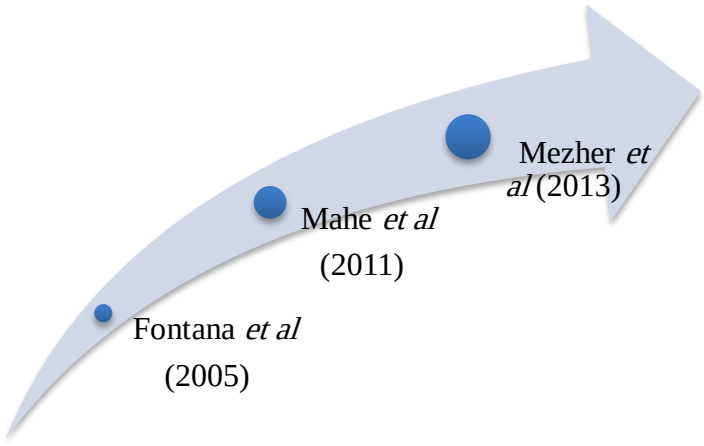

Figure III-9 – Transfer Function Model History

As depicted in Table III-1, model's utility can be discussed regarding seven main parts: identification, integration, time gain, model precision, model validation and temperature parameter integration.

Table III-1 – Evaluation of the different transfer function methodologies

	Fontana *et al.*	Mahe *et al.*	Mezher *et al.*
Identification	✓	✓	✓
Integration	-	✓	✓
Time Gain	-	-	-
Model Precision	-	✓	✓
Model Validation	-	✓	✓
Temperature Parameter Implementation	-	✓	-

✓ **Good** ✓ **Good but** - **Not Included**

Concerning identification procedure, previous works showed different ways of identifying a measured transfer function: Fontana and Mahe used an automated identification process based on least squares method whereas Mezher used a new methodology of identification based on Bode diagram. Both methods showed good ability of identifying a transfer function. In comparison between both methods, the advantage of Mezher's work is that the physical significations of the parameters of the transfer function are conserved. In other words, by applying numerical identification method, the physics behind each parameter of the transfer function is lost. However, numerical identification allows a better identification of the system with low error level especially for complex geometries (the coefficients of the transfer functions are calibrated using optimization algorithms). In terms of integration, the main purpose of the transfer function model is to replace the tested intake geometry by its transfer function in the simulation software. Fontana was not interested in simulation; he only used transfer function model for a better understanding of the pressure wave's propagation in the intake system of an internal combustion engine. Mahe and Mezher used a coupled simulation to integrate the transfer function in the simulation code. Simulink allowed them to replace the intake system of a single cylinder engine by its transfer function. However, the coupling between two simulation software makes the model vulnerable to numerical instabilities at some points and the results can be affected. Both authors were not interested in time gain factor; they were searching for a new high detailed methodology of simulation that can

replace one-dimensional schemes in the simulation software. Good agreement between transfer function model results, one-dimensional GT-Power native model and experimental results on a single cylinder engine at some operation points. However, their works only concern simple geometries. The main reason behind this can be:

- The high computational time of the new 0D/1D model (Transfer Function) compared to 1D representation (GT-Power Native model). Then, by using many transfer functions in the same code, the simulation time of the final model will be very high especially when a coupling with Simulink is performed.
- The error in transfer function identification procedure increases when complex geometries are used.

Finally, the temperature parameter in the transfer function methodology is not taken into consideration in the previous work. Only Mahe quantified the influence of the temperature variation on the frequency of the peaks. But at the end, the transfer function at ambient temperature is used to replace tested geometry.

III.3. Transfer Function Model Optimization

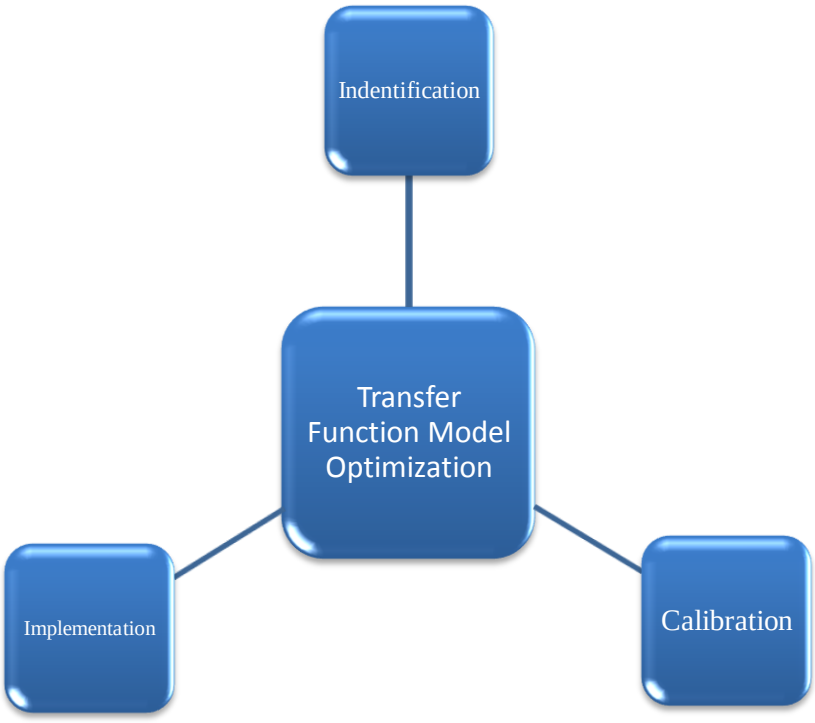

Figure III-10 – Transfer Function model optimization chart

The work performed in this PhD is based on the previous work of Fontana, Mahe and Mezher. The transfer function model optimization is done by focusing on three main parts (Figure III-10):

- *Identification:* a new identification procedure of a measured transfer function will be presented. The new methodology is fast, robust, easy and can take into consideration the half wave resonance mode. The previous work showed that this later can be neglected while identifying a transfer function. However, by testing a complex geometry, these waves cannot be neglected. Later on, the effect of the half waves on the pressure signal at the intake valve in the case of a complex geometry will be presented.
- *Implementation:* the coupled simulation between GT-Power and Simulink, which was used before in order to replace the intake system of the internal combustion engine by the identified transfer function, is replaced by a transfer function from GT-Power library. This helps to reduce simulation time of the coupled 0D/1D (Transfer function) model. A comparison between both methods of integration will be presented later on.
- *Calibration:* In the previous work, only one transfer function was identified at Q_{mexc} =150 kg/hr on the dynamic flow bench. This function is used in simulation code instead of the intake system of an engine running at different speeds. However, a relation exists between damping factor of the transfer function and the initial air flow aspirated by the DFB. Therefore, this function cannot model perfectly the dynamic behavior of the air after closing the intake valve at different engine rotational speed. Later on, a study will show the relation between aspirated air flow, engine rotational speed and the pressure fluctuation after closing the intake valve. Based on this study, different transfer functions should be used in order to increase the precision of the final model. Also, a new function will be introduced, called real time exponential filter. This function helps to reduce the number of transfer functions in the code while conserving a good accuracy level. The final model is tested using a simple geometry of a single cylinder engine to predict the fluid dynamic in a transient engine operation (a NEDC cycle is tested).

III.3.1 Transfer Function Identification Procedure

As discussed earlier, the transfer function TF of the tested geometry is the ratio between relative pressure variable (output of the system) and air mass flow rate excitation (input of the system). The pressure signal, registered using a sensor with high acquisition frequency, contains two main parts: static part due to the steady state before closing the shutoff component on the DFB, and pressure fluctuation part after closing the shutoff valve. In this PhD work, static and relative pressures are dissociated. In other words, only fluctuations will be modelled in transfer function model and pressure losses will be added externally to the output of the transfer function in the simulation code.

Measured transfer function is then obtained from dynamic flow bench tests. The result is a complex vector with n lines and one column. The number of samples in the vector can be specified by user (using a window function). An identification of the measured transfer function is needed in order to replace the intake system of the engine in the simulation code (function can be used only in s-domain). Hence, the System Identification Toolbox (Ident) in Matlab is used. This advanced toolbox provides functions for constructing mathematical

models of dynamic systems from measured input-output data. The recent versions of this toolbox allow the identification of Transfer Function linear model. From MATLAB workspace, air mass flow rate and relative pressure vectors are imported to the Toolbox. Then, by simply indicating a transfer function desired model identification and specifying the numerator and denominator model order, the new identified model will be generated with an error percentage. An example of identifying a transfer function of a simple tube is presented in Annex I.

The influence of the closing time on the frequency bandwidth is demonstrated by well-known impulse characteristic. When the closing time tends to zero, the impulse width tends to zero corresponding to the Dirac peak, which is a theoretical signal (time domain) characterized by an infinite bandwidth (frequency domain). To avoid numerical problems, the profile of the air mass flow rate on DFB, which is a step function (Figure III-11), is converted to impulse excitation by using the derivative of the signal (Figure III-12).

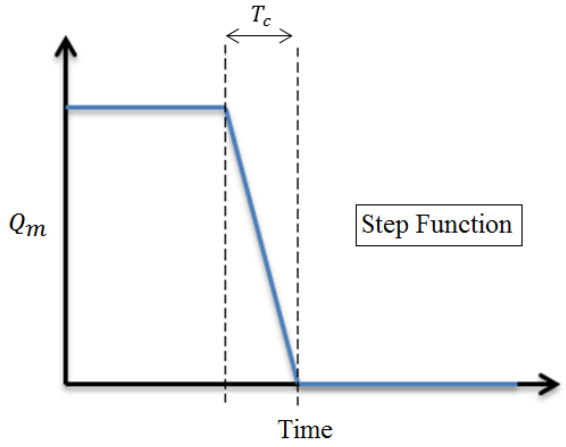

Figure III-11 – Step Function Profile

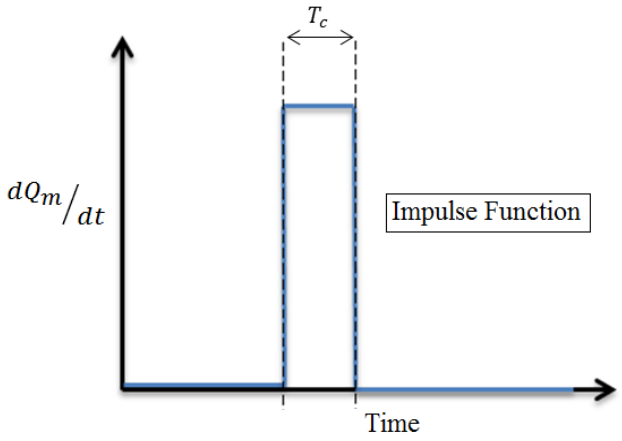

Figure III-12 – Impulse Function Profile

The measured transfer function is then:

$$TF_{measured} = \frac{Laplace(p_{relative})}{Laplace(\frac{dqm_{imp}}{dt})} \quad \text{(III-26)}$$

The advantages of System Identification Toolbox from MATLAB are:

- The Toolbox is easy to use. A transfer function estimation model already exists; user should only define the input and the output of the linear system in order to identify the model. User can define also the number of poles and zeros. It should be noted that for stability and causality criteria, number of poles should be bigger than number of zeros.
- For different intake geometry cases presented in this work, the convergence time needed for identifying a transfer function is too low.
- The toolbox provides at the end of the estimation an error percentage, which is a comparison between the output measured signal (experimental) and estimated one

(Equation (III-27)). Usually, according to the different cases studied in this thesis, the transfer function is identified with an error value of 5 to 10%. Error percentage can be decreased if the experimental output signal of the system is filtered (after removing high frequency and noise from the signal).

$$f_{error} = f_{exp} - f_{est} \tag{III-27}$$

- Compared to the identification procedure presented by Mezher[121], this way of identifying a transfer function of a linear system helps to take into consideration all the natural frequencies, including anti-resonance frequencies (half wave resonance modes).

III.3.2 Transfer Function Implementation

The GT-Power Native model of a single cylinder engine is presented is Figure III-13. Native model means that the intake system of the engine is modeled using GT-Power tube template. The flow inside this template is modeled using one-dimensional approach.

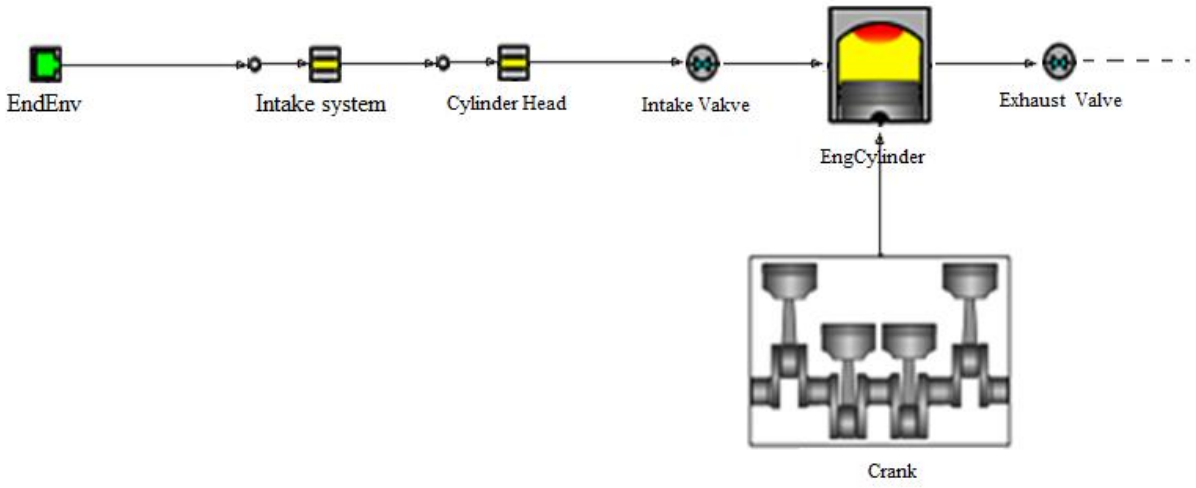

Figure III-13 - GT-Power Native Model

Once the transfer function is identified using the dynamic flow bench and calibrated, the next step is to replace the intake system from the native GT-Power model by its proper transfer function. In general, the coupling process is as follows: GT-Power provides the air mass flow rate instantaneous profile (via intake valve's motion), and then this information will be used as an input for the transfer function. Finally, calculation will be made inside of the transfer function bloc in time domain (after a transformation from complex frequency domain representation to discrete-time signal) and then the instantaneous relative pressure (which is the output of the transfer function) will be injected to GT-Power via EndEnvironment template after adding the related pressure losses.

The Transfer Function can be implemented to GT-Power using Simulink Bloc. The library of GT-Power offered the possibility to use Simulink in order to implement the identified transfer function. The intake system is then replace by the Simulink bloc as shown in Figure III-14.

This template is externally linked to a Simulink model (Figure III-15). The transfer function exists in Simulink code as a ration:

$$TF_{identified} = \frac{NUM}{DEN} \tag{III-28}$$

The numerator and the denominator of the identified transfer function are injected in Simulink s domain (continuous Transfer function). The simulation time can be specified by user. It should not be less than a certain value, which corresponds to the convergence time of the model.

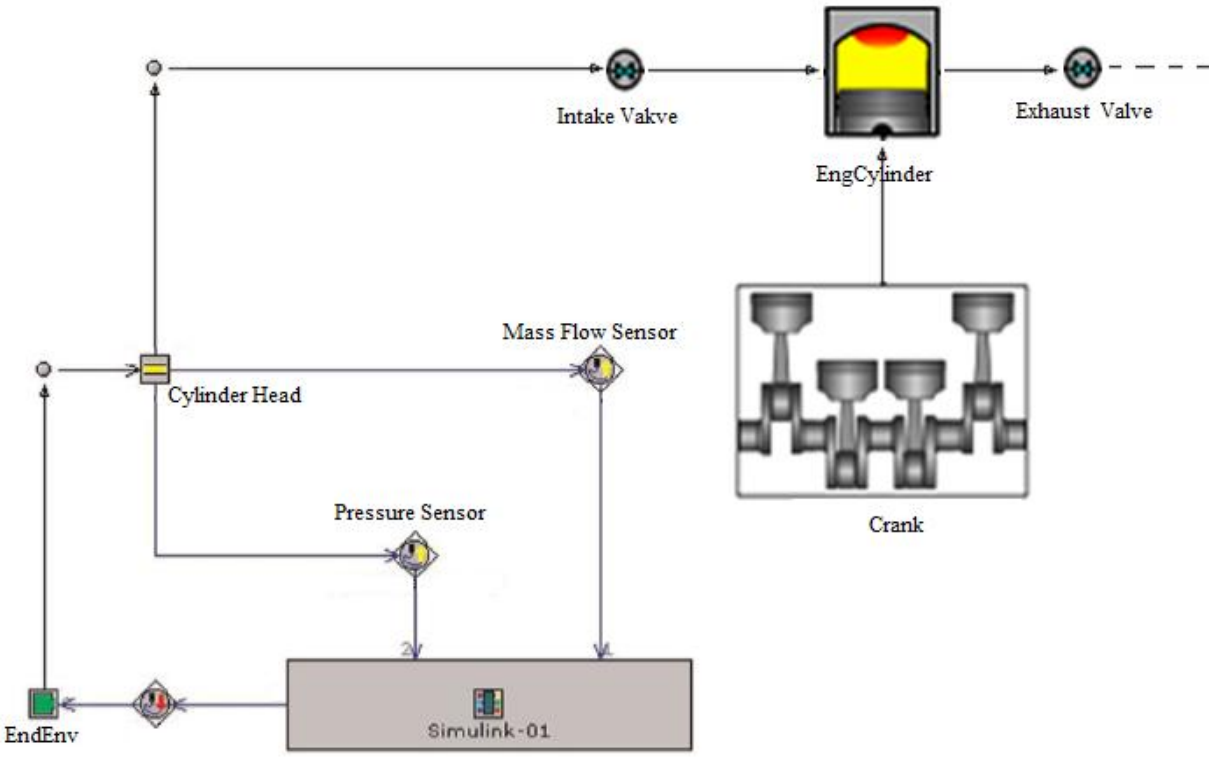

Figure III-14 - GT-Power/Simulink Coupling Model

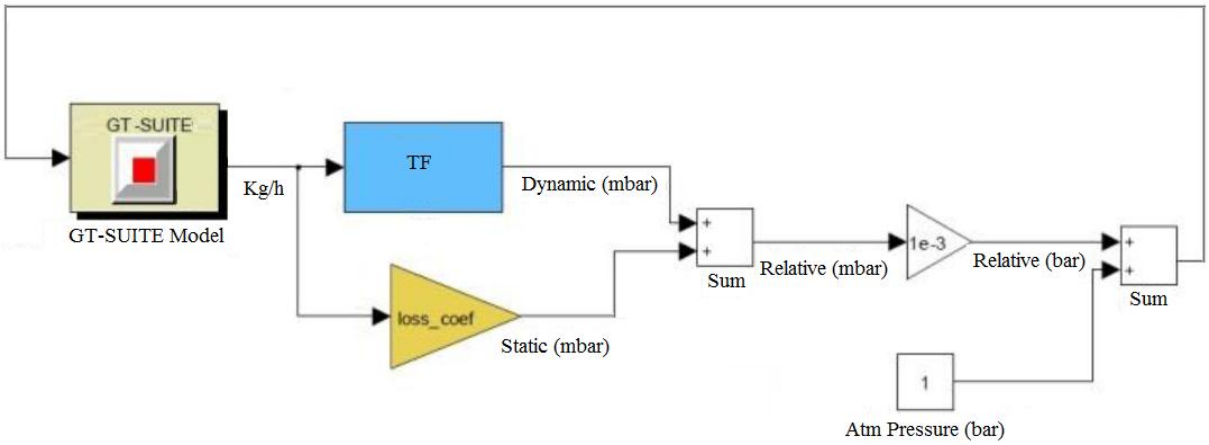

Figure III-15 - Simulink Transfer Function model

This model is time consuming. The simulation time of the coupled model compared to native model is too high. This is due to the coupling between different software. The final model shows some numerical instability as well. This can be the reason behind the high computational time of the model.

An alternative discovered option is the use of a transfer function template from GT-Power library. This coupling process will be called: GT/TF model. The same methodology will be applied but this time the Simulink model is replaced by a transfer function in GT-Power directly (Figure III-16).

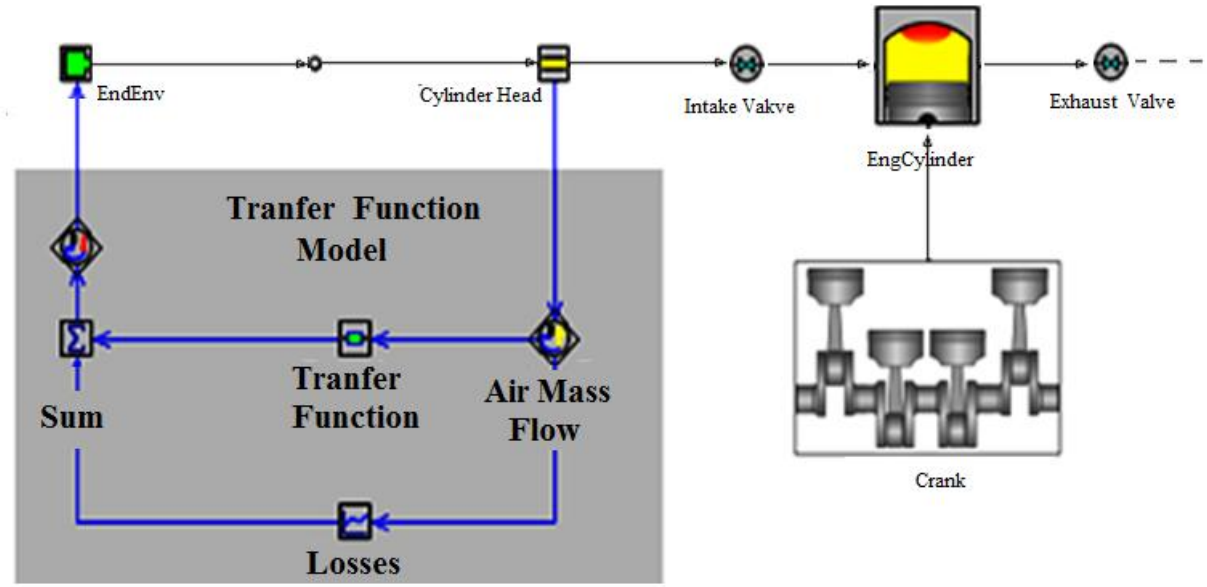

Figure III-16 - GT-Power/TF coupling Model

The transfer function template helps to implement a continuous transfer function. The transfer function is defined as:

$$TF_{(s)} = \frac{O(s)}{I_{tf}(s)} = \frac{a_1 s^n + a_2 s^{n-1} + \ldots + a_{n+1}}{b_1 s^m + b_2 s^{m-1} + \ldots ba_{m+1}} \quad \text{(III-29)}$$

This equation is internally rewritten in state-space form as:

$$\dot{x} = \hat{A}x + \hat{B}i_{tf} \quad \text{(III-30)}$$

$$y = \hat{C}x + \hat{D}i_{tf} \quad \text{(III-31)}$$

The numerator and the denominator of the transfer function start with the highest desired power of s. The number of denominator coefficient must be greater than or equal to the number of coefficients. The initial condition can be added to the function. The initial states were not calculated since the relation between the pressure and air mass flow rate at the intake

valve is considered as black box model. The code offers to initiate the simulation with random initial values.

Both methods showed the same results at different engine operating point. But the new coupling model was around fifty times faster than the coupling with Simulink in the case of a single cylinder engine, even faster than the native (which is the objective behind this methodology)

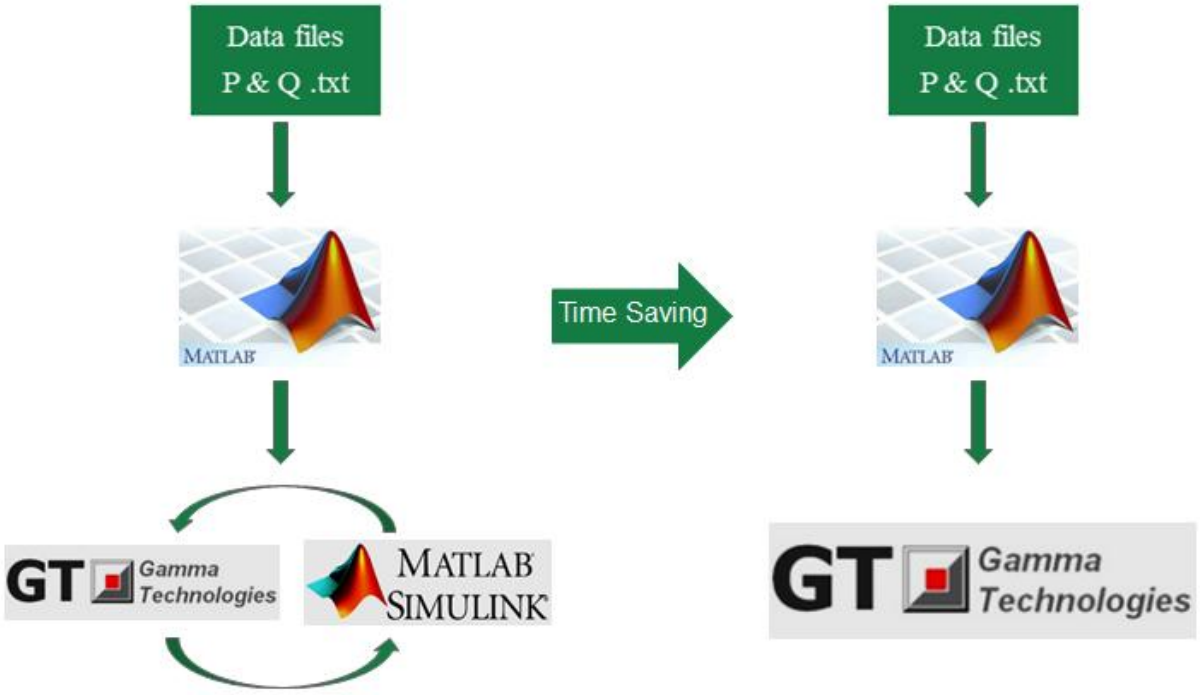

Figure III-17 - Coupling Model Transformation

The GT/TF coupling methodology will be adopted in this PhD. The time gain for the different application and model validation is presented in chapter V.

III.3.3 Transfer Function Model Calibration

The air mass flow rate in the intake system varies with the engine operating points. When different engine speeds are demanded, the air mass flow rate set point changes according to a calibrated value. This means that for a better modeling of that physical parameter, the new model should take into consideration this phenomenon. Since dynamic flow bench gives the possibility to change the initial aspirated air mass flow by simply regulating the pump to a certain value, the relative pressure response in function of air mass flow rate is studied in the case of the simple tube. Three different air mass flow rate values were chosen (60, 95 and 115 kg/h) on the dynamic flow bench (Figure III-18). At 0.1 second, the shut-off component is activated and then the air mass flow rate is suddenly interrupted. This mechanical movement creates a high pressure, then wave propagation in the tested geometry. The amplitude of the pressure decreases in time. The oscillation is damped due to the friction, which is a characteristic of the tested geometry.

The dependency between initial air mass flow excitation and the pressure response can be easily noticed in Figure III-19. It can be also better identified in frequency domain. The amplitude of the lowest natural frequency is high when the air mass flow excitation initial value is high (Figure III-20). According to equation (III-12), the damping coefficient varies in function of the amplitude of the frequency peak. This means that when a transfer function is identified at a certain air mass flow, only this function can lead to an accurate modeling of the flow in this condition. Thus, a model with many transfer functions, which correspond to different engine operating points, will be presented in details in chapter V.

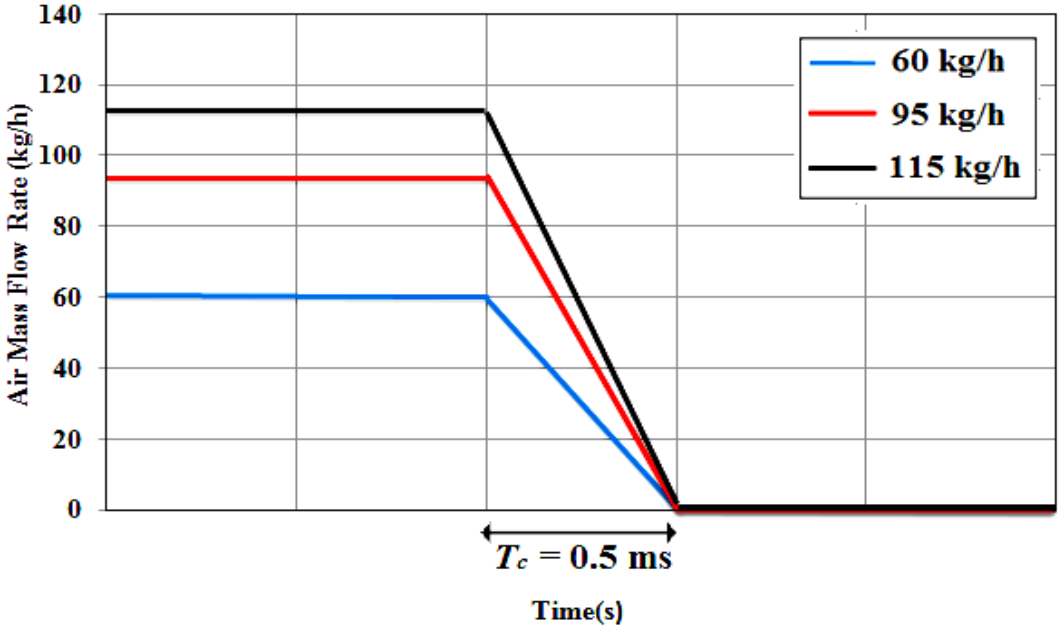

Figure III-18 - Air flow excitation profile on DFB

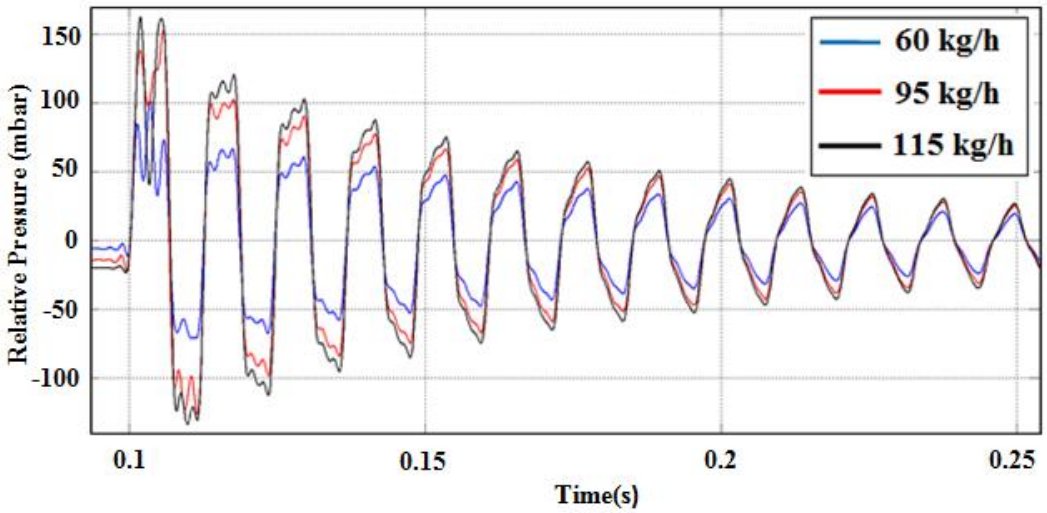

Figure III-19 - Relative pressure in function of time for different value of air mass flow rate

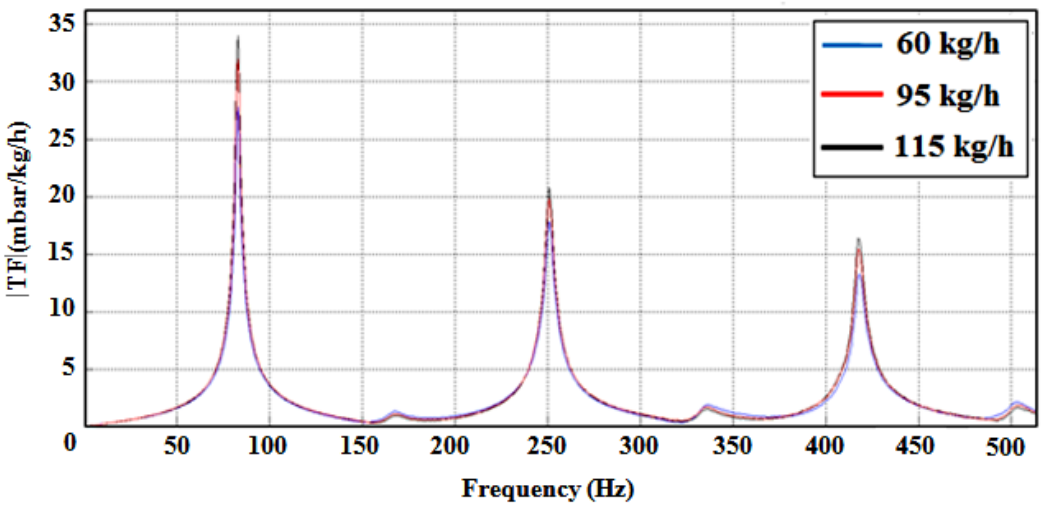

Figure III-20 - Relative pressure in function of air mass flow rate in frequency domain

To resume, many transfer functions where identified and implemented in the same code to cover the whole engine map. The disadvantage of this approach is the high computational time compared to a model where only one transfer function is used. In order to optimize the new model, a new function called exponential filter is introduced and implemented in the simulation software to reduce the number of transfer functions.

III.3.3.1. Exponential filter model

A very important physical phenomenon is shown in Figure III-19 and will be discussed. The amplitude of the wave after closing the valve is higher when the initial aspirated air mass flow is high, but after few oscillations, the amplitude of the waves converge to the same value. In order to quantify the effect of the damping parameter on the pressure response, a virtual dynamic flow bench is used. Three tests were done with different values of damping factor ϑ (Figure III-21). This parameter can be easily modified in the simulation software. For a fixed initial air mass flow rate value ($qm_{imp} = 115\ kg/h$), the results show that the first oscillation has the same amplitude after closing the shut-off valve. When the damping factor is high, the amplitude of the oscillation converges faster to zero than the other cases.

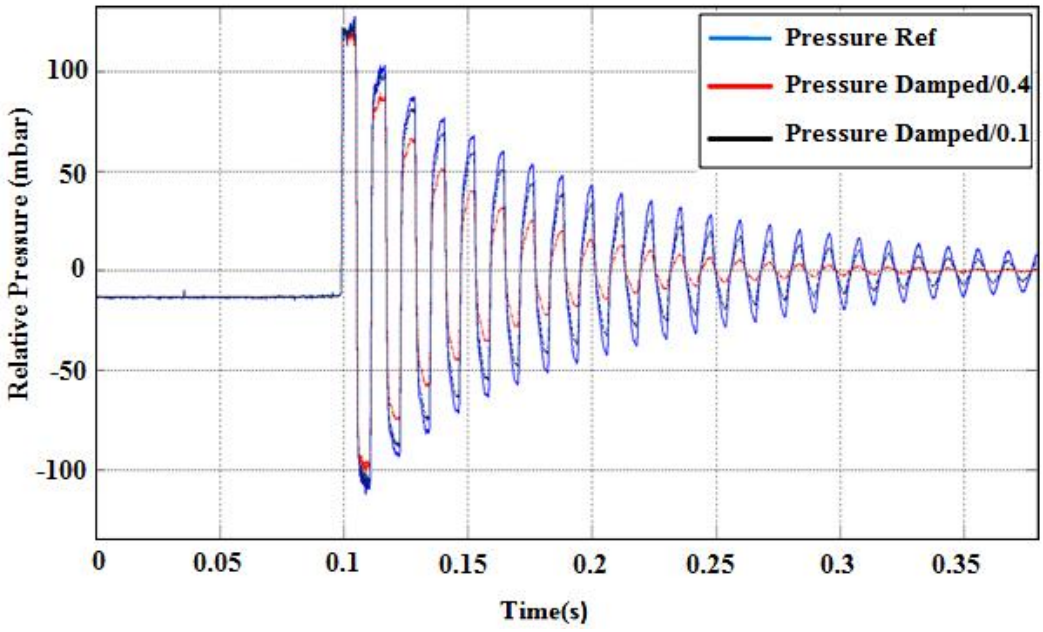

Figure III-21 - Relative pressure in function of damping parameter

After a comparison between Figure III-19 and Figure III-21, the signal filtration should be applied only at the beginning of pressure response oscillation in order to damp the peaks after closing the valve. The function which helps to achieve this objective is the exponential filter. In time domain, the form of the exponential filter is as follows:

$$F_{exp} = exp\left(\frac{-t}{\vartheta}\right) \tag{III-32}$$

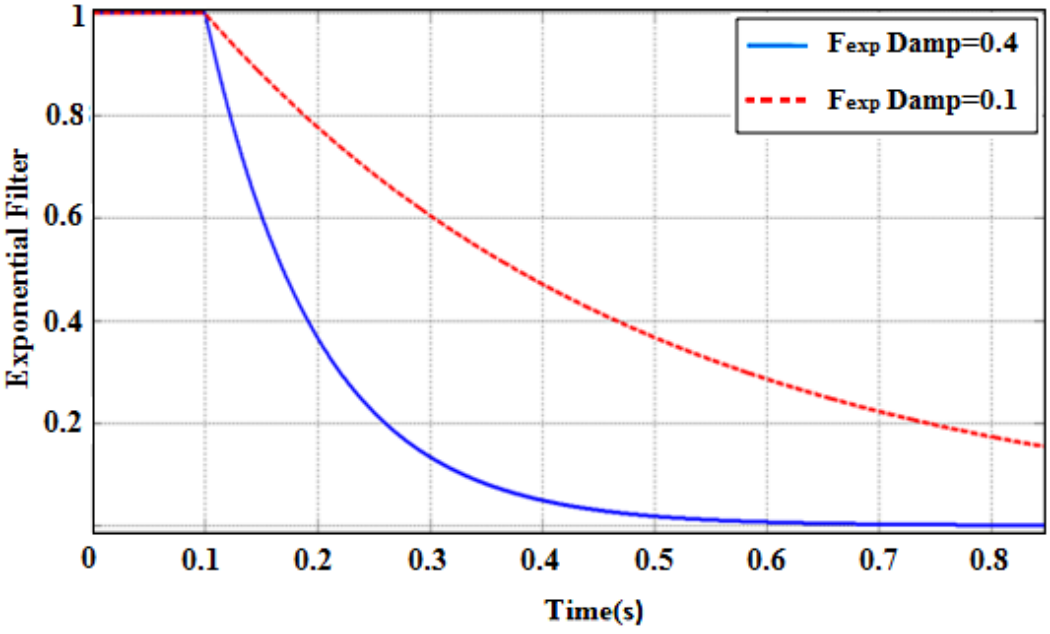

Figure III-22 - Exponential filter in function of ϑ

Generally, the filter helps damping the signals by applying a convolution product. Hence, in this work, the exponential filter will be used to damp the output of the transfer function (the relative pressure). The downward slope can be changed by simply varying the damping coefficient ϑ. This latter can be identified as follow:

- Using equation (III-12), the damping coefficient of the main frequency of the pressure signal, which is identified at certain air mass flow rate excitation, should be calculated
- Defining the main transfer function which will be used as a main function in the simulation code.
- Damping coefficient calculation of the main frequency of the pressure signal response of the main defined transfer function.
- The damping coefficient parameter of the exponential filter can thus identified using convolution product on both damping coefficient identified in the previous steps.

The complete procedure of damping coefficient identification will be detailed in chapter V.

Once the relative pressure signal is multiplied by the exponential filter, the amplitude of the pressure fluctuation will decrease. This filter will be integrated directly in the GT-Power code coupled with the transfer function, to damp the instantaneous pressure fluctuation after closing the intake valve. A switch was added to the model to activate the filter only for this period. For a good integration of this filter in GT/FT code, it will be better to be used in function of Crank Angle (°CA). In this case, the form of the filter will be as follows:

$$F_{exp} = exp\left(\frac{-(^{\circ}CA)}{\vartheta}\right) \tag{III-33}$$

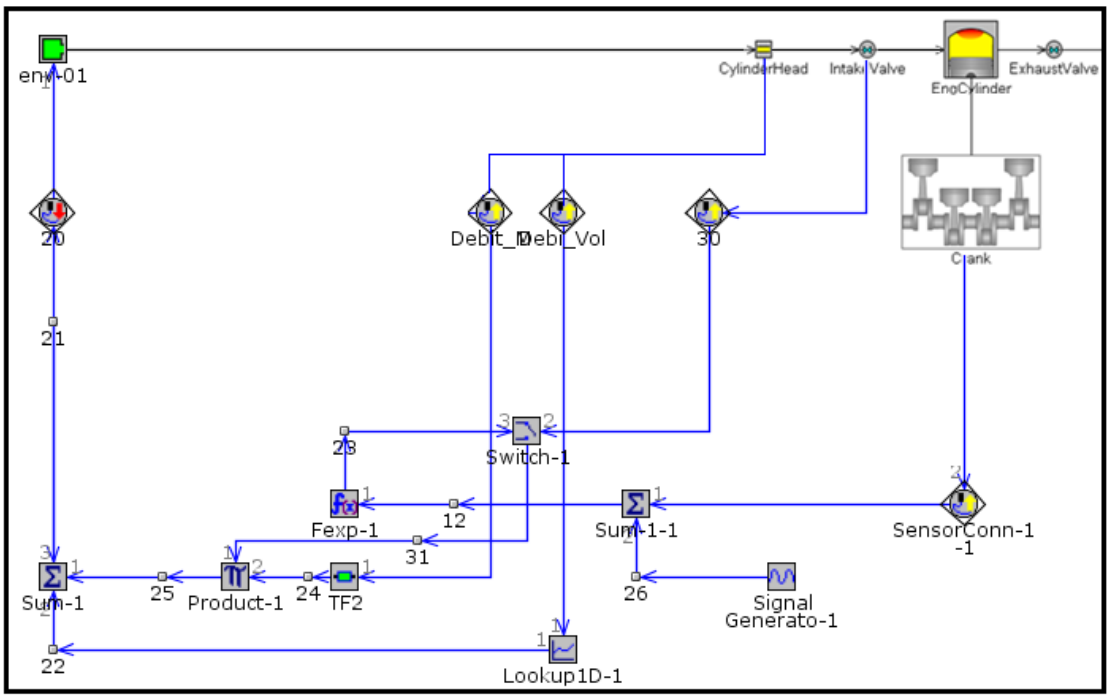

Figure III-23 - GT-Power coupled model

Therefore, only one transfer function is used, and then during the simulation, the damping coefficient of the filter will change with the rotational engine speed. The application of the methodology will be detailed later in chapter V.

III.3.3.2. Transfer function for modelling the temperature variation

In the previous sections, once the transfer function is subjected to sudden air mass flow variation, the model allows prediction of the pressure oscillation in the intake system of an internal combustion engine. This function only contains information related to dynamic pressure. In the simulation software, the transfer function should replace the one-dimensional schemes of the intake system. Thus, with only pressure information, the model convergence time will be high.

In this section, a new concept will be added to the previous model: the transfer function of temperature, which is considered as solver improvement for simulation time. It helps to model the temperature variation due to dynamic pressure fluctuation. The transfer function of temperature will be coupled with the transfer function of pressure in the same code in order to help GT-Power to decrease the convergence time of the model (Figure III-24). The objective consists on giving more information to the simulation software code (temperature evolution for the energy equation).

The same principle as the transfer function for pressure is used. The new transfer function is a relation between instantaneous temperature and air mass flow rate excitation:

$$TF_{Temperature} = \frac{T}{Qm_{exc}} \tag{III-34}$$

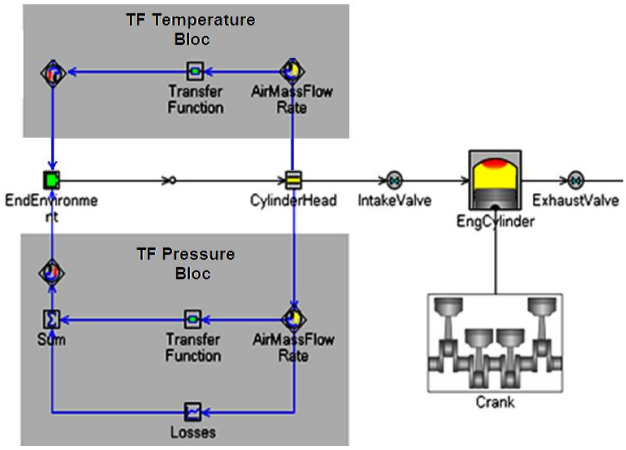

Figure III-24 - Transfer Function coupling model

Using Virtual Dynamic Flow Bench, the instantaneous temperature, placed at the same place of the pressure sensor, will be registered. This gives the possibility to get different thermodynamic parameters easily (virtual sensors). The same identification procedure for identifying a pressure transfer function is be used to identify a transfer function of temperature. It should be noted that this new function does not contain information related the heat exchange between the air in the intake system and the walls. The methodology application will be detailed later in chapter V.

III.3.4 Pressure losses

The pressure losses are dominating in the intake system of the internal combustion phase during admission phase. For this reason, the model should take into consideration this phenomenon. Since the Transfer Function models the pressure fluctuation at the intake system after closing the intake valve, another function should be added to the main model which includes information related to the behavior of an intake system when air flow is passing through it. In this work, the pressure drops of a tested geometry are identified using dynamic flow bench. In Figure III-25, the pressure drop curve in function air mass flow rate is identified or the case of a tube of 985mm length and 30 mm diameter.

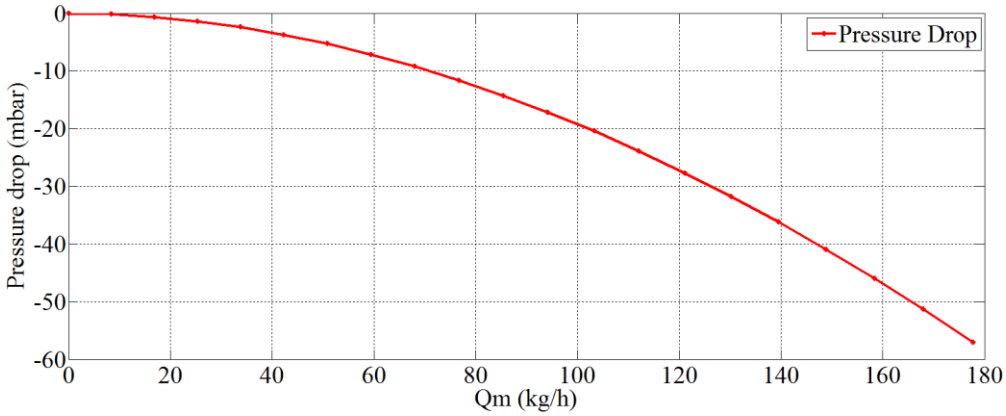

Figure III-25 - Pressure drop in function of air mass flow rate for a simple tube of 985 mm length and 30 mm diameter

Table III-2 – Pressure losses in function of air mass flow rate

$Q_m(kg/h)$	P_{losses}
0	0
8.433	-0.1743
16.87	-0.6489
25.33	-1.405
33.806	-2.436
42.308	-3.738
50.843	-5.309
59.417	-7.149
68.03	-9.26
76.70931	-11.64
85.44	-14.3
94.23	-17.23
103.408	-20.44
112.06	-23.94
121.105	-27.74
130.247	-31.83
139.498	-36.23
148.869	-40.94
158.368	-45.97
168.011	-51.35
177.81	-57.07

The red curve in Figure III-25 is not linear. The hypothesis of the linearity in equation (III-25) is not valid. Thus, the pressure losses will be integrated in the simulation code in a form of table, were data from experimental tests from the dynamic flow bench are implemented. This will be the most accurate way for pressure losses calculation in the simulation software. This step very important and should be taken into consideration, since the pressure upstream the intake is highly influenced by the pressure losses values. It should be noted that the

identification of the table of pressure losses variations is fast. In other words, once the geometry is installed on the dynamic flow bench, and before shut-off component activation, the air mass flow rate is modified (from 10 to 250 kg/h, with a step of 20 kg/h) and then pressure upstream the shut-off valve is registered and then saved in a table form in GT-Power.

In this chapter, the theory behind the transfer function model is presented. Model improvement is also detailed. The aim is to increase the accuracy of the model and reduce the simulation time of the complete engine model. The validation of this latter will be presented separately in chapter V.

IV. Acoustic Transfer Function

In this chapter, a new transfer function identification procedure will be presented. The aim of this new approach is to replace the tests on the dynamic flow bench by a mathematical tool which allows characterizing the wave action in a tested geometry. Linearized acoustic approach will be used in order to identify the transfer function of different geometries of the intake system of an internal combustion engine, starting from simple geometry (a tube of length L and diameter D) to a complex one (the intake system of a three cylinder engine).The transfer function methodology, presented in the previous chapter, will be used after identifying the relative pressure at the end of the runners from acoustic approach. Both functions are complementary and they should be applied together in order to model the relative pressure upstream the intake valve of an internal combustion engine.

IV.1. Introduction

In internal combustion engine, the pressure waves are generated by following four sources:

- Piston displacement that influences the intake and the exhaust pressure when the valves are open.
- The reciprocating movement of the valves that generates pressure waves at each opening-closing cycle. When the valve closes, a local overpressure at the valve is created.
- Presence of supercharger or turbocharger.
- Reflection and transmission of the wave generated by one or many previous sources, when these latter faced a sudden section or temperature variation.

These waves are considered as acoustic waves. The pressure sources mentioned above imply a periodic nature to the pressure waves; the amplitude and the frequency of the pressure waves are not the same and do not have the same effect on the engine filling. In addition they depend on the engine speed and the layout of the different parts of the intake line.

Two types of elements are to be distinguished at the intake system of an internal combustion engine:

- Passive elements: Tube, Junction, Section change, etc… These elements influence the propagation of pressure waves but do not create additional waves.
- Active elements: the valves and the compressor. The pressure waves are created by these elements.

In internal combustion engine, valve closing creates a compression wave; as long as the opening of the valve communicates the piston to the intake line generates expansion wave. These waves influence the flow in the intake system and thus the torque and engine performance:

- Effect of valve opening:

The waves generated during this phase are reflected at the open end and then transformed into compression waves that propagate towards the cylinder and coincide just before the intake valve closing (IVC) to fill more air in the cylinder (Figure Figure IV-1). At the end of admission phase, the valve is still open and the piston begins to slow down at the bottom dead center (BDC). The volume in the cylinder decreases once the piston begins to compress the fluid mixture. The pressure in the cylinder then increases. However, the intake air has sufficient kinetic energy to continue to fill the cylinder (Kadenacy effect). The wave generated in this phase is a half wave resonance

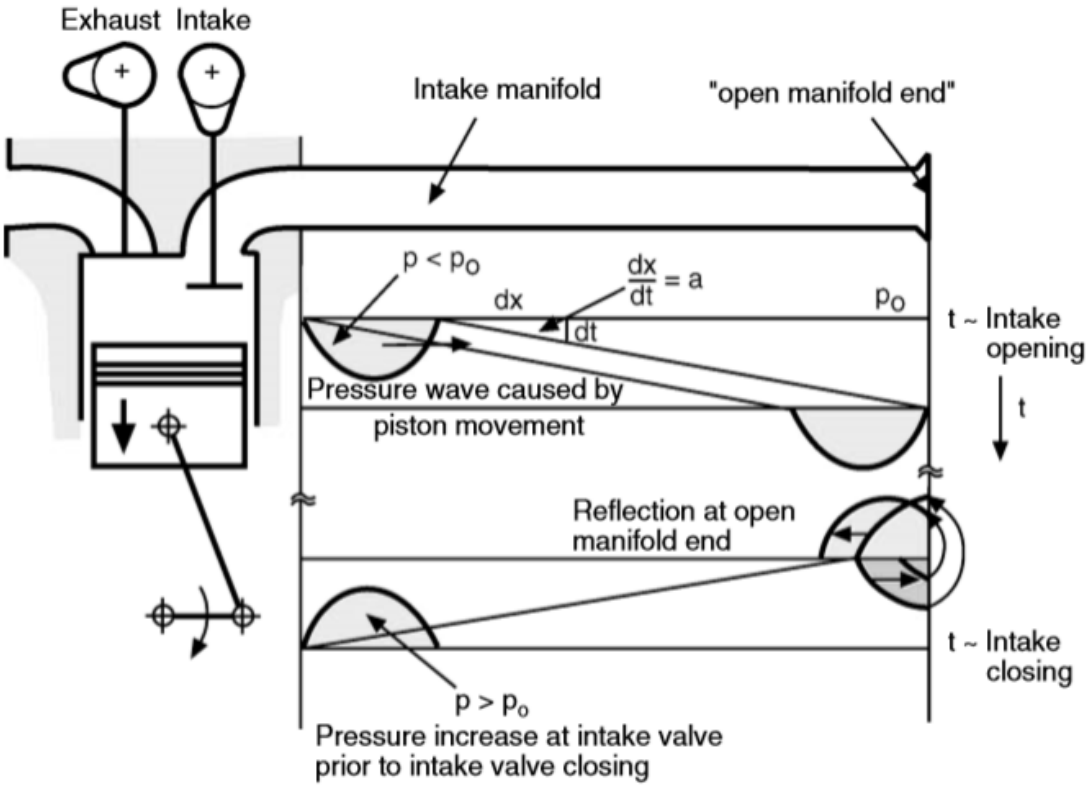

Figure IV-1 -Excitation and propagation characteristic of a pressure wave at the intake system [112]

- Effect of valve closing:

The wave generated in this phase is a quarter wave resonances and it occurs at the end of the admission phase (Figure Figure IV-2):

1. Valve closing creates a pressure wave: overpressure.
2. This wave crosses the intake line and reaches the open end of the manifold. Due to a sudden section variation, the wave is reflected and propagated again to the intake valve in the form of expansion wave.
3. The wave is reflected against the valve, which is always at a closing state. It propagates once more at the section variation where it undergoes a second reflection and becomes again a compression wave.
4. It propagates again towards the valve and coincides with its opening time.

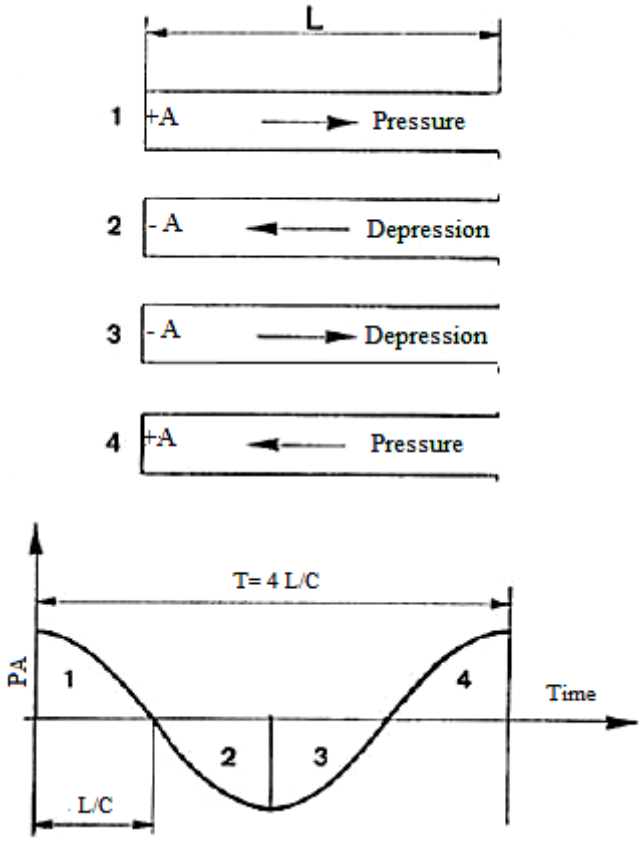

Figure IV-2 - Quarter wave resonances in the runner [112]

This phenomenon is called: "Acoustic supercharging". A natural supercharging then occurs, which allow to increase the air mass through the valve. Hence a good synchronization between the opening time of the intake valve (which depends on the engine rotational speed) and the propagation time of the pressure waves (which depends essentially on the length of the duct and the speed of sound) allow a better engine breathing.

IV.2. The use of the method

The acoustic method will be used only in order to replace the tests on the dynamic flow bench. As presented before, in the previous chapter, the first step which allows identifying a transfer function is to make few tests on the dynamic flow bench. These tests will give the pressure response on a tested geometry.

IV.3. Using Acoustic Equations

On the dynamic flow bench, the tube of length L is open at both ends before closing the dynamic component (Figure IV-3). Once the flow is interrupted by closing the excitation source, the system is then open at one end and close at the second end (Figure IV-4). From acoustic modelling point of view, the amplitude of pressure waves generated in the first configuration case is negligible. Furthermore, the impedance tends to infinity at the close end in the second configuration where air mass flow rate value is zero. However, sudden air flow change cannot be modelled using acoustic approach. For this reason, the close end (near

dynamic component) in the second configuration is considered as open, but it is subjected to acoustic excitation generated by the sudden obstruction of the air flow. This assumption will be clarified after presenting acoustic equations later on.

In Figure IV-3, white arrows represent the flow direction and the blue ones represent the propagation of the acoustic waves (Figure IV-4). Thus, by applying the equations of acoustic approach, the positive direction chosen is that of displacement of the acoustic waves.

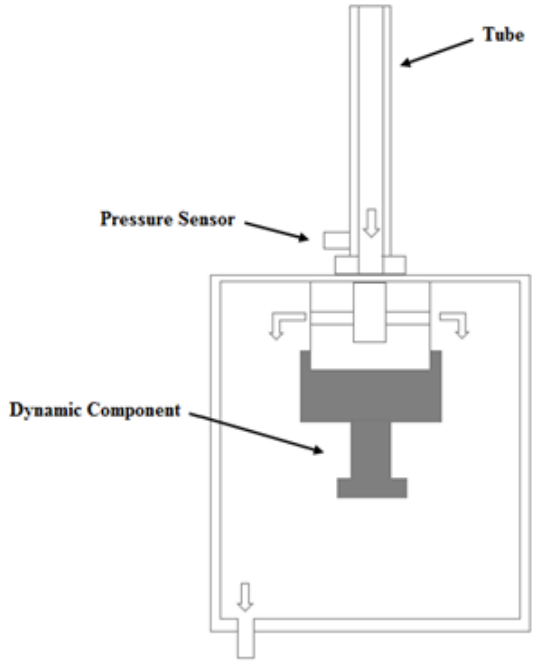

Figure IV-3 – Configuration 1

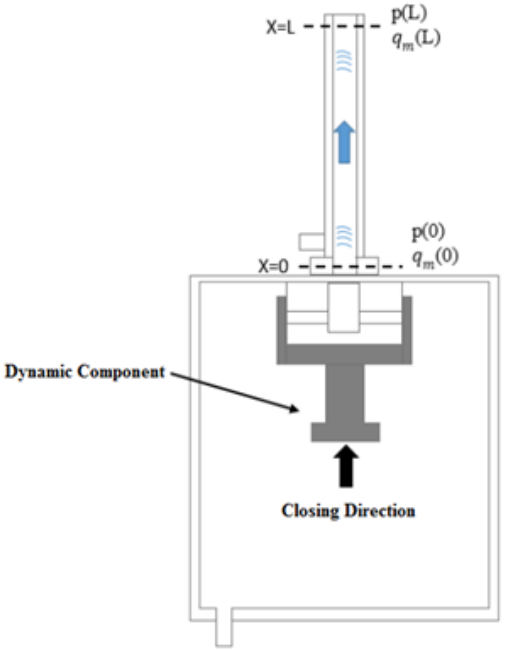

Figure IV-4 – Configuration 2

The analytical solutions of one-dimensional waves in a viscous moving medium are presented in Chapter 0I. In order to find the linear system between both ends of the tested geometry, the term $\exp(j\omega t)$ is integrated in the constant coefficients C_1 and C_2. Thus, the solutions become:

$$p(x) = \hat{A}.\exp(\beta^{+}x) + \hat{B}.\exp(\beta^{-}x) \tag{IV-1}$$

$$q_m(x) = \frac{1}{z_{c0}}\left[\hat{A}.\exp(\beta^{+}x) - \hat{B}.\exp(\beta^{-}x)\right] \tag{IV-2}$$

In the case of a simple tube of length L:

- For x=0:

$$p(0) = \hat{A} + \hat{B} \tag{IV-3}$$

$$q_m(0) = \frac{1}{z_{c0}}\left[\hat{A} + \hat{B}\right] \tag{IV-4}$$

- Similarly, for x=L:

$$p(L) = \hat{A}.\exp(\beta^{+}L) + \hat{B}.\exp(\beta^{-}L) \tag{IV-5}$$

$$q_m(L) = \frac{1}{z_{c0}}\left[\hat{A}.\exp(\beta^{+}L) - \hat{B}.\exp(\beta^{-}L)\right] \tag{IV-6}$$

A relation between $p(0)$ and $p(L)$ can be then deduces:

$$p(L) = p(0).\left[\frac{\exp(\beta^{+}L)+\exp(\beta^{-}L)}{2}\right] + z_{c0}.q_m(0).\left[\frac{\exp(\beta^{+}L)-\exp(\beta^{-}L)}{2}\right] \tag{IV-7}$$

$$q_m(L) = \frac{p(0)}{z_{c0}}.\left[\frac{\exp(\beta^{+}L)-\exp(\beta^{-}L)}{2}\right] + q_m(0).\left[\frac{\exp(\beta^{+}L)+\exp(\beta^{-}L)}{2}\right] \tag{IV-8}$$

In order to find the impedance at the close end (near the dynamic component), it is better to write the previous system as follow:

$$X(0) = function(X(L)) \tag{IV-9}$$

While X (x) is the thermodynamic variable (p at qm) at x position.

Thus, by reversing the equations (IV-7) (IV-8), the new equation system will be:

$$p(0) = p(L).\left[\frac{\exp(\beta^{+}L)+\exp(\beta^{-}L)}{2}\right] + z_{c0}.q_m(L).\left[\frac{\exp(\beta^{-}L)-\exp(\beta^{+}L)}{2}\right] \tag{IV-10}$$

$$q_m(0) = \frac{p(L)}{z_{c0}}.\left[\frac{\exp(\beta^{-}L)-\exp(\beta^{+}L)}{2}\right] + q_m(L).\left[\frac{\exp(\beta^{+}L)+\exp(\beta^{-}L)}{2}\right] \tag{IV-11}$$

The boundary conditions for the case of a simple tube of length L are:

- $p(L) = 0$, at x=L the tube is open to the atmosphere.
- $q_m(L) = Q_{imp}$, this value of air mass flow rate is fixed using the SuperFlow of the dynamic flow bench.

Hence,

$$p(0) = z_{c0}.\left[\frac{\exp(\beta^{-}L)-\exp(\beta^{+}L)}{2}\right].Q_{imp} \tag{IV-12}$$

$$q_m(0) = \left[\frac{\exp(\beta^{+}L)+\exp(\beta^{-}L)}{2}\right].Q_{imp} \tag{IV-13}$$

The characteristic impedance z and the complex Mach numbers $\beta^{+}$and β^{-} are already defined in Chapter 0. It should be noted that the values of these parameters change in function of flow types presented in Chapter I.

Knowing the relative pressure and the air mass flow rate at x=0, the characteristic impedance z (0), which is similar to the Transfer Function concept, is then:

$$z(0) = TF_{acoustic} = \frac{p(0)}{q_m(0)} = \frac{z_{c0} \cdot \left[\exp\left(\beta^- L\right) - \exp\left(\beta^+ L\right)\right]}{\left[\exp\left(\beta^+ L\right) + \exp\left(\beta^- L\right)\right]} \quad \text{(IV-14)}$$

IV.3.1 Effect of flow type on acoustic Transfer Function

This section is devoted to study the plane wave propagation along circular duct of length L using an acoustic transfer function, for different type of flow (with and without mean flow and viscous friction). It is important to check the effect of flow type on the acoustic response. For this reason, the evolution of acoustic transfer function modulus in frequency domain is compared to experimental data (measured transfer function identified using the dynamic flow bench) for the four different types of flow:

a. Inviscid stationary medium
b. Viscous stationary medium
c. Inviscid moving medium
d. Viscous moving medium

The tested geometry is a simple tube of 368 mm length and 30 mm of internal diameter. The air mass flow rate is fixed at $Q_{imp} = 80\ kg/h$ on the dynamic flow bench.

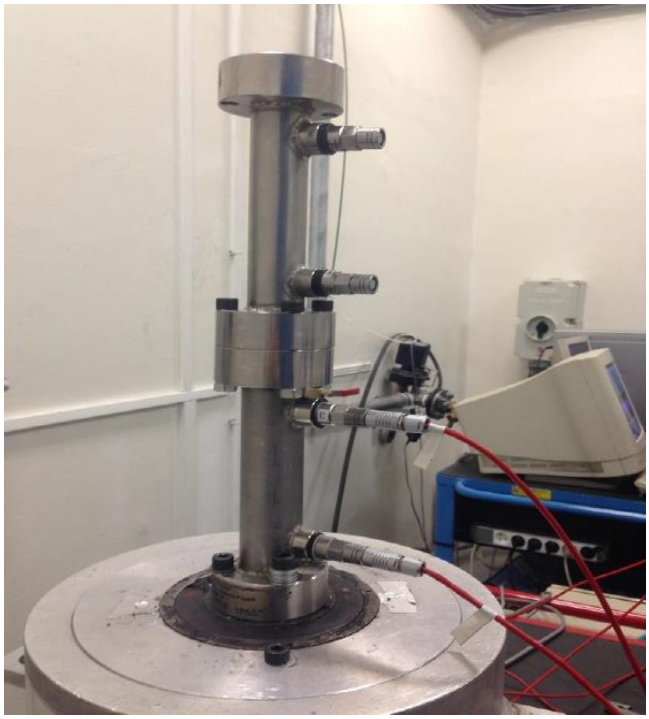

IV-5 - Dynamic flow bench test on a tube (L=368 mm, D=30 mm)

IV.3.1.1. Inviscid stationary medium

The blue curve represents the modulus of the measured transfer function (using dynamic flow bench) and the red one represents the modulus of the acoustic transfer function. However, the fact of not taking into consideration neither viscosity nor mean velocity effect, leads to an impedance far from the experimental one in terms of amplitude.

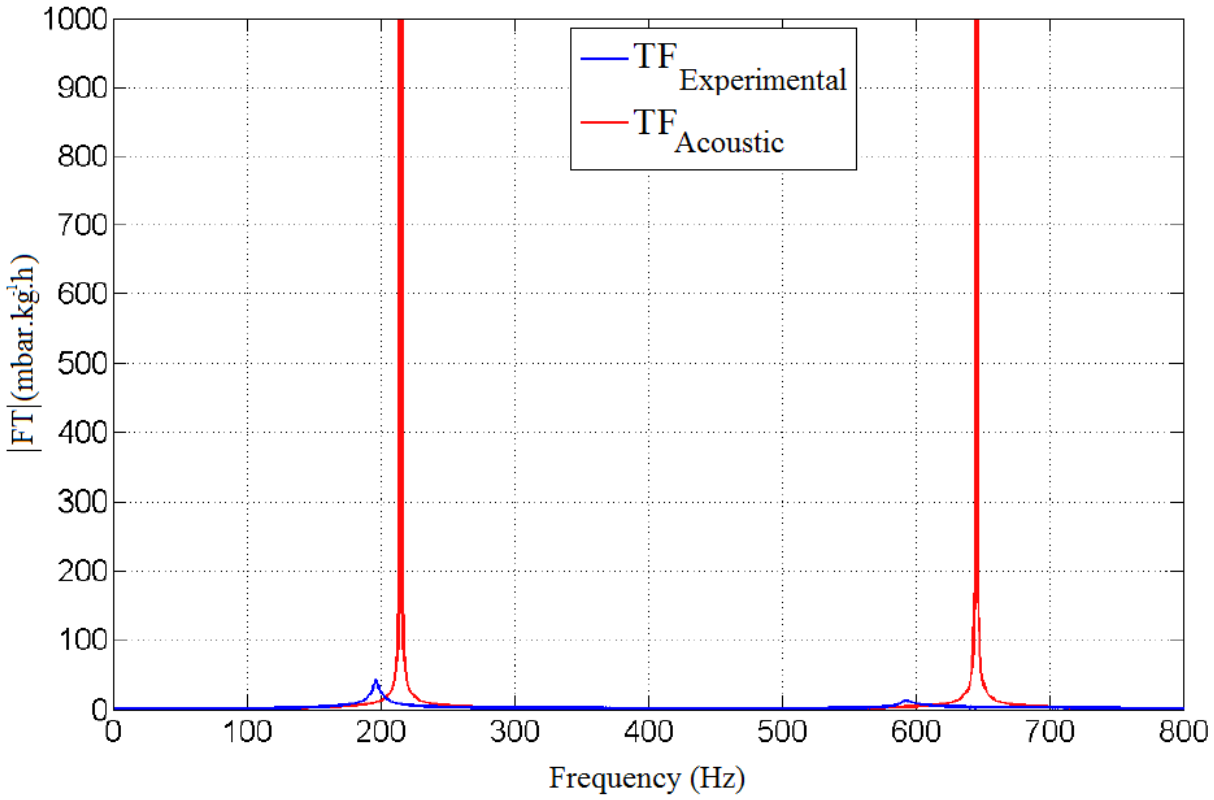

Figure IV-6 – Modulus of experimental and acoustic Transfer Function

The difference between fundamental frequencies in the modulus of transfer functions is around 15 Hz. The ambient pressure and temperature values used in the acoustic equations are the same as the values measured during the tests on the dynamic flow bench (P_{atm}= 1.01223 bar and T_{atm}= 292 K).

IV.3.1.2. Viscous stationary medium

Once the viscosity is taken into consideration, the amplitude of the peaks in red curves decreases and now it can be comparable to the ones of experimental peaks (as depicted in Figure IV-7). This is logical because the viscosity increases the damping coefficients of the medium. Regarding the frequency, the viscosity factor did not change the frequency of the peaks in red curve. Thus, it can assume that the viscosity does not affect the natural frequencies of the acoustic transfer function response.

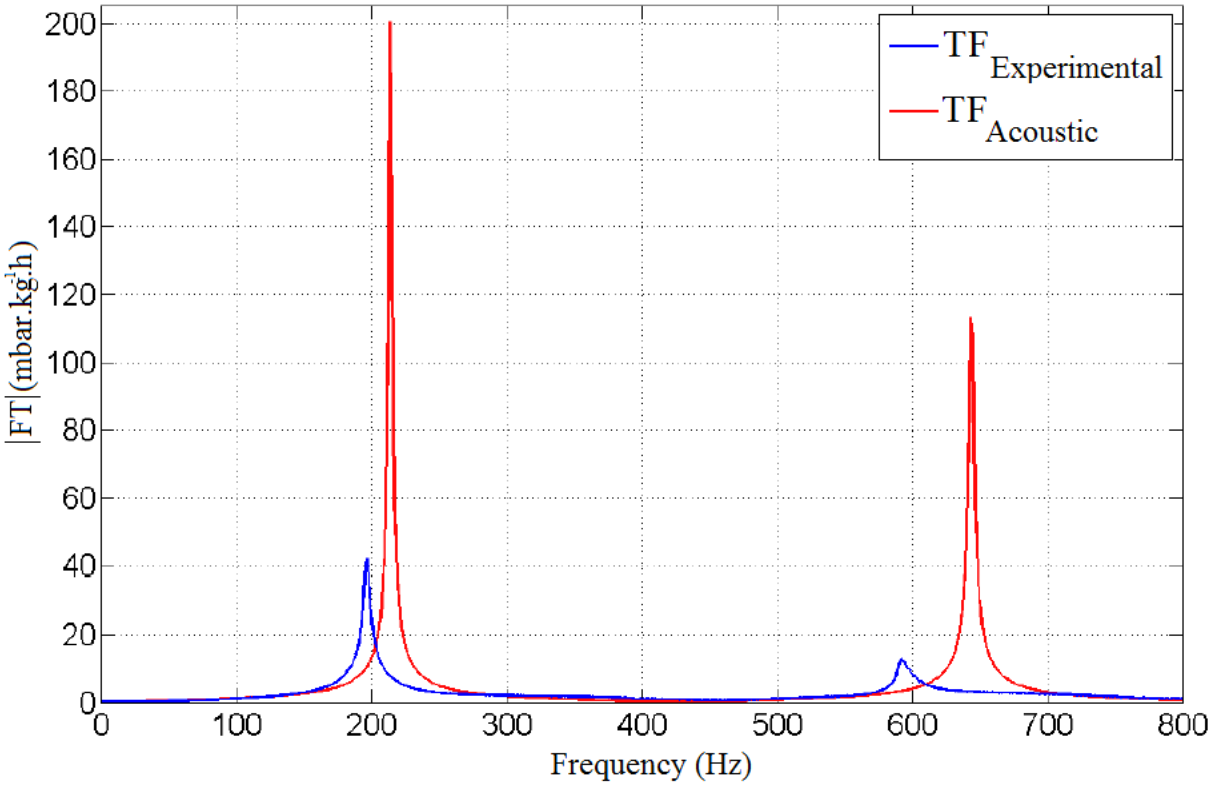

Figure IV-7 – Modulus of experimental and acoustic Transfer Function

IV.3.1.3. Inviscid moving medium

In this case, only mean velocity effect on the acoustic response is studied. Refereeing to Figure IV-8, the amplitude of the peaks in red curve decreased compared to the first case (in IV.1.1.1). However, by simply comparing this case to the previous one, it is easy to notice that the viscosity plays the main role in damping the amplitude of the red curve. In term of frequency of the peaks, the mean velocity parameter does not affect also the natural frequencies of the acoustic transfer function response.

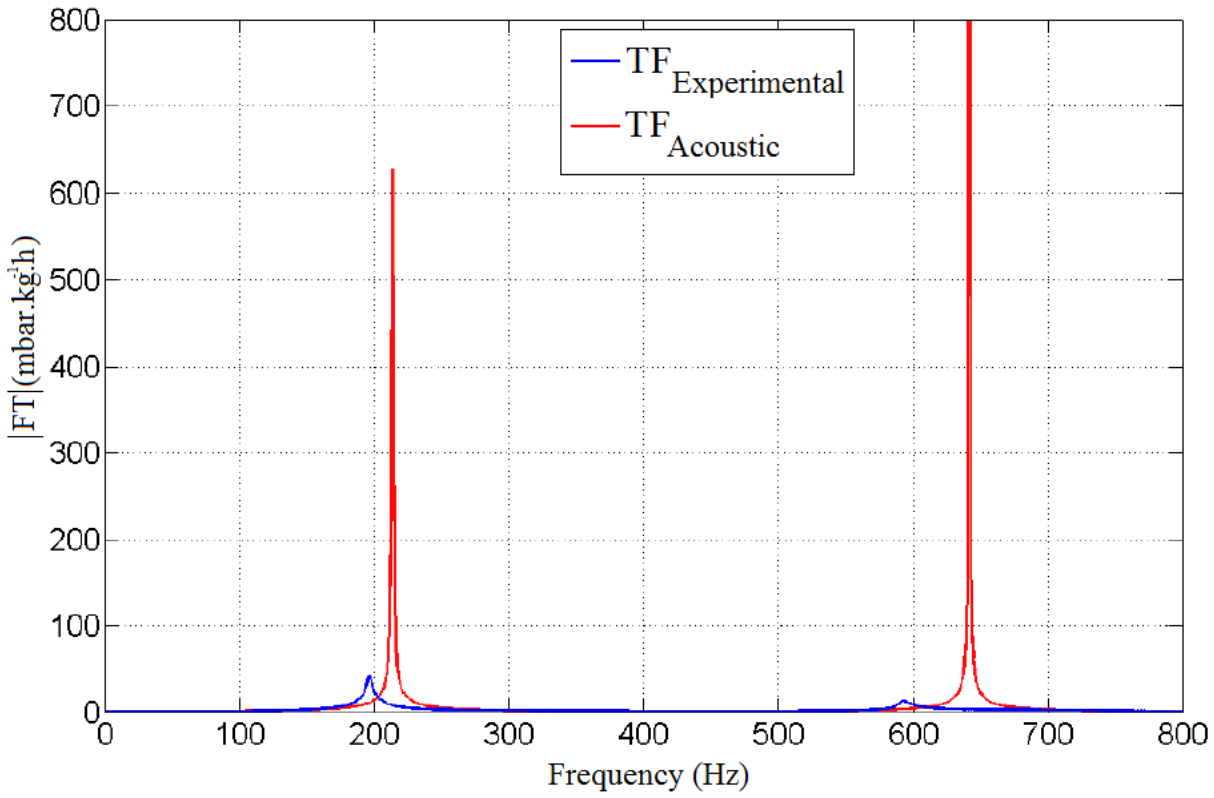

Figure IV-8 – Modulus of experimental and acoustic Transfer Function

IV.3.1.4. Viscous moving medium

The equations used to identify the acoustic impedance are extended in this case to account for the additional aero-acoustic losses due to turbulent friction, and also the convective effect of mean flow. The result is then a model which is the closest to the real case (Figure IV-9). However, the frequency and the amplitude of the peaks in red curve are still different than those in experimental one. In fact, the same length L is used in the equations in order to identify the acoustic transfer function model. This shift in frequency is mainly caused by the length of modeled tube. Theoretically, the absolute pressure at the open end of the tube is equal to atmospheric pressure. In other words, there is no pressure fluctuation at the open end of the tube and the pressure reflection coefficient is equal to one. However, it has been proven in acoustic domain that the total reflection does not occur exactly at the open end of the tube but in a small area outside of it [33]. For this reason, a length correction ΔL must be added to the acoustic equations to take into consideration this pheromone and to get the same natural frequency values. Based on experimental tests, many authors have worked on this topic in order to find the empirical equation for this length correction [35], [50], [127]–[131]. In addition, the effects of Mach number and Helmholtz number on the pressure reflection coefficient at the open end of a tube have been studied [34], [35], [132], [133].

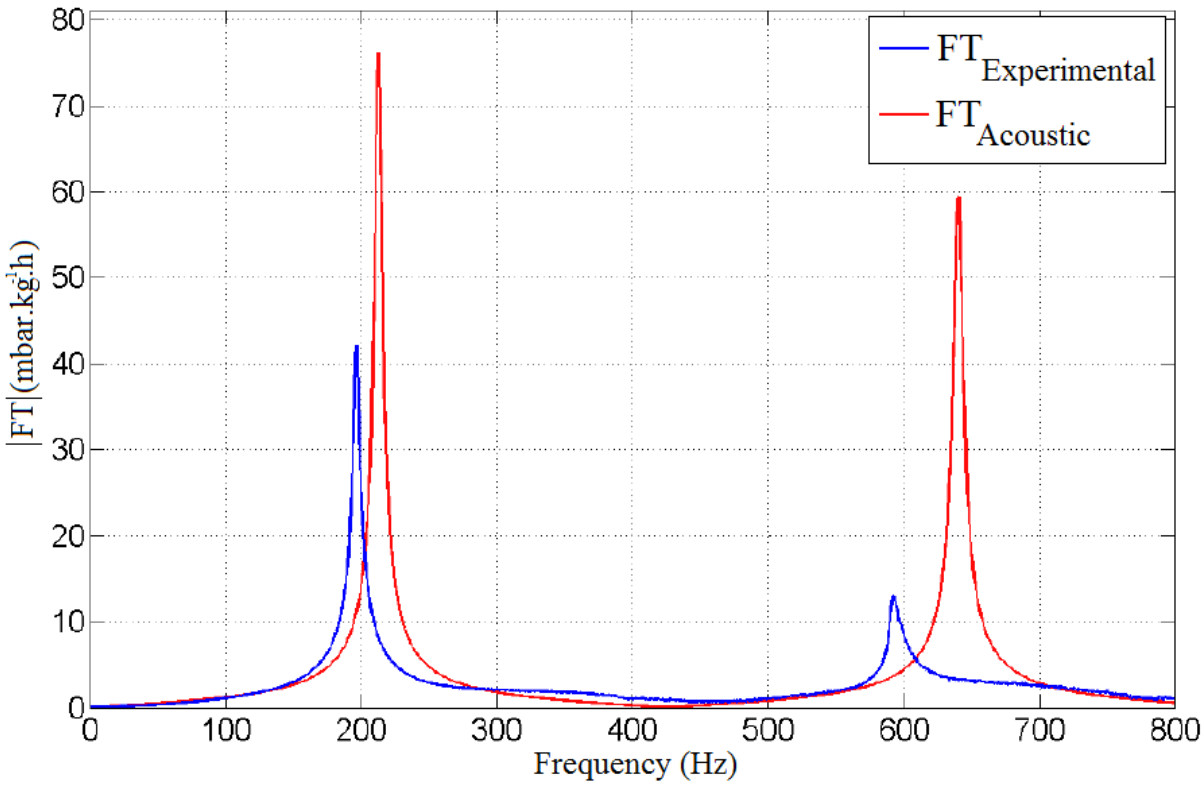

Figure IV-9 – Modulus of experimental and acoustic Transfer Function

IV.3.2 Acoustic Model Calibration

Here onwards, the viscous moving medium flow type is considered. According to equation (IV-14), the length of the tube and the Mach number are the main parameters which affect the response of the identified transfer function. A correction of these two parameters is needed to minimize the error between the fundamental frequencies and the modulus of experimental and acoustic transfer functions. The Mach number is corrected for different reasons:

- The temperature and the atmospheric pressure are considered constants in the acoustic equations, which imply a constant density of the flow. This is not guaranteed during the experimental test since the air is a highly compressible fluid.
- The complex geometry of the hole on the dynamic flow bench, where the air is aspirated, and the local pressure losses are not taken into account in the acoustic transfer function model.

Always in the case of a simple tube (L=368 mm, D_i=30 mm) and for $Q_{imp} = 80\ kg/h$, the corrected parameters are $\Delta L = 24.9\ mm$ and $Mach_{corrected} = 0.16$.

The length and the Mach number correction should be done for different imposed air mass flow rate in order to get a correction law of these two parameters. The correction laws give the exact values of ΔL and Mach number which must be implemented in equation (IV-14) to correct the response of acoustic transfer function according to experimental data. The calibration is done to target the fundamental peak. Figure IV-10 and Figure IV-11 show the correction law on Mach number and ΔL for different air mass flow rates between [20 160](kg/h). Two interpolation modes can be considered. The green curve represents the best interpolation while red line represents the linear interpolation.

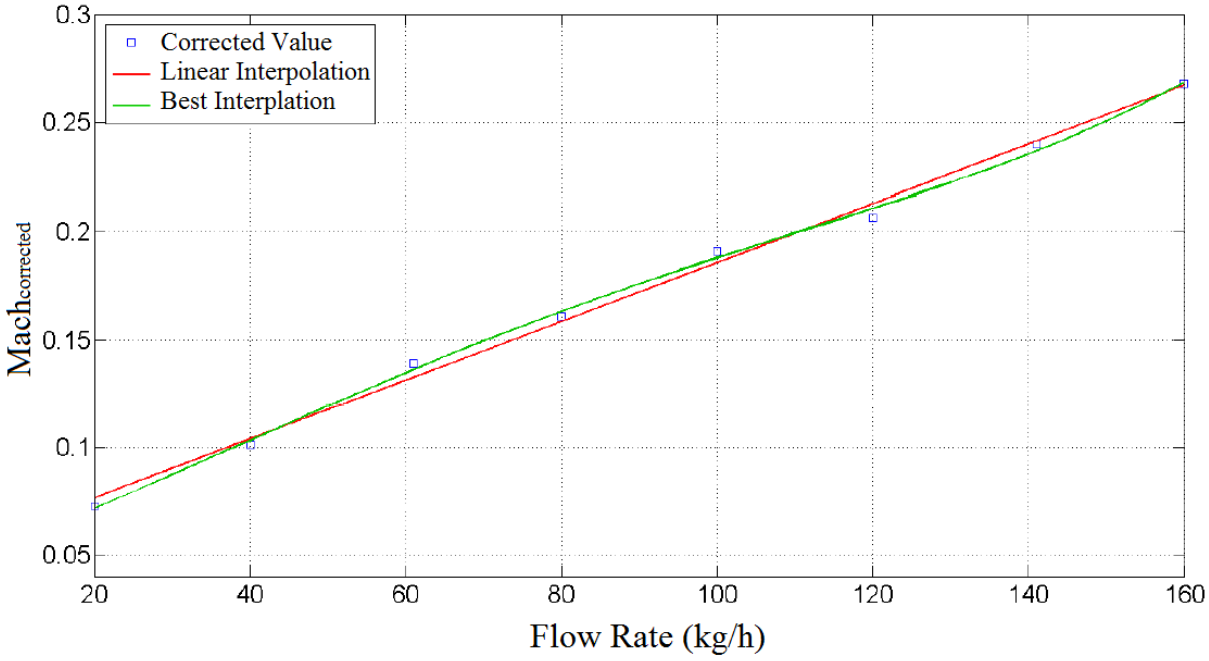

Figure IV-10 – Mach number correction law in function of air mass flow rate (L=368mm)

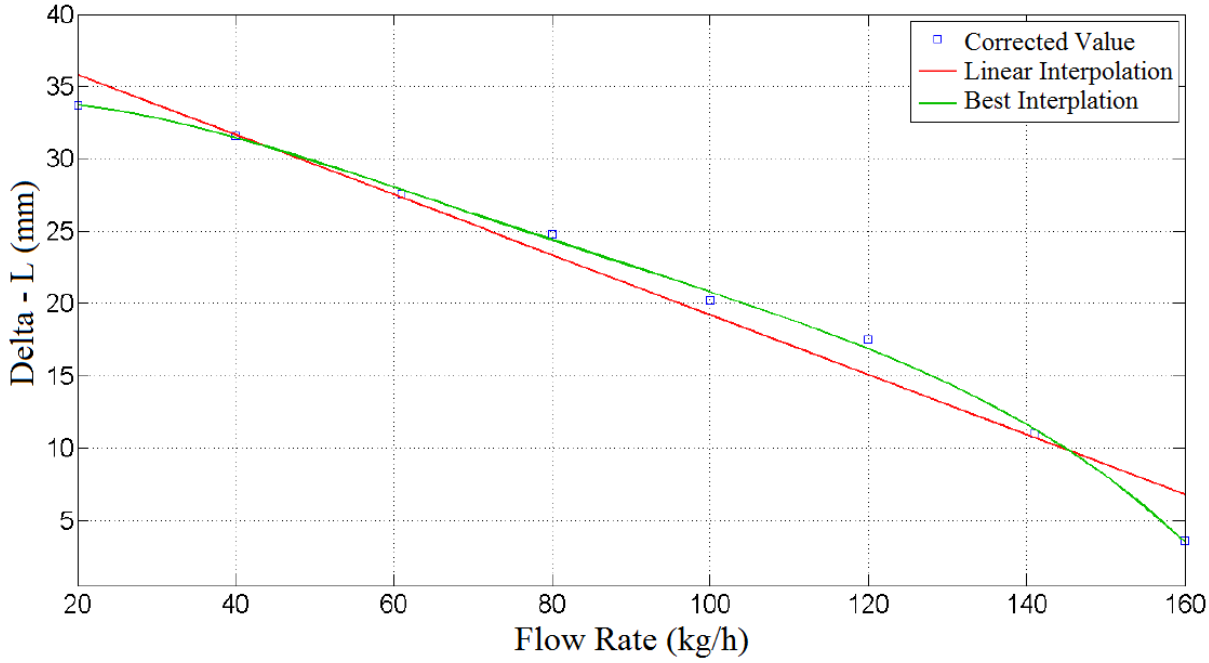

Figure IV-11 – Length correction law in function of air mass flow rate (L=368mm)

It is also important to show the evolution of corrected Mach number in function of calculated one. Apparently, a linear relation between these two parameters can exist (Figure IV-12).

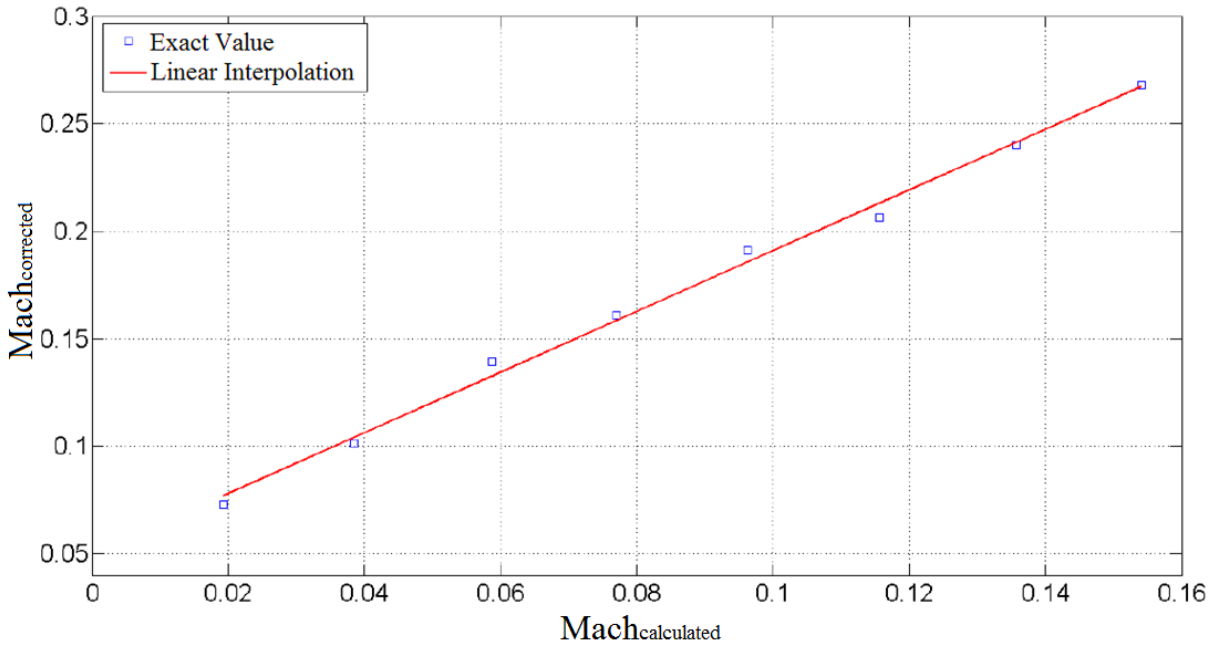

Figure IV-12 – Corrected Mach number in function of calculated Mach number (L=368mm)

Figure IV-13 and Figure IV-14 show the comparison between experimental and corrected acoustic transfer function (by applying respectively the best interpolation then the linear interpolation), for a mass flow rate of 80kg/h. Correction application on acoustic transfer function allowed the passage from Figure IV-9 to Figure IV-13.

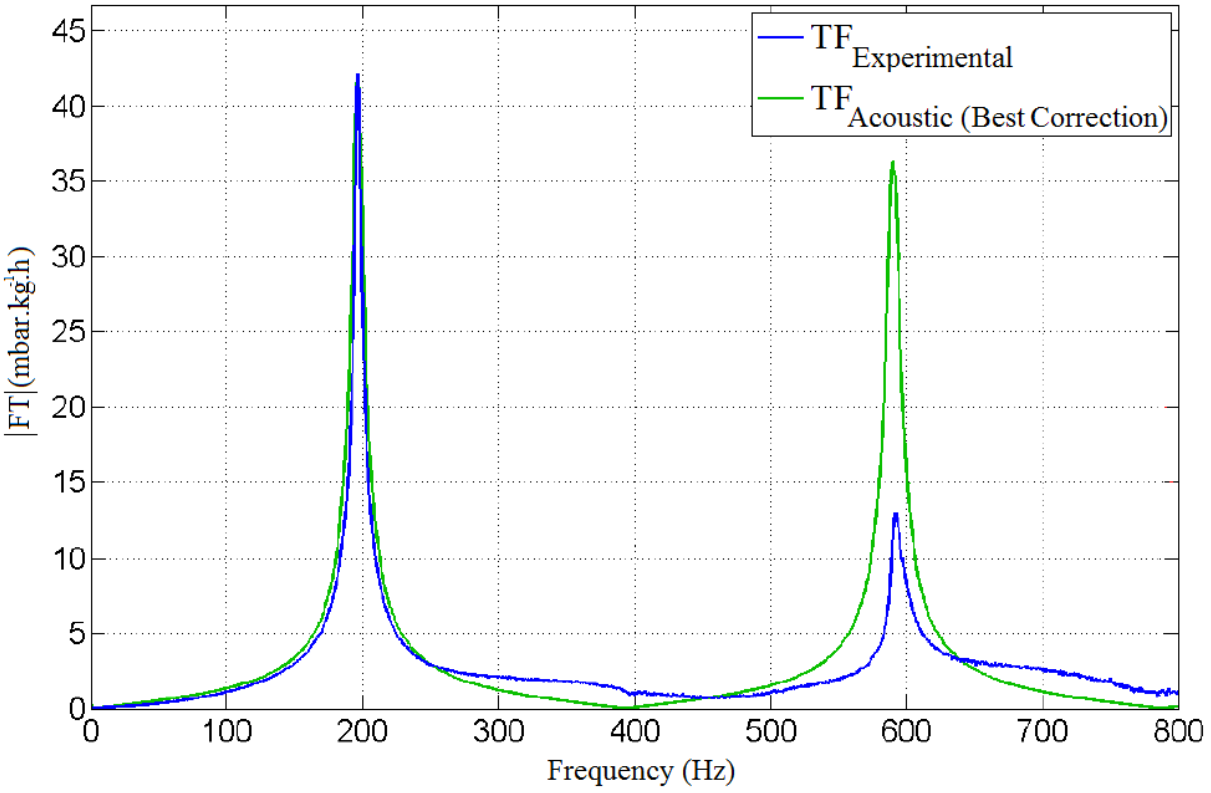

Figure IV-13 – Modulus of experimental and corrected acoustic Transfer Function (Best Correction)

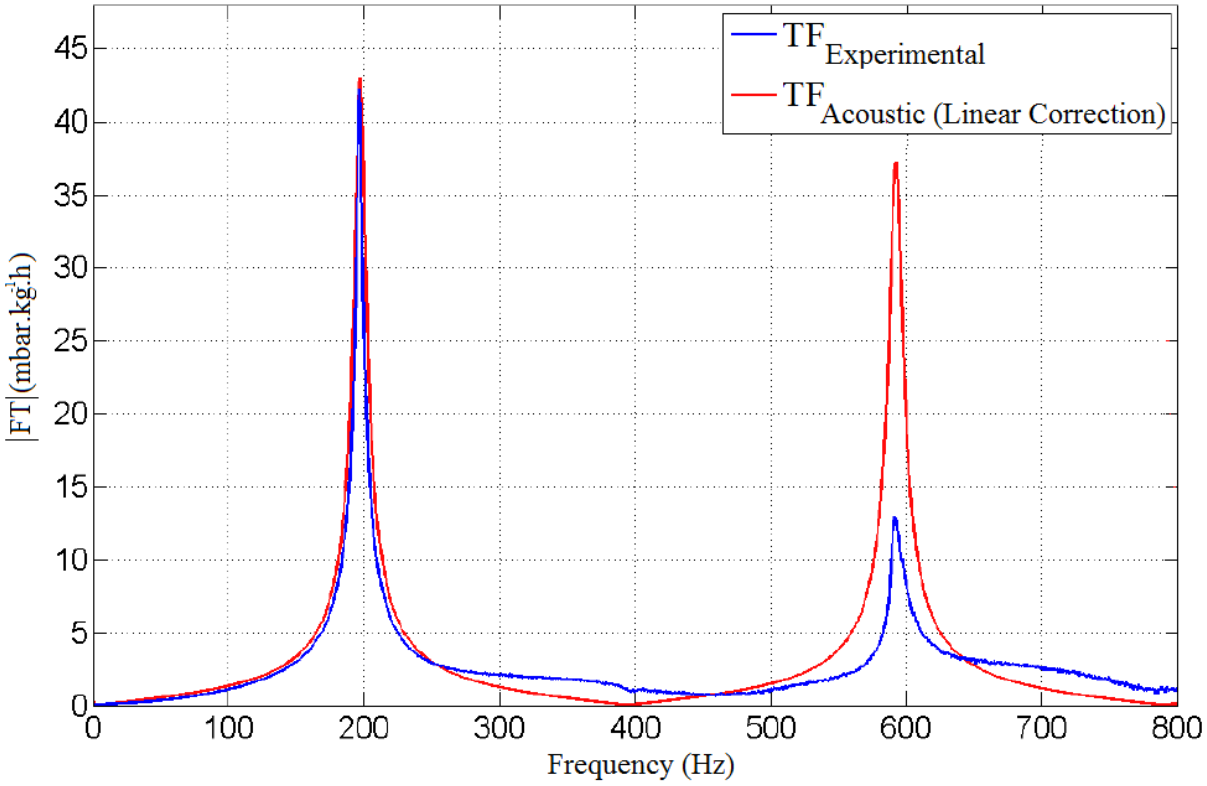

Figure IV-14 – Modulus of experimental and corrected acoustic Transfer Function (Linear Correction)

By comparing Figure IV-13and Figure IV-14, linear interpolation proved itself in the identification of the correction law. This method of calibration yielded to correct the fundamental frequency and the harmonic of the acoustic transfer function. However, only the amplitude of the fundamental peak is successfully corrected by using this method of calibration. The harmonics can be also corrected by dividing the identified function into different subsystems, each harmonic is considered then as a fundamental frequency of the new system. This work was not done in this PhD since engine sensitivity is about nearly 500 Hz, then a perfect modelling of the harmonics of the system is not needed.

The same work must be carried out for different length of the tube with same diameter (185, 985 and 1086 mm). The correction laws are shown in Figure IV-18 and Figure IV-19. Therefore, it will be possible by using acoustic impedance model and these corrections laws to identify a transfer function of a tube without doing tests on the dynamic flow bench.

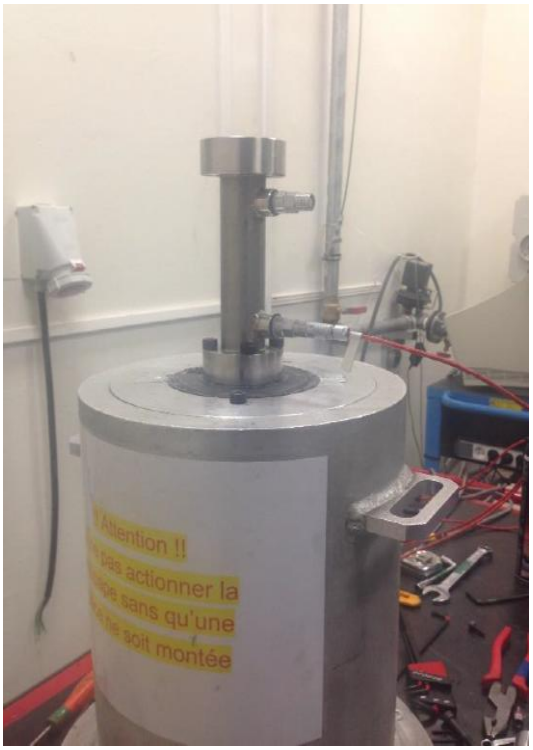

IV-15 - Dynamic flow bench test on a tube (L=185 mm, D=30 mm)

IV-16 - Dynamic flow bench test on a tube (L=968 mm, D=30 mm)

IV-17 - Dynamic flow bench test on a tube (L=1086 mm, D=30 mm)

It should be noted that this study was done on different geometries with the same diameter. In order to take into consideration this physical characteristic, the same study should be done on different geometries with the same length but different diameters. This study was not taken into consideration in this work, only length variation effect considered.

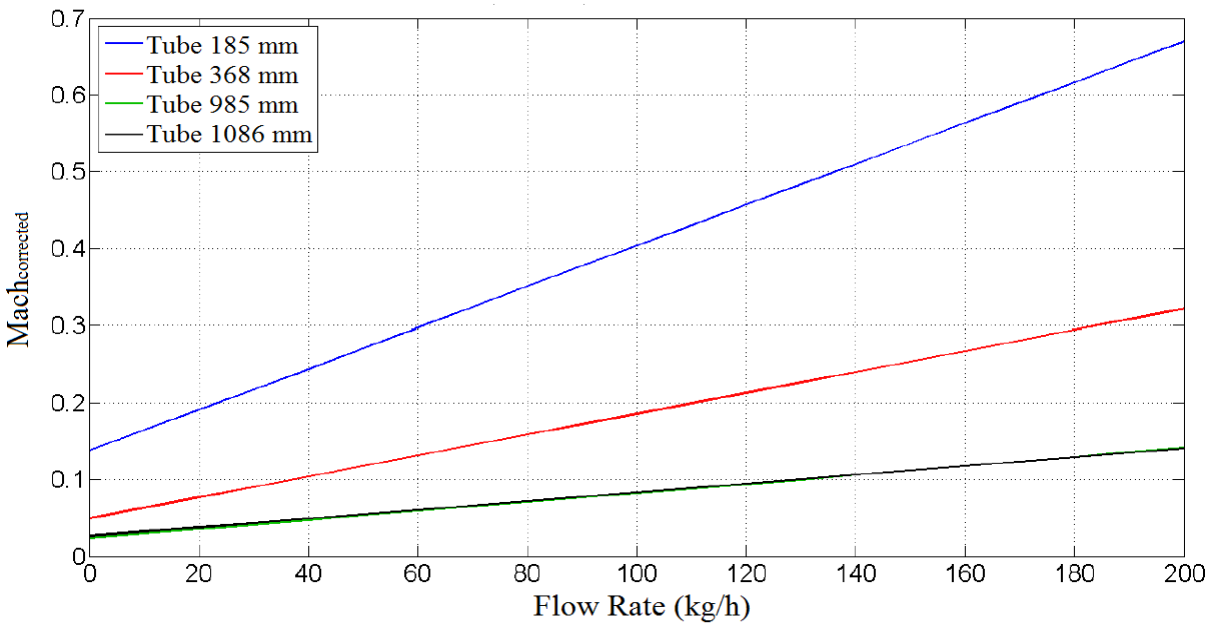

Figure IV-18 – Mach number correction law for different length of tube in function of air mass flow rate

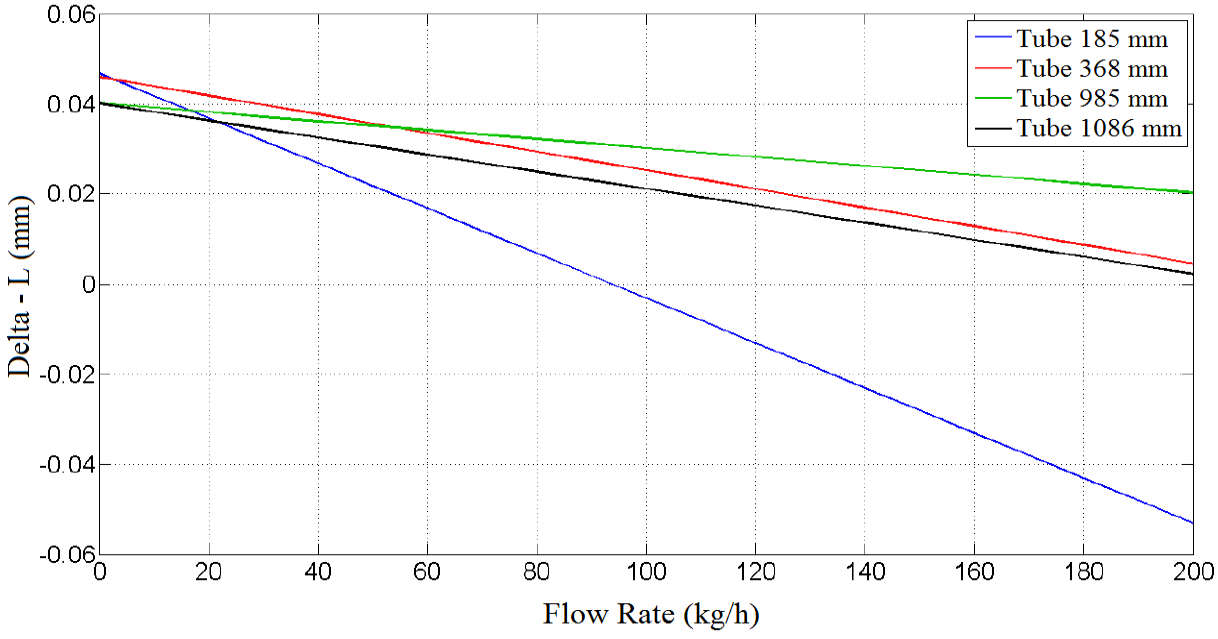

Figure IV-19 – Length correction law for different length of tube in function of air mass flow rate

Based on this study, the following conclusions can be drawn:

Length variation:

- Influences the natural frequencies of the system
- Its influence on the amplitude of the peaks become greater with the reduction of the length of the tube
- Decreases with the increase of the imposed air flow

Mach number variation:

- Influences the amplitude of the peaks
- Its influence on the natural frequencies of the system become greater with the reduction of the length of the tube
- Increases with the increase of the imposed air flow

IV.3.3 Conclusion

The identified transfer function using acoustic theory will replace the measured transfer function from the dynamic flow bench in chapter III. The complete model identification and validation, based on the acoustic transfer function model, will be presented in details in chapter V. Two applications will be presented:

- A single cylinder engine, where a simple intake geometry is used
- A three cylinder engine, where the intake system is a complex geometry

In this chapter, acoustic theory of the wave propagation is used in order to identify a transfer function, which should be similar to the one measured on the dynamic flow bench. The objective is to shorten the identification procedure of the transfer function model. In the next chapter, the model validation of the transfer function model based on acoustic theory is presented.

V. Model Validation

In this chapter all the experimental tests benches (the Dynamic Flow bench, the single cylinder engine and the three cylinder engine) and numerical tools (GT-Power and Matlab) helped to elaborate the transfer function model, and allowed a multi-physical representation in which the acoustic waves were taken into consideration. The model will be validated against experimental data of two engines: a single cylinder engine and a three cylinder engine. Obviously, the single cylinder engine is an easy application for transfer function model since only one excitation source is generating the pressure waves during engine cycles. However, the three cylinder engine is more complicated for model validation, since the interaction between cylinders can affect substantially the pressures upstream the valves. In this case, and for a better air flow modeling, this phenomenon should be taken into account. Two methodologies for cylinder's interactions modeling will be presented.

V.1. Model Algorithm

The general model algorithm is illustrated in Figure V-1. The intake system of the internal combustion engine is removed from the engine and installed on the dynamic flow bench. A prototype of the intake system can also be used, but it is better to use the same geometry used on engine in order to take into account the surface roughness and the real configuration of the parts connection. The link between the tested part and the dynamic flow bench can be done using a specific part. This latter takes into consideration the geometrical specifications of the shut-off valve and the intake system. Once the geometry is mounted on the bench and ready to use, a linkage test is primordial in order to check whether the complete configuration is isolated. The next step is to simulate the response of the geometry when it is subjected to a brutal excitation (shut-off valve closing). The pump is regulated to a certain air mass flow rate value. This pressure sensor measures the relative pressure upstream the valve. Before closing the shut-off valve, the pressure losses can be determined (open ended configuration). The relative pressure at the inlet of the geometry is considered negligible. Thus, the sensed value measured corresponds to the pressure losses of the intake valve at a certain air mass flow value. By simply regulating the air mass flow rate using the pump, the pressure losses profile of the tested part can be identified. These values are registered in a table (Pressure losses in function of air mass flow rate). After closing the shut-off valve, the geometry is in open-close ended configuration. The air mass flow is brutally interrupted. The pressure variation upstream the valve corresponds to the wave propagation in the tested geometry. This signal is registered and filtered with a high sampling frequency (2^{15}=32768 points). The signal is windowed to only one second, which is enough to maintain the complete informations related to the natural frequencies of the signal. Data are registered in Matlab workspace as vectors. One vector corresponds to the air mass flow rate excitation and the other one corresponds to the pressure fluctuation. Using "Ident" toolbox, a transfer function of the system can be identified (for more details please refer to the Annex I). The stability of this function should be also studied in order to check the robustness of the system. This study can be also done using Matlab. In order to check the good operations of identified system, the coefficients of the identified transfer function are implemented in a GT-Power model were only a transfer function exists with an excitation source (air mass flow signal variation) (for more details please refer to Annex II). The output response of the system is compared to the measured relative pressure from the dynamic flow bench. The function is considered as a robust model when good correlation between both signals is shown. Once this step is validated, the next step is to build a GT/TF coupled model in GT-Power. The intake geometry of the engine in the simulation native code is replaced by the transfer function and the pressure losses table. The final results (pressure upstream the intake valve and the volumetric efficiency) of the new model are compared to the data from GT-Power native model and experimental results. The model importance can be accessed through simulation time and model accuracy comparison.

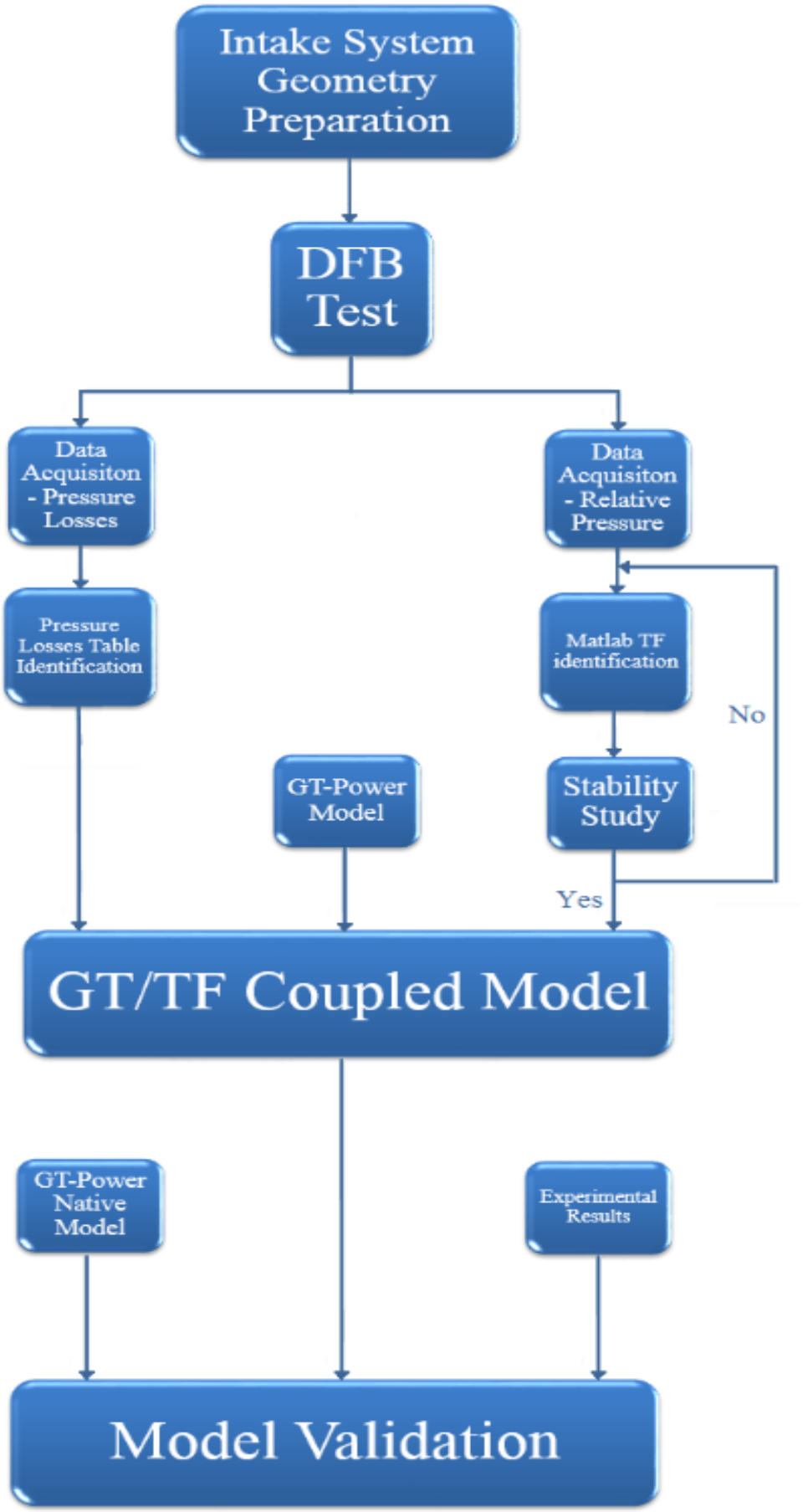

Figure V-1 - Model Algorithm

V.2. Single Cylinder Application

The single cylinder engine is shown in Figure II-27. The intake system is a simple tube of 985 mm length and 30 mm diameter. Many tests were done on this bench. Different engine rotational speeds were tested, in which the pressure upstream the intake valve and the mean air flow value aspirated during the cycles were registered and are presented in Table V-1.

Table V-1 - Mean air mass flow rate in function of engine rotational speed

N (rpm)	1265	1501	1604	1709	1789	1910	2085	2207
qm_{act} (kg/h)	5.82	6.28	6.83	7.29	8.06	8.30	9.56	11.13

N (rpm)	2313	2510	2604	2792	3000
qm_{act} (kg/h)	11.33	11.73	12.12	13.96	15.37

The actual mean air mass flow rate values allow calculating the volumetric efficiency of the engine in function of engine rotational speed. The GT-Power native model was calibrated according to the experimental results (Figure II-29). Good correlation between the simulation and experimental results were obtained. These later will be presented later in this chapter. Unfortunately, the hot film does not allow an instantaneous measurement of the air mass flow rate at the intake valve. In order to identify the maximum air mass flow rate at a particular engine rotational engine, the Barré-Saint-Venant model can be used [18]:

$$q_m = \frac{p_{cyl} A_{valve} C_d}{a} \left[\left(\frac{2\gamma^2}{\gamma - 1} \right) \left(\frac{p_{valve}}{p_{cyl}} \right)^{\frac{2}{\gamma}} \left[1 - \left(\frac{p_{valve}}{p_{cyl}} \right)^{\frac{\gamma - 1}{\gamma}} \right] \right]^{\frac{1}{2}} \quad \text{(V-1)}$$

The discharge coefficient C_d in equation (V-1) is determined using the dynamic flow bench. The cylinder head is mounted on this latter and the discharge coefficient is identified for different air mass flow rate. In-cylinder pressure and the pressure upstream the intake valve are already registered during the tests. Thus, the maximum air mass flow rate at each engine rotational speed is identified, and presented in Table V-2.

Table V-2 - Maximum air mass flow rate in function of engine rotational speed

N (rpm)	1265	1501	1604	1709	1789	1910	2085	2207
qm_{max} (kg/h)	59.24	69.12	72.76	74.80	75.98	78.68	81.01	87.29

N (rpm)	2313	2510	2604	2792	3000
qm_{max} (kg/h)	90.26	95.33	98.65	104.41	118.89

These values are necessary in order to identify the transfer function for each engine rotational speed. The next step is to begin the test campaign on the dynamic flow bench. The intake system of the single cylinder engine is mounted on the dynamic flow bench (Figure V-2). The pressure sensor is located at the same position on the real engine. The ambient pressure and temperature are registered during the test as well.

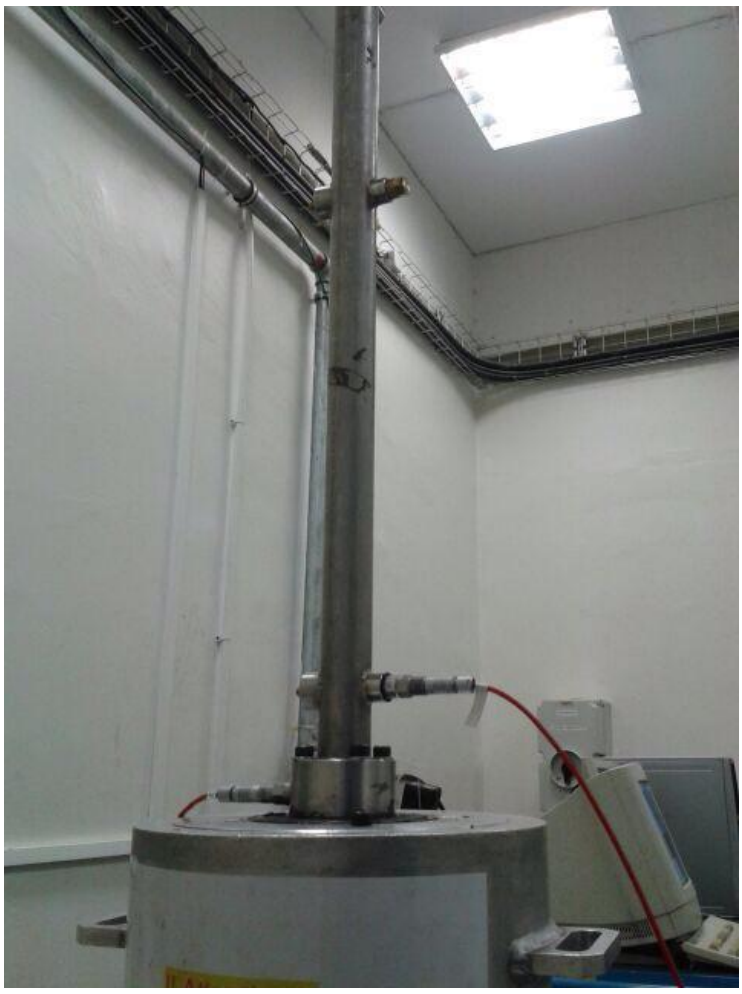

Figure V-2 - Dynamic flow bench test on a simple tube (L= 985 mm, D= 30 mm)

The transfer functions were identified at different air mass flow excitation according to Table (V-2). Table (V-3) presents the different notations of the identified transfer functions.

Table V-3 - Transfer Function identification at each engine rotational speed

N (rpm)	1265	1501	1604	1709	1789	1910	2085	2207
TF	TF_1	TF_2	TF_3	TF_4	TF_5	TF_6	TF_7	TF_8

N (rpm)	2313	2510	2604	2792	3000
TF	TF_9	TF_{10}	TF_{11}	TF_{12}	TF_{13}

The next step is to implement the transfer function in GT-Power code (as presented in Figure V-3). The pressure losses table is already calculated during the tests on dynamic flow bench and it is specific for each tested part. Before choosing the optimal way for implementing all the transfer functions in the coupled model, the functions presented in Table V-3 were tested in simulation. Firstly, the objective is to check the accuracy of the coupled model and the simulation time as well. Each transfer function parameters were implemented manually in the specific TF template for each engine rotational speed. The engine running was fixed in GT-Power at one second, which means that the real engine operating time is one second. The simulation time needed for GT-Power native model and GT/TF coupled model is shown at the end of the simulation. These data are presented in Figure V-4.

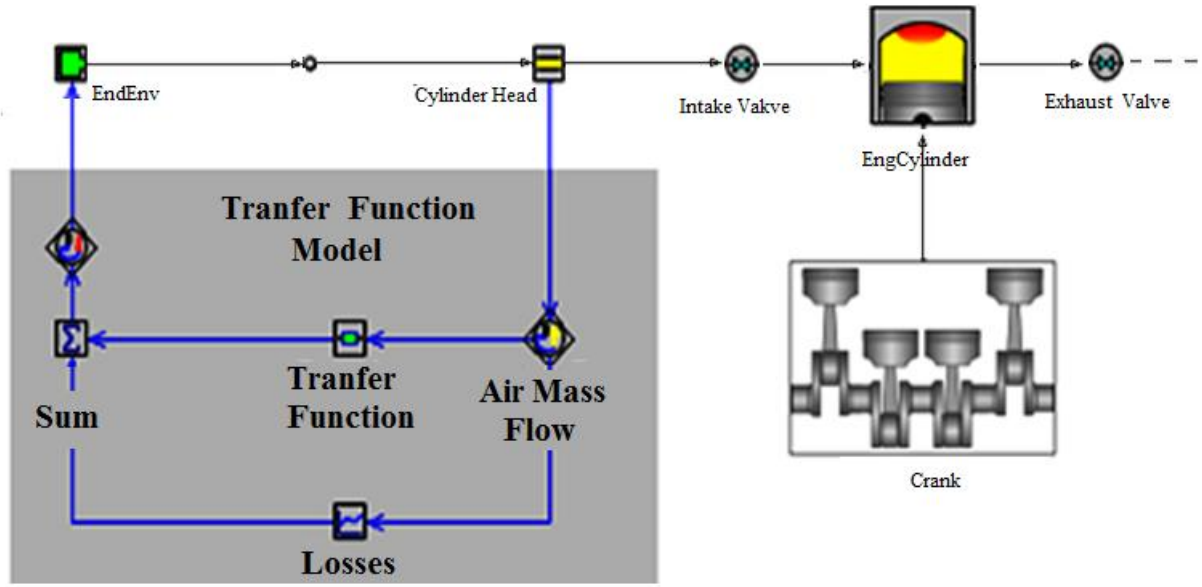

Figure V-3 - GT/TF coupled model

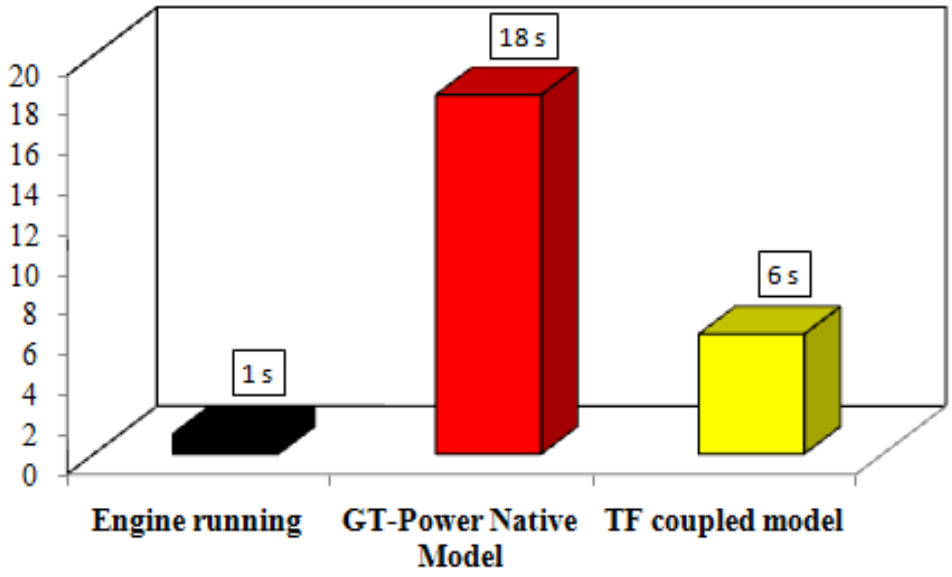

Figure V-4 - Simulation time in function of the model used for 1 second of Engine Running

For only one existing transfer function in the GT/TF coupled model, simulation time gain is about nearly 3 times. The simulation time needed for GT-Power Native to simulate 1 second of engine running is 18 seconds. The discretization number of the intake geometry in the native code was specified according to GT-Power recommendations (Table V-4). The discretization is the splitting of large geometries into smaller sections in order to improve modeling accuracy. In general, coarse discretization results in larger time steps and faster execution at the expense of model accuracy, while finer discretization results in better accuracy and frequency resolution at the expense of execution time. Beyond a certain limit, further reducing the discretization length does not bring benefits.

Table V-4- GT-Power recommendations

GT-Power recommendations
Intake system discretization $\cong 0.4\times$ Cylinder Bore
For detailed acoustic analysis (Straight tube)
Discretization Length = $\cong \frac{1}{2}\times$ Geometry Length

These meshes were removed by replacing the intake geometry of the single cylinder by its proper transfer function. As a consequence, the calculation time dedicated for thermodynamic variables calculation was saved. Thus the simulation time of the new model is reduced (three times faster than GT-Power native model.

In terms of accuracy, the volumetric efficiency criterion is used. The volumetric efficiency is the image of the pressure upstream the intake valve. For each engine rotational speed, this variable is calculated in the three studied cases:

- Using experimental results: for engine speed, the volumetric efficiency is calculated using the theoretical values of air mass flow rate, which are calculated using equation (III-7), and the real ones measured by the hot film.
- GT-Power native model: the volumetric efficiency is directly calculated by the simulation code.
- GT/TF coupled model: the volumetric efficiency is also calculated by the software.

The results are presented in Figure V-5. The relative errors are calculated in three cases:

- Relative error of GT-Power native model results compared to experimental data.
- Relative error of GT/TF model results compared to experimental data.
- It is interesting to show the relative error of GT/TF model results compared to GT-Power native model ones.

These values are presented in Tables (V-5), (V-6) and (V-7). The uncertainty of air mass flow rate measurements using the hot film ($e = 0.5/\sqrt{3}$) was taken directly into consideration in the data presented in the table (The worst case is presented).

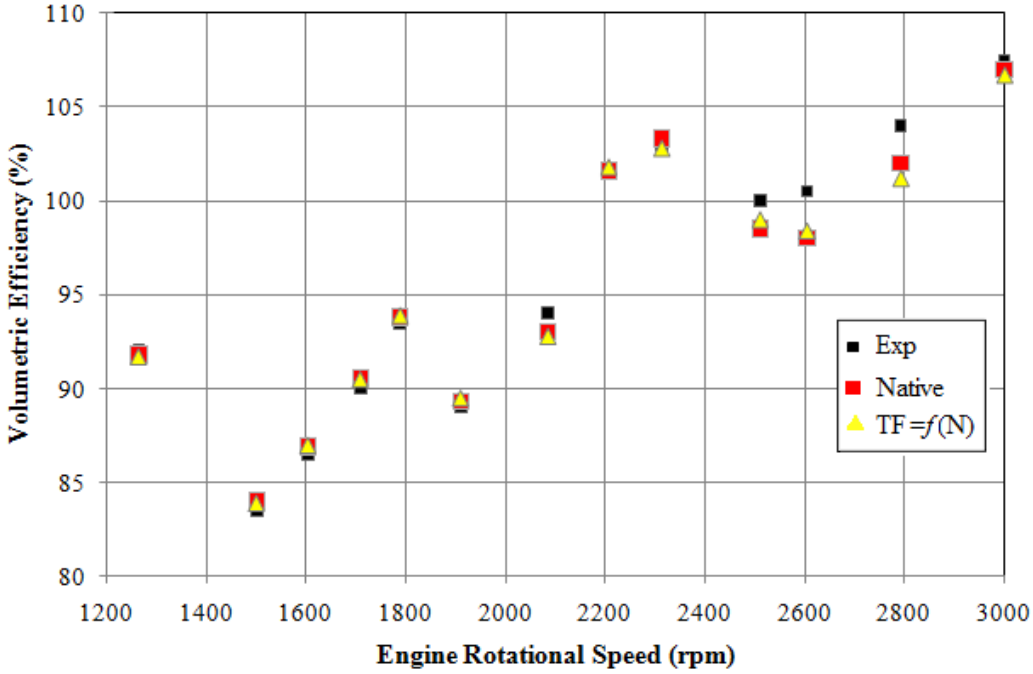

Figure V-5 - Volumetric Efficiency in function of engine rotational speed using many transfer functions identified at different $qm_{exc}=f(N)$

The results presented in Figure V-5 show good accuracy level of both models: GT-Power Native code and GT/TF coupled model. In the following tables, the maximum calculated relative error for the different cases cited previously, is marked by red boxes. The maximum error of GT-Power native model volumetric efficiency compared to experimental data is 2.55% at 2604 rpm. Concerning the relative error of GT/TF model results compared to experimental data, the maximum error on volumetric efficiency is 2.69% at 2792 rpm. Between both models, the maximum relative error on volumetric efficiency is always less than 1%. This letter proves that the coupled model is able to perfectly model the physical phenomena which occur in the intake system of the engine.

Table V-5 - Relative error of GT-Power native model results compared to experimental data

N (rpm)	1265	1501	1604	1709	1789	1910	2085	2207
Relative error (%)	0.217	0.595	0.46	0.662	0.319	0.335	1.07	0.09

N (rpm)	2313	2510	2604	2792	3000
Relative error (%)	0.29	1.522	2.551	1.96	0.467

Table V-6 - Relative error of GT/TF model results compared to experimental data

N (rpm)	1265	1501	1604	1709	1789	1910	2085	2207
Relative error (%)	0.326	0.479	0.578	0.555	0.427	0.561	1.276	0.295

N (rpm)	2313	2510	2604	2792	3000
Relative error (%)	0.194	1.05	2.089	2.692	0.744

Table V-7 – Relative error of GT/TF model results compared to GT-Power native model results

N (rpm)	1265	1501	1604	1709	1789	1910	2085	2207
Relative error (%)	0.109	0.119	0.115	0.110	0.106	0.224	0.215	0.196

N (rpm)	2313	2510	2604	2792	3000
Relative error (%)	0.484	0.507	0.408	0.784	0.280

In addition, three more transfer functions were identified at low, medium and high air mass flow rate excitation (40 kg/h, 80 kg/hr and 160 kg/h). The low value corresponds to the lowest minimum value of qm_0 in which the identified transfer function can be stable. The maximum value of air mass flow rate corresponds to the maximum set point regulated by the pump. This value depends on the tested geometry and the shut-off component slot presented in Figure II-6. The maximum air mass flow rate value increases when the slot of the shut-off component is big. Finally, the medium value of air mass flow rate corresponds to the average maximum air mass flow rate value calculated from Table V-2. These transfer functions were used in a three different GT/TF coupled models and implemented manually in the software. The purpose behind these three functions is to check the accuracy of the model for different engine rotational when only one equivalent transfer function is used.

In Figure V-6, the volumetric efficiency in function of engine rotational speed is presented. For the whole engine rotational speed, only one function identified at qm_{exc}=40 kg/h is used. The maximum relative error of GT/TF model results compared to experimental data is at 3000 rpm with 13.48%. Compared to the native model, the maximum relative error of GT/TF model is also at 3000 rpm with 13.08%. As a conclusion, the accuracy of the model using one transfer function identified at the lowest air mass flow rate value is not good. The model is improved by the use of the average air mass flow rate value (Figure V-7). The maximum relative error of GT/TF model results compared to experimental data is at 3000 rpm with 5.11%. Compared to the native model, the maximum relative error of GT/TF model is also at 3000 rpm with 4.67%. By simply comparing these values to the ones presented previously where TF = *f (N)* (Figure V-5), the model accuracy is high when many transfer functions are used in the code (higher accuracy level).

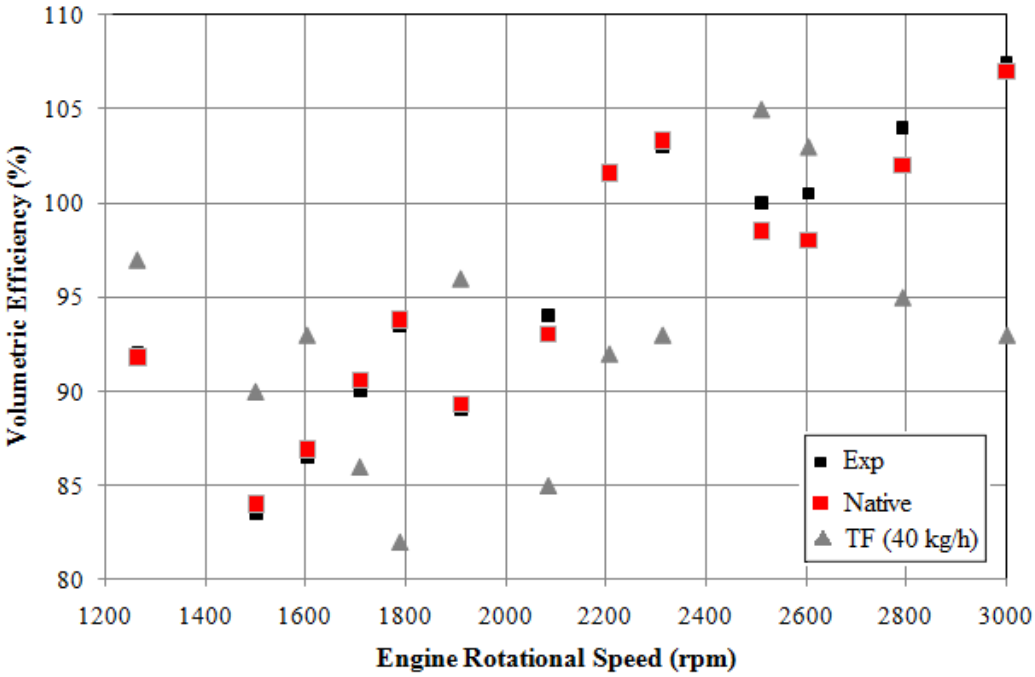

Figure V-6 - Volumetric Efficiency in function of engine rotational speed using a transfer function identified at qm_{exc}=40 kg/h

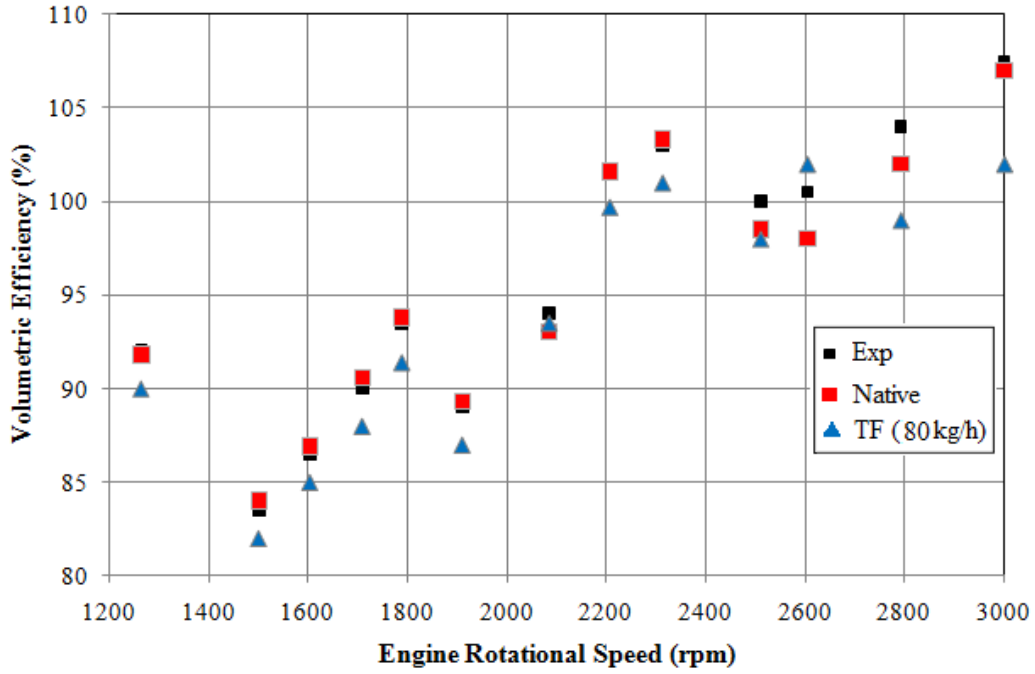

Figure V-7 - Volumetric Efficiency in function of engine rotational speed using a transfer function identified at qm_{exc} =80 kg/h

In Figure V-8, the volumetric efficiency in function of engine rotational speed using a transfer function identified at 160 kg/h is presented. The maximum errors of the GT/TF model compared to experimental and native ones are respectively 3.8 % and 4.3% at 1789 rpm and 2085 rpm. The model is improved compared to the case where the average air mass flow rate is used, especially at high engine rotational speed, but still in general the model accuracy is better using a transfer function for each engine rotational speed.

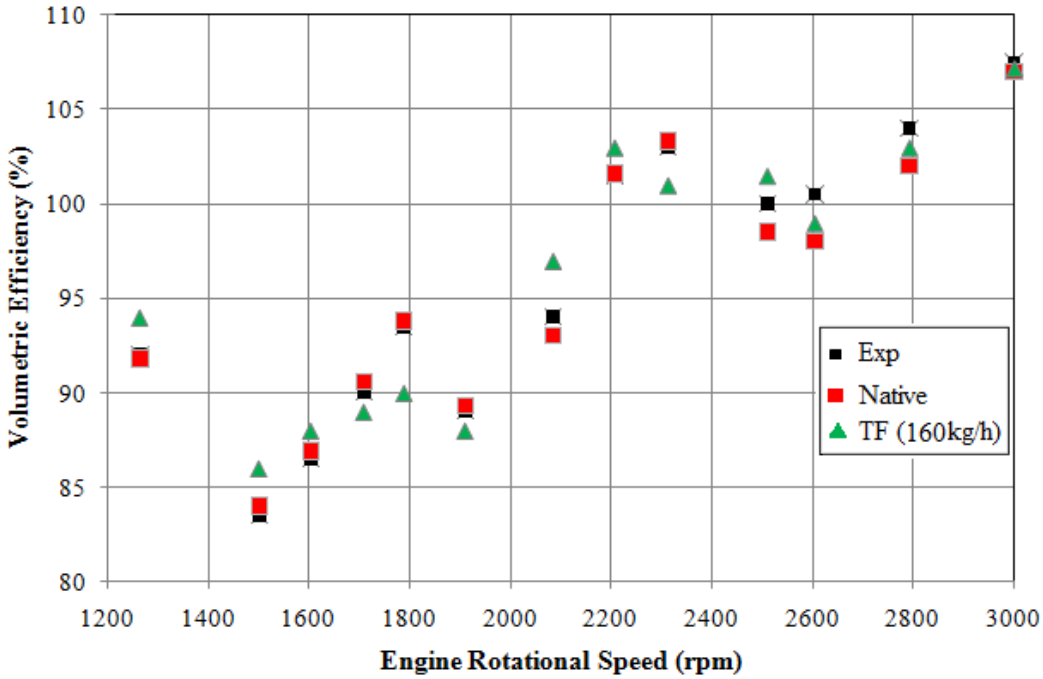

Figure V-8 - Volumetric Efficiency in function of engine rotational speed using a transfer function identified at qm_{exc} =160 kg/h

Thus, the work now should be focused on how these functions can be implemented in GT/TF coupled model. In the previous studied case, the functions were implemented manually by the user. In other words, for each engine rotational speed, the user has to change manually the coefficients of the transfer function template. This is not the best and easiest way for using the model. In the following section, a study was done in order to find the best way of making the transfer function implementation in the simulation software. A new methodology is then presented, based on exponential filter function.

In terms of simulation time, the GT/TF model in these three cases needs the same computational time as the coupled model presented in Figure V-4 since only one transfer function is presented in the code.

V.2.1 Transfer function implementation

V.2.1.1. Using Switch function

The transfer functions are implemented in the GT/TF Coupled code (Figure V-9). Switch functions were also added in order to switch between the functions according to the engine rotational speed. For example, when the engine speed is set to 1910 rpm, only the TF_6 should

be activated. Unfortunately, even when the other functions are disabled, calculations are done on these blocs. This affect the global simulation time of the final model and its convergence time as well. This means that this way of implementing the transfer functions is not the best way.

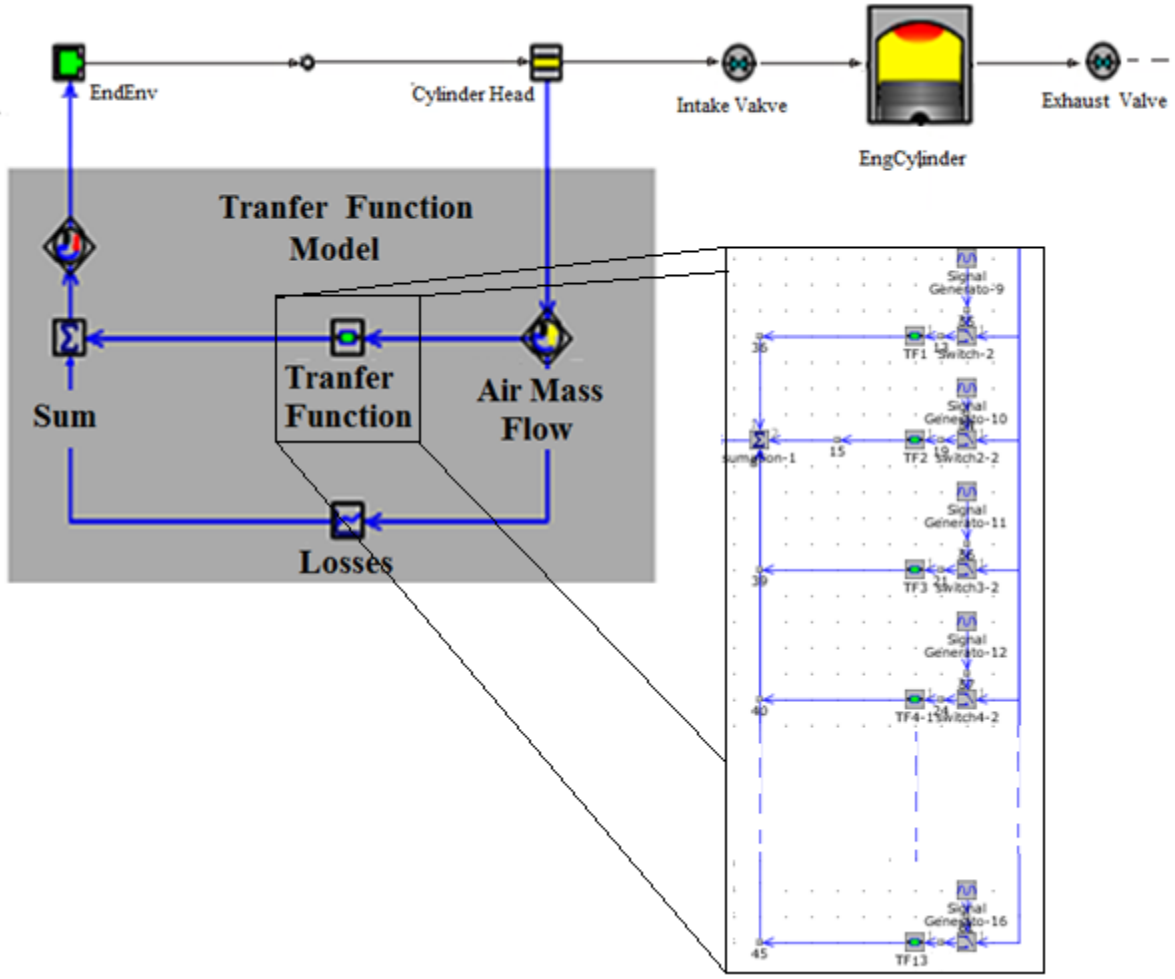

Figure V-9 - GT/TF coupled model

V.2.1.2. Using coefficient variation method

Another method for transfer function implementation in GT/TF code is tested. The objective is to use only one transfer function and changing the numerator and the denominator coefficient during the simulation (Figure V-10). This helps to reduce the simulation time since only one transfer function is used in the engine model.

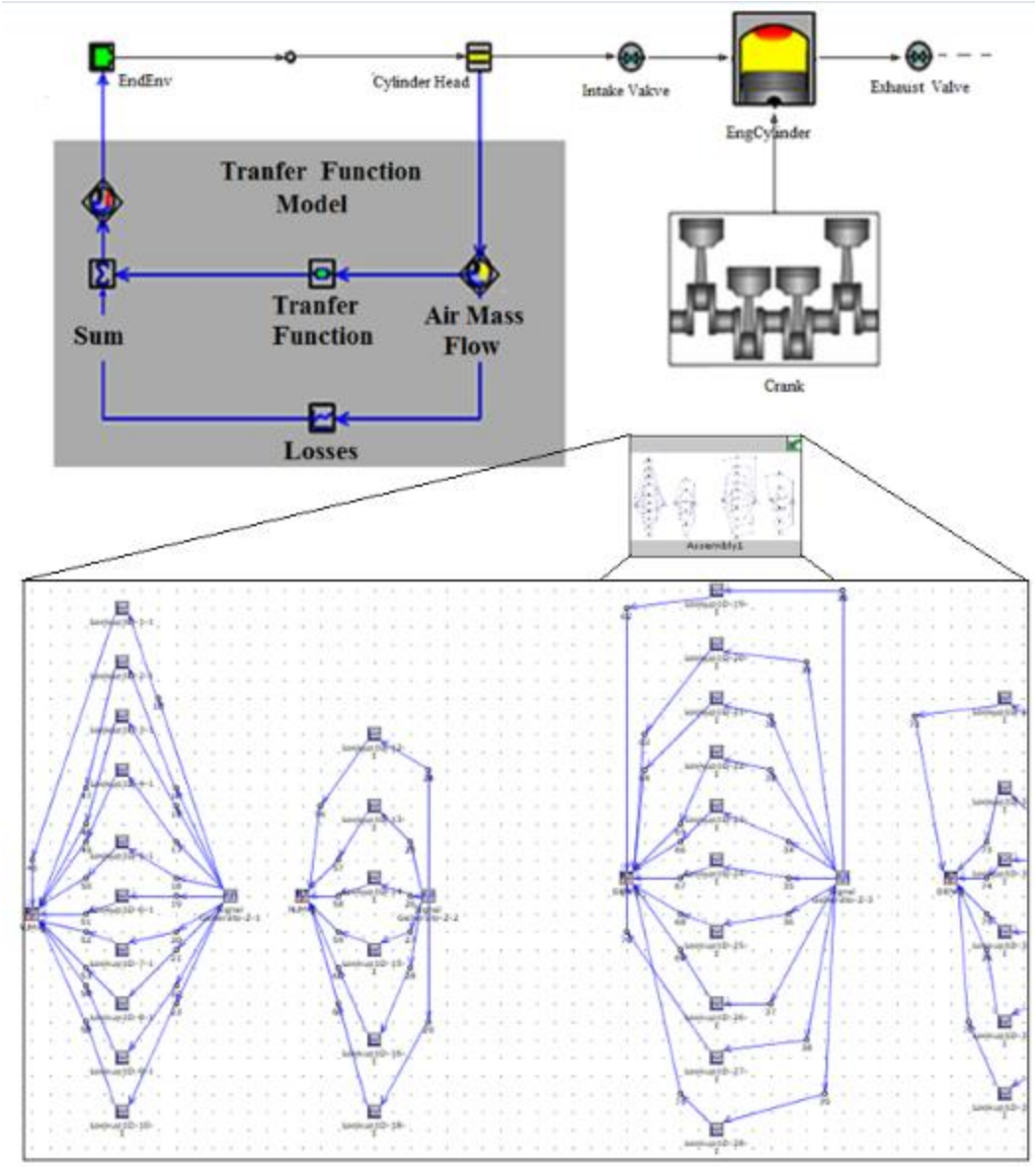

Figure V-10 - TF Coefficient changing Method

Unfortunately, the transfer function template in GT-Power version 7.5 does not allow user to modify the coefficient during simulation (Figure V-11). Thus, this way of implementing different transfer functions could not help to achieve the objective. It will be interesting to test this methodology of TF implementation in the future versions of GT-Power. Maybe this template will be updated to meet the needs of the user.

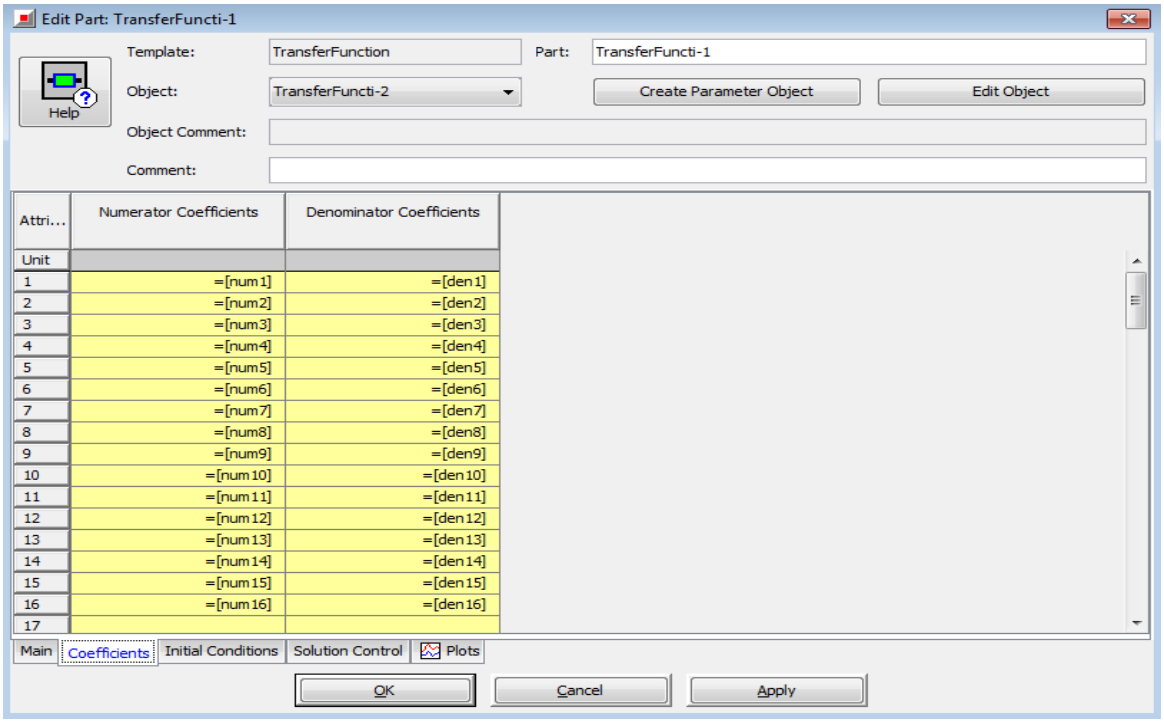

Figure V-11 - Transfer Function template

V.2.1.3. Using exponential filter

The best way discovered for transfer functions implementation is the use of exponential filter. This methodology allows using only one transfer function in the GT/TF model. This function is called basic transfer function. It is identified at a certain air mass flow rate (identification procedure is presented later). By choosing the right damping coefficient of the exponential filter in equation (III-33), the pressure response P_x calculated using equation (V-2) will be similar to the pressure response from the transfer function identified for a particular engine rotational speed.

$$P_x = FT_{basic} \otimes F_{\exp} \tag{V-2}$$

For example, the pressure response at 1910 rpm is called P_6. The corresponding transfer function is TF_6. The exponential transfer function helps to damp the output of the basic transfer function at 1910 rpm. Thus, the final response is almost similar to the response of TF_6 at the same engine rotational speed. For each speed, a specific damping coefficient is identified. The identification procedure of this coefficient is presented as follow:

- A transfer function is identified at the lowest air mass flow rate excitation value (40 kg/h). This latter is the basic transfer function. There are two reasons behind using this value: Firstly, it is the minimum value of qm_0 in which the identified transfer function can be stable. Secondly, compared to the other transfer functions identified at higher qm_0, the amplitude of the pressure fluctuation generated by this function, after closing the intake valve, is the highest one. This means that the pressure response of the corresponding transfer function covers the pressure response of other

transfer function. In this case, the output of the transfer function identified at 40 kg/hr will be damped using the exponential filter to get pressure values similar to the ones obtained by another transfer function.

- After identifying the basic transfer function, the next step is to identify the damping coefficient of the exponential filter, which depends on engine rotational speed. Only the low natural frequency of the transfer function is concerned by this study.

The identified damping coefficient of the exponential can be changed during the simulation according to engine rotational speed. Figure V-12 presents the GT/TF coupled model, where the exponential filter is added to the output of the transfer function.

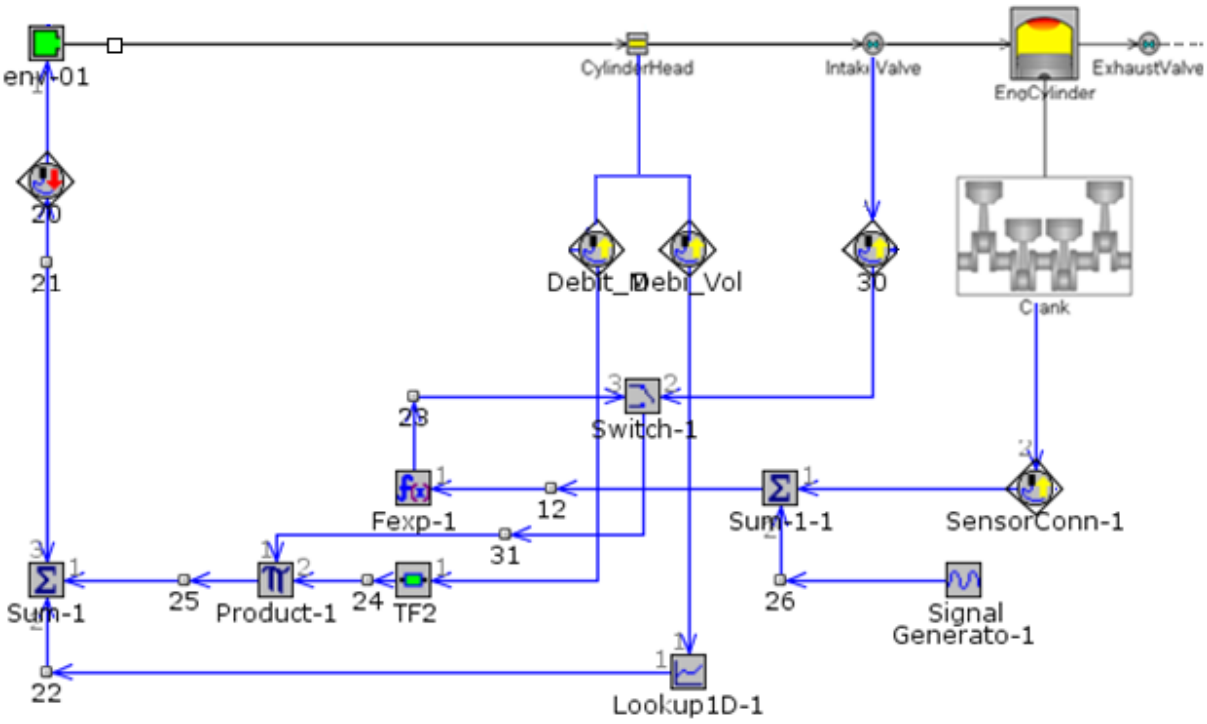

Figure V-12 - GT/TF coupled model including exponential filter function

Figure V-13 shows the volumetric efficiency in function of engine rotational speed when exponential filter is added to the transfer function main model. Compared to Figure V-5, the new model still shows good accuracy level compared to experimental data and GT-Power native model results. This methodology allows user to reduce the simulation time of the model where many transfer functions should be integrated. Transient engine operation can be also tested, since the coefficients variation of model are taken into account by changing the damping coefficient of the exponential filter according to engine rotational speed.

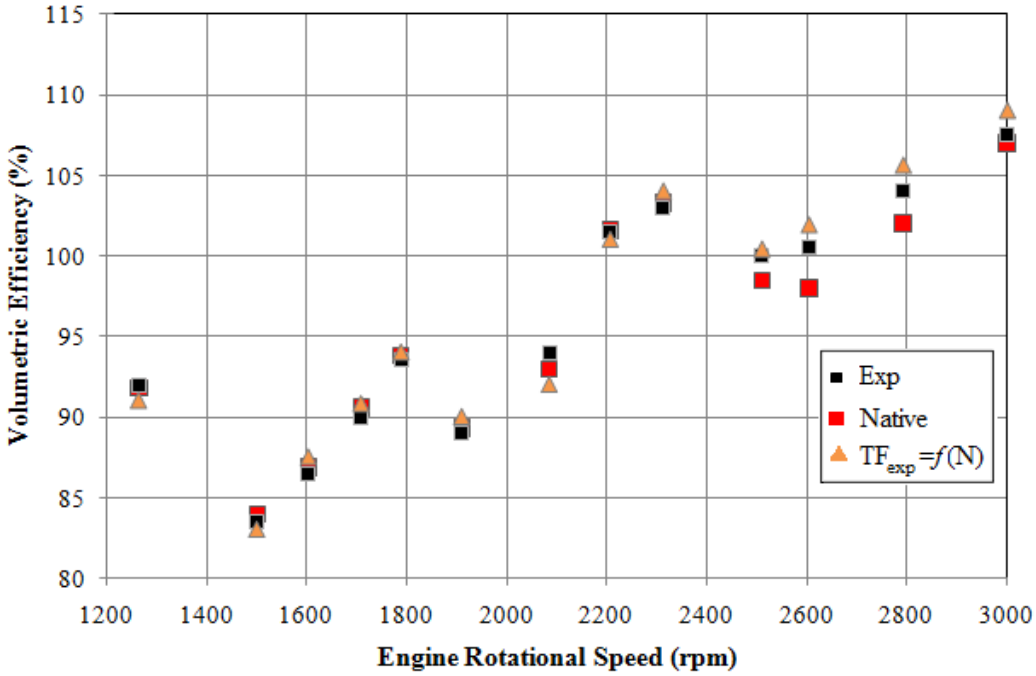

Figure V-13 -Volumetric Efficiency in function of engine rotational speed using a transfer functions identified at different $qm_{exc}=f(N)$ and filtered with the exponential filter

The next step to validate the model is to compare the instantaneous absolute pressure upstream of the intake valve. The following figures compare in-cylinder pressure and the instantaneous pressure in the inlet tube (located near the inlet valve) for different rotational engine speeds:

- **N=1265 rpm**

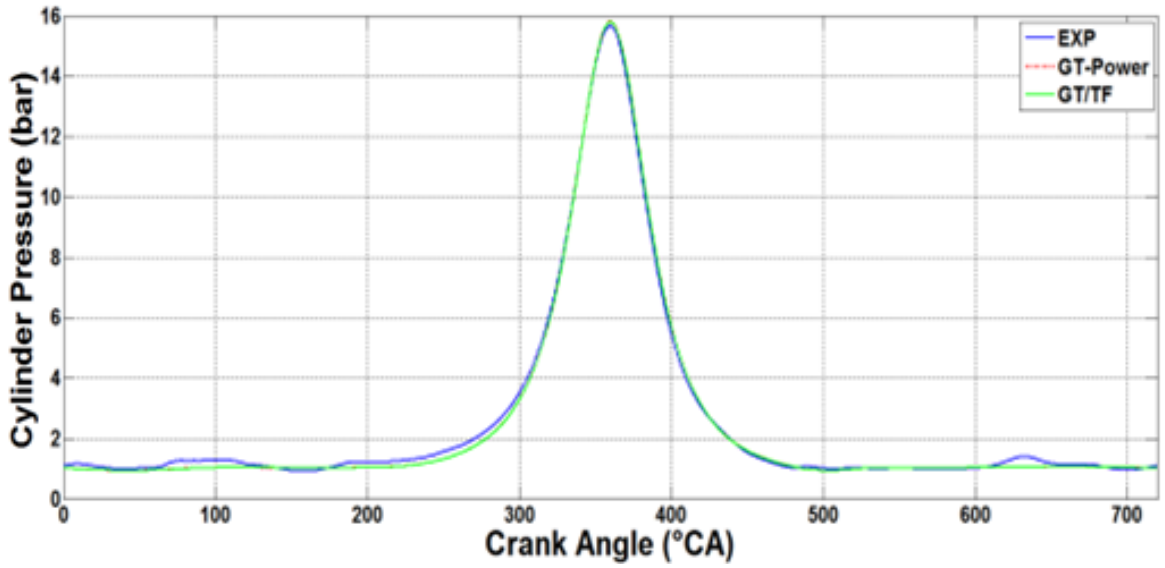

Figure V-14 - In-cylinder pressure in function of engine crank-angle at 1265 rpm

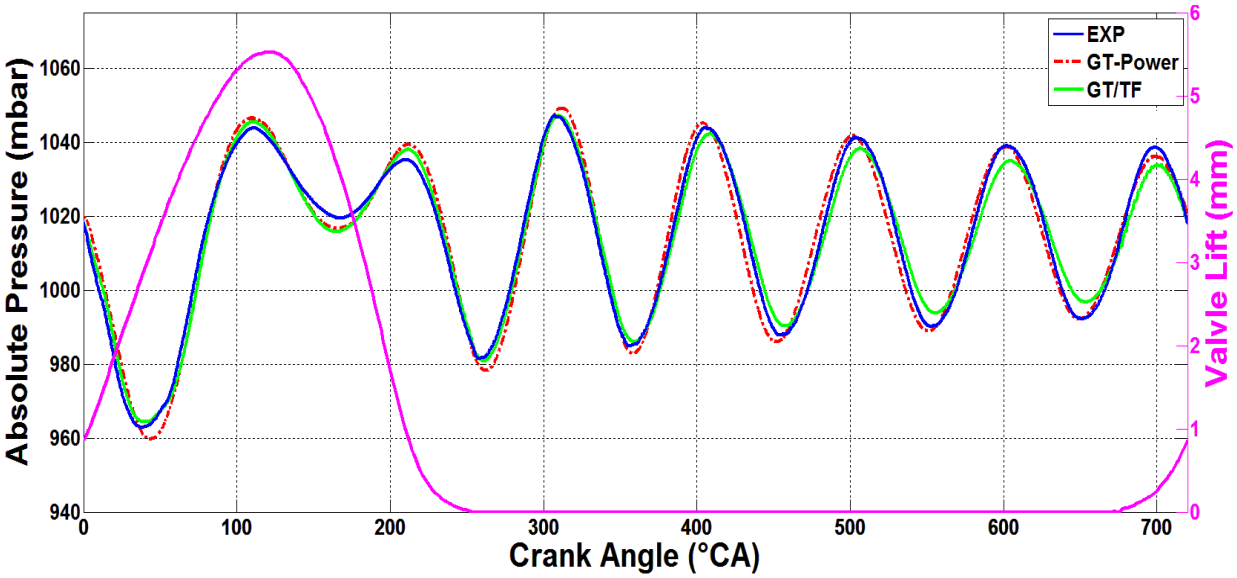

Figure V-15 - Intake absolute pressure in function of engine crank-angle at 1265 rpm

- **N=2085rpm**

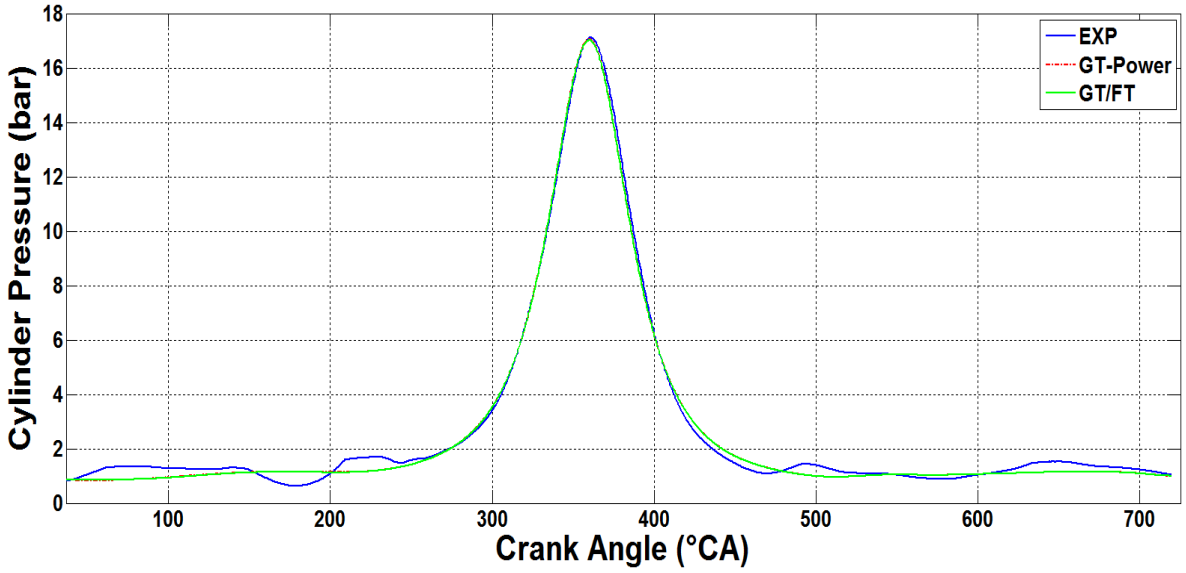

Figure V-16 - In-cylinder pressure in function of engine crank-angle at 2085 rpm

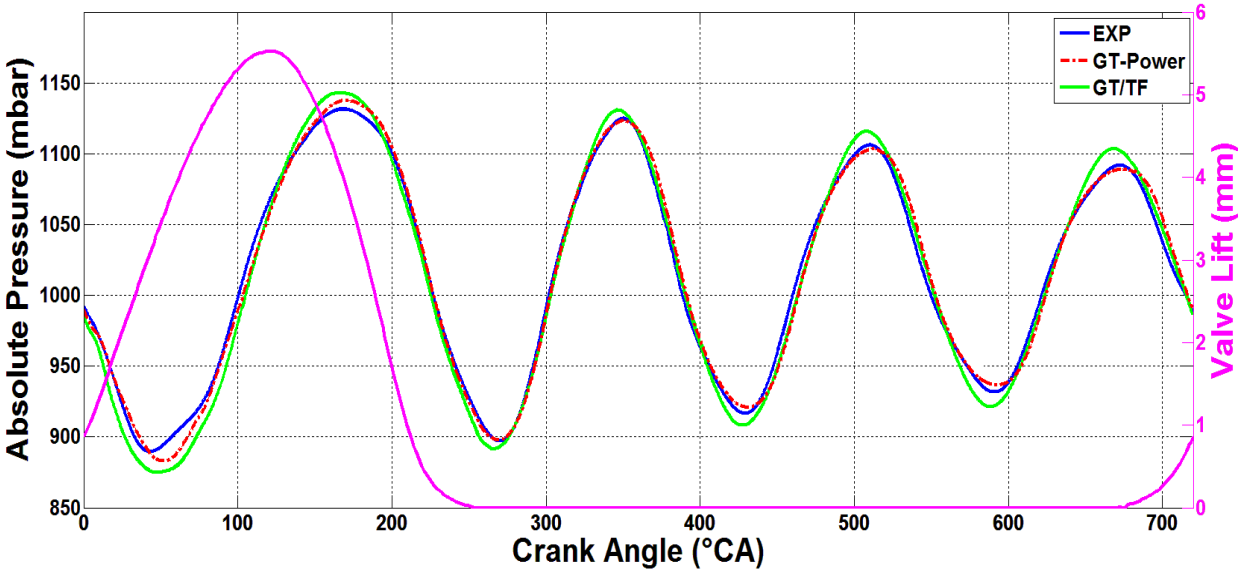

Figure V-17 - Intake absolute pressure in function of engine crank-angle at 2085 rpm

- **N=3000 rpm**

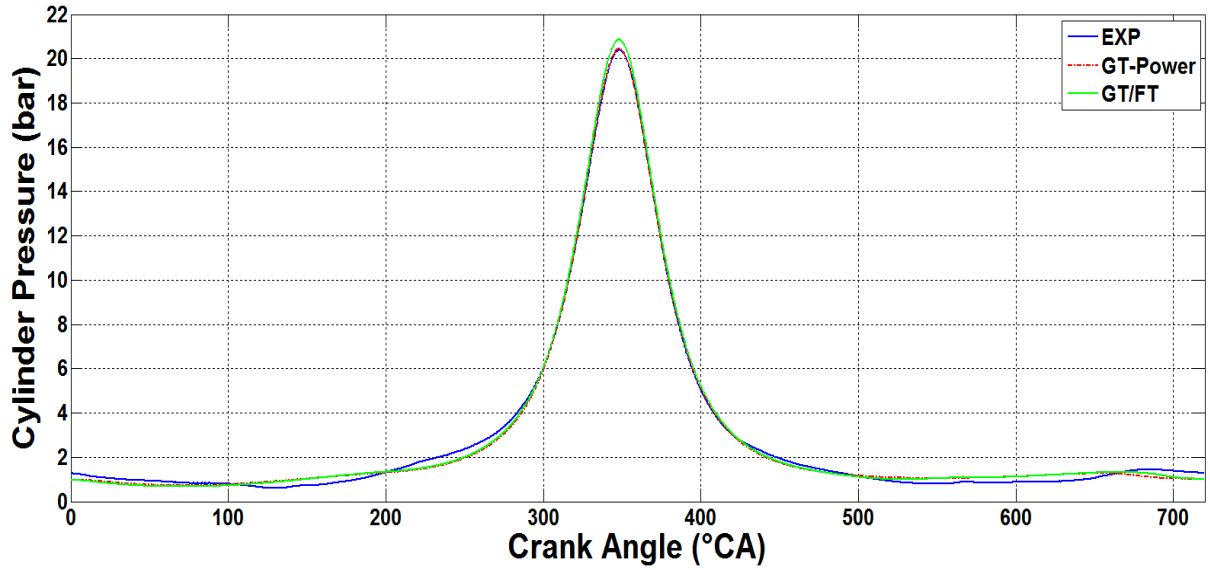

Figure V-18 - In-cylinder pressure in function of engine crank-angle at 30000 rpm

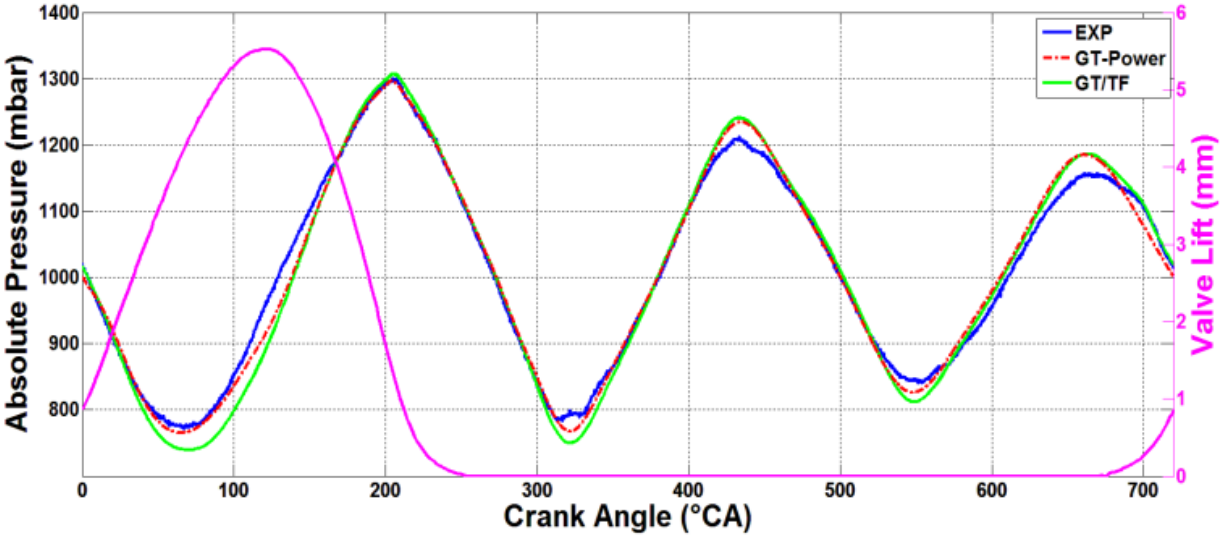

Figure V-19 - Intake absolute pressure in function of engine crank-angle at 3000 rpm

The crankshaft angle when piston is at TDC (end of compression stroke) is 360 °CA, and the intake valve closes completely at 253 °CA. As shown in Figures V.14 to V.19, there is good agreement between experimental data, GT-Power native code and GT/TF coupled model. According to Ohata *et al.* [3], the volumetric efficiency mainly depends on the pressure downstream the intake valve, chiefly during the short period before closing the intake valve. Therefore, when the pressure fluctuation is well modelled using transfer function model, the error on the volumetric efficiency as compared to experimental data is reduced. For the rotational engine speeds 1265 and 2085 r/min, the volumetric efficiency of the engine using transfer function model is very close to the experimental one. This can be explained using Figure V.15 and V.17, the error on the relative pressure is insignificant when the valve is opened, and also the amplitude of the fluctuations is not high. Considering Figure V.19, for the GT-Power and the new model, the amplitude of the pressure at the IVO was different than the experimental one, which is the reason of error increasing at 3000 r/min.

As a conclusion, the exponential filter helps to reduce the simulation time of the transfer function model, since only on transfer function in the code is used, while conserving good accuracy level of the main model. In the next section, a new concept is also added to the main model in order to reduce more the simulation time of GT/TF coupled model.

V.2.2 Transfer Function modeling the temperature variation

In this section, the application of transfer function of temperature variation described in chapter III is presented. The validation of this new concept is done on the single cylinder engine (without combustion).

As previously discussed, the aim of this function is to decrease the convergence time of the GT/TF model since new information (temperature variation) is added to the gas dynamics non linear equations of GT-Power. The temperature variation, due to pressure fluctuation, is modeled in this function. The effect of external heat exchange is not taken into consideration. This latter will be included in the model later in V.2.5.

Using the virtual dynamic flow bench, the temperature variation after closing the shut off valve is registered using a virtual temperature sensor. This latter is located at the same position of the pressure sensor. The methodology consists on separating the thermodynamic variables (relative pressure and temperature) by the use of two transfer functions. The same methodology of identification of the transfer function for pressure is used to identify a transfer function for temperature.

After identifying the coefficients, the transfer function for temperature is implemented into the previous model, which is presented in Figure V-12 (Figure V-20).

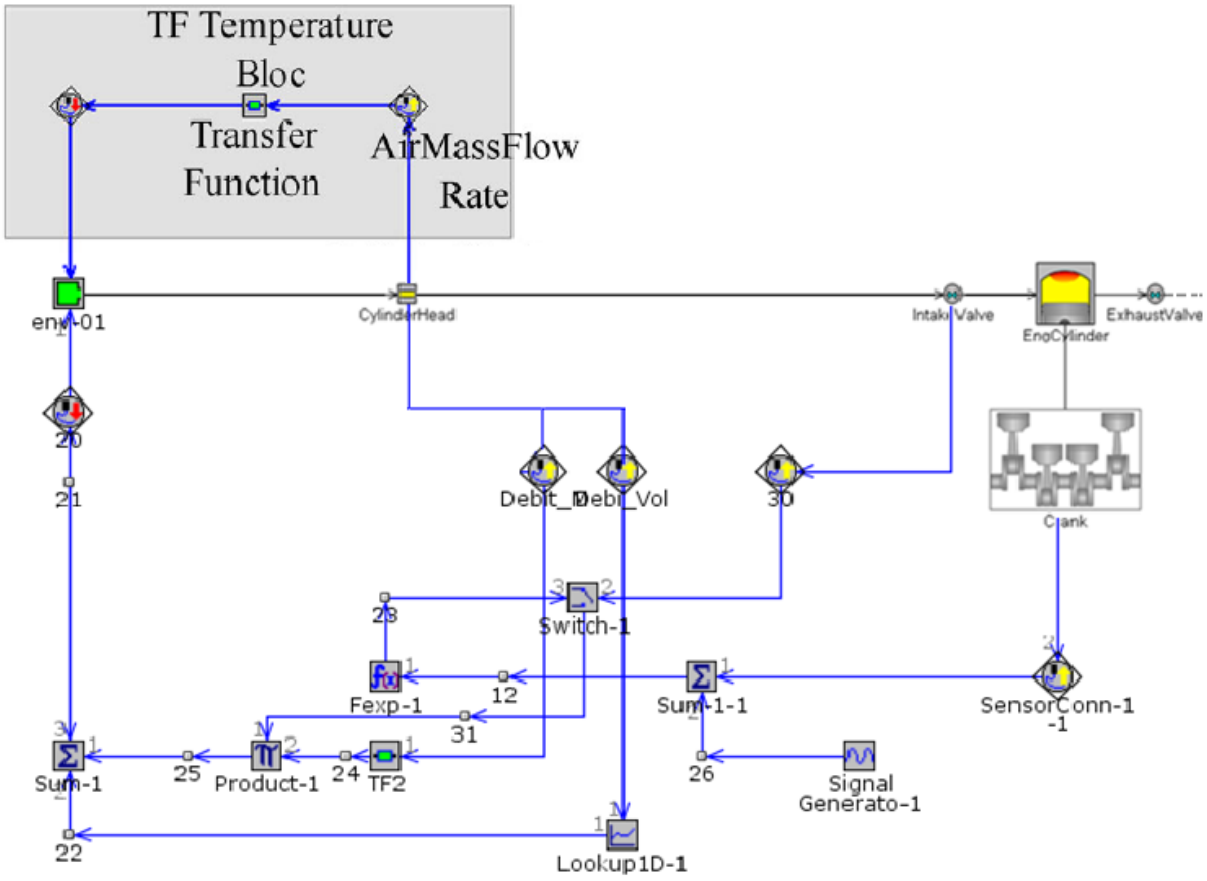

Figure V-20 - GT/TF coupled model including exponential filter function and transfer function for temperature variation

A simulation is done, and the temperature upstream the intake valve is measured. A comparison is made with the results from the native code (Figures V-21 and V-22). Good correlation between results, but this method did not show improving in term accuracy. The reason goes back to the small temperature variation in this case of application (single cylinder engine without combustion). Later, the effect of the temperature variation on transfer function model accuracy is studied.

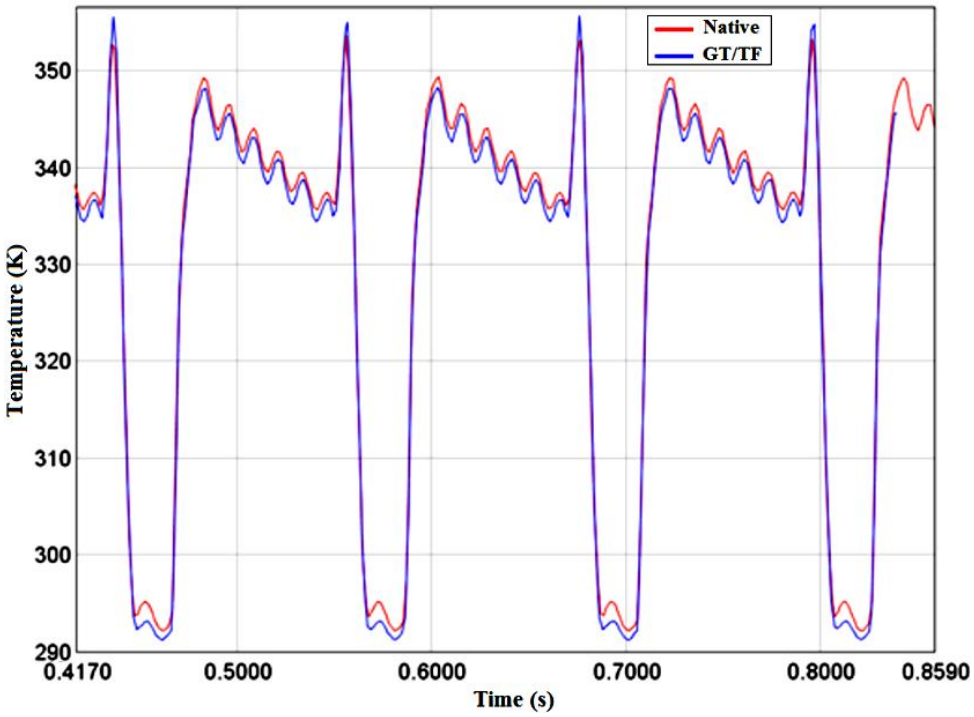

Figure V-21 - Temperature variation upstream the intake valve at 1265 rpm

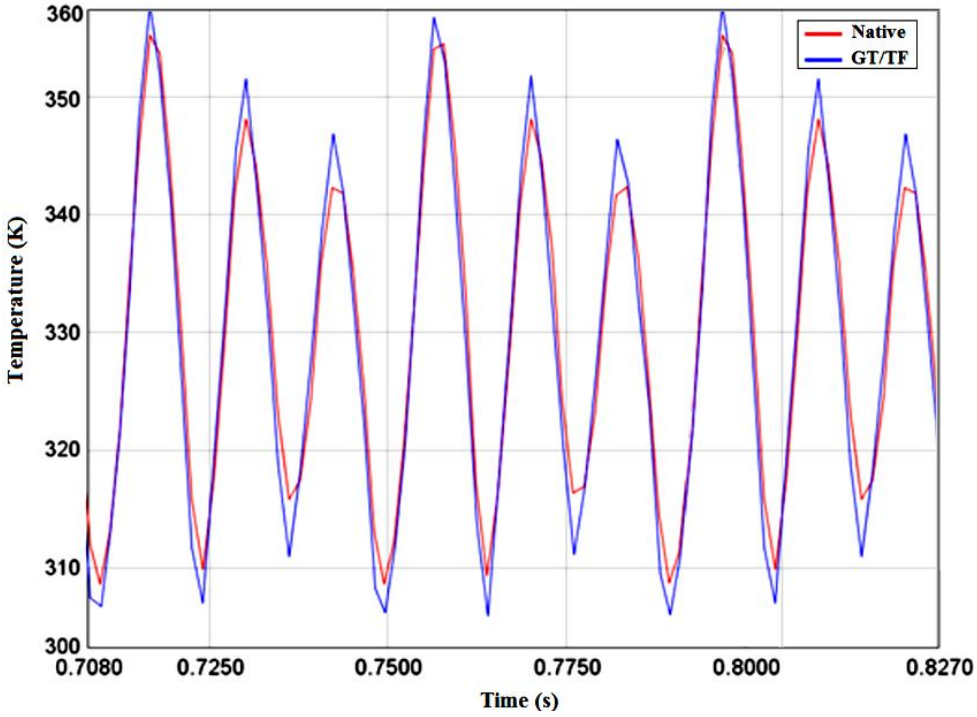

Figure V-22 - Temperature variation upstream the intake valve at 3000 rpm

In terms of simulation time, the new model allows saving 3 more seconds, compared to the previous model (where only transfer function for pressure is used). Compared to native model, the new model is six times faster.

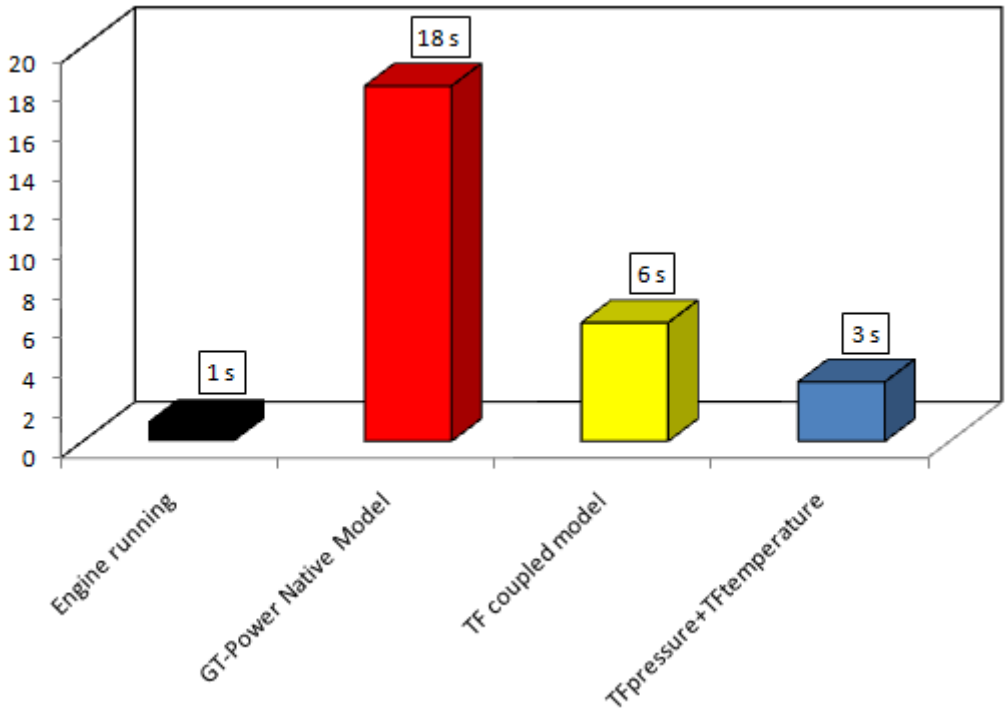

Figure V-23 - Simulation time in function of the model used for 1 second of Engine Running

V.2.3 Model efficiency using transient speed profile

In order to test the transfer function response in a transient engine operation, a cycle (inspired from the Extra Urban Driving Cycle (EUDC) of NEDC) is tested. The engine rotational speed variation in function of time is defined in GT-Power (as depicted in Figure V-25).

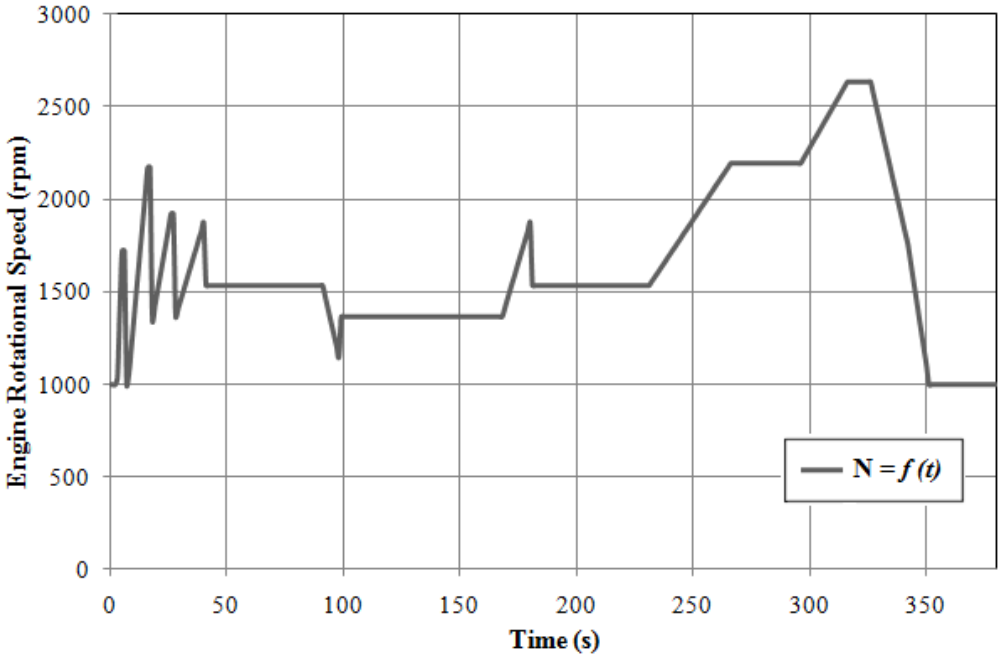

Figure V-24 - Engine rotational speed variation in function of time

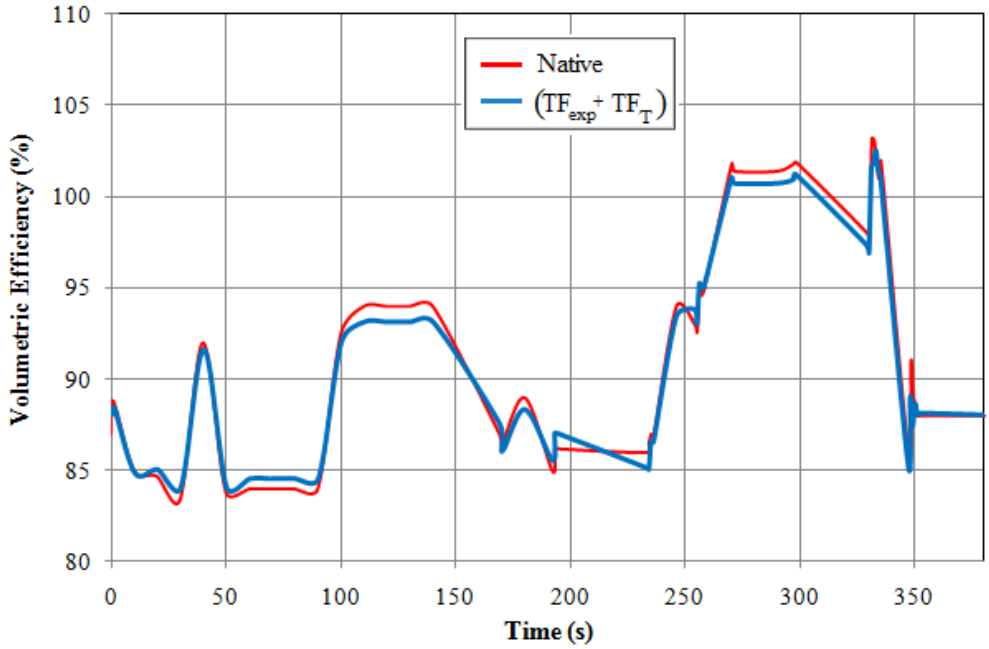

Figure V-25 - Volumetric efficiency comparison between GT-Power Native and GT/TF model using exponential filter function and the transfer function of temperature

Both GT-Power native code and GT/TF coupled model were run, and results in terms of volumetric efficiency are shown in Figure V-25. Again the model presents a great similarity with the native code even in transient engine operation (the error is less than 1%).

Table V-8 shows the simulation time of both models for 380 seconds of engine running. In general, when many cases are run in a GT-Power model, the initial conditions at instant (*t*) are taken from the results of simulation at instant (*t*-1). This option in the software helps to reduce the convergence time of the model.

Table V-8 - Simulation Time of models

Engine Running	380 seconds
GT-Power Native model	5890 seconds
GT/TF coupled model	980 seconds

The GT/TF coupled model is almost 6.1 times faster that the native code for the case of a simple geometry. It is a good time saving for such a model, in which the main physical phenomena (pressure losses, pressure wave propagation, fluid inertia, etc.) are taken into consideration. The good accuracy level of the model proves that this method includes all the necessary informations related to the flow in the intake system. The next step is to check the temperature variation influence on the transfer function model, since heat exchange is also a phenomenon which exists in an internal combustion engine.

V.2.4 Adding combustion to the engine

V.2.4.1. Indirect Injection

The single cylinder engine presented in the previous section does not take into account combustion. In other words, no fuel injection is available. The aim was to check the impact of the propagation of the pressure waves on cylinder filling. Once the native model is well calibrated according to experimental data, combustion is added in the next step. The first tested case is the indirect injection mode. An injector is added to the native model and GT/TF coupled model as presented in Figure V-26 and Figure V-27. Injection specifications are defined in a specific GT-Power template. This latter is located on the cylinder head. The length of the cylinder head is already defined and it corresponds to real length of the engine's cylinder head. Unfortunately, no experimental data are available to validate the GT-Power native model with combustion. The reference in this case for transfer function model validation is the results issued form native model.

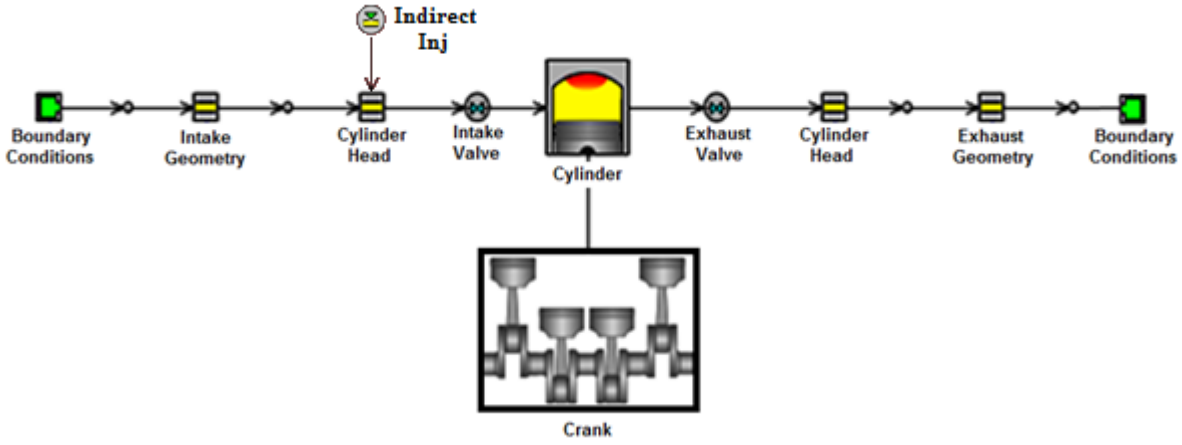

Figure V-26 - Indirect Injection Single cylinder engine native model

Once the coupling GT/TF is made. The distance between the intake valve and the transfer function corresponds to length of the cylinder head. When the valve is open, a depression occurs (values depend on the pressure losses of the whole intake geometry and the engine rotational speed). Thus, a quantity of fuel injected travels to 'EndEnvironment' template do to depression upstream the cylinder head. In this case, the simulation automatically stops and then an error message is sent, in which user is informed that a fuel backflow has occurred. As a conclusion, the coupled model cannot be used in the case of indirect injection mode. In the next section, the model will be tested in the case of direct injection mode.

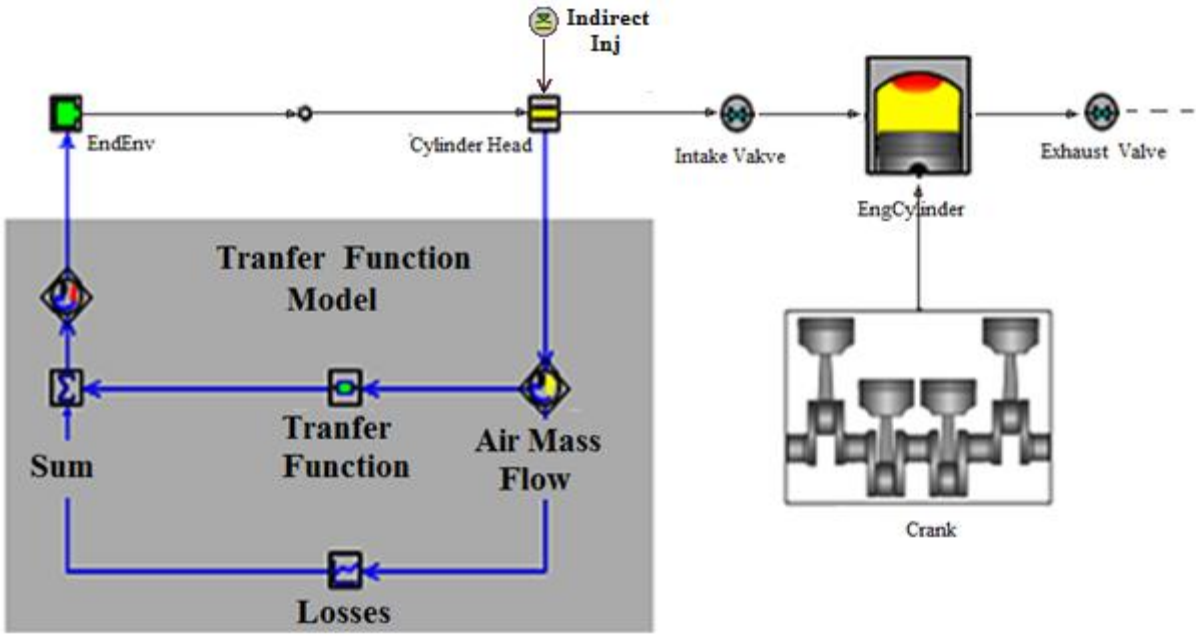

Figure V-27 - Indirect Injection Single cylinder engine GT/TF model

V.2.4.2. Direct Injection

The same injector is located in this case directly on the cylinder. This configuration corresponds to direct injection mode in GT-Power. In Figure V-28 and Figure V-29, GT-Power native model and GT/TF coupled model are presented respectively, in which direct engine mode is taken into consideration.

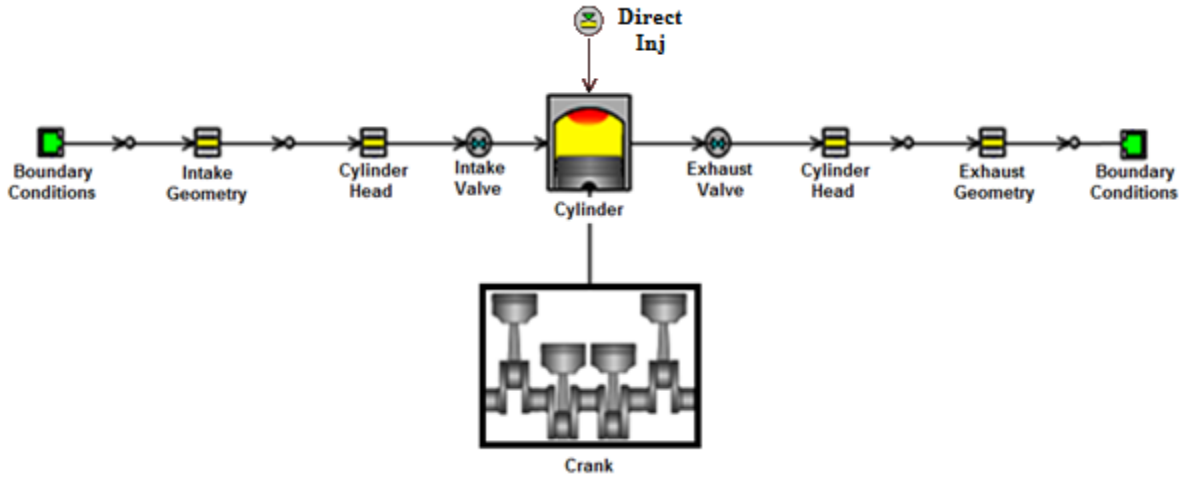

Figure V-28 - Direct Injection Single cylinder engine native model

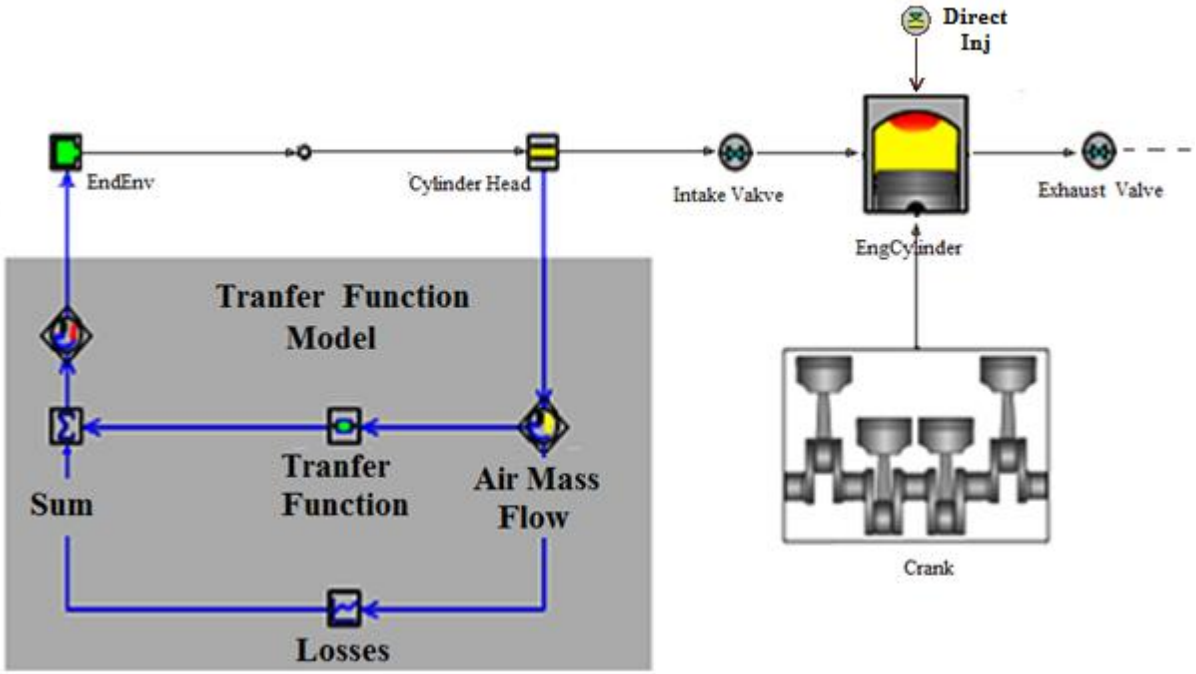

Figure V-29 - Direct Injection Single cylinder engine GT/TF model

The objective behind this test is to check the validity of the transfer function, identified at ambient pressure and temperature, when combustion is added to the model. The simulation is run in both models and the results are shown in Figure V-30. The transfer function parameters (for each engine rotational speed) were implemented manually in GT-Power. The exponential filter is not used in this case because the aim is to check the model validity when combustion is added, not reducing the simulation time of the global model.

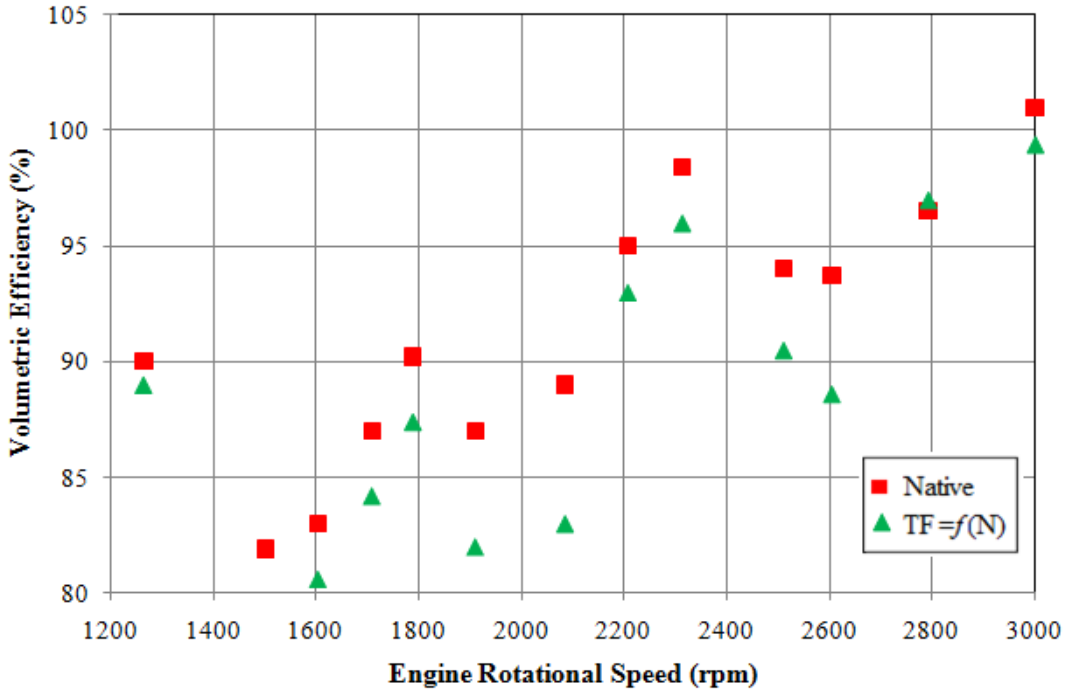

Figure V-30 - Volumetric Efficiency in function of engine rotational speed using a transfer functions identified at different *qmexc*=f (N)

The temperature increase in the air path, due to combustion, influences the volumetric efficiency of the engine. The density of in-cylinder fluid decreases when the temperature increases. Thus, compared to the case where no combustion of engine is added, the volumetric efficiency is lower for the different engine rotational speed. It is interesting to show the results of these comparisons models, with and without combustion (Figure V-31 and Figure V-32). In both models, the volumetric efficiency dropped.

According to Figure V-30, the maximum relative error between GT-Power Native model and GT/TF coupled model is 6.74 % at 2085 rpm. Before adding combustion, the maximum relative error was less than 1 % for the whole engine operating point. This means that the GT/TF model accuracy decreases when combustion is added. This error increasing is logical since the transfer functions are identified at ambient temperature. In the case where no combustion was taken into consideration, the mean temperature variation upstream the intake valve was almost close to the ambient temperature. Since combustion is added to the model, the temperature of air is not always close to the ambient temperature, especially upstream the intake valve location, where the transfer function is implemented. In fact, when the temperature of air is modified, the natural frequencies of the tested part can be modified. This latter can be corrected using equation (III-18). The transfer function identified at ambient temperature is no longer accurate for the whole engine operating points.

As a conclusion, in order to improve the transfer function model accuracy in the case where combustion exists, the transfer function identification should take into consideration the temperature variation at the intake valve. In the next section, this topic will be presented and discussed to find a solution.

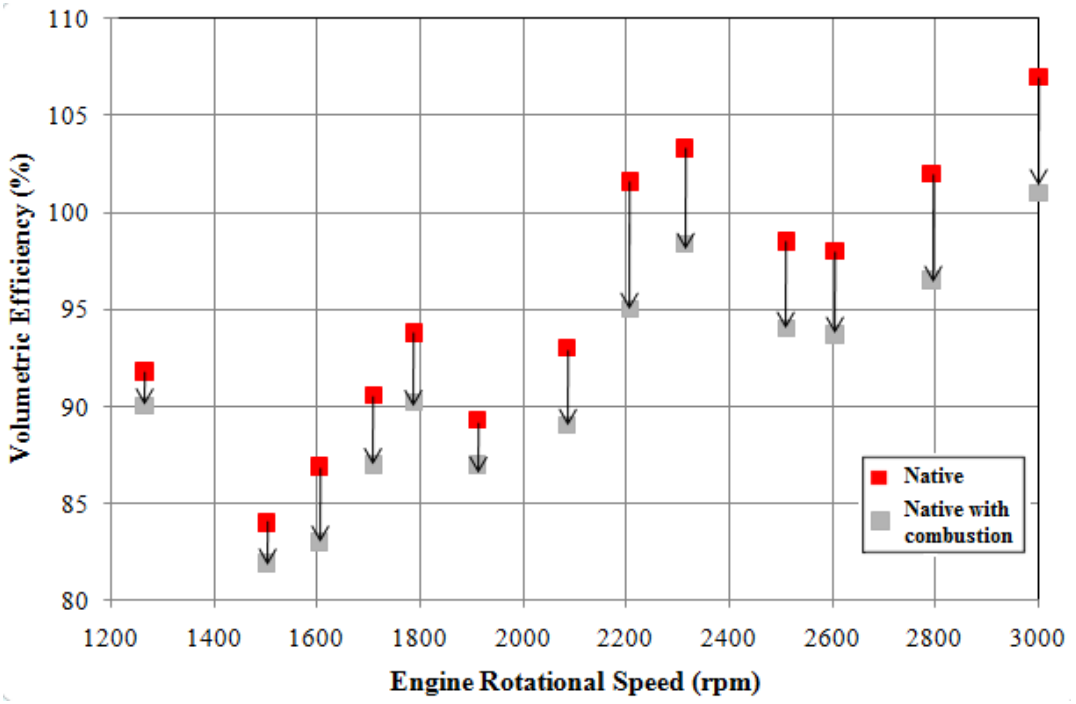

Figure V-31 – Volumetric Efficiency in function of engine rotational speed of GT-Power Native model

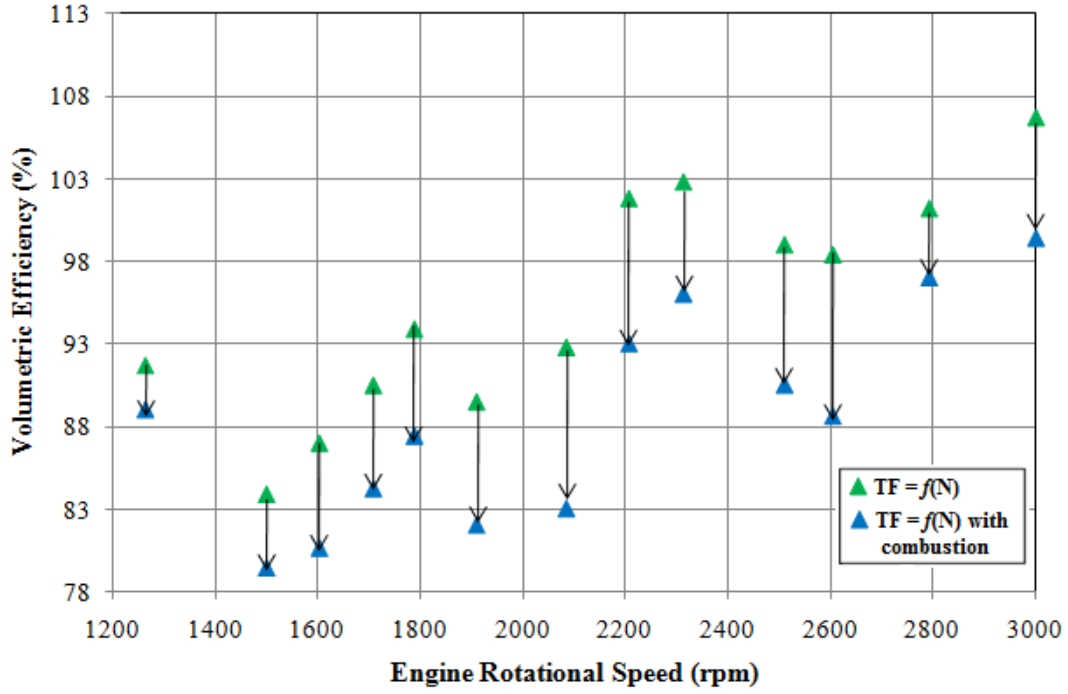

Figure V-32 - Volumetric Efficiency in function of engine rotational speed of GT/TF coupled model

V.2.5 Modeling the temperature upstream the intake valve

In this section, a new concept for improving the transfer function methodology is presented. In the previous section, when the combustion is added to model, the transfer function model accuracy was reduced, since these functions were identified only at ambient temperature. In the case of the single cylinder engine without combustion, the average temperature variation was close to the ambient temperature. That is the reason why the model was more accurate in this case.

As previously said, the temperature affects the natural frequencies of the intake geometry. These frequencies can be corrected using the following equation:

$$f(T) = f(T_{amb}) \cdot \sqrt{\frac{T_{amb}}{T}} \tag{V-3}$$

The average temperature at each engine rotational speed is calculated using a temperature sensor located at the intake valve. This value allows identification of the new natural frequencies.

The virtual dynamic flow bench is used in order to identify the transfer functions at different temperature (since the temperature modification on the real dynamic flow bench was not available). The same methodology of function identifications is used. Hence, for each engine rotational speed, a specific transfer function is used (a specific air mass flow rate excitation and temperature). In this case, the exponential filter cannot be used anymore, since no more equivalent transfer function can be identified. The coefficients of the transfer function are changed manually for each engine rotational speed.

Compared to Figure V-30, Figure V-33 shows improvement in terms of accuracy. When heat transfer is taken into consideration, the results of the new model show good agreement again compared to native data. The maximum relative error is reduced (2.66% at 2604 rpm). Compared to Figure V-5, where combustion was not taken into consideration (the average temperature was close to the ambient one), the new model is less accurate. The reason behind this is that the transfer functions were identified at average temperatures. In other words, the instantaneous temperature was not taken into consideration.

As a conclusion, the new model requires a new test campaign in order to identify new transfer functions that take into consideration the heat exchange at the intake valve.

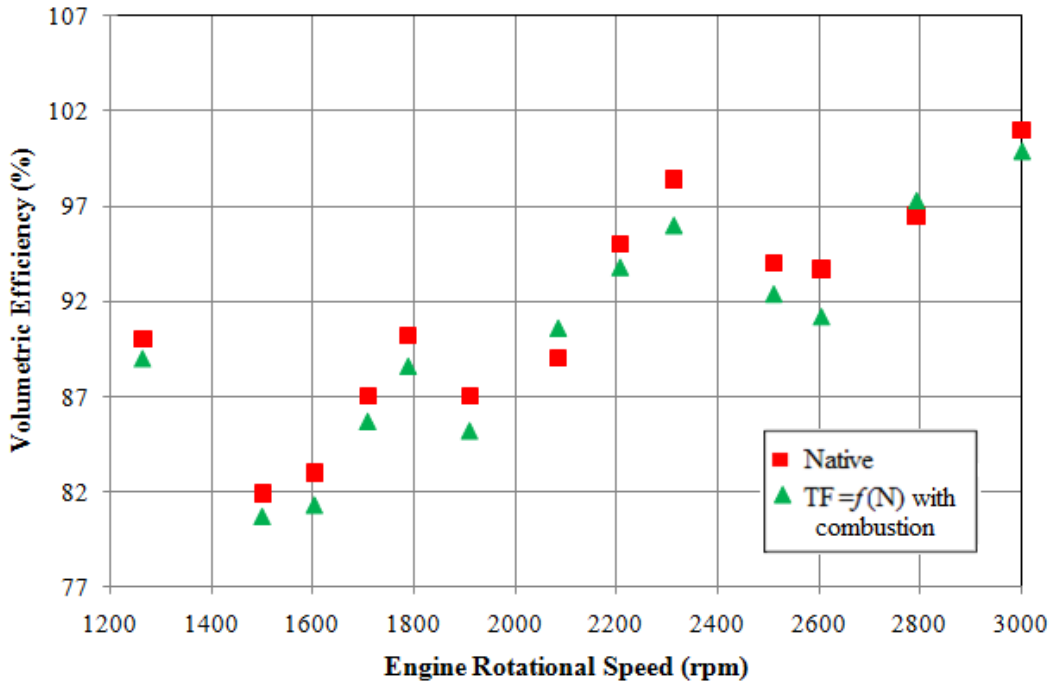

Figure V-33 - Volumetric Efficiency in function of engine rotational speed of GT/TF coupled model (combustion added)

V.3. Three cylinder application

In this section, the transfer function methodology was validated using 3-cylinder naturally aspirated engine. Engine specifications was already presented is chapter II. The same methodology applied on the single cylinder engine will be used for the model validation on a three cylinder engine. The objective is to test the accuracy of the transfer function model on a complex geometry.

Firstly, the intake system of the three cylinder engine (runners, manifold, throttle valve and air filter) was installed on the dynamic flow bench for transfer function identification (Figure V-34). In order to take into account the "self excitation effect" and "interference effect" between cylinders in the model, each runner was connected to the bench through a specific adaptation part. When a cylinder is connected, the others are completely closed (to simulate the case of a real engine operation). In general, at a certain time, only the intake valves of one cylinder are open, the others are closed. At the end of the admission phase of this cylinder, and after IVC, pressure waves are generated. These waves have a significant effect on the other cylinder (cylinder interferences effects produced by cycle overlap). These waves should be taken into consideration in the transfer function model for a better representation. Thus three configurations exist (Figure V-35): the first one consists on connecting the first runner to dynamic flow bench. The second and the third runners were closed at their end. Same procedure was done for the second and the third configurations (the second and the third runner were connected respectively to dynamic flow bench while the other runners were closed).

Figure V-34 - Dynamic flow bench tests using a complex geometry

For each runner, pressure signals were registered using three piezo – resistive KISTLER sensors (Calibrated Range: 0-5bar abs/±5 mbar error), one sensor placed at the end of each runner. These sensors are associated to 4624A Amplifiers. At the end, nine measurements were registered:

- Configuration 1: p_{11}, p_{12} and p_{13}
- Configuration 2: p_{21}, p_{22} and p_{23}
- Configuration 3: p_{31}, p_{32} and p_{33}

The pressure signals p_{ii} (p_{11}, p_{22} and p_{33}) correspond to the self excitation of cylinder i, while p_{ij} correspond to the interference effect of cylinder i on j.

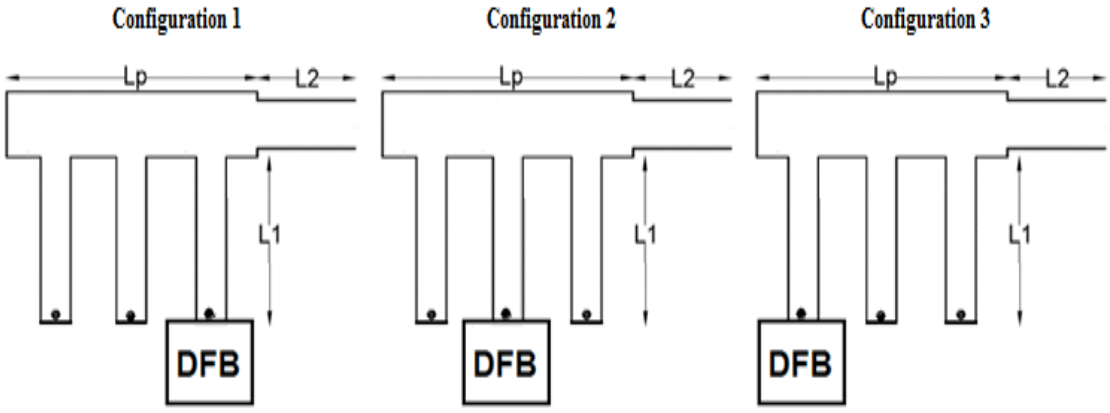

Figure V-35 – Transfer Function identification per cylinder

For the same air mass flow rate excitation value, nine transfer functions where identified (three transfer functions per cylinder). GT-Power native model is presented in Figure V-36.

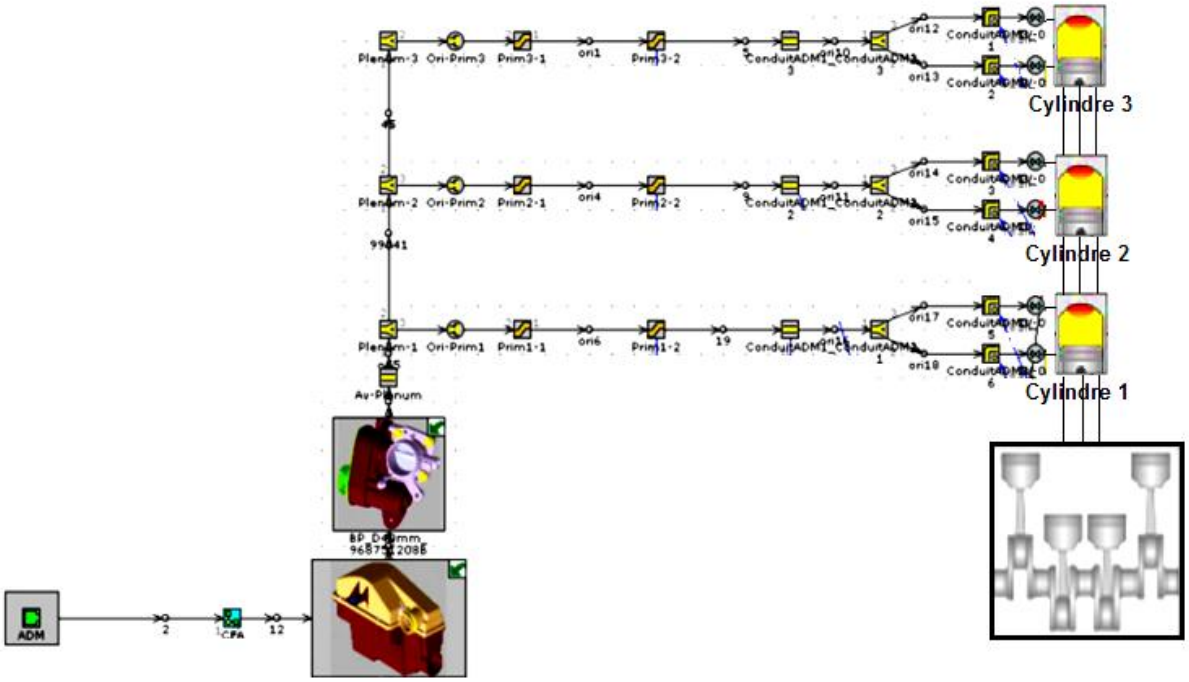

Figure V-36 - GT-Power native model of the three cylinder engine

Figure V-37 shows the implementation of the transfer functions in GT/TF coupled model. The transfer functions TF_{ii} correspond to the transfer functions which model the self excitation of cylinder i, and TF_{ij} correspond to the interference effect of cylinder i on j.

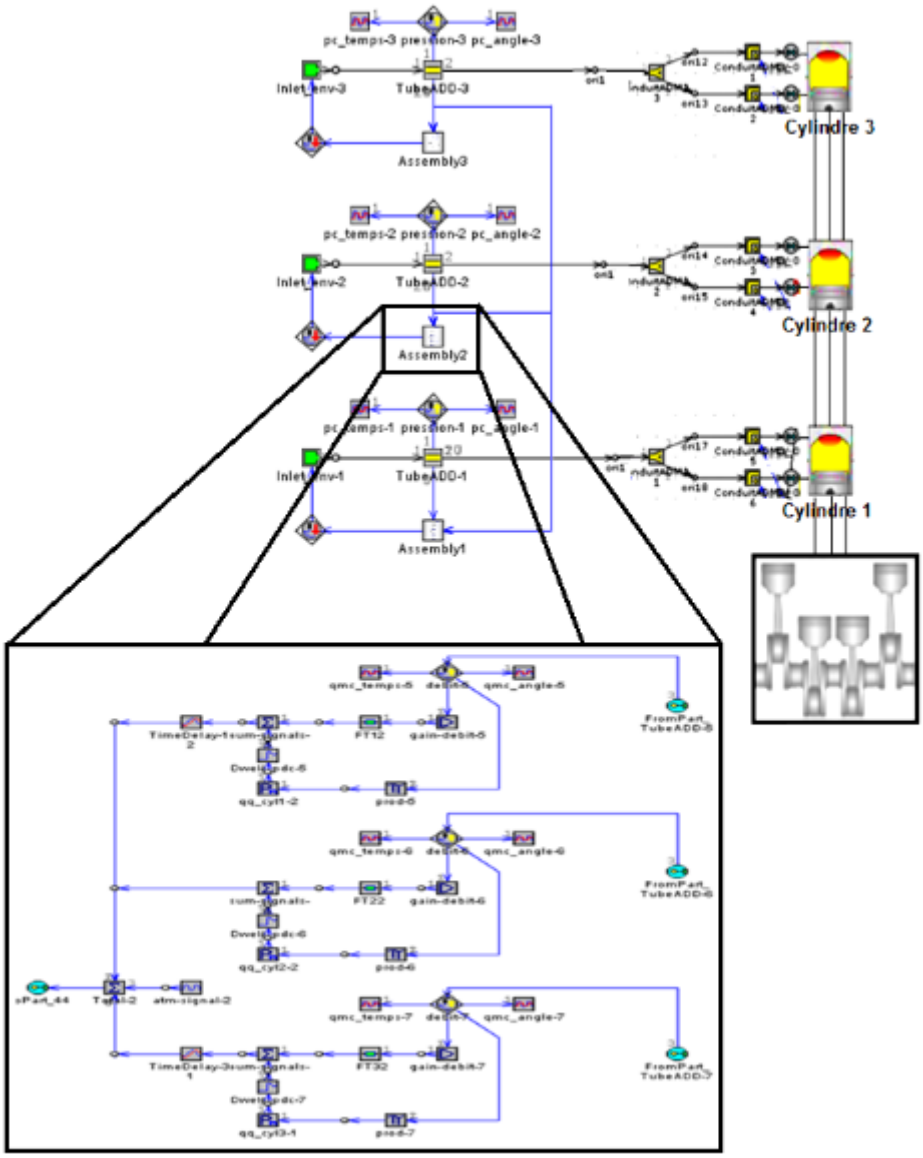

Figure V-37 - GT/TF model using 9 TF

For example, the transfer functions that should be applied on the second cylinder are:

- TF_{22}: corresponds to the self excitation of cylinder 2. The air mass flow rate signal (input of this transfer function) is taken from the cylinder head of the second cylinder.
- TF_{12}: corresponds to effect of intake valves closing of the first cylinder on the second one. The air mass flow rate signal is taken from the cylinder head of first cylinder, which represents its excitation source.
- TF_{32}: corresponds to effect of intake valves closing of the third cylinder on the second one. The air mass flow rate signal is taken from the cylinder head of third cylinder.

These functions are specific to each engine rotational speed. However, it is not the best way for implementing the transfer functions. The convergence time of such a model is relatively high since many transfer functions are working at the same time. And at a certain engine speed, some numerical instability leads to the interruption of the simulation. Thus, this configuration was not adopted in this PhD work. An alternative method is then used for modeling the flow behavior in a complex geometry. An equivalent transfer function at each cylinder is identified on the dynamic flow bench before the passage to Laplace domain. This function takes into account the self excitation and the effect of other cylinders in the same signal. Thus, the number of transfer functions reduces to 3 instead of 9.

The general form of the equivalent pressure at cylinder n is presented in equation:

$$\left(p_n\right)_{eq} = \sum_{j=1}^{j=3}\left(p_{jn}\right) \tag{V-4}$$

This letter strongly depends on the engine rotational speed and the firing order. In other words, the closing time of the intake valves of two successive cylinders should be taken into consideration. For example, the equivalent pressure at cylinder number 2 is the summation of the pressure signals p_{22}, p_{12} and p_{32}. A delay should be applied on p_{12} and p_{32} in order to take into account the traveling time of the pressure wave, which depends on the length of the geometry that separates consecutive cylinders. These delays factors can be identified on the dynamic flow bench during the identification process of the transfer functions. The superposition of these signals generates a new pressure signal which takes into account the self induction and the effect of other cylinders at instant t. An assumption is made for letting this superposition possible: the air mass flow rate is considered to be the same for the three cylinders. In reality, the air mass flow changes between cylinders (the volumetric efficiency as consequence).

Finally, three equivalent transfer functions are identified using the equivalent pressure data for each cylinder. In this way, only three transfer functions exist in the new GT/TF coupled model. This can reduce significantly the simulation time of the model compared to the one with nine transfer functions. However, logically this latter is more precise since the air mass flow rate is considered as different between cylinders.

Figure V-38 and Figure V-39 present the instantaneous pressure comparison respectively at 1200 rpm and 1500 rpm on the second cylinder. The obtained results seem to be very close to the experimental ones. The new methodology can be used in order to simulate the pressure waves in a complex system like a three cylinder engine manifold.

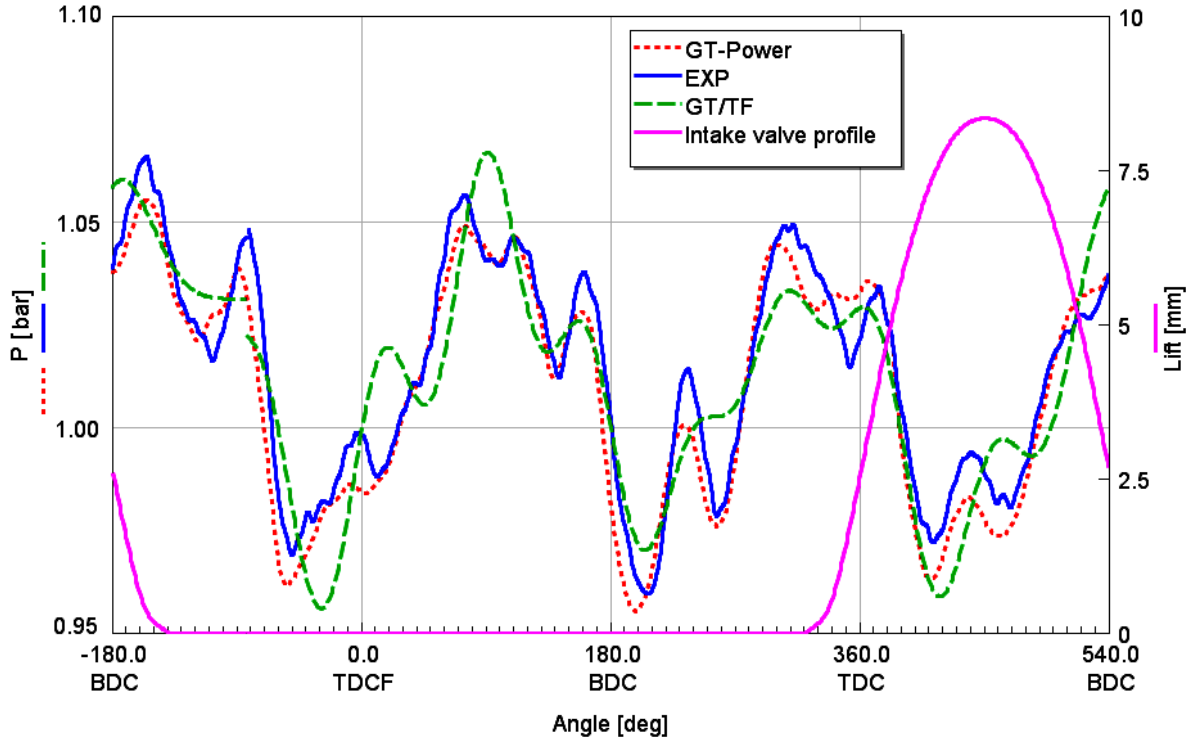

Figure V-38 – Instantaneous pressure comparison at 1200 rpm (cylinder 2)

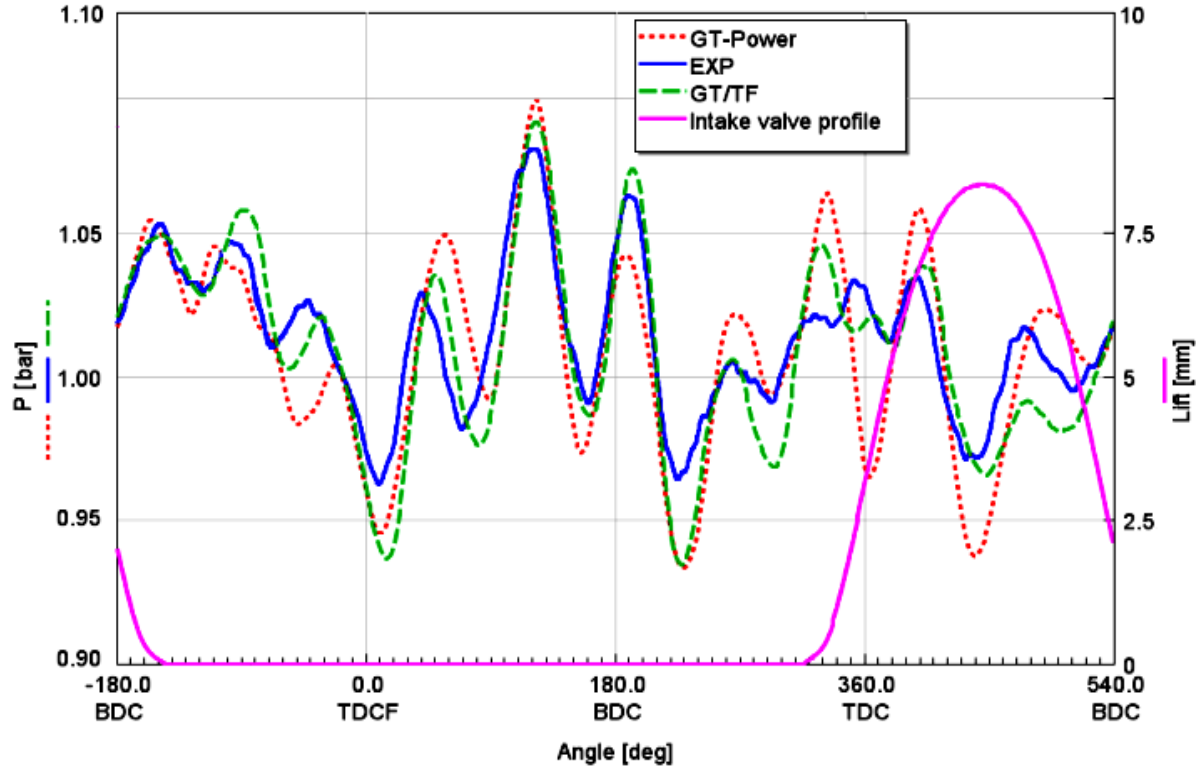

Figure V-39 - Instantaneous pressure comparison at 1500 rpm (cylinder 2)

In this chapter, the transfer function model validation was done using two different engines. The first one is considered as a simple application since only one excitation source exists. A compromise between accuracy and simulation time was done on the second application, the complex geometry of the three cylinder engine. The transfer function model shows a good accuracy level compared to experimental results and one dimensional non-linear approach.

Conclusion

The propagation of the pressure waves in the intake system of an internal combustion engine has a significant effect on engine behavior. These waves were studied using a frequency approach. This latter is based on a transfer function, which links the pressure and the air mass flow rate at the intake valve. The main challenge was clarified from the beginning of this manuscript, which is the accuracy of the model versus simulation time.

In the literature survey Chapter I, the air flow modeling approaches allowed a better understanding of some physical phenomena (especially the wave action).

The experimental and numerical tools presented in Chapter II allowed accomplishing this PhD work:

- *Using dynamic flow bench working under unsteady conditions, the transfer function was identified. It is the first step of the methodology. Based on quarter wave resonance phenomenon, the excitation on the dynamic flow bench allows identification of the natural frequencies of the tested geometry.*

- *Matlab helps to identify the transfer function in frequency domain, using a specific toolbox.*

- *GT-Power software was chosen for several reasons: firstly, it is reliable and friendly use software: The real engines presented in this PhD work were modeled and tuned according to experimental results. The results showed good ability of the model to reproduce the reality. Secondly, the methodology presented in this work consists on coupling the mathematical transfer function model with the one-dimensional non-linear representations. Thus, the model could not be useful if the multi-physics modeling is not allowed in this software. Finally, the software allows measuring the thermodynamic variables at any position on the intake system (using virtual sensors). This helped to identify the transfer function of temperature using a virtual dynamic flow bench.*

- *The experimental test benches helped to validate the accuracy of both models: native and 0D/1D coupled model.*

In Chapter III, the transfer function methodology is described. The model history as well as the optimization method is detailed. The main purpose of the 0D/1D transfer function model is to replace the native 1D intake system of the IC Engine in the simulation code. In other words, a coupling was made using the 1D simulation code of GT-Power, where the inlet system of the ICE was replaced by its transfer function. The optimization consists on three main parts: identification, implementation and calibration. Both transfer function for temperature and exponential filter function were added to the main model in order to improve the accuracy and decrease the simulation time.

The main purpose behind the acoustic model presented in Chapter IV *is to overcome the tests on the dynamic flow bench (which are time and cost consuming). The model allows identifying a transfer function, ideally equal to the measured transfer function issued from a dynamic flow bench test. The model was validated on a set of simple tubes with different lengths.*

Finally the model validation was performed in Chapter V. *The use of a single cylinder engine without combustion allowed focusing on the wave propagation phenomenon. Many transfer functions were identified for different engine speed for a better model accuracy. The way of implementing these functions in the simulation code allowed decreasing the simulation time (the use of exponential filter function). The filter coefficients are experimentally identified. However, these coefficients depend on engine rotational speed. The use of transfer function for temperature, due to pressure fluctuation, helps the coupled model to decrease its convergence time, since new information was added to the non-linear system of equations. This function has the same principle of the transfer function of pressure, and it is identified in the same way but in this case the virtual dynamic flow bench was used. This latter was already calibrated and validated using experimental data. The final model results were validated against experimental data. Good accuracy was discovered with less computational time compared to the native one-dimensional model (the model is three times faster in the case of a simple tube). A typical driving cycle is run in order to test the reliability of the model in transient engine operation phase. Since the convergence time of the transfer function model is too fast compared to one-dimensional representation. The model showed a better accuracy in the case of transient engine operation.*

The model validation also concerns a complex geometry of intake systems. The model presented in this PhD work showed a good ability to model the complex geometry of a three-cylinder engine (air filter + runners + intake manifold + throttle valve). The cylinder interferences were surely taken into consideration using related transfer functions. In this work, two ways of implementing the functions were proposed. Both methods showed a good ability to model the pressure waves propagation in the intake system. The method consisting in an equivalent transfer function is the best compromise between accuracy and simulation time. The model showed a good agreement with experimental results. For a certain engine operation point, the model showed a better accuracy than one-dimensional native. In terms of simulation time, the model was seven times faster than the traditional one-dimensional.

<u>Limitation:</u>

- *The transfer function corresponds for the whole tested geometry. This means that when a small modification is applied to the tested geometry (for example: changing the position of the throttle valve or adding a part), it is then necessary to identify a new transfer function which corresponds to this new configuration.*

- *The experimental tests done for identifying the transfer function are not easy to do, especially when the tested geometry is a complex configuration (for example: an intake system of a four cylinder engine). The whole intake system, from runners to the*

air filter, should be installed on the bench. This needs specific tools also to adapt this configuration to the bench.

- *Turbocharger obstacle: The model can perfectly work in the case of a naturally aspirated engine. A turbocharged engine could not be tested since the coupling between the turbocharger and the functions cannot be done. In fact, in transfer function model, the whole intake system was replaced by functions. Thus, the turbocharger cannot be implemented in the code.*

Finally, the transfer function methodology concept can be an alternative method for modeling the flow inside the intake geometry of an internal combustion engine.

Perspectives:

- *In this PhD work, only one transfer function for temperature is used per model. In fact, an equivalent function was identified for the whole engine speeds. The accuracy of the model can be improved by making these functions dependent on the engine rotational speed.*

- *Pressure and temperature variation were separately implemented in the simulation code using two different functions. In order to decrease the number of transfer function in the simulation code, an equivalent function which includes both parameter can be helpful.*

- *In acoustic model, the correction laws were identified for tubes with different lengths. Tubes with different diameters were not taken into consideration. In order to increase the identified transfer function library for different geometries, correction laws for diameter should be done.*

Articles in international journals

- *D. CHALET, H. MEZHER, M. YASSINE, J. MIGAUD, P.-E. PRETOT – Instantaneous mass flow rate measurements via transfer matrix and modal analysis for an internal combustion engine application – Journal of Modern Mechanical Engineering and Technology, Volume 3, n°2, pp. 41-55, ISSN 2409-9848, DOI: http://dx.doi.org/10.15377/2409-9848.2016.03.02.02, 2016.*

- *D. CHALET, M. YASSINE, J. MIGAUD – New 0D/1D physical approach for modelling the gas dynamics behavior inside the intake system of an engine – Journal of Thermal Science, Volume 27, n°4, pp. 394–403, ISSN 1003-2169, DOI: 10.1007/s11630-018-1027-y, 2018*

International conferences with technical papers

- *M. YASSINE, D. CHALET, J. MIGAUD – High precision and time saving method for modelling the inlet manifold of an internal combustion engine – FISITA World Automotive Congress, F2016-ESYG-005, Busan, Korea, September 26-30, 2016*

Seminar

- *May29 – June 02, 2017 - CRIEC 2017 (23ème édition du Colloque de Recherche Inter Ecoles Centrales et Centrale Supelec) | Campus de Centrale Marseille. Poster: M. YASSINE, D. CHALET, J. MIGAUD, "Transfer Function application for modeling the intake system of an Internal Combustion Engine"*

References

[1] "Emission Standards: Europe: Cars and Light Trucks." [Online]. Available: https://www.dieselnet.com/standards/eu/ld.php. [Accessed: 29-Oct-2018].

[2] "The NEDC value of a car increased suddenly, what happened? | WLTPfacts.eu." [Online]. Available: http://wltpfacts.eu/nedc-value-car-increased/. [Accessed: 29-Oct-2018].

[3] Y. Ohata, A., Ishida, "Dynamic Inlet Pressure and Volumetric Efficiency of Four Cycle Cylinder Engine," *SAE Technical Paper*, vol. 820407, 1983.

[4] R.W. MacCormack, "A Numerical Method for Solving the Equations of Compressible Viscous Flow," *AIAA journal, vol.20, no.9, p. 1275-1281.*

[5] M. Takizawa, T. Uno, T. Oue, and T. Yura, "A study of gas exchange process simulation of an automotive multi-cylinder internal combustion engine," SAE Techinacal Paper 820410, 1982, https://doi.org/10.4271/820410.

[6] D. Winterbone and R. Pearson, "Design techniques for engine manifolds," Professional Engineering Publishing, 1999.

[7] G. P. Blair, G. P. Blair, S. J. Kirkpatrick, D. O. Mackey, and R. Fleck, "Experimental Validation of 1-D Modelling Codes for a Pipe System Containing Area Discontinuities," *SAE Transactions*, vol. 104. SAE International, pp. 488–501, 1995.

[8] M. Fiocco, T. Lucchini, and G. Errico, "Modeling internal combustion engines using the OpenFOAM® library." In: Second OpenFOAM User Conference. Ed. by ESI-OpenCFD, Berlin, 2014.

[9] B. E. Launder and D. B. Spalding, "The numerical computation of turbulent flows," *Numerical Prediction of Flow, Heat Transfer, Turbulence and Combustion*, pp. 96–116, Jan. 1983.

[10] A. Bakker, "Lecture 5: Solution Methods. Applied Computational Fluid Dynamics," Instructor André Bakker, 2002.

[11] C. J. Lea and A. P. Watkins, "Differential stress modelling of turbulent flows in model reciprocating engines," *Proceedings of the Institution of Mechanical Engineers, Part D: Journal of Automobile Engineering*, vol. 211, no. 1, pp. 59–77, Jan. 1997.

[12] B. Baldwin and H. Lomax, "Thin-Layer Approximation and Algebric Model for Separated turbulentflows," In: 16th aerospace sciences meeting, p.257, Jan. 1978.

[13] A. Mahe, "Caractérisation du comportement non-stationnaire du système d'admission d'air d'un moteur à combustion interne. Incidence sur le remplissage," Thèse de Doctorat, Ecole Centrale de Nantes, 2011.

[14] M. Baum, T. J. Poinsot, D. C. Haworth, and N. Darabiha, "Direct numerical simulation of H 2 /O 2 /N 2 flames with complex chemistry in two-dimensional turbulent flows," *Journal of Fluid Mechanics*, vol. 281, no. 1, p. 1, Dec. 1994.

[15] M. Chapman, "Two Dimensional Numerical Simulation of Inlet Manifold Flow in a Four Cylinder Internal Combustion Engine," SAE Technical Paper, No 790244, 1979.

[16] J. L. Steger, "Implicit Finite-Difference Simulation of Flow about Arbitrary Two-Dimensional Geometries," *AIAA Journal*, vol. 16, no. 7, pp. 679–686, Jul. 1978.

[17] F. K. Bannister and G. F. Mucklow, "Wave Action following Sudden Release of Compressed Gas from a Cylinder," *Proceedings of the Institution of Mechanical Engineers*, vol. 159, no. 1, pp. 269–300, Jun. 1948.

[18] D. Chalet, "Etude et modélisation des ondes de pression dans les géométries complexes. Application à la simulation du fonctionnement d'un Moteur à Combustion Interne," Thèse de Doctorat, Ecole Centrale de Nantes, Dec. 2003.

[19] G. Blair, "Design and simulation of two-stroke engines," Warrendale, PA: Society of Automotive Engineers, pp. 472-511, 1996.

[20] R. Weast, M. Astle, and W. Beyer, "Chemical Rubber Company, CRC handbook of chemistry and physics: a readyreference book of chemical and physical data," 1985.

[21] CRANE CO. ENGINEERING DIVISION, "Flow of fluids through valves, fittings, and pipe," Crane Company, 1957.

[22] A. Rao, B. K.-J.-I. Waterworks, "Friction factor for turbulent pipe flow," *academia.edu.*, 2006.

[23] N. H. Chen, "An Explicit Equation for Friction Factor in Pipe," *Industrial & Engineering Chemistry Fundamentals*, vol. 18, no. 3, pp. 296–297, Aug. 1979.

[24] P. K. Swanee and A. K. Jain, "Explicit equations for pipeflow problems," *Journal of the Hydraulics Division*, vol. 102, no. 5, May 1976.

[25] L.F. MOODY, "Friction factors for pipe flow," *Trans. ASME*, vol. 66, pp. 671–684, 1944.

[26] D. Winterbone and R. Pearson, *Design techniques for engine manifolds: wave action methods for IC engines*. London and Bury St Edmunds, UK: Professional Engineering Publishing., 1999.

[27] T. Bulaty and H. Niessner, "Calculation of 1-D Unsteady Flows in Pipe Systems of I.C. Engines," *Journal of Fluids Engineering*, vol. 107, no. 3, p. 407, Sep. 1985.

[28] M. F. Harrison and P. T. Stanev, "Measuring wave dynamics in IC engine intake systems," *Journal of Sound and Vibration*, vol. 269, no. 1–2, pp. 389–408, Jan. 2004.

[29] M. F. Harrison and A. Dunkley, "The acoustics of racing engine intake systems," *Journal of Sound and Vibration*, vol. 271, no. 3–5, pp. 959–984, Apr. 2004.

[30] C. Chen, A. Veshagh, and F. J. Wallace, "A Comparison Between Alternative Methods for Gas Flow and Performance Prediction of Internal Combustion Engines," *SAE Transactions*, vol. 101. SAE International, pp. 1793–1824, 1992.

[31] M. Borel, *Les phénomènes d'ondes dans les moteurs*. Éditions Technip, 2000.

[32] R. J. Winterbone, D.E. and Pearson, *Theory of Engine Manifold Design: Wave Action Methods for IC Engines*. Professional Engineering Publishing., 2000.

[33] P. O. A. L. Davies, "Practical flow duct acoustics," *Journal of Sound and Vibration*, vol. 124, no. 1, pp. 91–115, Jul. 1988.

[34] M. C. A. M. Peters, A. Hirschberg, A. J. Reijnen, and A. P. J. Wijnands, "Damping and reflection coefficient measurements for an open pipe at low Mach and low Helmholtz

numbers," *Journal of Fluid Mechanics*, vol. 256, no. 1, p. 499, Nov. 1993.

[35] M. L. Munjal, *Acoustics of ducts and mufflers with application to exhaust and ventilation system design*. John Wiley & Sons, 1987.

[36] A. Chaigne, *Ondes acoustiques*. Les Editions de l'Ecole polytechnique, 2001.

[37] T. G. Prosser, "Induction Ramming a Motored High-Speed Four-Stroke Reciprocating Engine—Influence of Inlet Port Pressure Waves on Volumetric Efficiency," *Proceedings of the Institution of Mechanical Engineers*, vol. 188, no. 1, pp. 577–584, Jun. 1974.

[38] J. Taylor, D. Gurney, P. Freeland, R. Dingelstadt, J. Stehlig, and V. Bruggesser, "Intake Manifold Length Effects on Turbocharged Gasoline Downsizing Engine Performance and Fuel Economy," 2012.

[39] K. Banisoleiman, L. A. Smith, and B. A. French, "The Interaction of Diesel Engine Turbocharging and Tuned Inlet Manifold Systems under Steady State and Transient Operation," *Proceedings of the Institution of Mechanical Engineers, Part A: Journal of Power and Energy*, vol. 205, no. 4, pp. 269–281, Nov. 1991.

[40] H. Tiikoja, "Acoustic characterization of turbochargers and pipe terminations," The marcus Wallenberg Laboratory for sound and vibration research - Department of Aeronautical and vehicule Engineering , 2012.

[41] A. J. Torregrosa, J. R. Serrano, J. A. Dopazo, and S. Soltani, "Experiments on Wave Transmission and Reflection by Turbochargers in Engine Operating Conditions," 2006.

[42] L. Portier, "Experimental determination and prediction of turbocharger transfer matrix," in *In 7th Symposium–Automotive & Railway Comfort*, 2012.

[43] W. Polifke, A. Poncet, C. O. Paschereit, and K. Dobbeling, "Reconstruction of acoustic transfer matrices by instationary computational fluid dynamics," *Journal of Sound and Vibration*, vol. 245, no. 3, pp. 483–510, Aug. 2001.

[44] M. Knutsson, J. Lennblad, H. Bodén, and M. Abom, "A Study on Acoustical Time-Domain Two-Ports Based on Digital Filters with Application to Automotive Air Intake Systems," *SAE International Journal of Passenger Cars - Mechanical Systems*, vol. 4, no. 2, pp. 2011-01-1522, May 2011.

[45] M. Sekavčnik, T. Ogorevc, and L. Škerget, "CFD analysis of the dynamic behaviour of a pipe system," *Forschung im Ingenieurwesen*, vol. 70, no. 3, pp. 139–144, Sep. 2006.

[46] A. Torregrosa, F. Arnau, P. Piqueras, M. Reyes-Belmonte, M. Knutsson, and J. Lennblad, "Acoustic One-Dimensional Compressor Model for Integration in a Gas-Dynamic Code," 2012.

[47] M. Knutsson and M. Åbom, "Sound propagation in narrow tubes including effects of viscothermal and turbulent damping with application to charge air coolers," *Journal of Sound and Vibration*, vol. 320, no. 1–2, pp. 289–321, Feb. 2009.

[48] Y. El Nemr, "Acoustic modeling and testing of exhaust and intake system components," The marcus Wallenberg Laboratory for sound and vibration research - Department of Aeronautical and vehicule Engineering, Stockholm, Sweden , 2011.

[49] D. Chalet, A. Mahe, J. Migaud, and J.-F. Hetet, "A frequency modelling of the pressure waves in the inlet manifold of internal combustion engine," *Applied Energy*, vol. 88, no. 9, pp. 2988–2994, Sep. 2011.

[50] M. Bruneau, *Manuel d'acoustique fondamentale*. Paris: Hermes, 1998.

[51] B. Desmet, "Contribution à l'étude de l'influence du circuit d'aspiration sur le remplissage d'un moteur Diesel," Thèse de Doctorat, 1977.

[52] M. F. Harrison, I. De Soto, and P. L. Rubio Unzueta, "A linear acoustic model for multi-cylinder IC engine intake manifolds including the effects of the intake throttle," *Journal of Sound and Vibration*, vol. 278, no. 4–5, pp. 975–1011, Dec. 2004.

[53] V. Gibiat and F. Laloë, "Acoustical impedance measurements by the two-microphone-three-calibration (TMTC) method," *The Journal of the Acoustical Society of America*, vol. 88, no. 6, pp. 2533–2545, Dec. 1990.

[54] M. V. Walstijn and M. CAMPBELL, "Large-bandwidth measurements of the acoustic impedance using two microphones and four calibrations(TMFC)," in *Proceedings of the Stockholm Music Acoustics Conference*, 2003, pp. 759–762.

[55] M. F. Harrison and P. T. Stanev, "A linear acoustic model for intake wave dynamics in IC engines," *Journal of Sound and Vibration*, vol. 269, no. 1–2, pp. 361–387, Jan. 2004.

[56] W. M. Boehm, "A Determination of the Correction for the Open End of a Cylindrical Resonator," *Physical Review (Series I)*, vol. 31, no. 4, pp. 332–341, Oct. 1910.

[57] S. H. Anderson and F. C. Ostensen, "Effect of Frequency on the end Correction of Pipes," *Physical Review*, vol. 31, no. 2, pp. 267–274, Feb. 1928.

[58] D. J. Blaikley, "Blaikley, D. J. (1879). Experiments for Determining the Correction to be Added to the length of a Cylindrical Resonant Tube to Find the True Wave-length and the Velocity of Sound in Small Tubes," *Philosophical Magazine and Journal*, vol. 7, pp. 339–343, 1879.

[59] M. C. A. M. Peters, A. Hirschberg, A. J. Reijnen, and A. P. J. Wijnands, "Damping and reflection coefficient measurements for an open pipe at low Mach and low Helmholtz numbers," *Journal of Fluid Mechanics*, vol. 256, no. 1, p. 499, Nov. 1993.

[60] H. Mezher, D. Chalet, J. Migaud, V. Raimbault, and P. Chesse, "Wave dynamics measurement and characterization of a charge air cooler at the intake of an internal combustion engine with integration into a nonlinear code," *International Journal of Engine Research*, vol. 15, no. 6, pp. 664–683, Sep. 2014.

[61] H. Mezher, D. Chalet, J. Migaud, V. Raimbault, and P. Chesse, "Transfer matrix measurements for studying intake wave dynamics applied to charge air coolers with experimental engine validation in the frequency domain and the time domain," *Proceedings of the Institution of Mechanical Engineers, Part D: Journal of Automobile Engineering*, vol. 227, no. 9, pp. 1348–1359, Sep. 2013.

[62] C. W. S. To and A. G. Doige, "A transient testing technique for the determination of matrix parameters of acoustic systems, I: Theory and principles," *Journal of Sound and Vibration*, vol. 62, no. 2, pp. 207–222, Jan. 1979.

[63] C. W. S. To and A. G. Doige, "A transient testing technique for the determination of matrix parameters of acoustic systems, II: Experimental procedures and results," *Journal of Sound and Vibration*, vol. 62, no. 2, pp. 223–233, Jan. 1979.

[64] Z. Tao and A. F. Seybert, "A Review of Current Techniques for Measuring Muffler Transmission Loss," SAE transactions, p.2096-2100, 2003.

[65] H. Mezher, "Caractérisation du comportement dynamique d'un circuit d'admission : incident sur le remplissage d'un moteur à combustion interne suralimenté," Thèse de Doctorat, Ecole Centrale de Nantes, Jan. 2013.

[66] E. Jenny, "Unidimensional Transient Flow with Consideration of Friction, Heat Transfer, and Area Change of Section," *The Brown Boveri Review*, pp. 447–461, 1950.

[67] R. Benson, "The thermodynamics and gas dynamics of engine manifolds. Vol. 1, Eds. JH Horlock and DE Winterbone," 1982.

[68] W. J. M. Rankine, "On The Thermodynamic Theory of Waves of Finite Longitudinal Disturbance," in *Classic Papers in Shock Compression Science*, New York, NY: Springer New York, 1998, pp. 133–148.

[69] R. Benson and N. Whitehouse, "Internal combustion engines: a detailed introduction to the thermodynamics of spark and compression ignition engines, their design and development," Elsevier, Vol.1, 2013.

[70] P. H. Rankine, "Sur la propagation du mouvement dans les corps et spécialement dans les gaz parfaits," *Journal de l'École Polytechnique.*, vol. 57, pp. 3–97, 1887.

[71] R. J. LeVeque, *Numerical Methods for Conservation Laws*. Basel: Birkhäuser Basel, 1992.

[72] R. Courant, K. Friedrichs, and H. Lewy, "On the Partial Difference Equations of Mathematical Physics," *IBM Journal of Research and Development*, vol. 11, no. 2, pp. 215–234, Mar. 1967.

[73] P. D. Lax, "Weak solutions of nonlinear hyperbolic equations and their numerical computation," *Communications on Pure and Applied Mathematics*, vol. 7, no. 1, pp. 159–193, Feb. 1954.

[74] R. D. Richtmyer and K. W. Morton, "Difference methods for initial-value problems," *Malabar, Fla.: Krieger Publishing Co., |c1994, 2nd ed.*, 1994.

[75] R. Richtmyer, "*A survey of difference methods for non-steady fluid dynamics*." Boulder, Colorado: National Center for Atmospheric Research, 1963.

[76] R. W. MacCormack, "The Effect of Viscosity in Hypervelocity Impact Cratering," in *Frontiers of Computational Fluid Dynamics 2002*, World Scientific, 2001, pp. 27–43.

[77] A. Lerat and R. Peyret, "Noncentered schemes and schock propagation problems," *Computers & Fluids*, vol. 2, no. 1, pp. 35–52, Mar. 1974.

[78] J. VonNeumann and R. D. Richtmyer, "A Method for the Numerical Calculation of Hydrodynamic Shocks," *Journal of Applied Physics*, vol. 21, no. 3, pp. 232–237, Mar. 1950.

[79] A. Lapidus, "A detached shock calculation by second-order finite differences," *Journal*

of Computational Physics, vol. 2, no. 2, pp. 154–177, Nov. 1967.

[80] S. G.-M. Sbornik, "A difference method for numerical calculation of discontinuous solutions of the equations of hydrodynamics," *mathnet.ru.*, 1959.

[81] G. A. Sod, "A survey of several finite difference methods for systems of nonlinear hyperbolic conservation laws," *Journal of Computational Physics*, vol. 27, no. 1, pp. 1–31, Apr. 1978.

[82] E. F. Toro, *Riemann solvers and numerical methods for fluid dynamics : a practical introduction*. Springer, 1997.

[83] P. . Roe, "Approximate Riemann solvers, parameter vectors, and difference schemes," *Journal of Computational Physics*, vol. 43, no. 2, pp. 357–372, Oct. 1981.

[84] G. Martin, "0D-1D Modeling of the Airpath of IC Engines for Control Purposes," Thèse de Doctorat, Orléans,France, 2010.

[85] J. B. Heywood, *Internal combustion engine fundamentals*. New York: McGraw-Hill, 1988.

[86] D. Chalet, P. Chesse, X. Tauzia, and J.-F. Hetet, "Comparison of Different Methods for the Determination of Pressure Wave in the Inlet and Exhaust Systems of Internal Combustion Engine," 2006.

[87] A. Chevalier, M. Müller, and E. Hendricks, "On the Validity of Mean Value Engine Models During Transient Operation," *SAE Transactions*, vol. 109, pp. 1571–1592, 2000.

[88] M. Bordjane, "Modélisation et caractérisation dynamique des circuits d'admission et d'échappement des moteurs à combustion interne," Thèse de Doctorat, Université des Sciences et de la Technologie d'Oran, 2013.

[89] E. Arcaklioğlu and İ. Çelıkten, "A diesel engine's performance and exhaust emissions," *Applied Energy*, vol. 80, no. 1, pp. 11–22, Jan. 2005.

[90] M. Ayoubi, "Comparison between the dynamic multi-layered perceptron and the generalised Hammerstein model for experimental identification of the loading process in diesel engines," *Control Engineering Practice*, vol. 6, no. 2, pp. 271–279, Feb. 1998.

[91] V. Çelik and E. Arcaklioğlu, "Performance maps of a diesel engine," *Applied Energy*, vol. 81, no. 3, pp. 247–259, Jul. 2005.

[92] G. De Nicolao, R. Scattolini, and C. Siviero, "Modelling the volumetric efficiency of ic engines: Parametric, non-parametric and neural techniques," *Control Engineering Practice*, vol. 4, no. 10, pp. 1405–1415, Oct. 1996.

[93] R. S. Benson, J. H. Horlock, and D. E. Winterbone, *The thermodynamics and gas dynamics of internal-combustion engines*. Clarendon Press, 1982.

[94] D. Chalet, P. Chesse, and J. F. Hetet, "Boundary conditions modelling of one-dimensional gas flows in an internal combustion engine," *International Journal of Engine Research*, vol. 9, no. 4, pp. 267–282, Aug. 2008.

[95] G. H. Trengrouse and M. M. Soliman, "Effect of Sudden Changes in Flow Area on Pressure Waves of Finite Amplitude," *Journal of Mechanical Engineering Science*,

vol. 8, no. 2, pp. 198–206, Jun. 1966.

[96] M. Takizawa, T. Uno, T. Oue, and T. Yura, "A Study of Gas Exchange Process Simulation of an Automotive Multi-Cylinder Internal Combustion Engine," SAE transactions, p.1663-1676, 1982.

[97] S. Kirkpatrick, "An evaluation of one-dimensional simulation techniques for predicting unsteady gas flow in engine ducting,"PhD thesis, Queen's University of Belfast (UK), 1996.

[98] G. P. Blair, H. B. Lau, A. Cartwright, B. D. Raghunathan, and D. O. Mackey, "Coefficients of Discharge at the Aperatures of Engines," *SAE Transactions*, vol. 104. SAE International, pp. 2048–2062, 1995.

[99] G. P. Blair and F. M. M. Drouin, "Relationship Between Discharge Coefficients and Accuracy of Engine Simulation," SAE transactions, p.2456-2468, 1996.

[100] D. Chalet, P. Chesse, J.-F. Hetet, and X. Tauzia, "Inflow boundary condition for one-dimensional gas dynamics simulation code of internal combustion engine manifolds," *Proceedings of the Institution of Mechanical Engineers, Part D: Journal of Automobile Engineering*, vol. 223, no. 7, pp. 953–965, Jul. 2009.

[101] G. I. Chan, C. L., Winterbone, D. E., Nichols, J. R., & Alexander, "A Detailed Study of Compact Exhaust Manifolds Applied to Automotive Diesel Engines," in *Instn. Mech. Engrs. Conf.: Turbocharging and Turbochargers*, pp. 269–281.

[102] J. F. Bingham and G. P. Blair, "An Improved Branched Pipe Model for Multi-Cylinder Automotive Engine Calculations," *Proceedings of the Institution of Mechanical Engineers, Part D: Transport Engineering*, vol. 199, no. 1, pp. 65–77, Jan. 1985.

[103] W. A. Woods and S. R. Khan, "An Experimental Study of Flow through Poppet Valves," *Proceedings of the Institution of Mechanical Engineers, Conference Proceedings*, vol. 180, no. 14, pp. 32–41, Jun. 1965.

[104] L. J. Kastner, T. J. Williams, and J. B. White, "Poppet Inlet Valve Characteristics and Their Influence on the Induction Process," *Proceedings of the Institution of Mechanical Engineers*, vol. 178, no. 1, pp. 955–975, Jun. 1963.

[105] G. P. Blair, A. J. Blair, "Gas flow modelling of valves and manifolds in car engines," in *International Conference computers in Engine Technology*, pp. 24–25., 1987.

[106] G. P. Blair, E. Callender, and D. O. Mackey, "Maps of discharge coefficients for valves, ports and throttles," SAE Technical Paper, No. 2001-01-1798, 2001.

[107] R. S. Benson, P. C. Baruah, and R. Sierens, "Steady and Non-Steady Flow in a Simple Carburettor," *Proceedings of the Institution of Mechanical Engineers*, vol. 188, no. 1, pp. 537–548, Jun. 1974.

[108] X. Fontana, P., Jacquet, "Dynamic flow bench Report N °1- equipment reference document : development results and the way it works," Report, Laval, 2002.

[109] Manual, "GT-Suite^{TM} Version 7.4," 2004.

[110] S. BELL, "A Beginner's Guide to Uncertainty of Measurement," *Measurement Good Practice Guide*, vol. 11, p. 1, 1999.

[111] H. Mohtar, "Increasing surge margin of turbocharger centrifugal compressor automotive application," Ecole Centrale de Nantes (ECN), 2010.

[112] M. Harrison and P. Stanev, "A linear acoustic model for intake wave dynamics in IC engines," *Journal of Sound and Vibration*, vol. 269, no. 1–2, pp. 361–387, 2004.

[113] J. Heywood, *Internal combustion engine fundamentals*. New York: Mcgraw-hil:Automotive Technology Series, 1988.

[114] P. Fontana and B. Huurdeman, "A new evaluation method for the thermodynamic behavior of air intake systems," *SAE Technical Paper*, no. 01-1136, 2005.

[115] J. (Johan) Schoukens and R. (Rik) Pintelon, *Identification of linear systems : a pracatical guidline to accurate modeling*. Pergamon Press, 1991.

[116] D. Chalet, A. Mahé, J.-F. Hétet, and J. Migaud, "A new modeling approach of pressure waves at the inlet of internal combustion engines," *Journal of Thermal Science*, vol. 20, no. 2, pp. 181–188, Jun. 2011.

[117] D. Chalet, "Contribution à la compréhension et à l'analyse des écoulements dans les systèmes d'admission et d'échappement des Moteurs à Combustion Interne." HDR, Ecole Centrale de Nantes, 2011.

[118] D. Chalet, A. Mahe, J. Migaud, and J.-F. Hetet, "Multi-frequency modelling of unsteady flow in the inlet manifold of an internal combustion engine," *Proceedings of the Institution of Mechanical Engineers, Part D: Journal of Automobile Engineering*, vol. 226, no. 5, pp. 648–658, May 2012.

[119] A. Mahé, J. Migaud, D. Chalet, and J.-F. Hétet, "Comparison Between Two Experimental Characterization Setups of Unsteady Behavior of Internal Combustion Engine Intake Systems," SAE Technical Paper, No. 2008-01-0674, 2008.

[120] D. Chalet, "Modélisation des écoulements pulsés dans les géométries complexes Application à la simulation du fonctionnement d'un Moteur à Combustion Interne ," Thèse de doctorat de l'Université de Nantes et de l'Ecole Centrale de Nantes, 2003.

[121] H. Mezher, D. Chalet, J. Migaud, and P. Chesse, "Frequency based approach for simulating pressure waves at the inlet of internal combustion engines using a parameterized model," *Applied Energy*, vol. 106, pp. 275–286, Jun. 2013.

[122] M. H. Tooley, *Electronic circuits : fundamentals and applications*. Oxford:Linacre House: Elsevier, 2006.

[123] H. Mezher, J. Migaud, D. Chalet, V. Raimbault, and P. Chesse, "Transfer matrix computation for intake elements with large pressure fluctuations under mean flow conditions," SAE Technical Paper, No. 2012-01-0672, 2012.

[124] H. Mezher, D. Chalet, P. Chessé, J. Migaud and V. Raimbault, "Transfer Matrix Computation for Wave Action Simulation in an Internal Combustion Engine," In: ASME 2012 11th biennial conference on engineering systems design and analysis, p.167-175, 2012.

[125] D. Chalet, H. Mezher, M. Yassine, J. Migaud, and P.-E. Pretot, "Instantaneous Mass Flow Rate Measurements Via Transfer Matrix and Modal Analysis for an Internal Combustion Engine Application," *Journal of Modern Mechanical Engineering and*

Technology, vol. 3, no. 2, pp. 41–55, Dec. 2016.

[126] I.R Idel'chik, *Handbook of hydraulic resistance (2nd revised and enlarged edition)*. Washington DC: Hemisphere Publishing Corp., 1966.

[127] S. H. Anderson and F. C. Ostensen, "Effect of Frequency on the end Correction of Pipes," *Physical Review*, vol. 31, no. 2, pp. 267–274, Feb. 1928.

[128] W. M. Boehm, "A Determination of the Correction for the Open End of a Cylindrical Resonator," *Physical Review (Series I)*, vol. 31, no. 4, pp. 332–341, Oct. 1910.

[129] D. J. Blaikley, "On Quality of Tone in Wind Instruments," *Proceedings of the Musical Association*. Taylor & Francis, Ltd.Royal Musical Association, pp. 79–90, Vol. 6, 1879.

[130] P. O. A. L. Davies, M. Bhattacharya, and J. L. Bento Coelho, "Measurement of plane wave acoustic fields in flow ducts," *Journal of Sound and Vibration*, vol. 72, no. 4, pp. 539–542, Oct. 1980.

[131] P. O. A. L. Davies and P. O. A. L., "Plane wave reflection at flow intakes," *Journal of Sound and Vibration*, vol. 115, no. 3, pp. 560–564, Jun. 1987.

[132] R. M. Munt, "The interaction of sound with a subsonic jet issuing from a semi-infinite cylindrical pipe," *Journal of Fluid Mechanics*, vol. 83, no. 04, p. 609, Dec. 1977.

[133] H. Rammal, H. Lavrentjev , J. Tiikoja, "On the acoustic reflecion at pipe opening," In: 17th *International congress on sound and vibration*, Cairo 18-22 July, 2010.

Transfer function estimation using identification system toolbox in Matlab:

The derivation of the air mass flow rate input signal is needed for better system identification (Figure I and II).

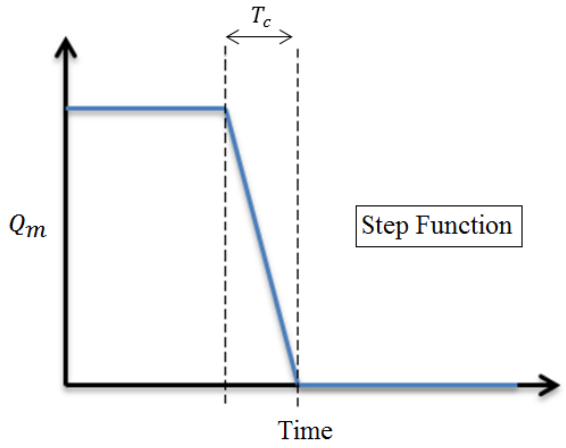

Annex I – Fig.I – Step Function

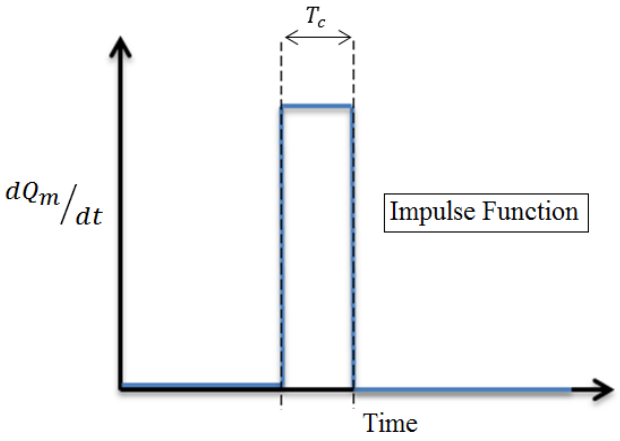

Annex I – Fig.II – Impulse Function

The final form of the transfer function is given as follow:

$$TF = \frac{P}{s \cdot Q_m} \tag{An.I.I}$$

The data are imported from Matlab workspace in time domain. Number of poles and zeros fields should be specified once the continuous transfer function estimation model is chosen (Annex I – Fig. III). The number of zeros should be greater than poles by one (Annex I - Fig IV) and can be specified by user.

In the toolbox, the transfer function form is given by the following equation:

$$Input(m) = \frac{NUM}{DEN} \cdot Output(m - \Delta_m) + e \tag{An.I.II}$$

The Δ_m represents the models delay. In this case of study, the delay term is equal to zero (system without delay). The term *e* represents the error of the system. The objective is to reduce the value of the error in the transfer function identified model. Usually, the transfer

function can be identified with good accuracy by well specifying the number of poles and zeros (up to 90 and 95 %). In this case, the *e* term is considered as negligible.

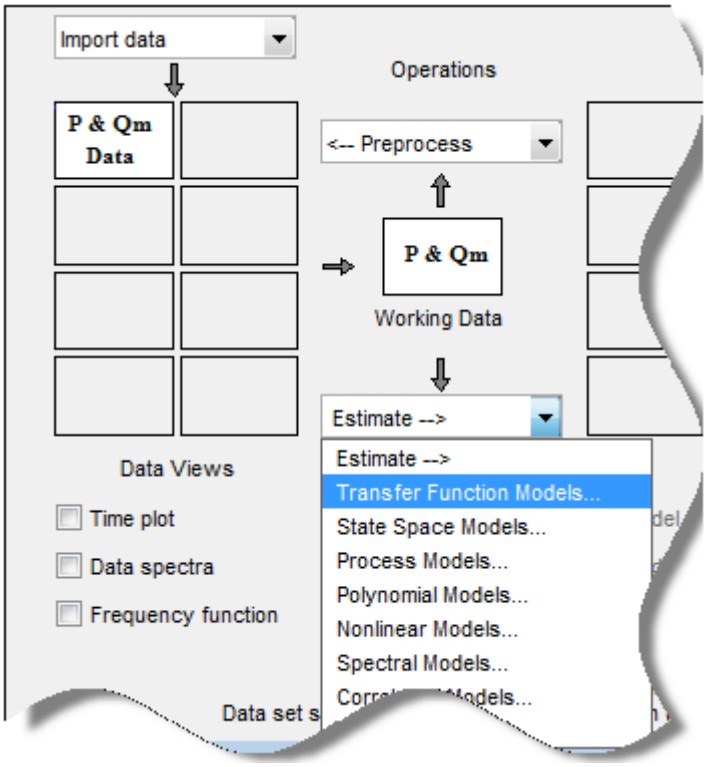

Annex I – Fig.III - System Identification Toolbox

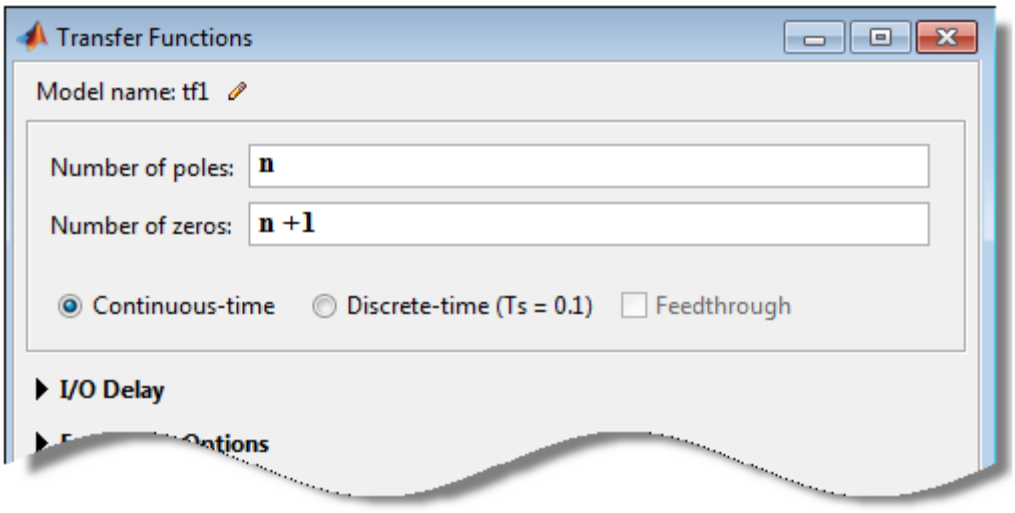

Annex I - Fig IV – TF Model specifications

The model validation can be checked by selecting the appropriate check box in the Model Views area of the System Identification app (Annex I - Fig V). The model in frequency domain is then identified. In order to export the model to the Matlab workspace, it is

sufficient to drag the model to the 'To workspace' rectangle in the System Identification app. Finally, according to equation (An.I.I), the numerator of the transfer function in Matlab workspace should be multiplied by's' (TF numerator order increasing). The coefficient of the transfer function is now well identified and ready to use.

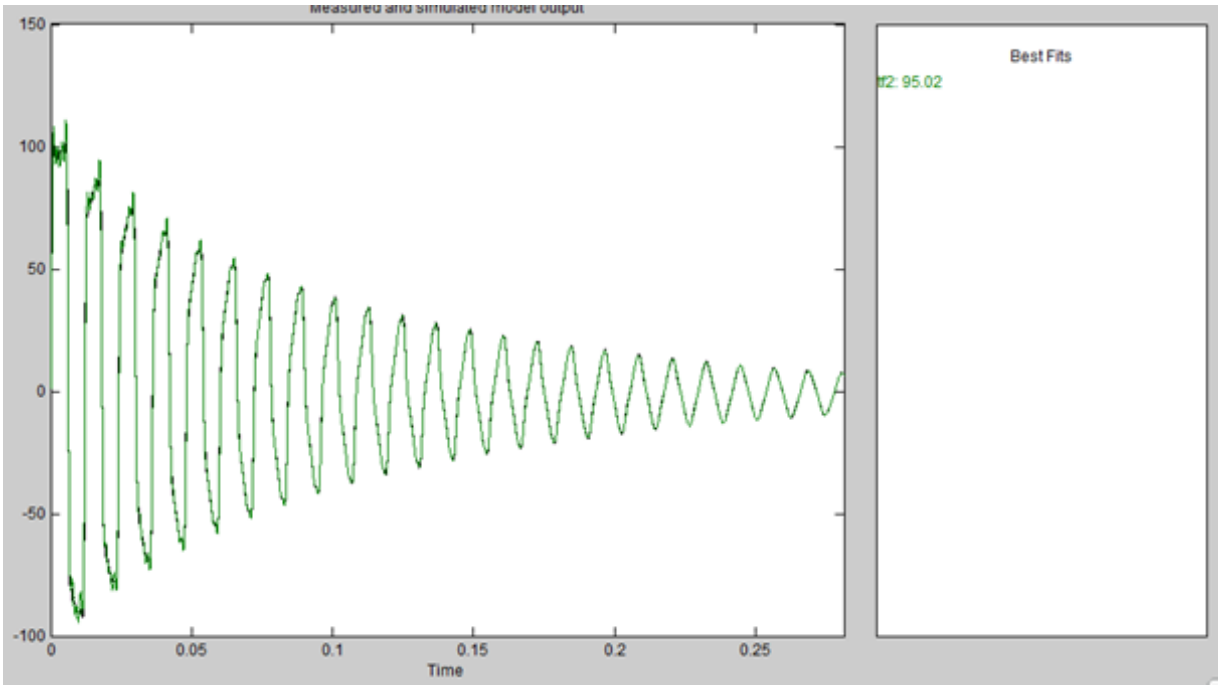

Annex I - Fig V – TF Model output in the case of the simple tube

Transfer function robustness verification:

Once the transfer function coefficients are well identified, the next step is to validate in GT-Power the good reaction of the system once it is subjected to sudden flow interruption. A specific GT-Power model is then built, where only an excitation source (air mass flow variation) (Figure) and a transfer function template exists. The transfer function output is compared to the pressure signal registered during the dynamic flow bench experiment tests.

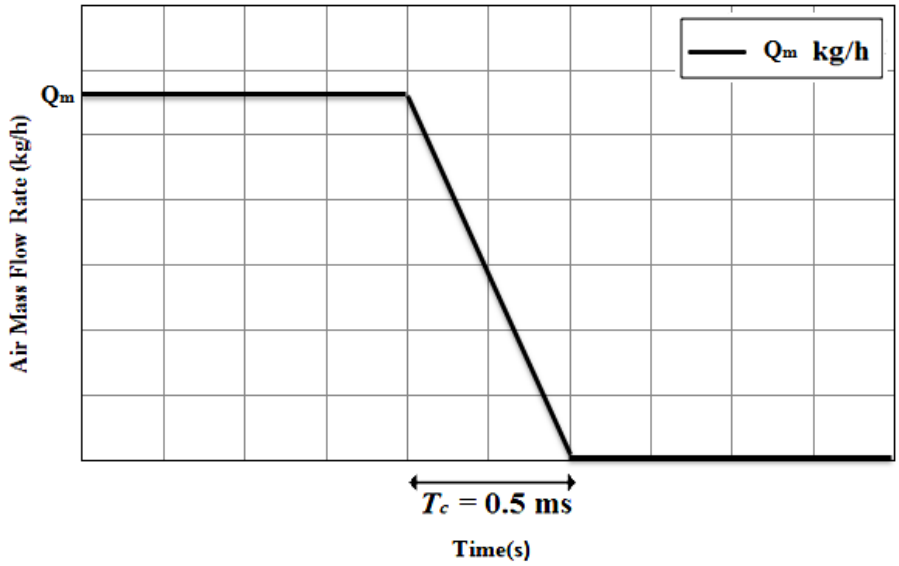

Annex II – Fig.I – Air mass flow profile

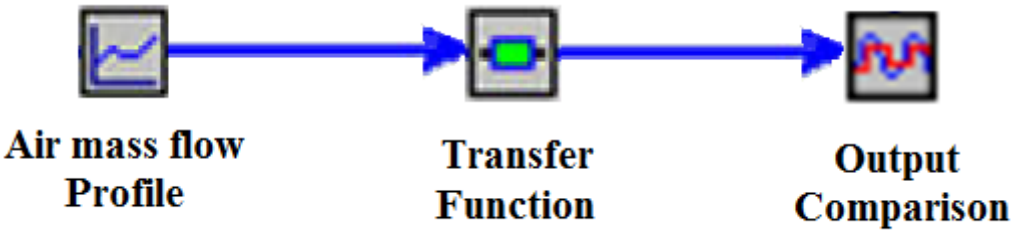

Annex II – Fig.II – GT-Power model verification

This step is necessary before fixing the transfer function coefficients. In all the studied cases, the identified transfer function system allowed a good pressure signal reproducing. This means that this function is able to model the pressure response of a system when this latter is subjected to sudden flow interruption.

French Resume

Aujourd'hui, les évolutions dans le domaine automobile sont relativement importantes. Les développements techniques et les nouvelles innovations contribuent à l'amélioration du fonctionnement des moteurs à combustion interne. A ce jour, les moteurs Diesel et les moteurs à essence dominent le marché en Europe, tandis que les autres technologies, comme par exemple les véhicules hybrides, électriques, etc., occupent un pourcentage assez faible du marché. Cependant, le moteur à combustion interne est susceptible de rester dominant à court et à moyen terme. Pour cette raison, les constructeurs automobiles sont concernés par la réduction des émissions polluantes, comme par exemple les: NO_x, CO, HC et PM, qui dégradent la qualité de l'air et contribuent au réchauffement climatique (causé en partie par les émissions de CO_2). L'objectif essentiel des nouvelles technologies appliquées aux moteurs thermiques est de permettre aux constructeurs automobiles de respecter les normes imposées par l'état qui deviennent de plus en plus sévères (Figure 1).

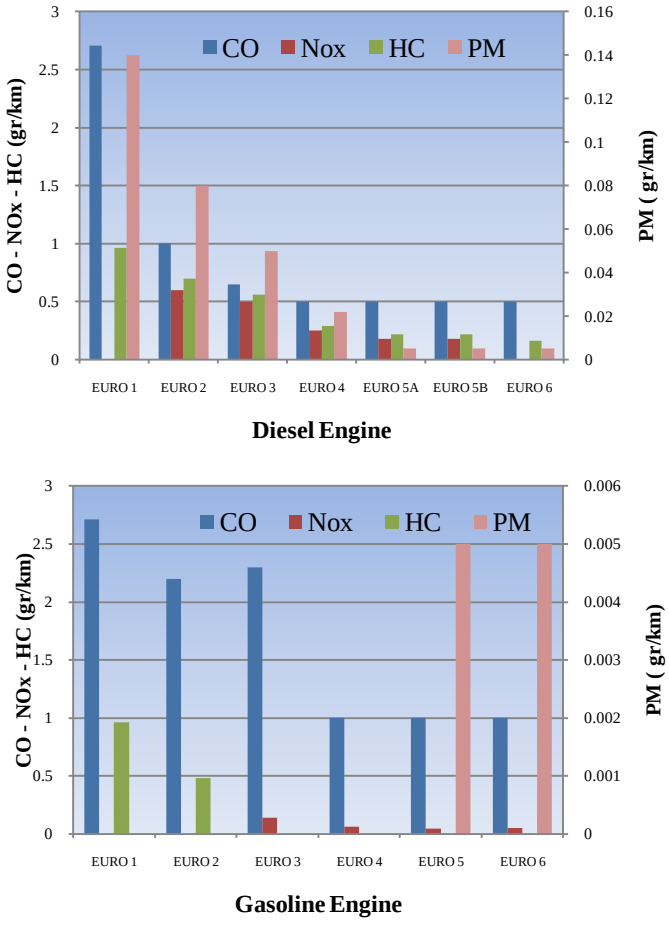

Figure 1 – Normes Européennes concernant les niveaux d'émissions polluantes pour les moteurs Diesel et Essence [1]

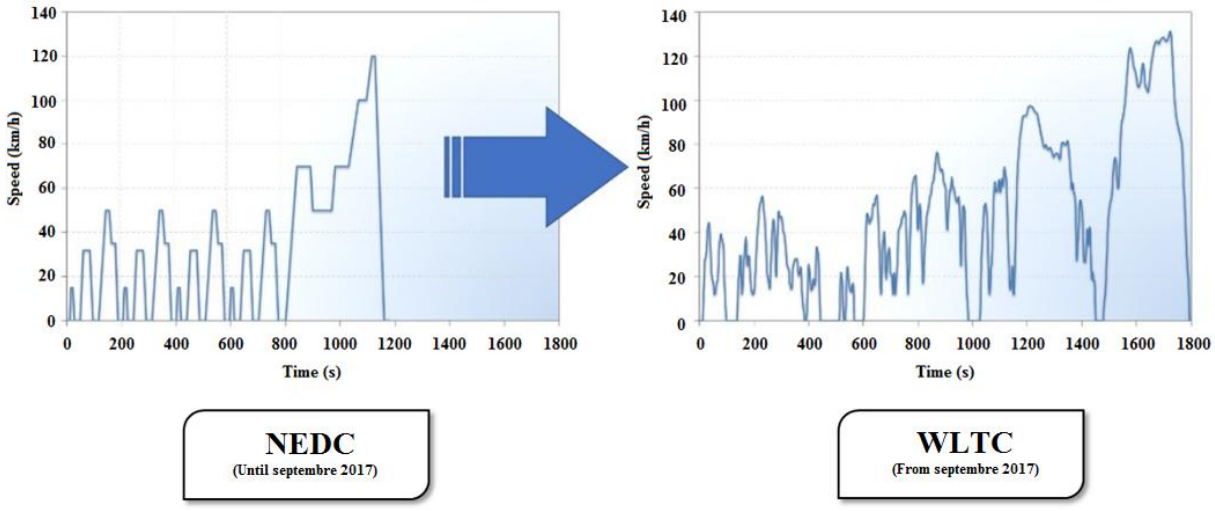

Figure 2 – Cycles NEDC et WLTC [2]

En Europe, les émissions polluantes sont mesurées sur différents cycles normalisés (NEDC, WLTC, RDE, etc.…) en fonction de la date de mise en service du véhicule. Les cycles diffèrent principalement selon leurs capacités de représenter statistiquement les conditions du monde réel. New European Driving Cycle (NEDC) était le cycle d'homologation de base jusqu'à Euro 6c. Ce dernier a été remplacé par le Worldwide harmonized Light vehicle Test Cycle (WLTC), qui couvre une bande plus large d'accélération, de variations de vitesses tout en étant plus dynamique (Figure 2). Un nouvel essai de régulations appelé "Real Driving Emissions" (RDE), a été introduit en parallèle avec les essais sur WLTC afin de garantir que les véhicules respectent les niveaux d'émissions pour des conditions d'utilisation plus étendues. L'industrie automobile est toujours en évolution et la compétition entre les constructeurs automobiles pour introduire les solutions innovantes augmente chaque jour dans le but d'améliorer les performances du moteur. Par exemple, afin de réduire les émissions polluantes, des nouvelles technologies ont été ajoutées à la ligne d'échappement. Ces système, nommés "systèmes de post-traitement", permet de réduire les niveaux des émissions générées par la combustion du carburant (DOC, SCR et FAP). Récemment un nouveau système (appelé CUC) a été ajouté au système précédent pour éviter les fuites de l'ammoniac. Par conséquent, le moteur à combustion interne devient de plus en plus sophistiqué et difficile à gérer. Suite à cela, des essais expérimentaux sur un moteur est une étape primordiale pour étudier le comportement du moteur sous différentes conditions. Cette étape est appelée «phase de calibration». Le but de cette dernière est de trouver un compromis optimal entre la puissance, la consommation, les émissions de polluant et le bruit. Cependant, la phase de calibration du moteur est généralement longue et coûteuse. D'où l'importance des codes de simulation qui sont basés sur des modèles physiques. A travers ces codes, la calibration « virtuelle » du moteur peut être faite. Actuellement, la simulation est largement utilisée dans le domaine d'automobile. Au lieu de construire des prototypes relativement coûteux et de consommer du carburant pour réaliser des essais, la simulation est devenue une solution fiable avant de prendre des nouvelles décisions. Par exemple, concernant l'étude du comportement de l'air dans la ligne d'admission d'un moteur à combustion interne, qui est de nature fortement compressible et instationnaire, les modèles de simulation sont basés sur des équations thermodynamiques. Ces dernières peuvent

être des équations 3D, 2D, 1D ou 0D selon les hypothèses adoptées par le modélisateur. Cependant, les logiciels commerciaux de simulation sont généralement basés sur des équations 1D et 0D. Les modèles basés sur les équations 3D et 2D sont gourmands en temps de calcul et ils sont rarement utilisés pour la simulation d'un moteur complet. Les modèles 1D garantissent une précision acceptable mais le temps de simulation est aussi élevé par rapport au temps réel. Pour cette raison, et dans le but de réduire le temps de simulation, des hypothèses ont permis aux modèles 0D de prendre leurs places dans les codes de simulation. Cependant, une modélisation 0D du moteur thermique ne permet pas de prendre en compte tous les phénomènes physiques qui prennent lieu dans le moteur. Par exemple, les modèles 0D ne sont pas suffisants pour bien modéliser l'écoulement de l'air dans les tubulures d'admission. Ceci revient au fait que certains détails ne sont pas pris en compte dans la modélisation, comme la propagation des ondes de pression, les échanges thermiques avec les parois, etc. De plus, les technologies ajoutées au système d'admission du moteur (on peut citer par exemple l'EGR, la suralimentation, le RAS, etc…) ont rendu la modélisation de l'écoulement de l'air dans ces systèmes très complexe. La capacité des modèles pour prendre en compte les phénomènes physiques qui existent dans le moteur face au temps de simulation demandé reste un défi (Figure 3).

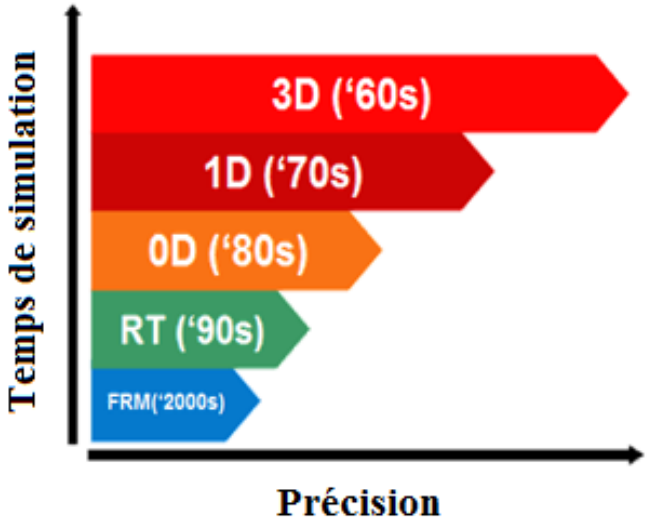

Figure 3 – Précision obtenue en fonction du type du modèle

Les niveaux des émissions polluantes ainsi que les performances du moteur sont influencés par la dynamique des gaz dans les tubulures d'admissions et d'échappements. Par exemple, le rendement volumétrique du moteur dépend fortement de la pression en amont de la soupape d'admission du moteur. Dans le but d'améliorer le remplissage du cylindre, la géométrie de la ligne d'admission doit être parfaitement conçue. Réduire les pertes de charge de différentes géométries de la ligne et assurer un bon accord acoustique permettent d'obtenir une pression plus élevée en amont soupape. Concernant l'étude de la dynamique des gaz et le phénomène de propagation des ondes de pression dans la ligne d'admission, un modèle physique précis est nécessaire afin d'obtenir des résultats fiables. Malheureusement, les modèles complets de l'écoulement de l'air dans la ligne d'admission qui prennent en compte tous les phénomènes physiques qui y ont lieu, sont gourmands en termes de temps de calcul et nécessitent des machines de calculs relativement puissantes. Face à ce constat, les travaux réalisés dans cette

thèse ont pour objectifs d'obtenir un compromis entre précision et temps de calcul. Le travail présenté dans le présent manuscrit fournit une étude complète sur la dynamique des gaz et de l'écoulement de l'air dans la ligne d'admission d'un moteur à combustion interne ainsi que les modèles physiques et numériques associés. Ce travail consiste à élaborer une nouvelle méthodologie qui permet de modéliser le comportement de l'air en amont de la soupape d'admission. Le modèle sera implémenté dans un logiciel de simulation commercial dans le but de réduire le temps de simulation d'un moteur virtuel complet. Les résultats seront comparés avec ceux issus de la modélisation classique utilisée par le logiciel commercial et des essais expérimentaux.

L'efficacité du modèle ainsi que sa capacité de prendre en compte les phénomènes physiques qui ont lieu dans la ligne d'admission d'un moteur à combustion interne seront démontrées selon les critères de précisions du rendement volumétrique et de la pression instantanée en amont de la soupape d'admission.

Après une brève introduction, la structure générale du manuscrit prendra la forme suivante:

- ***Chapitre I:*** *Une étude bibliographique sur le sujet est menée dans ce chapitre. Une brève description des modèles utilisés pour la modélisation de l'écoulement de l'air dans la ligne d'admission d'un moteur à combustion interne ainsi que leurs avantages/inconvénients permettent de comprendre l'objectif principal de ces travaux de recherche. Les modèles basés sur des équations permettent souvent de comprendre la physique associée à ce type de phénomène.*

- ***Chapitre II:*** *Les outils numériques et expérimentaux utilisés dans cette thèse sont présentés dans ce chapitre.*

- ***Chapitre III:*** *C'est la partie principale de mes travaux de recherche, où le modèle principal est présenté. Seule la théorie est présentée dans ce chapitre. La partie validation du modèle sera détaillée dans le chapitre V.*

- ***Chapitre IV:*** *Une nouvelle méthodologie d'identification de la fonction de transfert basée sur les équations acoustiques est présentée dans ce chapitre. Le but de cette nouvelle méthodologie est de réduire le temps de la procédure d'identification du modèle principal.*

- ***Chapitre V:*** *La validation du modèle de fonction de transfert est présentée dans ce chapitre. Des bancs d'essais expérimentaux ont été utilisés pour cette validation. Cette étape permet de montrer la capacité du modèle de reproduire la réalité en prenant en compte les phénomènes physiques qui ont lieu dans la ligne d'admission d'un moteur à combustion interne.*

Les performances du moteur à combustion interne sont directement conditionnées par la masse d'air introduite dans le cylindre. Cette masse détermine la quantité maximale de carburant pouvant être injectée et par conséquent l'énergie totale disponible. Cette dernière est transformée en énergie mécanique sur un arbre, des frottements et des pertes de chaleur. L'optimisation de cette quantité d'air nécessite l'étude du flux qui se produit dans le système d'admission. Cette optimisation est réalisée en déterminant les longueurs et les sections des conduits, les volumes des différents éléments, ainsi que les caractéristiques de la distribution (diamètre et nombre de soupapes, levée maximale, etc.,…). Cette section présente l'étude bibliographique réalisée concernant les modèles utilisés pour étudier et simuler le comportement de l'écoulement de l'air dans le système d'admission d'un moteur à combustion interne (Figure 4). Les modèles sont nombreux. Les avantages et les inconvénients de chaque modèle seront discutés, puis le défi principal sera identifié.

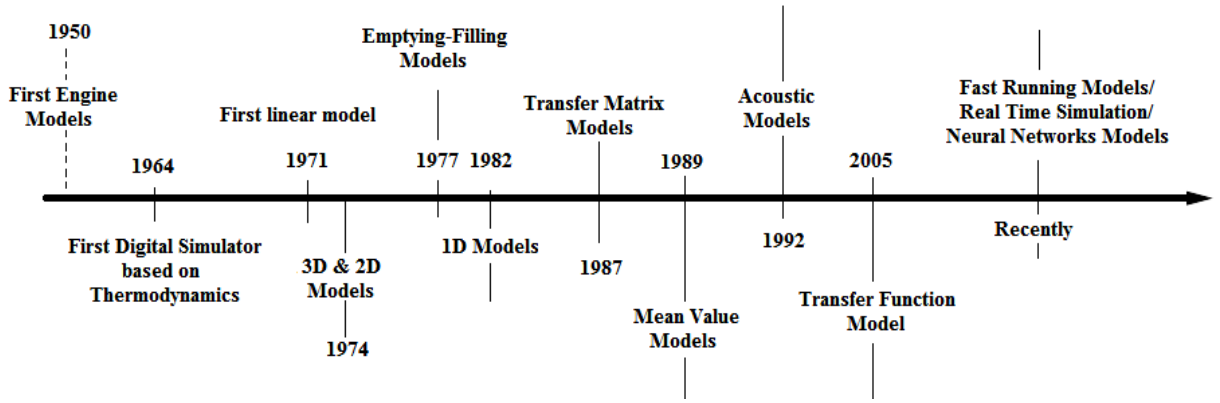

Figure 4 – Evolution des modèles

La simulation est largement utilisée dans le domaine automobile et ceci pour différentes raisons: réduire le coût total du projet, gagner du temps dans certains cas, comprendre certains comportements du moteur. Par contre, des inconvénients existent aussi, comme par exemple: les logiciels commerciaux peuvent être coûteux, l'utilisateur n'est pas toujours autorisé à effectuer des modifications dans les modèles de bases du logiciel, le temps de simulation est considéré élevé par rapport au temps réel ainsi que le temps consacré pour la phase de recalage du modèle construit est aussi élevé,… La tendance des ingénieurs aujourd'hui est l'utilisation des codes qui ne sont pas demandeur de temps de calcul trop important avec un niveau de précision acceptable. Généralement, plus le modèle est précis, plus le temps de calcul est élevé. Les codes de simulation peuvent être classés en fonction de leur complexité, de leur précision et de leur temps de calcul. Cependant, le critère de précision par rapport au temps de simulation reste un défi pour l'optimisation, la conception et la production du moteur.

Les approches tridimensionnelles permettent d'avoir un niveau de précision relativement important, en particulier pour les géométries complexes. Cependant, le temps de simulation associé à ces approches est très élevé et cela nécessite des machines de calculs relativement puissantes.

Les modèles unidimensionnels sont largement utilisés dans les logiciels de simulation. Ces modèles sont basés sur des équations d'Euler à une dimension. Le temps de calcul et la précision des schémas numériques utilisés pour résoudre les équations sont considérés comme acceptables. Cependant, ces modèles doivent être calibrés avec des données expérimentales, en particulier pour les géométries complexes. Dans ce chapitre, ces modèles ont été plus détaillés, plus précisément l'approche acoustique. En effet, l'idée du modèle proposé dans ces travaux de recherche est inspirée de la méthode acoustique. Un couplage entre modèles unidimensionnels et tridimensionnels peut être utilisé lorsque des données expérimentales ne sont pas disponibles afin d'optimiser les résultats.

Le système d'admission d'un moteur à combustion interne peut également être modélisé à l'aide de modèles 0D. Connus pour leur temps de simulation rapide, ils sont particulièrement recommandés lorsque des modèles détaillés ne sont pas nécessaires. En conséquence, certains phénomènes physiques ne sont pas pris en compte, tels que la propagation des ondes de pression dans le système d'admission d'un moteur à combustion interne. Pour augmenter le niveau de précision, ces modèles peuvent être associés à des approches unidimensionnelles. L'une de ces approches est le modèle de matrice de transfert. Cependant, la mise en œuvre de ces matrices nécessite parfois un couplage avec une bibliothèque de contrôles externe (Simulink par exemple), ce qui rend le modèle plus complexe mais aussi la possibilité d'avoir des discontinuités numériques non-physiques.

Récemment, de nombreux modèles différents ont été utilisés, tels que les modèles temps réel, basés sur l'approche de la valeur moyenne et sur des réseaux de neurones. Ces modèles étaient populaires parmi les développeurs du secteur de l'automobile et permettaient d'obtenir une vue d'ensemble des performances du moteur avec un temps de simulation rapide, voire supérieur au temps réel dans certains cas. Cependant, une description physique détaillée du composant de moteur individuel ne peut pas être incorporée dans ce type de modèles, comme par exemple la propagation des ondes acoustiques dans le système d'admission, après une fermeture soupape.

Dans le but de mieux comprendre la nature de l'écoulement dans des géométries spécifiques de la ligne d'admission, autre que les tubes droits, par exemple : les jonctions, les coudes, boitier papillons, élargissements et rétrécissements brusques, etc., une étude bibliographique a été menée sur ce sujet. Cette dernière permet aussi de bien pouvoir spécifier les différents paramètres de ces géométries dans le logiciel de simulation.

Pour conclure, l'objectif global a été identifié grâce à ce chapitre, qui est le compromis à définir entre la précision face au temps de calcul. Dans les prochains chapitres, une nouvelle approche fréquentielle basée sur l'idée de la fonction de transfert a été choisie.

Dans ce chapitre, les bancs d'essais expérimentaux ainsi que les logiciels numériques utilisés dans cette thèse sont décrits.

Dans le but d'étudier la propagation des ondes de pression dans les différents éléments de la ligne d'admission, un banc dynamique est utilisé. L'avantage de ce dernier est d'obtenir des fluctuations de pression qui sont comparables à celles observées dans un moteur à combustion interne (généralement générés par les soupapes et le compresseur). Ce banc permet d'obtenir les fréquences propres du système testé ainsi que les harmoniques. Le principe du banc dynamique est de générer initialement un débit masse stationnaire dans les éléments à tester (des tubes ou des géométries plus complexes) et de l'arrêter rapidement en 0.5 ms. La variation brusque de ce débit masse est assurée par un système muni d'une soupape et un piston pneumatique. La Figure 5 montre le principe de fonctionnement de ce système.

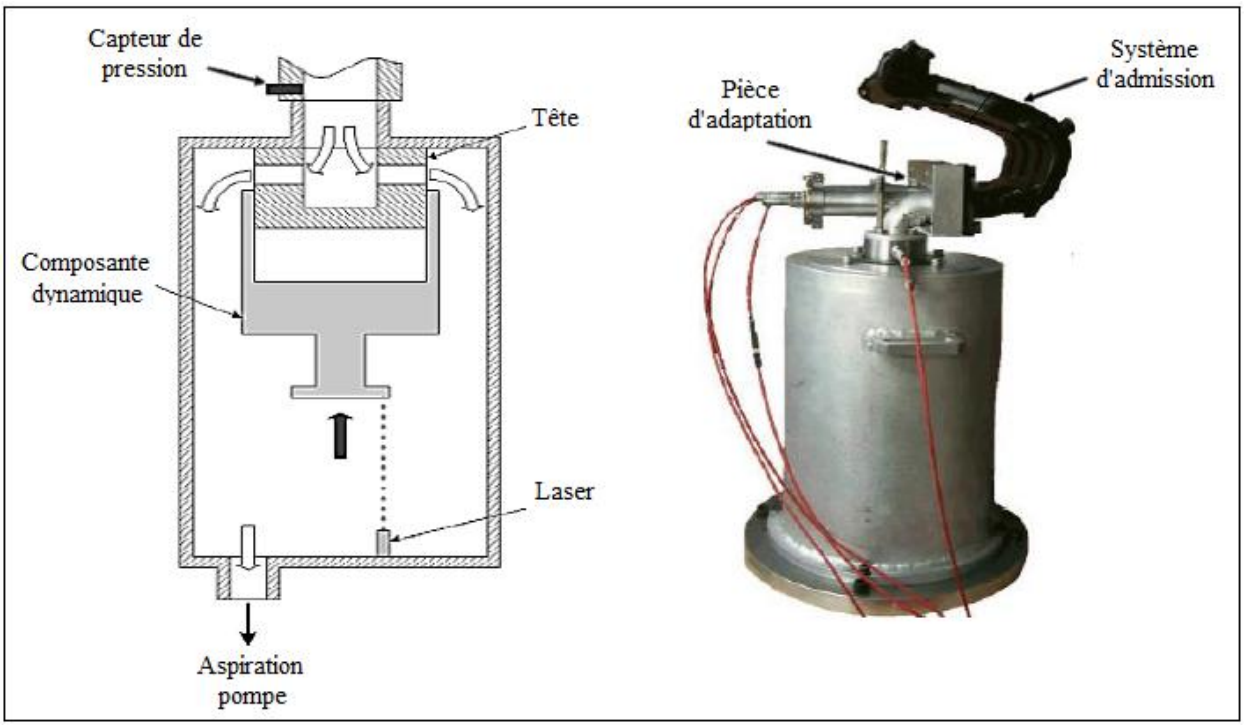

Figure 5 – Banc Dynamique

Le capteur de pression est installé à l'extrémité de l'élément testé, le plus proche possible du banc dynamique. Les données sont enregistrées avec une fréquence d'échantillonnage de 20 KHz. La fonction de transfert mesurée est ainsi le rapport entre la pression mesurée et le débit d'excitation. C'est la première étape de la méthodologie de fonction de transfert proposée.

L'outil Matlab est utilisé pour la partie traitement du signal. Plus précisément, la toolbox « Ident » a été utilisé pour identifier la fonction de transfert dans le domaine fréquentiel.

Le logiciel de simulation GT-Power a été choisi dans ces études de recherche et ceci pour plusieurs raisons :

- *C'est un logiciel fiable et facile à manipuler,*

- *Il contient une large librairie de composant de moteur,*
- *Il permet le couplage multi-physique,*
- *Utilisation des schémas 1D et 0D pour la modélisation du modèle complet du moteur.*

Les moteurs thermiques sont modélisés puis calibrés avec ce logiciel. Ces codes sont nommés: modèles natifs. Le banc dynamique est aussi modélisé dans ce logiciel. La fonction de transfert identifiée en utilisant le banc dynamique est implémentée dans GT-Power à la place de la ligne d'admission du moteur. Ce couplage multi-physique est nommé GT/TF. Les coefficients des fonctions de transferts sont intégrés dans le code via un template de la librairie de GT-Power.

La dernière étape de validation du modèle de la fonction de transfert est la validation expérimentale. Pour cela deux moteurs sont utilisés :

- *Moteur monocylindre (Figure 6)*
- *Moteur trois cylindres atmosphérique (Figure 7)*

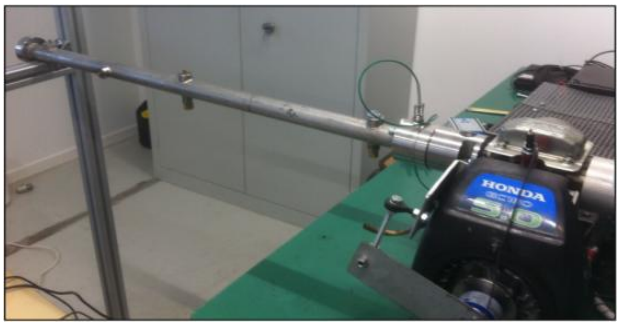

Figure 6 – Moteur Monocylindre

Figure 7 – Moteur trois cylindres atmosphérique

Des calculs d'incertitudes sont également effectués. Pour conclure, tous les outils numériques et expérimentaux présentés dans ce chapitre ont permis d'atteindre l'objectif principal de ces travaux de recherche.

D'un point de vue physique, lorsque la fréquence de la source d'excitation est égale à la fréquence naturelle d'un élément, le système a tendance à vibrer avec les valeurs d'amplitude les plus élevées. Ce phénomène s'appelle la «résonance». Dans les moteurs à combustion interne, la source d'excitation est la soupape d'admission. La fréquence d'ouverture-fermeture de ce dernier est liée à la vitesse de rotation du moteur. Pour certains points de fonctionnement du moteur, la fréquence de la soupape est égale à la fréquence naturelle du système d'admission. Ainsi, une résonance du système se produira. Une onde se propage ensuite dans le système avec une amplitude élevée. Ce phénomène conduit à une valeur de pression élevée à la position de la soupape d'admission. En exploitant cette énergie importante avant l'ouverture de la soupape d'admission (IVO), le remplissage du moteur peut être amélioré.

La fonction de transfert est une méthode de mesure de l'impédance de la source lorsque la géométrie testée est considérée comme la charge acoustique. Elle contient des informations relatives au comportement du flux, telles que l'inertie, le coefficient d'amortissement, les fréquences et les harmoniques. Dans ce chapitre, la méthodologie d'identification de la fonction de transfert et l'amélioration du modèle sont présentés.

La fonction de transfert est alors un modèle linéaire à zéro dimension qui corrèle les informations d'entrée à une réponse de sortie. Dans ce travail, la fonction de transfert est le rapport entre la pression relative (sortie du système) et le débit masse d'air (source d'excitation). Elle est égale à l'impédance à la sortie de la pièce (dans la position proche de la soupape d'admission). De plus, cette fonction mathématique permet de déterminer le comportement de l'onde de pression créé par toute excitation de flux instable.

Dans le cas d'un moteur multicylindre, le système d'admission est toujours dans une configuration où il est ouvert aux deux extrémités (car au moins une soupape est ouverte par cycle moteur). Par ailleurs, même les fréquences de résonance demi-onde devraient être prises en compte dans le modèle final.

Pour pouvoir identifier la fonction dans le domaine fréquentiel, un modèle physique est nécessaire. Des analogies électriques et mécaniques sont utilisées dans la littérature de ce modèle. Les résultats issus de ces analogies ont montré un bon niveau de précision dans le cas d'une simple géométrie. Cependant, une optimisation numérique est nécessaire dans le but d'améliorer le modèle. La méthodologie complète sera présentée dans ce chapitre: le processus d'identification, calibration, l'implantation dans le logiciel de simulation et enfin la procédure de validation.

Une étude sur l'optimisation du modèle de la fonction de transfert est menée selon 3 axes (Figure 8):

- *Identification: Un modèle numérique d'identification de la fonction de transfert est utilisé (utilisation du toolbox « Ident»). Cet outil permet des identifications rapides des systèmes avec un bon niveau de précision même dans les cas des géométries complexes. Les pertes de charge ont été dissociées de la fonction qui modélise*

seulement la variation dynamique de pression. Elles sont aussi identifiées sur le banc dynamique. Une fois que les deux fonctions sont identifiées, la prochaine étape sera de les implanter dans le code GT/TF.

- *Implantation: le couplage avec une librairie de contrôle extérieur est supprimé et remplacé par un couplage multi-physique dans le même code de simulation.*
- *Calibration: la fonction de transfert identifiée et le débit maximum d'excitation sur le banc dynamique sont liés. Par conséquent, pour chaque régime de rotation une fonction de transfert est utilisée. Afin d'intégrer ces fonctions dans le code GT-Power, une fonction filtre exponentiel a été ajoutée à la sortie de la fonction de transfert. Une fonction de transfert qui modélise la variation de la température est également ajoutée au modèle pour réduire son temps de convergence.*

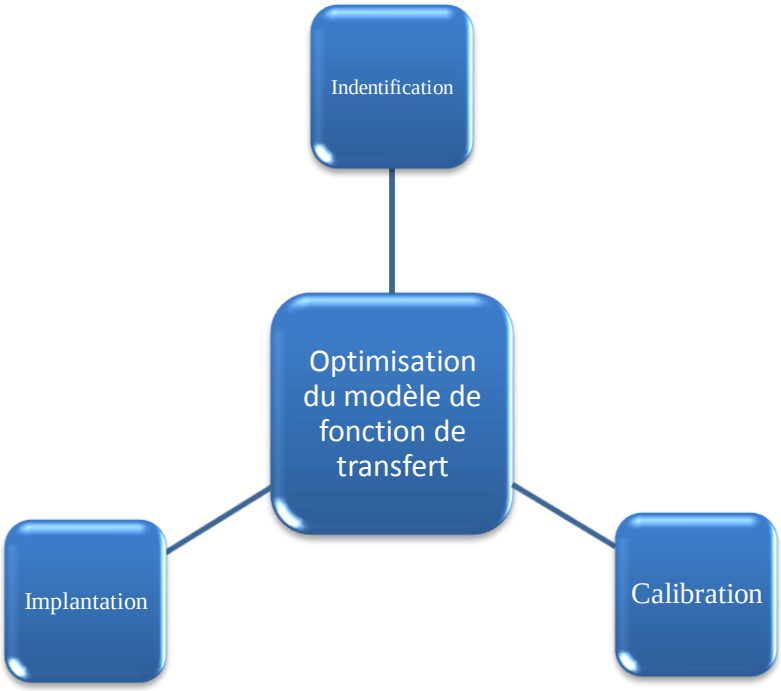

Figure 8 – Optimisation du modèle fonction de transfert

Pour conclure, l'objectif principal des optimisations effectuées sur le modèle de base est d'améliorer la précision et de réduire le temps de simulation du modèle de moteur complet modélisé dans GT-Power.

Dans ce chapitre, une nouvelle procédure d'identification de la fonction de transfert est présentée. L'objectif de cette nouvelle approche est de remplacer les tests sur le banc d'écoulement dynamique par un outil mathématique permettant de caractériser la propagation des ondes de pression dans une géométrie testée.

L'approche acoustique linéarisée est utilisée afin d'identifier la fonction de transfert de différentes géométries du système d'admission d'un moteur à combustion interne, à partir d'une géométrie simple (un tube de longueur L et de diamètre D) jusqu'à une forme complexe (le système moteur à trois cylindres).

Un lien entre le débit masse et la pression relative des deux côtés de la géométrie est établie. Ces équations ont permit au final de déduire la forme générale de la fonction de transfert acoustique (équation (IV-14)) en fonction de l'impédance spécifique et la longueur d'un tube. La viscosité du milieu ainsi que le nombre de Mach sont pris en compte dans cette fonction, ce qui l'a rendu robuste. Des lois de corrections sont ainsi établies par rapport aux essais au banc dynamique. Ces lois vont permettre d'identifier des fonctions de transfert, en fonction de la longueur du tube (pour un diamètre fixe), sans avoir à refaire des essais au banc dynamique. Dans le cas de la géométrie complexe (ligne d'admission d'un moteur à trois cylindres), une nouvelle méthodologie basée sur une méthode de décomposition des différentes parties de la ligne d'admission en prenant en compte certaines hypothèses, est utilisée pour pouvoir identifier des fonctions de transfert sans avoir recours à des essais au banc dynamique.

La méthodologie de la fonction de transfert, présentée dans le chapitre précédent, est utilisée après avoir identifié la fonction de transfert acoustique de la ligne d'admission. Les deux fonctions sont ainsi complémentaires et doivent être appliquées ensemble pour modéliser la pression relative en amont de la soupape d'admission d'un moteur à combustion interne.

La validation du modèle doit prouver la capacité de cette fonction à modéliser le comportement instationnaire et compressible du flux. Le défi reste la précision du modèle par rapport au temps de simulation. Après avoir effectué le couplage avec le code non linéaire à une dimension (Figure 9), les résultats sont discutés en fonction de la précision et de la durée de calcul du nouveau modèle par rapport à l'approche native à une dimension.

Le modèle est validé par rapport aux données expérimentales de deux moteurs: un moteur monocylindre et un moteur à trois cylindres. De toute évidence, le moteur monocylindre est une application relativement simple pour le modèle de fonction de transfert puisqu'une seule source d'excitation génère les ondes de pression pendant les cycles du moteur. La ligne d'admission est relativement facile à modéliser. Cependant, le moteur à trois cylindres est plus compliqué pour la validation du modèle, car l'interaction entre les cylindres peut affecter sensiblement les pressions en amont des soupapes. Dans ce cas, et pour une meilleure modélisation du débit d'air, il convient de prendre en compte ce phénomène. Deux méthodologies pour la modélisation des interactions de cylindre sont présentées. La première consiste à identifier des fonctions de transfert pour chaque interaction. En d'autres termes, dans le cas d'un moteur à trois cylindres, la ligne d'admission correspondante qui contient 3 conduits primaires, nécessite 9 fonctions de transfert pour modéliser toutes les auto-excitations ainsi que les interactions. La deuxième méthodologie consiste à identifier une fonction de transfert équivalente par cylindre, et qui prend en compte l'auto-excitation et les interactions des autres cylindres sur la réponse finale. En termes de temps de calcul, la deuxième méthodologie est plus rapide que la première parce que le nombre des fonctions de transferts existant dans le code de simulations est réduit à trois au lieu de 9. Par contre, la première méthodologie est plus précise que la deuxième vu que les interactions et les auto-excitations sont bien indépendantes et dissociés.

Dans le cas d'un simple tube, qui correspond à ligne d'admission du monocylindre, le modèle de la fonction de transfert complet est six fois plus rapide que le modèle natif avec un très bon niveau de précision (erreur relative maximum par rapport à GT-Power native de moins de 1 % et de 2.69 % par rapport aux essais expérimentaux).

Dans le cas d'une géométrie complexe, qui est le cas pour le moteur à trois cylindres, le modèle de la fonction de transfert est sept fois plus rapide que le modèle natif avec aussi un bon niveau de précision (erreur relative maximum par rapport à GT-Power native de 2.88 % et de 3.4% par rapport aux essais expérimentaux).

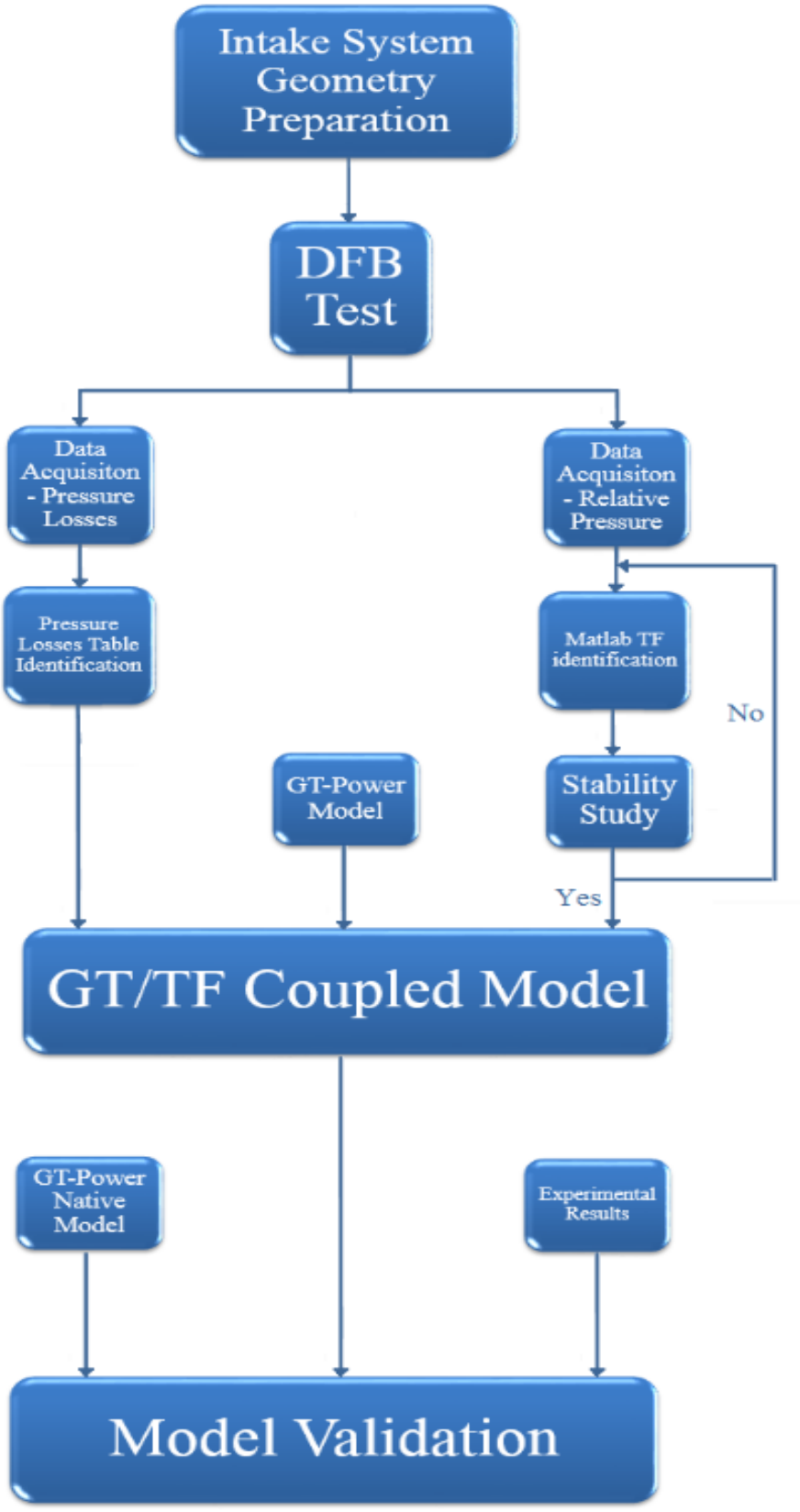

Figure 9 – Algorithme de la méthodologie de la fonction de transfert

Conclusion

La propagation des ondes de pression dans la ligne d'admission d'un moteur à combustion interne a des effets significatifs sur le comportement du moteur. Une étude a été menée sur ce phénomène en utilisant une approche fréquentielle, basée sur l'idée de la fonction de transfert. Cette dernière permet de lier la pression relative et le débit masse d'air en amont de la soupape d'admission. L'enjeu principal de cette méthodologie est d'avoir un bon niveau de précision d'un modèle virtuel modélisé dans un logiciel de simulation, avec un temps de calcul rapide.

L'étude bibliographique présentée dans le Chapitre I permet de mieux comprendre certains phénomènes physiques, surtout le phénomène de propagation des ondes de pression dans la ligne d'admission d'un moteur à combustion interne.

Les outils numériques et expérimentaux présentés dans le Chapitre II ont aussi permis de réaliser le travail du présent manuscrit :

- *En utilisant le banc dynamique, les fonctions de transfert ont été identifiées. C'est la première étape de la méthodologie proposée. Les fréquences propres des systèmes testés ont été identifiées en se basant sur le phénomène de la résonance en quart d'onde.*

- *Matlab permet de transformer le système identifié dans le domaine temporel en un système robuste dans le domaine fréquentiel, en ayant recours à un outil spécifique nommé « Ident ».*

- *Le logiciel de simulation GT-Power a été choisi pour plusieurs raisons: d'abord, c'est un outil fiable et facile à utiliser. Les moteurs thermiques présentés dans le Chapitre II ont été modélisés dans GT-Power et calibrés selon les essais expérimentaux. Les résultats ont montré la bonne capacité des modèles virtuels à reproduire les essais réels. Ensuite, le logiciel autorise la modélisation multi-physique. En effet, la méthodologie présentée consiste à coupler une fonction de transfert mathématique avec une modélisation unidimensionnelle non-linéaire. Enfin, le logiciel permet de mesurer les variables thermodynamiques à n'importe quelle position du système d'admission en utilisant des capteurs virtuels. Cette propriété a été utilisée pour identifier la fonction de transfert de la température à l'aide d'un banc dynamique.*

- *Les bancs moteurs ont aidé à valider la précision des modèles natifs et des modèles 0D/1D couplés.*

Dans le troisième chapitre, la méthodologie de la fonction de transfert a été présentée. L'historique du modèle ainsi que la méthode d'optimisation sont détaillés. L'objectif principal de la méthodologie 0D / 1D est de remplacer le système d'admission du moteur à combustion interne par sa propre fonction de transfert dans le code de simulation. En d'autres termes, un couplage a été effectué à l'aide du code de simulation 1D de GT-Power, dans lequel le système d'admission du moteur à combustion interne a été remplacé par sa fonction de transfert. L'optimisation comprend trois parties principales: identification, implémentation et calibration.

Les fonctions de transfert de température et les filtres exponentiels ont été ajoutées au modèle principal afin d'améliorer la précision et de réduire le temps de simulation

L'objectif principal du modèle présenté dans le chapitre IV est de réduire le nombre d'essais sur le banc dynamique. Le modèle permet d'identifier une fonction de transfert, idéalement égale à la fonction de transfert mesurée issue d'un essai sur le banc dynamique. Le modèle a été validé sur un ensemble de simples tubes de différentes longueurs.

Enfin, la validation principale du modèle a été effectuée dans le chapitre V. L'utilisation d'un moteur monocylindre sans combustion a permis de se concentrer sur le phénomène de propagation des ondes. De nombreuses fonctions de transfert ont été identifiées pour différentes vitesses de moteur pour une meilleure précision du modèle. La manière d'implémenter ces fonctions dans le code de simulation a permis de réduire le temps de simulation (utilisation de la fonction de filtre exponentiel). Les coefficients de filtrage sont identifiés expérimentalement. Cependant, ces coefficients dépendent de la vitesse de rotation du moteur. L'utilisation de la fonction de transfert pour la température, due aux fluctuations de pression, aide le modèle couplé à diminuer son temps de convergence, étant donné que de nouvelles informations ont été ajoutées au système d'équations non linéaire. Cette fonction a le même principe que la fonction de transfert de pression, et elle est identifiée de la même manière mais dans ce cas, le banc dynamique virtuel a été utilisé. Ce dernier a déjà été calibré et validé à l'aide de données expérimentales. Le modèle final garanti une bonne précision avec un temps de calcul réduit par rapport au modèle natif de GT-Power (le modèle est trois fois plus rapide dans le cas d'un tube simple). Un cycle équivalent à un NEDC est exécuté afin de tester la fiabilité du modèle en phase de fonctionnement transitoire du moteur. Le temps de convergence du modèle de fonction de transfert est relativement rapide par rapport à la représentation unidimensionnelle. Le modèle a montré aussi une meilleure précision en cas de fonctionnement transitoire du moteur.

La validation du modèle concerne également une géométrie complexe des systèmes d'admission. Le modèle présenté dans ce travail de recherche a montré une bonne capacité à modéliser la géométrie complexe d'un moteur à trois cylindres (filtre à air + collecteur d'admission + papillon). L'effet d'interférence entre les cylindres a été pris en compte en utilisant les fonctions de transfert correspondantes. Dans ce travail, deux manières d'intégrations de ces fonctions ont été proposées. Les deux méthodes ont montré une bonne capacité à modéliser la propagation des ondes de pression dans le système d'admission. La méthode consistant à utiliser une fonction de transfert équivalente est le meilleur compromis entre précision et temps de simulation. Le modèle a montré un bon accord avec les résultats expérimentaux. Pour certains points de fonctionnement du moteur, le modèle a montré une meilleure précision que le mode natif unidimensionnel. En terme de temps de simulation, le modèle était sept fois plus rapide que le modèle unidimensionnel traditionnel.

<u>Limitations:</u>

- *La fonction de transfert correspond à toute la géométrie testée. Par conséquent, lorsque cette géométrie est modifiée, une nouvelle identification du nouveau système est nécessaire (par exemple : changement d'angle d'ouverture du papillon).*

- *Les essais expérimentaux effectués pour identifier les fonctions de transfert ne sont pas faciles à réaliser, en particulier lorsque la géométrie testée est une configuration complexe (par exemple: un système d'admission d'un moteur à quatre cylindres). L'ensemble du système d'admission, des conduits primaires jusqu'au filtre à air, devront être installés sur le banc. Ceci nécessite également des outils spécifiques pour adapter cette configuration au banc.*

- *Modélisation du turbocompresseur: le modèle de fonction de transfert peut parfaitement fonctionner dans le cas d'un moteur atmosphérique. Un moteur suralimenté n'a pas pu être testé parce que le couplage entre le turbocompresseur et les fonctions est impossible à réaliser dans la configuration actuelle du modèle. En fait, dans le modèle de la fonction de transfert, l'ensemble du système d'admission a été remplacé par des fonctions. Ainsi, le turbocompresseur ne peut pas être implémenté dans le code.*

Enfin, la méthodologie de la fonction de transfert peut être une méthode alternative pour modéliser l'écoulement à l'intérieur de la géométrie d'admission d'un moteur atmosphérique à injection directe.

Perspectives:

- *Dans le présent travail, une seule fonction de transfert équivalente de température est utilisée par modèle pour toutes les vitesses de rotation du moteur. La précision du modèle peut être améliorée en rendant ces fonctions dépendantes de la vitesse de rotation du moteur.*

- *Les variations de pressions et de températures ont été implémentées séparément dans le code de simulation en utilisant deux fonctions de transfert différentes. Afin de réduire le nombre de fonctions de transfert dans le code de simulation, une fonction équivalente comprenant les deux paramètres pourrait être utile.*

- *En modèle acoustique, les lois de correction ont été identifiées pour des tubes de différentes longueurs. Les tubes de différents diamètres ne sont pas pris en compte. Afin d'enrichir la bibliothèque des fonctions de transfert identifiée pour différentes géométries, en établissant une loi de correction pour le diamètre, il convient de réaliser une campagne d'essais, durant laquelle le diamètre est pris en compte.*

Titre : Modélisation multi-physique de la ligne d'admission d'un moteur à combustion interne

Mots clés : Moteur à combustion interne, dynamique des gaz, écoulement compressible, domaine fréquentiel, ligne d'admission, fonction de transfert.

Résumé : La concurrence entre les constructeurs automobiles pour introduire les solutions les plus innovantes est de plus en plus importante. Depuis quelques années, la simulation est largement utilisée dans le domaine d'automobile. Concernant l'étude de la dynamique des gaz et de la propagation des ondes de pression dans le système d'admission d'un moteur à combustion interne, qui ont des effets significatifs sur le comportement du moteur, une modélisation précise est nécessaire afin d'obtenir de bons résultats. L'objectif principal de la méthodologie présentée dans cette thèse est de réduire le temps de simulation permettant d'étudier le fonctionnement de moteurs à combustion interne tout en conservant un bon niveau de précision.

Les ondes de pression ont été étudiées en utilisant une approche fréquentielle. Cette dernière est basée sur une fonction de transfert, qui relie la pression relative au débit masse d'air en amont de la soupape d'admission. Un couplage multi-physique avec le logiciel de simulation a été établi. La validation du modèle a été effectuée à l'aide d'un critère de précision relatif au rendement volumétrique et à la pression instantanée en amont de la soupape d'admission. Les résultats ont montré un bon niveau précision. En termes de temps de calcul, la méthodologie de la fonction de transfert est plus rapide que le code de simulation natif. Cette méthodologie peut être une méthode alternative pour modéliser la géométrie d'admission d'un moteur à combustion interne.

Title : Multi-physics modeling of the intake line of an internal combustion engine

Keywords : Internal combustion engine, gas dynamics, compressible flow, frequency domain, intake system, transfer function.

Abstract: The competition among carmakers to introduce the most innovative solutions is growing day by day. Since few years, simulation is being used widely in automotive industries. Concerning the study of gas dynamics and pressure wave's propagation in the intake system of an internal combustion engine, which have a significant effect on engine behavior, a precise modelling is needed in order to obtain good results. The main objective of the methodology presented in this PhD thesis, is to shorten the simulation time in order to study the behavior of an internal combustion engine, while conserving a good accuracy level.

The pressure waves are studied using frequency approach. This latter is based on a transfer function, which links the relative pressure and the air mass flow rate upstream the intake valve. A multi-physics coupling model in the simulation code was established.
The model validation was conducted using precision criterion on volumetric efficiency and on instantaneous pressure upstream of the intake valve. The results showed good accuracy level. In terms of computational time, the transfer function methodology is faster than the native one-dimensional non-linear code.
This methodology can be an alternative method for modeling the intake geometry of an IC engine.